UNIVERSITY OF SOUTHAMPTON
FACULTY OF PHYSICAL AND APPLIED SCIENCES
PHYSICS AND ASTRONOMY

An X-Ray, Optical and Infra-red study of High-Mass X-Ray Binaries in the Small Magellanic Cloud

by

Lee John Townsend

Thesis for the degree of Doctor of Philosophy
March 17, 2012

UNIVERSITY OF SOUTHAMPTON

ABSTRACT

FACULTY OF PHYSICAL AND APPLIED SCIENCES

PHYSICS AND ASTRONOMY

Doctor of Philosophy

AN X-RAY, OPTICAL AND INFRA-RED STUDY OF HIGH-MASS X-RAY BINARIES IN THE SMALL MAGELLANIC CLOUD

by Lee John Townsend

The known population of high-mass X-ray binaries in the Small Magellanic Cloud is continually growing and is now a similar size to that of the Milky Way, despite a significant mass difference between the two galaxies. In this thesis, I present multi-wavelength observations of Be/X-ray binaries that have undergone an outburst during the past three years, including the discovery of new systems and extended outbursts from previously known sources. The results are discussed in terms of both the underlying physics of individual outbursts and how the growing SMC population is helping our understanding of the formation and evolution of high-mass X-ray binaries. In particular, I describe the orbital analysis of every extended X-ray outburst detected by the *Rossi X-ray Timing Explorer* and present the first significant sample of systems outside of the Milky Way for which a binary orbital solution is known.

CONTENTS

LIST OF TABLES

LIST OF FIGURES

DECLARATION

I, Lee John Townsend, declare that the thesis entitled *An X-Ray, Optical and Infrared study of High-Mass X-Ray Binaries in the Small Magellanic Cloud* and the work presented in the thesis are both my own, and have been generated by me as a result of my own original research. I confirm that:

- this work was done wholly or mainly while in candidature for a research degree at this University;
- where any part of this thesis has previously been submitted for a degree or any other qualification at this University or any other institution, this has been clearly stated;
- where I have consulted the published work of others, this is always clearly attributed;
- where I have quoted from the work of others, the source is always given. With the exception of such quotations, this thesis is entirely my own work;
- I have acknowledged all main sources of help;
- where the thesis is based on work done by myself jointly with others, I have made clear exactly what was done by others and what I have contributed myself;
- parts of this work have been published as:
  - Be/X-ray binary SXP6.85 undergoes large Type II outburst in the Small Magellanic Cloud, 2010, MNRAS, 403, pp. 1239-1245
  - The orbital solution and spectral classification of the high-mass X-ray binary IGR J01054–7253 in the Small Magellanic Cloud 2011, MNRAS, 410, pp. 1813-1824
  - On the orbital parameters of Be/X-ray binaries in the Small Magellanic Cloud, 2011, MNRAS, 416, pp. 1556-1565

Lee John Townsend, March 17, 2012

ACKNOWLEDGEMENTS

First and foremost I would like to thank my supervisor, Malcolm Coe, for his continued guidance and support. His drive to obtain and exploit all manner of data has given me a wealth of information on which to base my thesis and sent me to some of the world's most incredible places in the process. I feel extremely lucky to have been able to use my Ph.D. as a stepping stone to visit many a beautiful city and inspiring mountain top, and I thank Malcolm for being so insistent that I go to as many as possible! When Malcolm wasn't around there was always two people I could turn to for advice. Matthew and Vanessa, thank you for all your help during the early years of my Ph.D. and your continued willingness to lend a helpful ear. I'll always be thankful to Matthew for providing me with such a bumpy introduction to observing at SAAO. Everything since then has been a breeze! Whilst my love for astronomy sometimes dwindled here in Southampton it has always been renewed by observing runs at SAAO and visiting Cape Town, a city that I love so much. A special thanks must go to Jose. Whilst we never crossed paths in Southampton, the plethora of IDL codes you left behind have helped me enormously in my work and saved me many an hour of staring blankly at the screen. If only you had done the same with IRAF! I am also indebted to Simon, without whom, I'm sure, no student would ever finish their Ph.D.

And so to the students, past and present, who have helped me and kept me going in less obvious ways. Matthew, again, for our Friday lunchtime snooker sessions. Whilst often prime examples of how not to play the game, they made the prospect of Friday morning meetings much more bearable. We must also not forget to publish the paper we discussed in Valencia. Does the April 1st deadline still seem doable...? Thank you Grace for listening to and joining me in countless hours of Ph.D. bashing at lunchtimes and for opening up your home for many a classy night of binge drinking! To Tony, Pablo, Anna and the others fortunate enough to go to Hawaii. It is a truly beautiful place that will stay in my memories forever, as will the carnage that often followed one too many cocktail in the sun. Special thanks to Tony, for helping me to fully exploit said cocktails on many occasions with the arduous cynicism only you can manage! Thank you Sadie for putting up with me as a housemate for a year. Your drunken escapades always make me smile. My office mates, Mark, Martin, Dan & Dan for providing help and distraction when needed. I think we were all brought closer by a common enemy... And thank you Martin for your thesis advice, I can only hope it wasn't in vain. Thanks to Seb for all your help with INTEGRAL data and for making it that little bit easier to drag myself to circuits each week. Though you have started to win too many squash games, so it may be for the best I am finishing. A final thank you goes to Tony Bird. Though banished to work in the student quarters you were always happy to lend a hand, or a sarcastic comment. To everyone else that I have forgotten to mention, its been a pleasure.

To my parents, Mum, Dad, Barb and Vic. You have supported me in so many ways (often financially!) from my very first day as a undergraduate here 8 years ago. I cannot thank you all enough for the countless hours you spent reading with me, doing homework with me and generally driving me to do the best I could possibly do, at school and elsewhere in life. I certainly wouldn't be where I am today if it weren't for you. Thank you.

Finally, Liz. Traditionally people would dedicate their thesis to the special someone in their life, but as you will have one of your own soon it seems a little out of place! Thank you for being there for me and for traversing the ups and downs of Ph.D. life with me. Working so close to you has never been a chore, and I'm incredibly happy I've had the chance to share with you some of the amazing experiences that I've had during my studies. The next challenge is finding our way to the same city and, I'm sure, whichever far flung corner of the world that may be, we'll be just fine. From the bottom of my heart, I love you.

Lee John Townsend, March 17, 2012

Astronomy's much more fun when you're not an astronomer.

BRIAN MAY (1947 – PRESENT)

To Grandad

The release of atom power has changed everything except our way of thinking...the solution to this problem lies in the heart of mankind. If only I had known, I would have become a watchmaker.

ALBERT EINSTEIN (1879 - 1955)

I know the human being and fish can coexist peacefully.

GEORGE W. BUSH (1946 – PRESENT)

The history of astronomy is a history of receding horizons.

EDWIN P. HUBBLE (1889 – 1953)

1 X-ray Binaries

The following chapter is an introduction to physics of X-ray binaries. As this thesis records a multi-wavelength study of high-mass X-ray binaries (HMXB), this too is the focus of this chapter. The formation channel and evolutionary pathways of HMXBs are discussed in terms of the different sub-classes of this type of system. A detailed description of the observational properties of both the X-ray source and the counterpart star is given for HMXBs with a Be star counterpart, as these are the most numerous of the HMXB family and are the sub-class on which this thesis is based. The accretion physics and emission mechanisms that underlie these properties are also discussed towards the end of the chapter.

1.1 Introduction

X-ray binaries are some of the most variable and volatile objects in the universe. Much of this variability is caused by the accretion of matter from a companion star onto a compact object. In most cases, the companion is a 'normal' star on the main sequence or a more evolved giant or supergiant star and the compact object is a neutron star, black hole or white dwarf. Each combination produces wildly different observational properties across all spectral frequencies. From here on, I

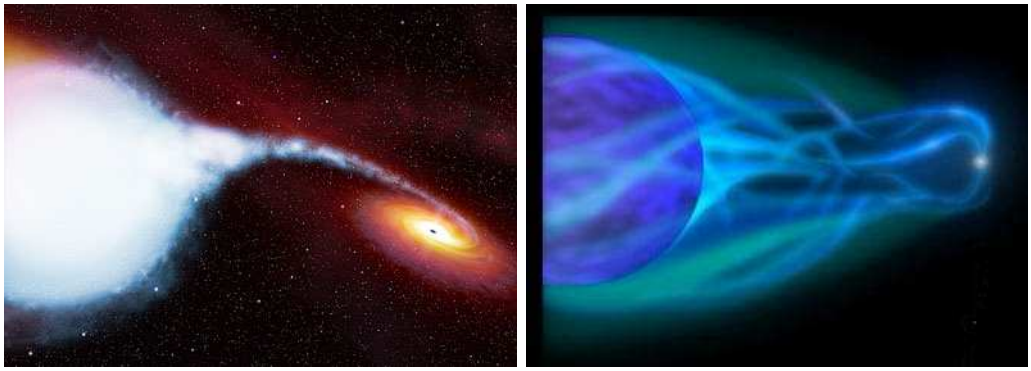

Figure 1.1: Artist impression of an accreting black hole in an X-ray binary (*left*) and an accreting neutron star in an X-ray binary (*right*). Image credit: ESA.

will reserve the term 'X-ray binary' (XRB) for neutron star and black hole systems, as accreting white dwarfs are much fainter in the X-ray than the other two types. They are classified separately as cataclysmic variables (CV), due to large dynamic ranges caused by nova events. Figure 1.1 gives an artists view of what a black hole XRB and a neutron star XRB might look like. The left-hand image depicts material being accreted from a low-mass companion and forming an accretion disk around the black hole. The right-hand image depicts a neutron star accreting from the stellar wind of a high-mass star down its magnetic poles. These are two specific types of binary and will be discussed, along with the other types, in detail here.

The emission properties seen from an XRB are largely determined by the type of compact object, the accretion geometry and, in the case of a neutron star, the strength and geometry of the magnetic field. A magnetic field is the easiest way to determine whether the compact object is a neutron star or black hole. The magnetic field around a neutron star will disrupt the accretion disk or spherical inflow, causing material to funnel down the field lines onto the magnetic poles. If the rotation and magnetic axes are misaligned and one or both poles move through our line-of-sight, X-ray pulsations will be seen by the observer. However, a lack of pulsations does not rule out a neutron star accretor. A geometry other than that discussed above, a weak magnetic field or a number of other reasons discussed throughout this work can result in pulsed emission either not being produced or not reaching the observer. In this case we rely on other methods to distinguish between accreting objects, such as spectral differences or mass measurements.

Despite the heavy dependence of the observational properties on the compact object, the 3 main types of XRB are divided into groups based on the mass of the companion star. These are low-mass X-ray binaries (LMXB), intermediate-mass X-ray binaries (IMXB) and high-mass X-ray binaries (HMXB).

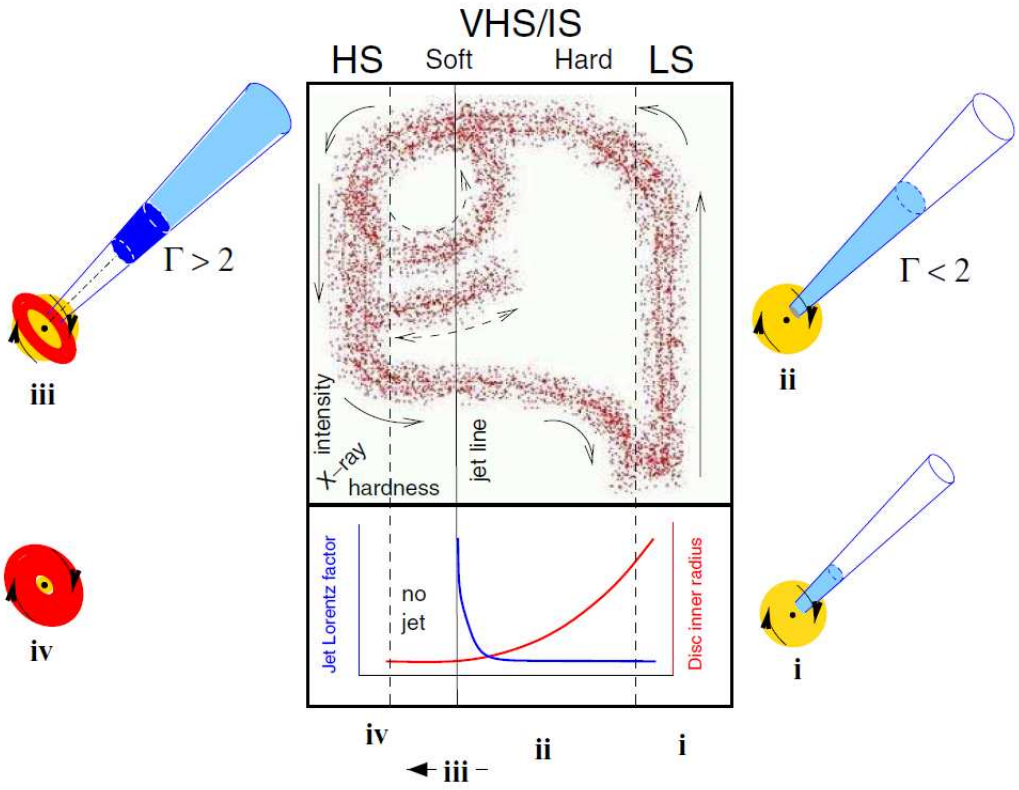

Figure 1.2: Hardness-intensity diagram for a black hole X-ray binary (taken from Fender, Belloni & Gallo 2004).

1.1.1 Low-mass X-ray binaries

An LMXB is made up from a companion star of approximately stellar mass and a neutron star or black hole compact object. The companion is usually a main sequence or evolved star, but can also be a white dwarf. They are old systems, having a typical age of around 10^9 years, and are usually found in globular clusters or toward the Galactic centre. Matter is accreted onto the compact object via Roche-lobe overflow through the inner Lagrangian point. The initial angular momentum of the material prevents it being accreted directly to the surface of the neutron star or event horizon of the black hole. Instead, the material follows a spiral path toward the compact object and forms an accretion disk. It is the accretion disk that causes most of the optical and X-ray variability observed in LMXBs.

The key areas of LMXB research are variability within the accretion disk, production of radio jets and the similarities and differences with active galactic nuclei (AGN). Time and spectral variability are known to be related and presumably originate from the inner accretion flow, where X-ray emission and reprocessing are thought to occur. These spectral and timing characteristics produce different source

'states', identifiable by luminosity, hardness and quasi-periodic oscillation (QPO) type. Specifically, black hole systems undergo state changes in a manner of hysteresis, as in Figure 1.2. Fender, Belloni & Gallo (2004) present a model based on these state changes to describe the disk-jet coupling in black hole binaries. The source starts in the low-hard state (lower right corner, Figure 1.2) where the jet emission is steady and dominates the disk emission. It will evolve up the right-hand side of the plot as the X-ray luminosity increases. The source evolves anti-clockwise around the figure entering the high-soft state where the Lorentz factor of the jet increases sharply. This is followed by a quenching of the jet as the source luminosity decreases, entering the disk dominated state. The final stage is for the source to become harder and fainter, moving back into quiescence.

Both variability and disc-jet coupling seen in black hole X-ray binaries have been linked to what is seen in AGN. In particular, it is seen that variability timescales scale with mass (e.g. Uttley, McHardy & Papadakis 2002, McHardy et al. 2004), suggesting that the same processes causing the variability in LMXBs are also present in AGN. Similarly, Maccarone, Gallo & Fender (2003) show that the radio emission from a sample of AGN is quenched at a similar fraction of the Eddington luminosity as in black hole binaries, and that the radio to X-ray luminosity correlation is the same in both type of objects. This suggests that a similar 'state' evolution and disk-jet coupling exist in both AGN and X-ray binaries.

1.1.2 Intermediate-mass X-ray binaries

The mass of the optical counterpart in LMXBs is $\lesssim 1\,M_{\odot}$. The mass of the counterpart in HMXBs is usually between 10–30 $M_{\odot}$ (see the next section for more details). Thus, it stands to reason that there should exist a population of binaries with a counterpart of mass between 1–10 $M_{\odot}$. These are designated as Intermediate-mass X-ray binaries. In comparison to LMXBs and HMXBs, the number of IMXBs is very small. The reasoning for this was first put forward by van den Heuvel (1975): HMXBs have evolved companions massive enough to have a stellar wind strong enough to power the X-ray source. LMXBs accrete via Roche-lobe overflow (RLO), but evolve very slowly due to the low mass difference between the two stars. In IMXBs the companion is not massive enough to produce a strong enough stellar wind to power the X-ray source. Thus, they must evolve through RLO. The larger mass ratio between the two stars causes the binary to evolve very quickly through this pathway, on the order of a few thousand years (Lewin & van der Klis, 2006), meaning very few would be expected to be observed at any given time.

1.2 High-mass X-ray Binaries

High-mass X-ray binaries (HMXB) consist of a massive early type main sequence or supergiant star and a neutron star or black hole compact object. They are found in regions of high gas and dust, such as the spiral arms of the Milky Way, where massive stars can form. As such, they are an excellent tracer of star formation and an ideal object through which to study star forming galaxies. Figure 1.3 is a Hertzsprung-Russell diagram showing the luminosity, temperature, mass, radius and lifetime of different types of stars. The OB stars that form HMXBs have typical main sequence effective temperatures of between 15000–30000 K and luminosities between 10^3–$10^5\,L_\odot$. Their masses are generally between 10–30 $M_\odot$ whilst their radius is of the order of 10–20 $R_\odot$. This class of star spends typically 1–10 Myrs on the main sequence before evolving into a supergiant and eventually undergoing a supernova explosion. During this transition, the star will become much larger and cooler, resulting in an increase in luminosity of around an order of magnitude.

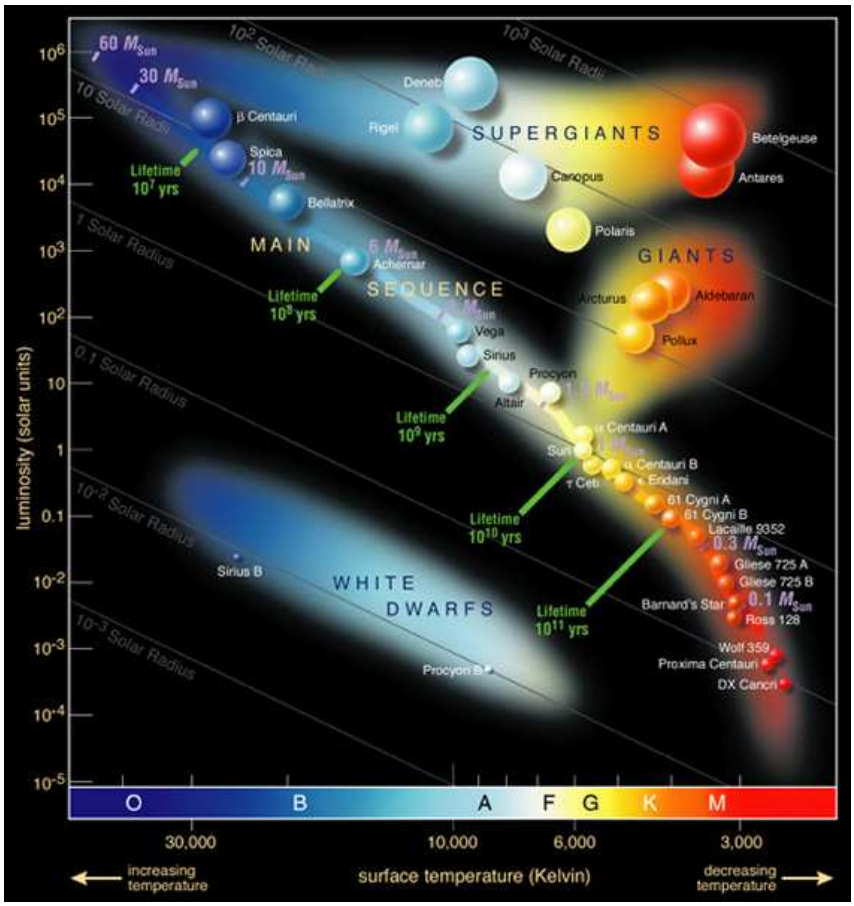

Figure 1.3: Hertzsprung-Russell (HR) diagram showing the stellar distribution on the luminosity-temperature plane, as well as their expected radius, mass and lifetime.

Whether the star is a supergiant or on the main sequence largely determines the characteristics of the HMXB. The main sub-groups of HMXB are the Be/X-ray binaries (BeXRB) and supergiant X-ray binaries (SGXB), making up a large fraction of the known population. The newly emerging classes of supergiant-fast X-ray transients (SFXT, e.g. Sguera et al. 2005, Sidoli 2011) and gamma-ray binaries (e.g. Hill et al. 2010) complete the HMXB family.

1.2.1 Formation

The formation of X-ray emitting compact objects is an inevitable conclusion of the binary evolutionary process. When one, or both, progenitor stars are of a certain mass (typically above $8\,M_\odot$), the binary will evolve such that one or more neutron stars or black holes will form from one or both progenitor stars undergoing a supernova explosion. If the binary remains bound after the initial supernova, it is this evolutionary pathway that produces the HMXBs we observe today. The basic stages of the evolution are depicted in Figure 1.4 and are described below, though it is stressed here that the details depicted and described here are just one possible evolutionary scenario, of which there are actually many. A broader and more detailed review on binary formation and evolution is available by Tauris & van den Heuvel (2006).

In the initial situation of two massive ($\geq 8\,M_\odot$) zero-age main sequence (ZAMS) stars in orbit about each other, normal stellar evolution will take place. Specifically, each star will burn hydrogen and radiate heat under their own gravitational contraction, as described by the virial theorem. The initially more massive star will evolve faster and will be the first to expand. On its expansion and filling of its Roche-lobe, the initially less massive star will begin to accrete from the more massive star through the inner Lagrangian (L_1) point. The transfer of mass and angular momentum will act to disrupt the orbit, changing the orbital period and separation of the system. This will also increase the angular velocity of the less massive star, spinning it up. This type of accretion, known as stable mass transfer, is depicted in the first two stages of Figure 1.4. An alternative to this scenario might occur if the donor star is already a supergiant. In this case, the secondary star cannot accrete all of the material funnelling through the L_1 point, causing a common envelope to form. This is known as unstable mass transfer. This phase of common envelope evolution, though short-lived, causes the orbital period and separation to shrink markedly, resulting in a much more compact X-ray binary or, indeed, a complete merging of the core of the donor star and the companion.

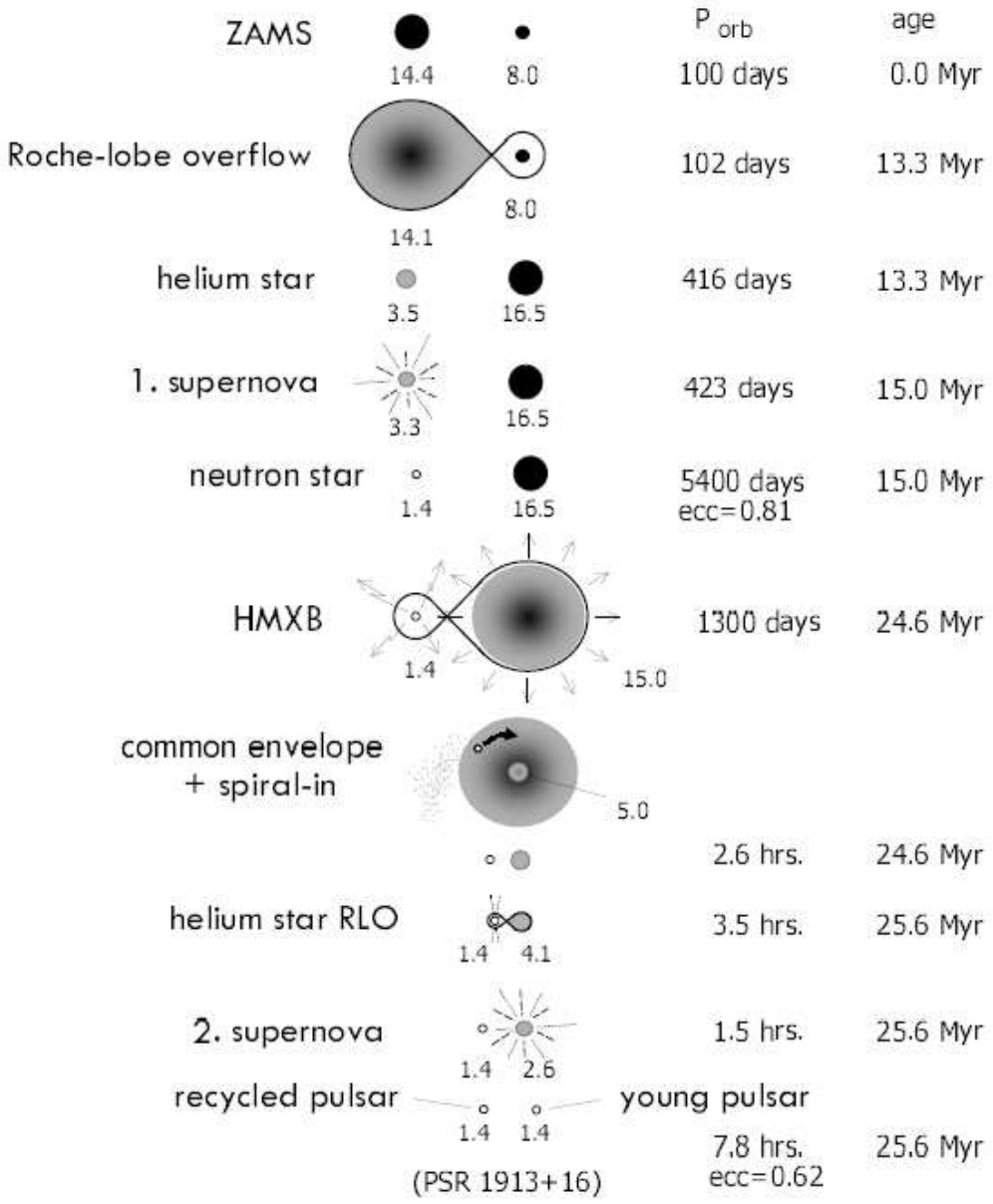

Figure 1.4: Example of an evolutionary path of a HMXB (taken from Lewin & van der Klis 2006). The sequence starts with two massive main sequence stars that evolve through Roche-lobe accretion until the initially more massive star goes supernova. The system then spends around 10 Myrs as an X-ray emitting binary before a common envelope phase causes the system to spiral in, finally becoming a compact object binary.

Once the initially more massive star has lost its hydrogen envelope, a helium star core will be left. When the helium star no longer has the radiative pressure to withstand its own gravitation, it will collapse in on itself. Most of the remaining mass of the star is lost in the subsequent supernova explosion, leaving a neutron star (or black hole) with a spin and mass largely determined by the amount of material expelled in the explosion (stages 3, 4 & 5 in Figure 1.4). The kick imparted onto the neutron star by the (usually asymmetric) supernova explosion severely disrupts the orbit of the system. The most notable changes being a substantially increased orbital period, separation and orbital eccentricity. Should the binary system survive the kick, the properties of the HMXB system are now established and will only change slightly over the lifetime of the X-ray source (stage 6 in Figure 1.4). Depending on the initial conditions the, now very massive, companion star will lose material either via a substantially increased stellar wind, an equatorially enhanced outflow or by direct accretion onto the compact object via the L_1 point. The differences in the properties of the companion and, as such, the way in which the compact object accretes, produces the sub-classes of HMXB. Each class is described in detail below. The point at which the primary star loses its hydrogen envelope also affects the type of supernova that occurs and the resultant compact object. If the envelope is lost before helium ignition in the core, the final mass of the iron core is lower than if hydrogen burning had continued into the core helium burning phase. Thus, it is expected that all supernovae occurring from hydrogen-deficient stars result in a neutron star. This pathway usually occurs if the primary is extremely massive ($\geq$50 $M_\odot$), as these stars will likely evolve into Wolf-Rayet (WR) stars that are characterised by very high mass-loss rates. Indeed, there is a growing number of WR/X-ray binaries known, in addition to the more common OB/X-ray binaries, though it is also worth noting that a majority of these are WR–WR binaries (i.e. systems that have not yet undergone a primary supernova) that emit X-rays through colliding winds (e.g. Pollock 1987).

Eventually, the massive companion star will likely expand to encompass most or all of the orbit of the compact object (stage 7 in Figure 1.4). This is another example of a common envelope phase. This usually coincides with an increase in X-ray luminosity from enhanced interaction between the compact object and the secondary star. This also causes the compact object to spiral-in until it is in a very tight orbit with the core of the secondary and the hydrogen shell has been exhausted. A final stage of accretion takes place as helium from the core of the secondary funnels onto the compact object via the L_1 point. A second supernova explosion will take place once the secondary has lost all of its fuel. A compact object binary is

formed (stages 8, 9, 10 & 11 in Figure 1.4). These systems may continue to interact, causing the orbit to shrink further via gravitational wave radiation. Again, this post-XRB evolution is just one of many different possible pathways. The compact object and the core of the secondary star could merge during the common envelope phase, or the binary could be disrupted by the second supernova before a compact object binary can be produced.

1.2.2 Be/X-ray Binaries

Be/X-ray binaries (BeXRBs) are systems in which a compact object orbits a massive, early type star that at some stage has shown evidence of line emission in the Balmer series. These are main sequence stars with a luminosity class of III–V. To date there are no BeXRBs that contain a confirmed black hole (Belczynski & Ziolkowski, 2009) meaning the detection of pulsed X-ray emission (caused by the strongly magnetised neutron star) is a useful tool in identifying these systems. However, the presence of pulsations does not immediately mean that your HMXB is a BeXRB. Likewise, the lack of pulsations does not rule out it being a BeXRB, as will be discussed throughout this work. The neutron star accretes via interactions with an extended envelope of material in the equatorial plane of the Be star. This outflow originates from the stellar atmosphere of the Be star and is known as a 'circumstellar disk'. It is highly variable due to the rapid rotation and internal dynamics of the Be star and is an important factor to consider when looking at the X-ray properties of the system. The optical properties of the circumstellar disk will be discussed later in this chapter.

X-ray emission in BeXRBs is transient and can occur over a wide range in luminosity. This transient nature is due to the intermittency with which these systems accrete. Generally this occurs because most BeXRBs have highly eccentric orbits, periodically taking the neutron star far away from the mass donor (see Figure 1.5 for a schematic of such an orbit). Systems with a circular orbit are more likely to accrete continuously (c.f. the supergiant systems; see next section), though transient outbursts from near-circular orbit systems have been observed (e.g. Pfahl et al. 2002). In outburst, some systems have reached a peak X-ray luminosity of $\geq 10^{38}$ ergs s^{-1}, close to the Eddington limit for a standard mass neutron star. In contrast, some systems have not been detected in observations sensitive to luminosities of around 10^{32} ergs s^{-1}, demonstrating a huge dynamic range. Most systems spend a large fraction of time in quiescence, in which very little accretion is taking place onto the neutron star. Luminosities in this regime tend to be around 10^{34} ergs s^{-1}. Laycock

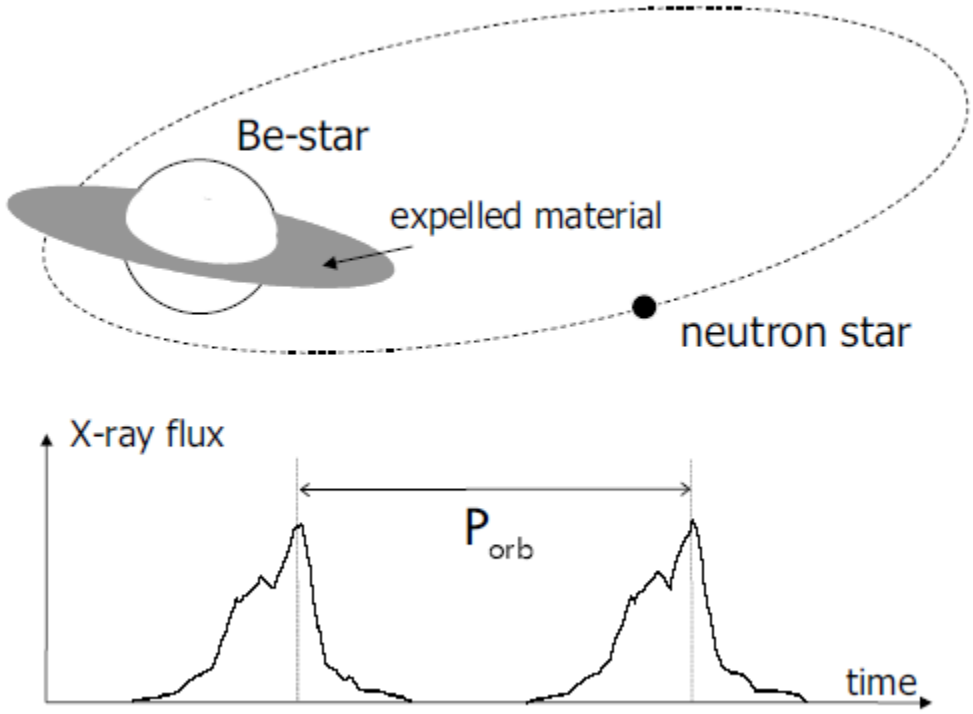

Figure 1.5: Schematic of a neutron stars orbit around a Be star in a typical Be/X-ray binary. The plot shows how the X-ray flux is modulated at the orbital period of the system, caused by an eccentric orbit. The orbital period can be determined from timing analysis of the light curve (taken from Lewin & van der Klis 2006).

et al. (2010) show that even at this low level of accretion, pulsations are still seen in many systems. This was the first time that material was observed to be accreted down the magnetic poles of the neutron star at this accretion rate for a substantial fraction of the BeXRB population. There are two reasons why a BeXRB will emerge from quiescence into outburst: the orbit of the neutron star brings it into contact with the mass outflow of the Be star near its periastron passage, or the Be star enters a period of enhanced mass outflow such that its disk engulfs the orbit of the neutron star. These occurrences result in the two types of transient outburst in BeXRBs: Type I and Type II (Stellar, White & Rosner, 1986). Type I outbursts occur near periastron passage of the neutron star, where there is more accretable material. They are generally in the luminosity range $10^{36} - 10^{37} \mathrm{ergs\,s^{-1}}$ and last from a few days to a few weeks, depending on the binary period of the system. Studying these outbursts allows orbital periods to be derived through timing analysis of their light curves (see Figure 1.5). Type II outbursts are typically an order of magnitude brighter than Type I outbursts and last much longer. The cause of this is

likely due to an enhancement of the circumstellar material or radially driven wind around the companion star (e.g. Negueruela & Okazaki 2000), allowing accretion to occur at any orbital phase and at a higher rate (see Stellar, White & Rosner 1986, for further details of these outburst types).

The rapid rotation of Be stars that most likely causes the disk-like structure in the equatorial plane of the star has recently been ascribed by McSwain & Gies (2005) to spin-up caused by mass transfer in a binary system, as opposed to being born as rapid rotators (Zorec & Briot, 1997). This particular evolutionary pathway, in which the primary star undergoes stable mass transfer onto the secondary prior to the primary supernova, is identical to the pathway that a HMXB moves through before undergoing an electron-capture supernova (ECS; Linden et al. 2009). Linden et al. (2009) also show the production of bright, wind-fed HMXBs is significantly enhanced between 20–60 Myrs after the initial star formation in a starburst galaxy – coincident with the population in the Small Magellanic Cloud (SMC; see Chapter 2). This led those authors to conclude that BeXRBs primarily form through ECS creation channels.

1.2.3 Supergiant X-ray Binaries

Supergiant X-ray binaries (SGXB) consist of a compact object orbiting an OB supergiant star (i.e. a luminosity class of I–II). The optical star emits substantial stellar winds, with mass loss rates of between 10^{-6}–10^{-8} $M_{\odot}\,yr^{-1}$, although these are somewhat reduced in lower metallicity environments such as the Magellanic Clouds (Kudritzki, Pauldrach & Puls, 1987). The winds are highly supersonic, with speeds up to around $2000\,km\,s^{-1}$. This is much higher than the orbital velocity of the compact object, therefore the accretion can be approximated by the classical Bondi-Hoyle formula. This is discussed in more detail later.

A neutron star or black hole can accrete from the stellar wind producing X-rays. In almost all systems the orbit is circular, meaning accretion takes place continuously and with very little variation in luminosity, which is around the level of a typical Type I outburst in a BeXRB. If the companion has evolved to fill its Roche-Lobe, mass transfer occurs at a much higher rate. X-ray emission in this case is highly enhanced ($L_X \sim 10^{38} erg\,s^{-1}$) and an accretion disc is formed around the compact object. At the time of writing, only 3 disk-fed SGXBs are known: Cen X-3, SMC X-1 and LMC X-4. The large majority of the known population of SGXBs reside in the Galaxy. Historically this has always been the case, though it is even more apparent since the *INTEGRAL* discovery of a substantial population of

obscured SGXB in the Galaxy (e.g. Bird et al. 2007, Bodaghee et al. 2007). This hard X-ray population is evidence that the stellar wind in many HMXBs (mostly SGXBs) absorbs much of the soft X-ray component, meaning instruments such as *RXTE, XMM-Newton* and *Chandra* would not have detected them.

1.2.4 New classes of HMXB: SFXTs & γ-ray binaries

A third type of transient X-ray outburst has recently been detected in addition to the Type I & II outbursts in BeXRBs, and is now accepted to originate from a new class of HMXB known as supergiant fast X-ray transients (SFXT). These sources are characterised by rapid X-ray outbursts on the order of minutes to hours (Sguera et al., 2005), large dynamic ranges of order 10^4–10^5 and are associated with OB supergiant companion stars (Chaty et al., 2008). The final sub-class making up the known HMXB family is the small, but growing class of γ-ray binaries, in which very high energy radiation is thought to be produced via interaction of the pulsar wind with the stellar atmosphere of the secondary star (e.g. Hill et al. 2010) or from a micro-quasar.

1.2.5 The relationship between neutron star spin and the binary orbit

A significant number of the HMXBs in the Milky Way and Magellanic Clouds have both their orbital and spin periods known. The orbital periods are usually derived in two distinct ways: from the timing analysis of long-term X-ray and optical light curves that bear evidence of periodic Type I outbursts, or from X-ray pulse arrival time analysis. The latter is the focus of Chapter 5. Figure 1.6 plots the orbital and spin periods of all HMXBs that were known at the time of writing. The figure is more commonly known as the Corbet diagram and is adapted from Corbet (1986). Thorough investigation of this parameter space has yielded the classical picture that the 3 types of HMXB (wind-fed SGXBs, disk-fed SGXBs and BeXRBs) occupy different areas. In particular, the BeXRBs show a large variation in the periods seen and seem to show a positive correlation between the two parameters. In the past, this correlation has been assigned a numerical equation that could be used to predict one parameter should the other be known. However, the most recent plots of the available data show a large spread in the correlation and even merging of some extreme systems with the SGXB region. Thus, it is proving less and less reliable to use this relationship as a tool to predict one of the parameters to any

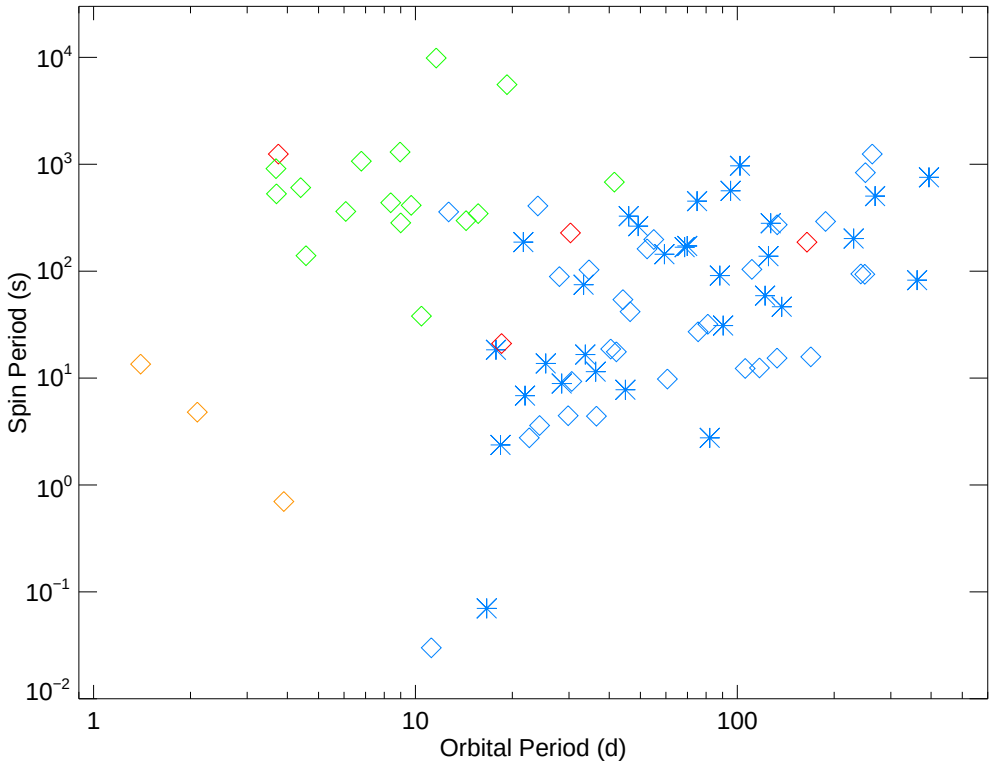

Figure 1.6: The Corbet diagram of HMXB pulsars. The green data points are the wind-fed SGXBs, orange are the disk-fed SGXBs, red are the SFXTs and blue are the BeXRBs. The blue diamonds are the Galactic systems and the blue stars are the Magellanic systems. Private communication from Corbet (2011).

degree of precision, though a ball-park estimate can certainly be made. Even more interesting is the recent emergence of several SFXTs with known orbital and spin periods. The four systems with both periods confirmed are also plotted in Figure 1.6 and appear to occupy both the SGXB and BeXRB regions. This may be telling us something very fundamental about the nature of SFXTs; are they progenitors of the classical HMXBs we see, or do they mark a transitionary state between a BeXRB and a SGXB? There are currently many programmes dedicated to finding and classifying more SFXTs in order to understand where they fit into the standard model of HMXBs.

The classical view on why there may exist a correlation between spin and orbital periods in the BeXRBs involves the spin-down time of the neutron star in the time between its formation and the time the binary starts to accrete. Immediately after the primary supernova, the neutron star is rotating rapidly. The neutron star must spin-down significantly in order to allow inflowing material to overcome the outward force and be accreted. Once the neutron star is rotating slowly enough for material

to be accreted, it will undergo a period of alternating spin-up and spin-down as it moves around its orbit, accreting, or not, at different phases. The amount of time the neutron star spends away from its companion, and hence the amount of time it accretes, is largely dependent on the period and eccentricity of the orbit. As such, a neutron star in a longer orbit will tend to have a longer spin period as it has had more time to spin down. A counter argument to this is that it predicts all systems should be hovering around their equilibrium spin periods. However, this seems not to be the case as there is evidence of a strong bias towards long term spin-up or spin-down trends (e.g. Coe, McBride & Corbet 2010).

1.3 Optical emission from BeXRBs: the Be star

The large mass ratio in HMXBs means that all optical emission seen in such systems comes for the optical counterpart (the accretion disk being much less optically bright in comparison). This is opposite to what is seen in LMXBs where the optical emission from the accretion disk can be studied and the light from the counterpart is swamped. As such, HMXBs offer the best chance to study the donor star in an XRB. In particular, the diversity and variability offered by a Be star counterpart makes the optical properties of the BeXRBs one of the most exciting fields to study. In this section I will introduce some properties of Be stars and discuss what has been learnt from optical observations of BeXRBs.

The Be phenomenon of mass ejection from the equatorial plane of the B star is not well understood (see Porter & Rivinius 2003 for a detailed review). It is thought that the rapid rotation of the photosphere plays a part but that this is not sufficient to explain the disk emission alone as most Be stars rotate just below the critical limit. It has been suggested that non-radial pulsations (the simultaneous expansion and contraction at different radii within the stellar atmosphere) could be the additional trigger needed to push matter at the surface above the escape velocity of the star (see e.g. Emilio et al. 2010 and references therein), though evidence for this is sparse. Regardless of the mechanism(s) that produces the circumstellar emission, its effect is key in our understanding of the optical and X-ray activity we see in BeXRBs.

1.3.1 Spectral classification and the distribution of spectral types

A star can be classified as emission line if Hα (or any other Hydrogen line usually seen in absorption in the hot, ionised photosphere) is filled in or is in emission, and so spectral coverage of the red part of the spectrum is vital. However, the spectral

classification of emission line stars suffers many difficulties due to their very nature; the Balmer lines in particular will be rotationally broadened due to the high rotational velocities of Be stars and hence may obscure any comparisons to closely neighbouring lines, whilst the filling-in of lines caused by the disk emission also makes classification harder. Thus, it is beneficial to perform classification observations when the disk emission is minimal. Further difficulties arise when observing in the Magellanic Clouds. Classification of Galactic Be stars relies on using the ratio of many metal-helium lines (Walborn & Fitzpatrick, 1990). However, this type of classification, based on the Morgan-Keenan (MK; Morgan, Keenan & Kellman 1943) system, is particularly difficult in the low metallicity environment of the Magellanic Clouds because these metal lines are either very weak or not present at all. Using high signal-to-noise ratio spectra of SMC supergiants, Lennon (1997) devised a system for the classification of stars in the SMC that overcomes the problems with low metallicity environments. This system is normalised to the MK system such that stars in both systems exhibit the same trends in their line strengths. Thus, in the spectral classification presented in Chapters 4 & 6 I have used the classification method as laid out in Lennon (1997) and utilised further in Evans et al. (2004). For the luminosity classification I adopted the classification method set out in Walborn & Fitzpatrick (1990).

Negueruela (1998) were the first to show a significant difference between the distribution of spectral types of Be stars in binaries and those in isolation. The three panels in Figure 1.7 show this comparison for the SMC, LMC and Milky Way, running top to bottom respectively (Antoniou et al., 2009). As can be seen, the difference in the Milky Way populations is apparent, though the reasons are unclear. It has been suggested by Ekström et al. (2008) that the observed cutoff in spectral type for Be stars is due to higher mass loss in early type stars (meaning the critical velocity limit is never approached) and due to a lower rate of angular momentum transfer from the core to the surface of later type stars (meaning the photosphere is not accelerated as much). McBride et al. (2008) suggest that the cutoff for Be stars in BeXRBs may be due to high angular momentum loss before the supernova that produces the XRB. On examination of the SMC and LMC distributions, Antoniou et al. (2009) find the BeXRB and isolated Be systems in the SMC to be consistent with each other and find the total SMC sample to be similar to that of the LMC. These conclusions are based on Kolmogorov–Smirnov (K–S) tests to see if the two populations are distinct. In the case of the Be star distribution being similar to the BeXRB distribution in the SMC and LMC, where it is clearly not in the Galaxy, it is very hard to explain why. There seem to be no obvious reasons why stars

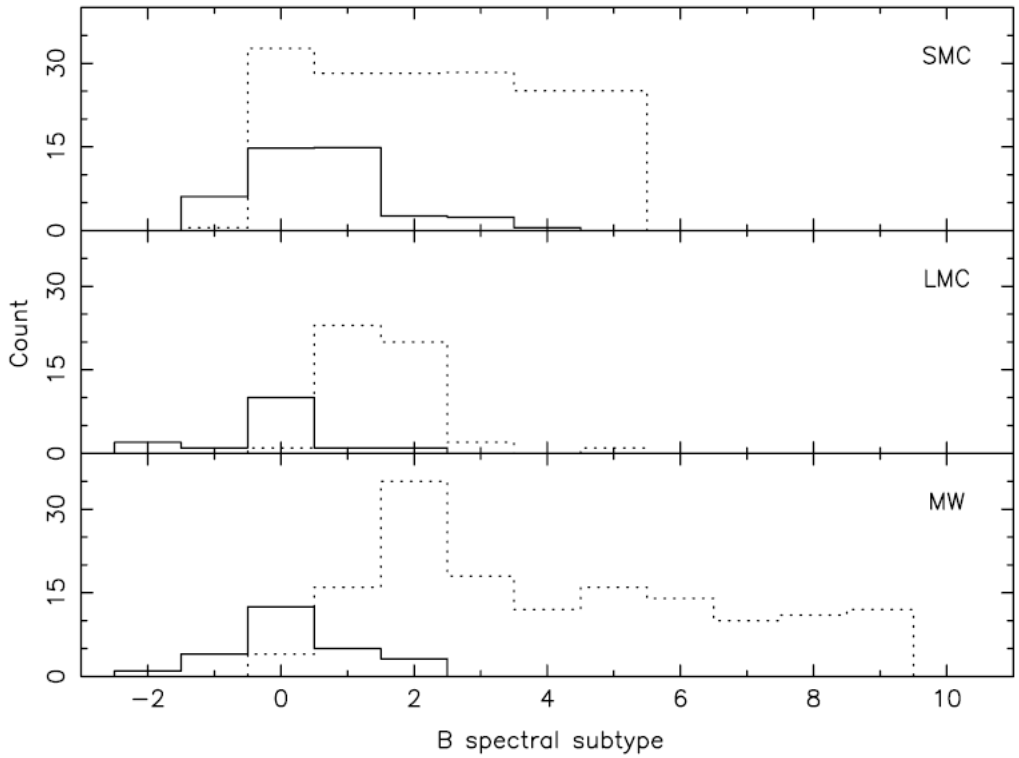

Figure 1.7: Distribution of the spectral subtypes of BeXRBs (solid histograms) and isolated Be stars (dashed histograms) for the SMC, LMC and Milky Way. Negative subtypes correspond to O-type stars. Taken from Antoniou et al. (2009).

should be of lower spectral type than those in binaries in the Milky Way but not in other galaxies. It may be more likely that the current data are biased towards higher spectral types in the Magellanic Clouds, as later type stars are harder to classify at these distances.

1.3.2 The circumstellar disk

A Be star will be forever known as a Be star once the line emission and IR continuum excess have been observed, even though they can transition from Be to B and back again throughout their time on the main sequence through the loss and reformation of the disk. O and A type stars that show the same behaviour are also referred to generically as Be stars, though sometimes as Oe and Ae stars. The line emission in the Balmer and Paschen series' produced in the disk is a result of temperatures being lower that in the photosphere, whilst free–free and free–bound hydrogen emission is presumably responsible for the observed IR excess.

When observing the continuum and line emission from the disk, it is important to consider the region of the disk in which the emission comes from. Carciofi (2010)

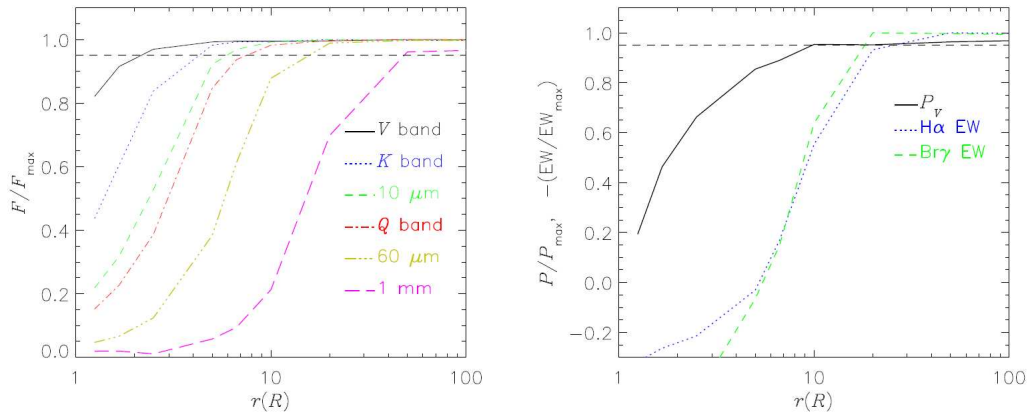

Figure 1.8: The formation radii of different disk observables as shown by recent numerical simulations (Carciofi, 2010). The calculations are based on a rapidly rotating B1 Ve star, where r(R) is the disk radius in stellar radii. *Left:* continuum emission at various wavelengths, where F_{max} is the flux in a simulation with a disk outer radius of 1000 $R_\star$. Specifically, this is the maximum flux that the disk can produce. The longer wavelength emission is shown to be produced further out in the disk. *Right:* disk polarisation and line emission as a fraction of the maximum possible polarisation and line equivalent width. The polarisation is shown to originate from much closer to the star than the hydrogen line emission. Taken from Carciofi (2010).

state that the size of the disk is a function of the wavelength at which you are looking. The left-hand side of Figure 1.8 shows this for several specific wavelengths. Thus, if you observe in the NIR, you would expect much of the flux to come from the inner few stellar radii. Whereas, much of the sub-millimeter flux is produced between 10 and 50 $R_\star$. The right-hand side of Figure 1.8 shows how the line emission and polarisation grow with disk radius. Not until the disk size is about 5 $R_\star$ is there enough emission at Hα and Brγ to fill in the absorption from the photosphere. Much like the IR continuum emission, this line emission continues out to a few ten's of stellar radii. The polarised light is produced out to around 10 $R_\star$. The results of this simulation (see Carciofi & Bjorkman 2006 for details of the code) support the excellent spectropolarimetric observations by Wisniewski et al. (2010) that suggest disk-loss in Be stars proceeds from the inside out. Those authors show an approximate 120 d (190 d) lag in the maximum (minimum) Hα equivalent width from the maximum (minimum) in V-band polarisation in the Be star 60 Cyg. This means the polarised flux is lost before the Hα flux. Figure 1.8 supports the interpretation of Wisniewski et al. (2010) that the inner part of the disk dissipates first and proceeds outwards.

Other informative ways of looking at the circumstellar disk is through IR colours derived from the continuum flux and so-called V/R variations derived from the ratio

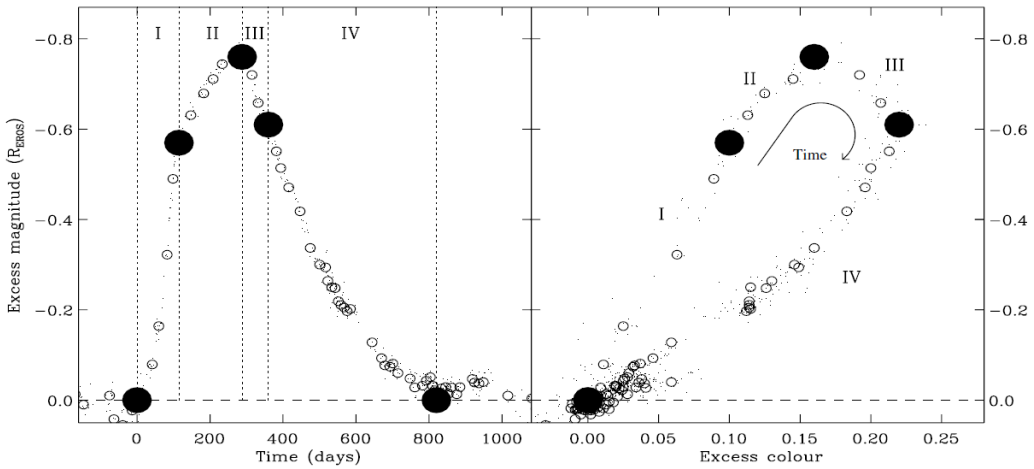

Figure 1.9: Light curve (*left*) and colour-magnitude diagram (*right*) for a Be star in the SMC. Excess magnitude and excess colour are the difference between the observed magnitude and colour and that observed at time = 0. The larger the excess, the brighter or redder the star is. It is shown that the star gets redder as it gets brighter and bluer as it gets fainter, as is the case for most Be stars. The important deviation from this occurs just after the peak flux where, for a short time, the star continues to redden as it gets fainter. This is a signature of the inside-out manner by which the star losses its disk. Taken from de Wit et al. (2006).

of violet and red peak intensities in the double-peaked disk line emission. The latter, together with the long-term Be to B transitions and NRPs mentioned previously, make up the three main types of variability seen in isolated Be stars. V/R variability has been observed in many Be stars (e.g. Mennickent & Vogt 1991) and is generally accepted to arise from global one-armed oscillations within the circumstellar disk (Okazaki, 1991). Theoretically, these one-armed oscillations are born from global oscillations thought to occur in quasi-keplerian disks (Kato 1983; Okazaki 1991). The finer details of this is beyond the scope of this work. For a nice review of the theoretical aspects of global oscillations and summary of recent observations of V/R variability see Mennickent, Sterken & Vogt (1997).

The long-term process in which the disk grows and shrinks is generally accepted to cause changes in surface brightness of any Be star. It is also seen in many cases in the literature that Be stars become redder as they get brighter (e.g. Percy & Bakos 2001; McGowan et al. 2008a). This is thought to arise from a density change within the disk which leads to a change in the continuum emission so long as this is optically thin (de Wit et al., 2006). A small fraction of Be stars with a high inclination angle (viewed side-on) are known to redden with *decreasing* luminosity (the most famous example of which is probably the counterpart in the BeXRB A 0535–26). This is likely due to the enlarged disk blocking out some of the blue light from the

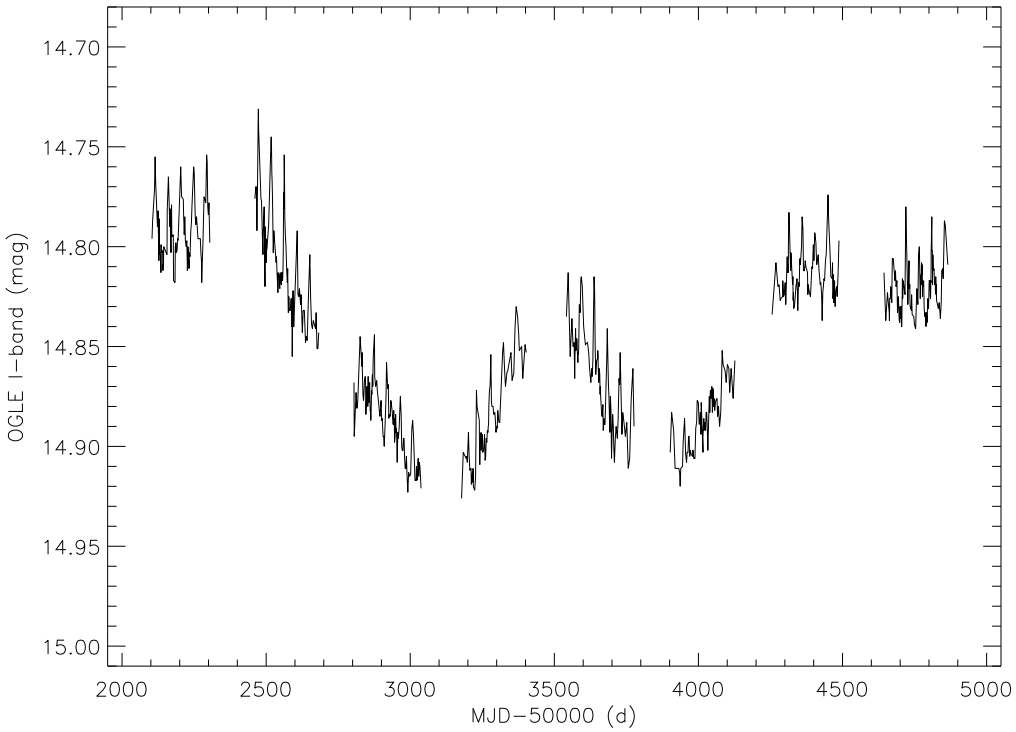

Figure 1.10: I-band light curve of the SMC BeXRB SXP7.78 from the OGLE III photometric survey. The periodic brightening is attributed to the neutron star interacting with the disk during periastron, whilst the longer aperiodic changes are likely due to changes in the size of the disk.

photosphere. Figure 1.9 shows not only this relationship between luminosity and colour, but also that the colour change proceeds in a manner of hysteresis (right panel). The key phase of the four labelled is phase III, in which the star continues to redden despite reducing in flux. This occurs because of the inside-out nature of disk-loss as described earlier, such that the blue flux produced at smaller radii than red flux is decreasing faster. This reverses in phase IV where the standard flux-colour relationship is resumed.

1.3.2.1 Introducing the neutron star

Interaction between the neutron star and the companion star is an important factor in determining the X-ray activity and optical variability of any particular system. Probably the two most significant affects the neutron star has on the optical emission we see are through the tidal truncation of the disk and the orbitally induced modulation of the flux. I will briefly describe these two effects, starting with the latter.

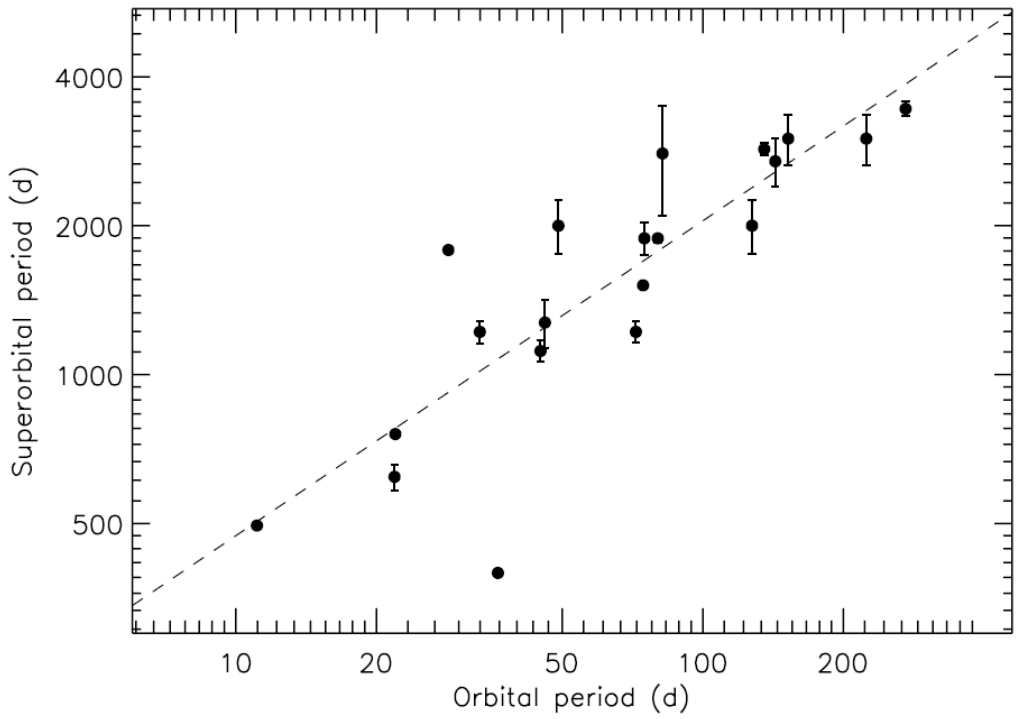

Figure 1.11: The long-term periods seen in the optical light curves of BeXRBs in the SMC are plotted against the binary period of that system. A linear trend between the parameters is noted by a line of best fit plotted over the data. Taken from Rajoelimanana, Charles & Udalski (2010).

Optical monitoring by the Optical Gravitational Lensing Experiment[1] (OGLE) on the 1.3m Warsaw telescope at Las Campanas observatory, Chile, has provided several years of I-band photometry of Magellanic Cloud stars. As such, we can use the variability seen in the OGLE light curves of BeXRBs as a tracer of changes in the structure or size of the circumstellar material. Figure 1.10 presents the OGLE light curve of a 7.8s BeXRB pulsar in the SMC[2]. It shows a periodic brightening of around 0.05 magnitudes every 45 days over a longer aperiodic variation. The long term changes are intrinsic to the Be star and is thought to signify the loss and reformation of the disk as described earlier. The periodic variation is the orbital period of the system and is caused by the neutron star interacting with the disk. This variability is seen in many of the optical light curves of SMC binaries and is extremely useful in determining orbital periods (e.g. Schurch et al. 2011; Schmidtke & Cowley 2006a). As well as finding the orbital signature of a system, it is also useful to

[1]The OGLE experiment and data products will be discussed in detail in section 2.3 as the long-term light curves produced by the survey have been used extensively as an optical monitor of the SMC BeXRB population.

[2]This light curve is part of the OGLE real time monitoring of X-ray variables (XROM) programme. See http://ogle.astrouw.edu.pl/ogle3/xrom/xrom.html and Udalski (2008) for details.

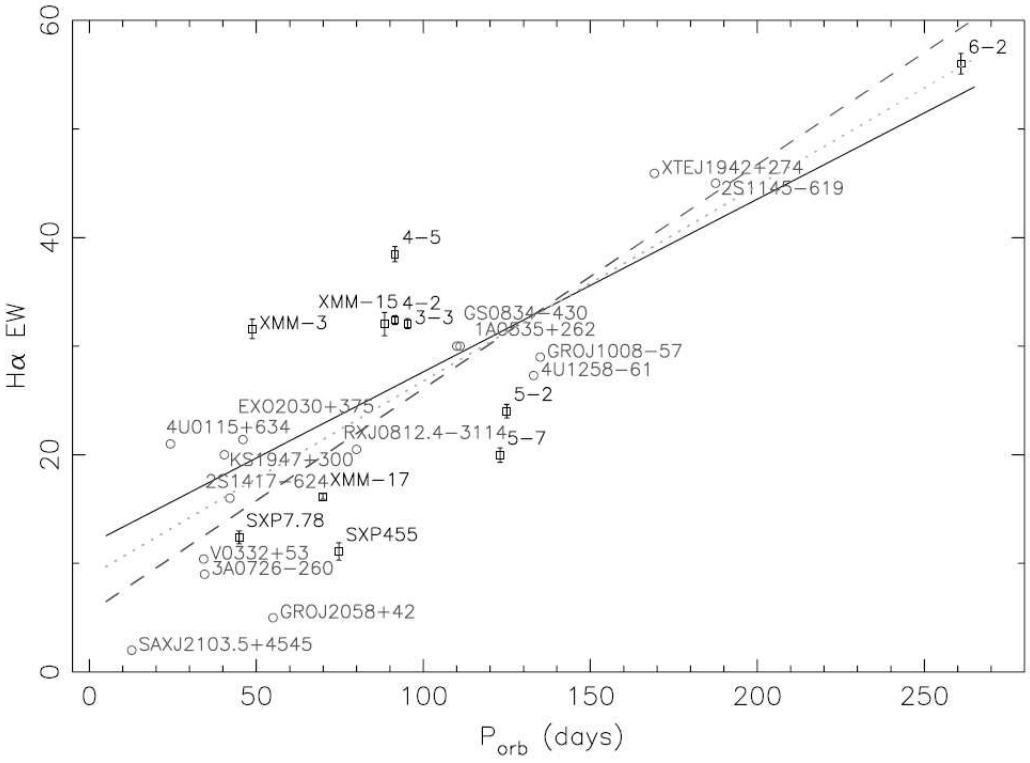

Figure 1.12: Hα equivalent width against orbital period for SMC (squares) and Milky Way (circles) BeXRBs. The solid, dashed and dotted lines represent the best-fit to the SMC, Galactic and total populations respectively. Taken from Antoniou et al. (2009).

compare the longer variations with the X-ray light curve. In Chapter 3, I will show that an X-ray outburst can be predicted in some systems based on the timescale of growth and decay of the circumstellar disk. Moreover, a much more detailed study of these long-term changes in SMC BeXRBs by Rajoelimanana, Charles & Udalski (2010) seems to suggest that there exists an intrinsic link between the decay time of the disk and the binary period of the system[3] (Figure 1.11). Those authors find a correlation between the periods that suggests the disk size can be modulated by the orbital period of the system in addition to the disk-loss episodes driven by the Be star itself. However, this relationship may not be as significant as first thought according to recent findings by Bird et al. (Priv. Comm., 2011). They show that many periods found in the optical light curves of BeXRBs are merely beats of stellar pulsations with the sampling of the light curve. Some periodicities previously assigned as orbital periods in the SMC population have been shown to be non-orbital in nature. If Figure 1.11 is redrawn with these systems removed, the significance of the

[3]Note that whilst the long-term periods are labelled as superorbital periods, they are discussed in terms of changes in the size of the circumstellar disk and does not mean the disks are precessing as may be the more common use of the term.

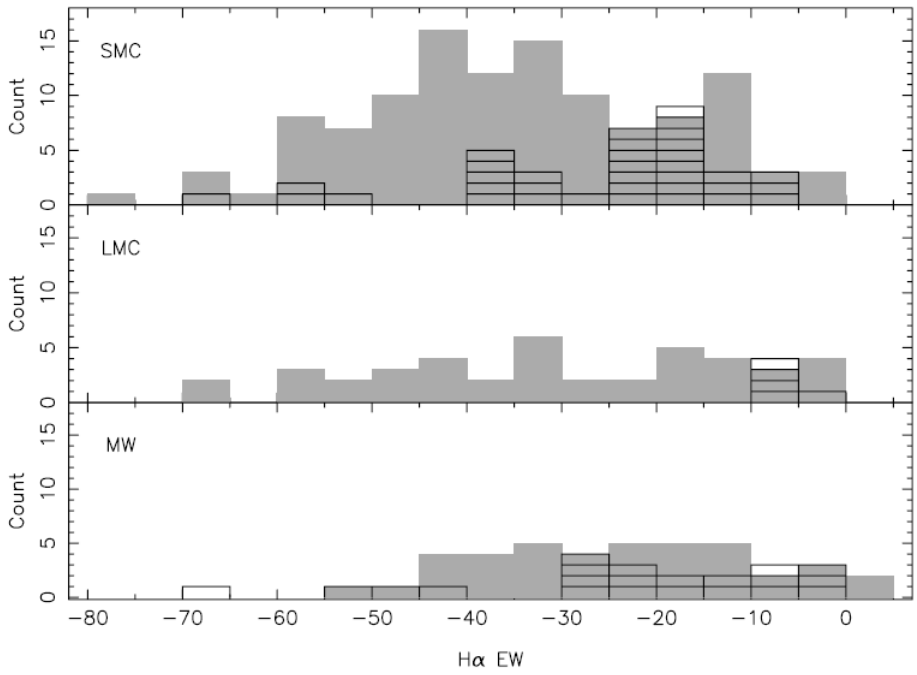

Figure 1.13: Distribution of Hα equivalent widths for BeXRBs (open histograms) and isolated Be stars (solid histograms) for the SMC, LMC and Milky Way. The isolated Be stars are shown to have an average disk size much larger than that of BeXRBs. Taken from Antoniou et al. (2009).

correlation reported by Rajoelimanana, Charles & Udalski (2010) is reduced. Reig, Fabregat & Coe (1997) demonstrated that the observed Hα equivalent width is also correlated with the binary period, a relationship verified by more the recent work of Antoniou et al. (2009). Figure 1.12 shows this relationship for SMC and Galactic systems. It tells us that a neutron star in a shorter orbit, must be more effectively reducing the size of the disk. This is exactly what is shown to happen in current viscous decretion disk models.

Whilst the mechanism for disk formation is not understood, the model that appears to best describe observations is the viscous decretion disk model (Lee, Saio & Osaki, 1991). This is because it is the only model that naturally yields quasi-Keplerian disks around the Be star, which is supported by both theory and observation. The model produces a stable disk from matter that drifts outwards from the stellar surface by viscous torques. These can be thought about in the opposite sense to the torques at work in an accretion disk around the compact object. The reader is referred to Okazaki (2001) for a detailed discussion of the model. When applied to BeXRBs, the model also describes much of the observed behaviour. In particular, work by Negueruela & Okazaki (2001) found that the tidal interaction of the neutron star causes the circumstellar disk to be truncated. This agrees with many

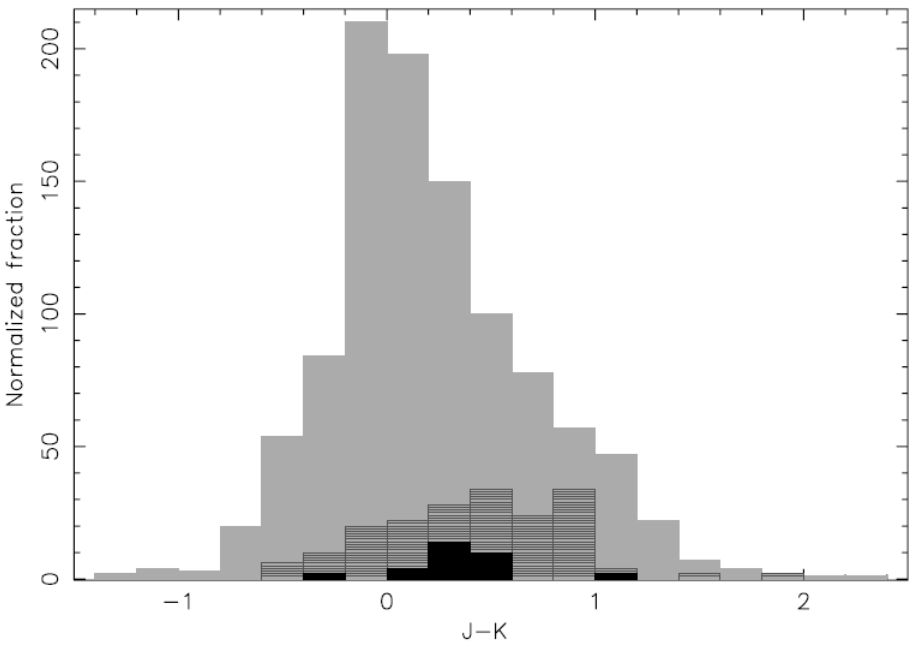

Figure 1.14: Distribution of J–K colour of BeXRBs (black histogram), Be stars (hatched histogram) and B stars (solid grey histogram). Taken from Antoniou et al. (2009).

observables such as the Hα equivalent width – orbital period relationship of Reig, Fabregat & Coe (1997) (see also Figure 1.12) and the distribution of Hα equivalent widths and of NIR colours of BeXRBs compared to that of isolated Be stars (see Figures 1.13 and 1.14). Figure 1.13 shows the Hα equivalent width in isolated Be stars is significantly higher than that of BeXRBs, in line with the disk truncation model. Figure 1.14 shows the obvious difference between the J–K colour of Be and B stars (a clear signature of a disk), but also the difference between the colour of isolated and binary Be stars. The difference is not obvious by eye, but Antoniou et al. (2009) show that the distribution for BeXRBs peaks at ~ 0.3 mags, whereas that of the isolated Be stars peaks at ~ 0.5–0.9 mags. However, it is noted that Antoniou et al. (2009) do not specify whether the sample of isolated B and Be stars are limited to spectral types in a range consistent with those of the BeXRBs, since including systems of differing spectral type could affect the interpretation of this figure. Should the differences be real, this may also represent the tidal truncation of the disk by the neutron star (see, for example, the colour change of A 0535+26 during its disk-loss phase; Coe et al. 2006). Further work on the disk-neutron star relationship by Atsuo Okazaki has shown several things[4]:

[4]Noted as part of various discussion sessions at the 2011 BeXRB conference in Valencia, Spain unless a specific reference is given.

- The truncation efficiency increases for decreasing eccentricity, though the disk is smaller for larger eccentricities when the neutron star is at periastron. Low eccentricity systems truncate the disk well within the critical lobe radius, whereas high eccentricity systems truncate the disk much closer to the critical lobe radius. As such, the more circular BeXRBs tend not to be able to accrete from the disk and only show Type II outbursts. High eccentricity systems can accrete from the disk and display regular Type I outbursts (Okazaki & Negueruela, 2001).

- Truncation can only occur at low misalignment angles between the disk and orbital plane. Above ~ 30 degrees truncation starts becoming less efficient. This means systems with a significant misalignment between orbit and disk may be prone to outburst more often or to more luminous outbursts.

- One of the 2 arms of the 2-armed density wave that is produced in the disk by the tidal interaction with the neutron star connects with the accretion disk for some phase of the orbit around periastron.

- Tidal truncation doesn't stop the intrinsic mass-loss within the Be star. This means that matter can be lost from the photosphere into the disk whilst it remains at the same tidally locked radius. The disk gets denser and is then more likely to snap into a large mass ejection, resulting in a Type II outburst.

Some data in support of this idea that shorter orbit systems are more likely to Type II outburst and less likely to Type I outburst (and vice-versa) will be presented in Chapter 5 and discussed further in Chapter 7.

1.4 Accretion and emission mechanisms

The transfer of matter in a binary system is not only a key stage in its evolution, but also drives the X-ray activity we see. To fully understand the accretion process in X-ray binaries is almost impossible as the accreting plasma will undoubtedly suffer from thermal and magnetic instabilities that are hard to quantify. The following is a simplistic account of the important regions within the accretion flow, assuming spherical accretion initially through the L_1 Lagrangian point that does not suffer from plasma instabilities. After passing through L_1, the material will form an accretion disk at the radius at which the initial angular momentum carried by it is equal to the angular momentum of material in a Keplerian orbit at that radius. Viscosity

within the disk will redistribute angular momentum and energy allowing material to progress inwards towards the neutron star. At some point between the disk outer-edge and the surface of the neutron star, matter will cease to follow the keplerian orbit of the disk and begin funnelling down the magnetic field lines of the neutron star. The radius at which this occurs depends on the strength of the magnetic field and is called the magnetospheric or Alfvén radius, defined as the radius at which the magnetic pressure balances the thermal and ram pressure of the accreting matter (e.g. Lamb, Pethick & Pines 1973). This is presented in terms of the observable X-ray luminosity by Shtykovskiy & Gilfanov (2005b)

$$R_m = 1.4 \times 10^9 R_6^{10/7} M_{1.4}^{1/7} B_{12}^{4/7} L_{35}^{-2/7} \,\mathrm{cm} \tag{1.1}$$

where R_6 is the radius of the neutron star in units of 10^6 cm, $M_{1.4}$ is its mass divided by $1.4\,\mathrm{M}_\odot$, B_{12} is the magnetic field strength at the surface of the neutron star in units of 10^{12} Gauss and L_{35} is the X-ray luminosity in units of 10^{35} ergs s^{-1}. The luminosity was introduced assuming it is related to the mass accretion rate via $L_\mathrm{x} = GM_\mathrm{ns}\dot{M}/R_\mathrm{ns}$. In practice however, the accretion flow is not spherical and the material may not be captured by the neutron star through Roche-lobe overflow. Frank, King & Raine (2002) show that the magnetospheric radius for disk accretion is usually of the order half that of the spherical magnetospheric radius. Moreover, those authors show that amount of deviation from spherical accretion (i.e. the fraction of the neutron star surface that actually accretes) is a function of the ratio of neutron star radius and magnetospheric radius. This means that a stronger magnetic field, which would truncate the Keplerian disk at a larger radius, would cause the fraction of the neutron star surface that accretes to reduce.

Another factor that will affect the accretion in an X-ray binary is the spin period of the neutron star, which in turn is changed by the act of accretion. The corotation radius is defined as the radius at which a particle attached to a magnetic field line would rotate at the Keplerian rate (e.g. Frank, King & Raine 2002)

$$R_\Omega = \left(\frac{GMP_\mathrm{spin}^2}{4\pi^2}\right)^{1/3} = 1.5 \times 10^8 P_\mathrm{spin}^{2/3} M_1^{1/3} \,\mathrm{cm} \tag{1.2}$$

where P_spin is the spin period of the neutron star in seconds and M_1 is its mass in solar masses. In the case of $R_\Omega > R_\mathrm{m}$, straightforward disk accretion can proceed as

discussed above. During phases of accretion, the pulse period of the pulsar is often seen to decrease, suggesting that angular momentum is being transferred from the accreting material to the neutron star. This is known as *spin-up*. This phenomenon can be seen on both long-term (several years) and short-term (several days) time scales (e.g. SXP46.6, SXP144; Galache et al. 2008). Long-term changes in spin period are a complex mixture of spin-up from periods of accretion and spin-down caused either by accretion coming to a halt or by a change in the internal structure of the neutron star. Short term changes are most apparent under larger accretion rates and hence, high rates of angular momentum transfer. The case of $R_\Omega < R_\mathrm{m}$ signifies the neutron star is rapidly rotating. This can occur either when the neutron star is born from a supernova or if it accretes enough angular momentum that it becomes substantially spun up. In this situation, matter can no longer be accreted down the magnetic field lines as the outward force from the rotation of the neutron star is greater than the ram pressure of the plasma. The plasma is expelled from the system. This is known as the *propeller effect*. Whilst accretion is inhibited, the neutron star will spin-down under magnetic braking torques. This acts to bring the spin of the neutron star into a quasi-equilibrium with the disk rotation ($R_\Omega \sim R_\mathrm{m}$). The spin period at which this happens can be calculated from equations 1.1 and 1.2. If L_{35} in equation 1.1 is changed to L_{37} (the standard luminosity of an X-ray outburst from a BeXRB being 1×10^{37} erg s^{-1}) and $M_{1.4}$ changed to M_1 to conform with equation 1.2, the equilibrium spin period is approximated by

$$P_{eq} \sim 2R_6^{15/7} M_1^{-2/7} B_{12}^{6/7} L_{37}^{-3/7} \,\mathrm{s} \tag{1.3}$$

from which it can be inferred that either very few of the known X-ray pulsars can be near their equilibrium periods (e.g. Frank, King & Raine 2002), or the standard values indicated in equation 1.3 are deviated from significantly in many systems, such that their equilibrium periods are much longer than a few seconds. The latter seems most likely as it is a natural explanation for the relationship between the spin and orbital periods of BeXRBs as discussed previously.

It is not only the surface accretion and propeller regimes that are important to understand. King & Cominsky (1994) and Campana et al. (1995) point out that energy can also be released from accretion onto the magnetosphere. This type of accretion is expected to be observed during the propeller regime, when the accretion flow is unable to penetrate the magnetospheric boundary. Whilst much of the material may be propelled from the system, gravitational energy may be released from matter ro-

tating at the magnetospheric boundary. The theory of such accretion is summarised by Corbet (1996) and the X-ray luminosity produced is given by $L_{\rm x} = GM_{\rm ns}\dot{M}/R_{\rm m}$. Whilst at the equilibrium period where $R_\Omega \sim R_{\rm m}$, a small increase in the accretion rate will allow material to penetrate the magnetospheric boundary and accretion to begin onto the neutron star surface. The opposite is also true for a small decrease in the accretion rate (i.e. accretion onto the neutron star surface can stop with the onset of the propeller regime). The difference in the observed luminosity and spectral characteristics of these two accretion modes is marked. The former is observed as a significant jump (or drop), referred to as the luminosity gap. This is described in terms of the ratio between the minimum luminosity produced from neutron star accretion and the maximum luminosity produced from magnetospheric accretion. The latter occurs at $R_{\rm m} = R_\Omega$. The luminosity gap is thus

$$\Gamma = \frac{L_{\rm ns,min}}{L_{\rm mag,max}} = \frac{GM_{ns}\dot{M}/R_{ns}}{GM_{ns}\dot{M}/R_\Omega} \tag{1.4}$$

which from equation 1.2 becomes

$$\Gamma = (GM_{\rm ns})^{1/3}(P_{\rm spin}/2\pi)^{2/3}R_{ns}^{-1} \tag{1.5}$$

$$= (G\rho_{\rm ns}/3\pi)^{1/3}(P_{\rm spin})^{2/3} \tag{1.6}$$

where $\rho_{\rm ns}$ is the density of the neutron star. Thus, the size of the luminosity gap is dependent only of the spin period and density of the neutron star. The magnetic field strength will affect the actual luminosity seen in each regime, but will not change the difference between them. To give the reader a reference frame for the size of typical luminosity gaps, a 2 s, 40 s and 100 s pulsar will have a gap of ~ 270, ~ 1950 and ~ 3600 respectively. This illustrates the necessity of having either a small spin period or large luminosity (magnetic field) when trying to observe the transition between accretion regimes. So far there has been no conclusive evidence for such a luminosity gap in a BeXRB, though several authors claim to have observed accretion onto the magnetospheric boundary (e.g. Corbet 1997; Campana et al. 2002; Doroshenko, Santangelo & Suleimanov 2011).

Finally I will consider the properties of the accretion flow close to the polar caps of the neutron star. In the 'slow rotator' regime described above in which a neutron star will accrete freely, the accretion rate is limited purely by the amount of material available. Figure 1.15 shows the accretion column geometry near the surface of the

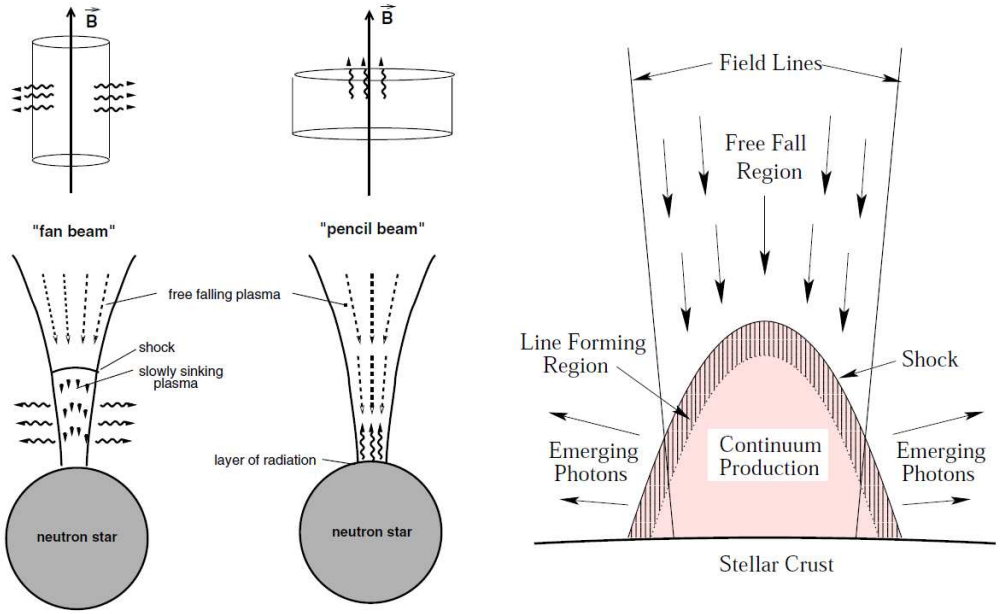

Figure 1.15: Left: accretion column geometries (taken from Schönherr et al. 2007). Right: blow up of the column near the neutron star surface (taken from Heindl et al. 2004). Fan beam scenario: at very high accretion rates a shock front is formed and the up-scattered photons are forced out from the accretion column perpendicular to the magnetic field. Pencil beam scenario: at low accretion rates no shock front is formed and the high energy photons escape in a narrow 'pencil' beam along the accretion column. The schematic shows the thermal mound on the surface of the neutron star and identifies the line forming region and continuum production zone.

neutron star and where the X-ray continuum and line features that we observe are produced. The left-hand side of the figure shows the two extreme cases of the type of emission we see. In the high $\dot{M}$ regime, a collisionless shock front is formed above the accretion mound which forces the photons that are up-scattered to very high energies at the neutron star surface out the sides of the accretion column. This is known as 'fan beam' emission. At low $\dot{M}$, no such shock front is formed and the plasma can free-fall directly onto the polar cap of the neutron star. The radiation produced is emitted back up the accretion column in a narrow beam. This is known as 'pencil beam' emission. These two types of emission can be observationally distinguished by features in the folded X-ray light curves (e.g. Blum & Kraus 2000). The right-hand side of Figure 1.15 shows the line and continuum forming regions near the neutron star surface. The X-rays are produced via inverse comptonisation of soft seed photons with relativistic electrons in the infalling plasma within the 'accretion mound'. This consists of the continuum producing zone above which photons must propagate through the line forming region which is characterised by a

magnetic field strength, an electron temperature and an optical depth. Schönherr et al. (2007) present a concise quantum mechanical treatment of the electron motion within the plasma and use this to show that absorption within the line forming region produces absorption features in the photon energy spectrum at quantised energies. We observe these features as cyclotron lines and their harmonics, from which we can infer properties of the accretion column and magnetic field of the neutron star. Going beyond the fan beam scenario described above, an even higher $\dot{M}$ could halt the accretion process all together. If we, again, assume spherically symmetric accretion, the radiation emitted from the compact object will exert a force on the ionised plasma being accreted. If you also assume the plasma is made up of fully ionised hydrogen, the radiation exerts a force mainly on the electrons in the plasma through Thompson scattering, due to the electron having a much larger scattering cross-section than a proton. As the radiation pushes electrons out, the electrostatic attraction between electrons and protons in the plasma causes the electrons to pull out protons with them. At the point of equilibrium, in which matter is neither accreted nor expelled, the radiative force acting against the gravitational force of the plasma are equal. This scenario causes accretion to halt and is known as the Eddington limit. The corresponding luminosity at which this occurs is the Eddington luminosity given by

$$L_{Edd} = 4\pi GMm_p c/\sigma_T \tag{1.7}$$

$$\simeq 1.3\times10^{38}(M/M_\odot)\,\mathrm{ergs\,s^{-1}} \tag{1.8}$$

where G is the gravitational constant, M is the mass of the compact object, m_p is the proton mass, c is the speed of light and σ_T is the Thompson cross-section (Frank, King & Raine, 2002). So for a $1.4\,M_\odot$ neutron star, the Eddington luminosity is approximately $2\times10^{38}\,\mathrm{ergs\,s^{-1}}$.

The photons that result from this accretion process hold the information we need to derive the physical properties of any particular system. Photons produced in this way have a wide range of energies. Their X-ray spectra are generally well characterised by a power-law in the soft (2–15 keV) X-ray regime. Some systems require the addition of a thermal component at lower energies (e.g. McCray et al. 1982) or a high-energy break in the power law (e.g. White, Swank & Holt 1983) to be well modelled. The thermal component likely originates as thermal blackbody emission from the neutron star or some other thermal emission from the magnetosphere, or from reprocessed X-rays near the surface of the neutron star. The

power law emission is likely generated by Compton up-scattering from an accretion disk or synchrotron emission from close to the polar regions. A break in the energy spectrum, if needed, would most likely indicate a separate electron population or that the energy distribution of the electron population does not follow a power-law model at higher energies. This simple idea of the emission regions in an X-ray binary will be used when fitting energy spectra in later chapters.

1.5 Thesis overview

In this chapter, I have presented an overview of the X-ray binary family. In particular, I have described the optical and X-ray properties of the BeXRB sub-class and the relevant accretion and emission characteristics that are used throughout this thesis. Chapter 2 gives an introduction to the Magellanic Clouds, providing the relevant history, structure and observations to put the work presented into context. I include an overview of the ongoing *RXTE* programme to monitor BeXRB activity in the Small Magellanic Cloud (Galache et al., 2008), as data from this programme form a major part of the work presented. In Chapter 3 I present X-ray observations of the second largest outburst seen from a BeXRB in the SMC and subsequent optical and NIR follow-up observations. In Chapter 4 I present X-ray and optical observations of a newly discovered pulsar in the SMC. These data allowed for the spectral classification of the counterpart and the calculation of the orbital parameters of the system. Chapter 5 furthers the orbital analysis work introduced in Chapter 4 by looking at outbursts from four other systems in the SMC. I discuss the derived parameters for each system before comparing the results with what is known from systems in the Milky Way and exploring the spin period, orbital period and eccentricity parameter space. In Chapter 6 I describe the results of a newly implemented method to locate pulsars discovered with *RXTE*. This resulted in the discovery and localisation of one new pulsar and the association of a suspected new pulsar with an already known system. The latter informed that this particular pulsar seemed to show very high spin-up of the neutron star during apparent phases of negligible accretion. I conclude with a discussion of the possible implication of this observation. I conclude this thesis with a summary of key scientific results and future work in Chapter 7.

Common sense is the collection of prejudices acquired by age eighteen.

ALBERT EINSTEIN (1879 - 1955)

2

The Magellanic Clouds and *RXTE* long-term monitoring programme

For hundreds of years, two fuzzy blobs in the Southern sky have provided people with their first look into a world beyond our own galaxy. The Magellanic Clouds were named after Ferdinand Magellan whose expedition led to one of the first European documentations of the Clouds. Both the Large and Small Magellanic Clouds (LMC, SMC) are dwarf irregular galaxies that resemble tidally disrupted barred spirals. In fact, the tidal interaction between both Clouds and between the Clouds and the Milky Way has caused huge streams of material to stretch across much of the sky. In this chapter, I will discuss the structure, history and observations of the Magellanic system and will describe the ongoing programme to monitor the SMC; the data from which has made much of the following work possible.

2.1 The Magellanic system

The Magellanic Clouds lie within the dark matter halo of the Milky Way at a distance of around 60 kpc. Their proximity to each other and to the Milky Way causes tidal disruption and stripping of gas from the galaxies. This has the greatest effect

Figure 2.1: Photograph of the Magellanic Clouds (left), Milky Way (centre) and the VLT Unit Telescope 1 (right). Image credit ESO/Y. Beletsky.

on the less massive SMC which has experienced substantial star formation and has had much of its gas stripped from the bar region by the LMC. This material connects the two galaxies and is known as the Magellanic Bridge. Figures 2.1 and 2.2 demonstrate the proximity of the galaxies and the scale of the Magellanic system on the sky. Figure 2.2 also shows the different regions of the Magellanic system in HI column density. The HI, or 21 cm, emission line is one of the most prominent in the radio regime. This line arises from a forbidden hyperfine spin-flip transition of the electron in neutral hydrogen, resulting in the release of a photon at 21cm, or 1.4 GHz, from which maps such as that in Figure 2.2 can be produced. The hydrogen gas content of a galaxy is often used as a representation of its physical extent and structure. Neutral hydrogen maps can also be used as locators of star formation regions, as massive, young stars are likely to form in such regions of dense gas. Evidence of this can also be seen by plotting a galaxy's HMXB population onto its HI map (see section 2.1.2). The LMC, SMC and Bridge represent most of the material in the Magellanic system and span several degrees on the sky. Even this large structure is dwarfed by the plume of material extending out from the Clouds known as the Magellanic Stream. Recent observations at the Green Bank Telescope estimate the angular size of the Magellanic system to be $\sim 200^\circ$ (Nidever et al., 2010), a 20° increase on previous measurements. Critically, this increases the estimated age of the Stream to ~ 2.5 Gyr, which coincides with a burst of star formation in the SMC (Harris & Zaritsky, 2004). A close approach between the LMC and SMC is thus the favoured scenario to explain the existence of the Stream.

Recent proper motion measurements of the Clouds using the Advanced Camera for Surveys (ACS) aboard the *Hubble Space Telescope (HST)* by Kallivayalil et al.

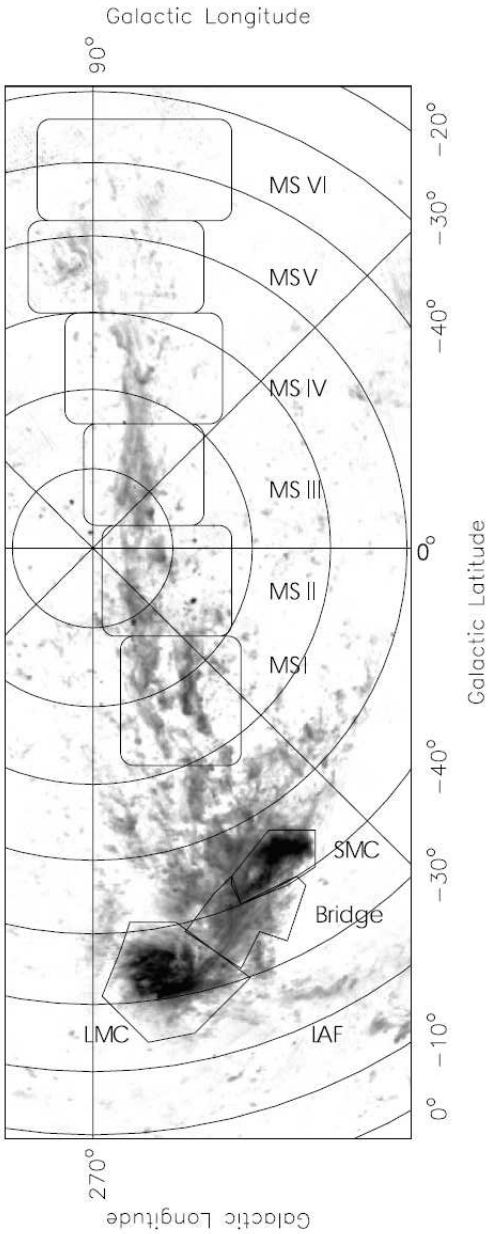

Figure 2.2: HI column density map of the Magellanic system. The LMC, SMC and Bridge are labelled, as is the Magellanic Stream (MS) and start of the Leading Arm Feature (LAF). The entire system stretches nearly 180° across the sky. Taken from Putman et al. (2003).

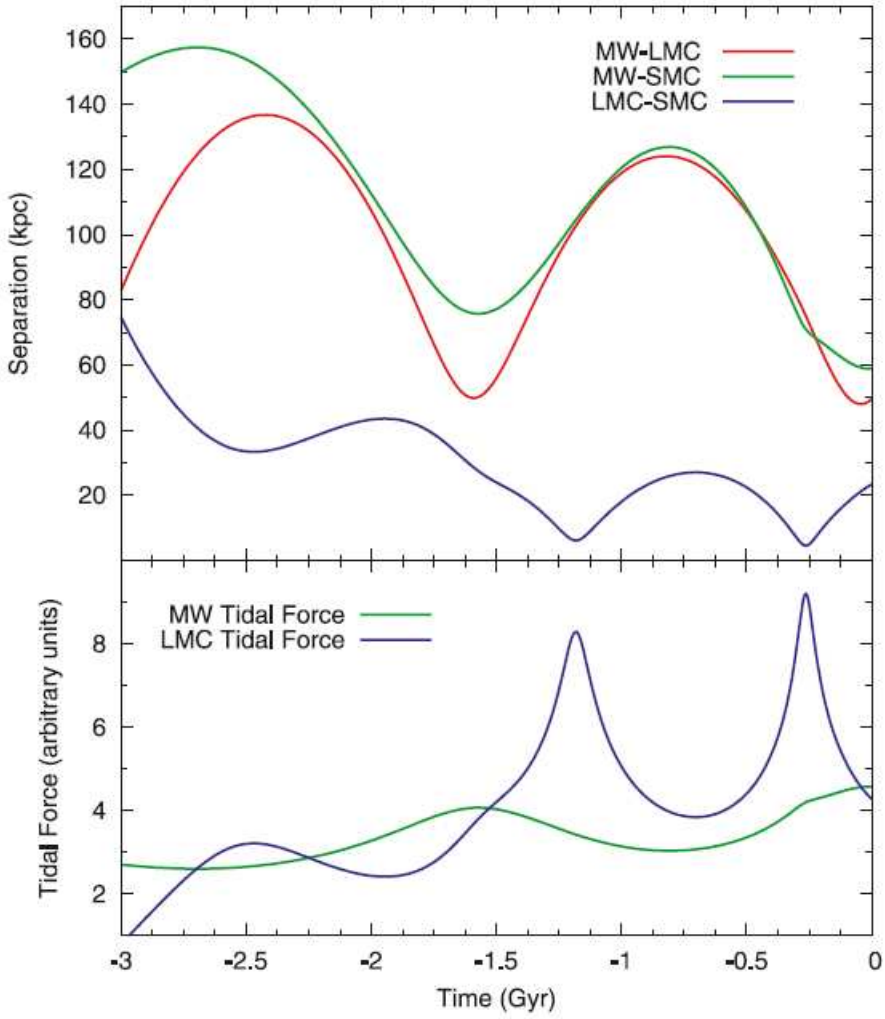

Figure 2.3: *Top:* The separation history of the SMC, LMC and MW from each other. *Bottom:* The tidal force exerted by the Galaxy and LMC on the SMC as a function of time. The spikes at 1.6 Gyr and 0.25 Gyr are thought to have formed the Magellanic Stream and Bridge respectively. Taken from Diaz & Bekki (2011).

(2006) and Kallivayalil, van der Marel & Alcock (2006) suggest that their estimated three-dimensional galactocentric velocities are as much as 100 km s^{-1} higher than previously estimated values (Gardiner & Noguchi, 1996). Besla et al. (2007) use these velocities to re-examine the orbital history of the Clouds about the Milky Way. Their main conclusion is that the LMC and SMC are either currently on their first passage about the MW or that their orbital period and apogalacticon distance must be a factor of 2 larger than previously estimated, increasing to 3 Gyr and 200 kpc, respectively. This cast a major doubt over the previously accepted scenario put forward by Gardiner & Noguchi (1996) that the Clouds had completed many orbits of the MW during a Hubble time. However, Diaz & Bekki (2011) present

Table 2.1: HMXB populations in the Galaxy and Magellanic Clouds.

Population	Number of HMXBs	Number of pulsars
SMC	92[1]	65
LMC	36[1]	10
Bridge[2]	3	1
Milky Way[3]	114	66

[1]Liu, van Paradijs & van den Heuvel (2005), [2]McBride et al. (2010), [3]Liu, van Paradijs & van den Heuvel (2006).

a numerical model that is based upon the traditional tidal model (e.g. Gardiner & Noguchi 1996) but with the important inclusion of the proper motion measurements. Those authors show that it is in fact possible to reproduce the result of a tidally bound Magellanic-MW system with the newly measured velocities, though they admit the model is somewhat idealised at the present time. Figure 2.3 shows some of the results of their simulations. The top panel shows the Magellanic system bound to the MW and having an orbit of around 1.6 Gyr. It also shows the SMC and LMC have been in separate orbits around the Galaxy and have only recently become tidally locked themselves. This has never been suggested in earlier work. It does, however, reproduce the HI structures in the system. The two close passages of the SMC and LMC at around 1.6 and 0.25 Gyr are predicted to have formed the Stream and Leading Arm and the Bridge respectively, though this age is now at odds with that calculated by (Nidever et al., 2010). More modelling seems to be necessary in order to fully understand the dynamical history of the Magellanic system.

2.1.1 The X-ray binary population

The Galactic population of HMXBs includes all of the different types described in the previous chapter. This is markedly different to the population in the SMC, which includes only BeXRBs and one SGXB, all of which have a neutron star accretor. The number of HMXBs in the SMC is also at odds with what we know from the Galaxy. A simple mass comparison suggests there should be only one or two such systems, and yet there are over 60 now known (Coe et al., 2008; Corbet et al., 2008) and many more good candidates. Population synthesis models by Dray (2006) predict the low metallicity environment in the SMC could increase the number of HMXBs by a factor of 3. However, this is still not sufficient to explain the SMC population on its own. A recent episode of star formation, possibly due

to an increase in the tidal force exerted on the SMC by a close approach with the LMC, is the current favoured scenario to explain the number of XRBs seen. This close approach has not been disputed in the wake of the new Hubble proper motion measurements. Recent work by McBride et al. (2010) shows that such tidal interaction seems to be inducing binary formation in the Bridge itself, as well as the SMC. Those authors show a population of at least 3 confirmed and 3 candidate HMXBs that must have formed *in situ* rather than being expelled from the SMC. This number has recently increased to 5 candidates with the detection of two more hard X-ray transients in an *INTEGRAL* observation of the SMC (Drave, 2011, Priv. Comm.). Table 6.1 summarises the population of HMXBs in the Galaxy and Magellanic system. The data in Liu, van Paradijs & van den Heuvel (2005) and Liu, van Paradijs & van den Heuvel (2006) are outdated, but are still the most recent published catalogues of HMXBs. It is certain that the number of HMXBs in the LMC, SMC and Milky Way and the number of pulsars in the Milky Way have substantially increased from these figures in the past five years, though precise cataloguing of these systems has not been carried out in this work. The Bridge population is as described in McBride et al. (2010). The number of pulsars in the LMC and SMC are correct at the time of writing.

2.1.2 HMXBs in the SMC

The SMC provides an excellent laboratory to study both the fundamental physics of individual HMXB systems and the global properties of a substantial population formed at the same time and at a well defined distance (60 kpc; Harries, Hilditch & Howarth 2003)[1] and absorption column ($6 \times 10^{20}\,\mathrm{cm}^{-2}$; Dickey & Lockman 1990). The latter can give an insight into the star-forming history of the galaxy and improve our understanding of how differences in the local environment (e.g. metallicity) affects the formation and evolution of the binary system. The former allows us to observe the interaction between a compact object and a massive star and how the compact object behaves under varying levels of accretion. In turn, this can provide information about the fundamental properties of the compact object such as the neutron star equation of state or black hole masses. The metallicity difference between the SMC and Galaxy ($\sim$ a factor of 5; Russell & Dopita 1992) is of particular rele-

[1] This is the most widely accepted distance estimate to the SMC. A more recent study of eclipsing binary systems in the SMC by North et al. (2010) yields a distance of 66.4 ± 0.9 kpc and a $2\,\sigma$ line-of-sight depth of 7.6 kpc. This means an estimate of a source luminosity, for example, could carry up to a 20% error. Despite this, the HMXB population in the SMC is still much more homogeneous than that of the Milky Way.

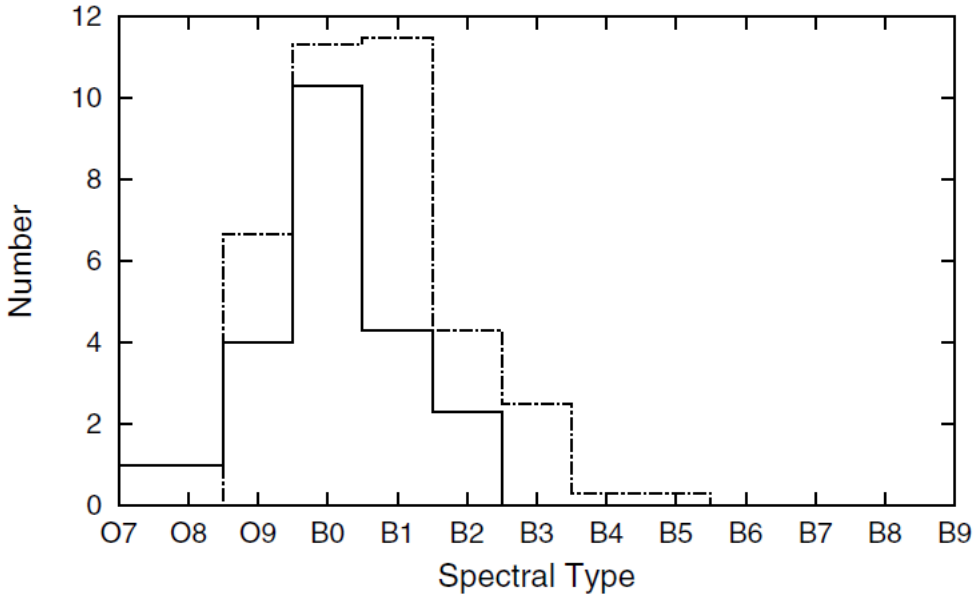

Figure 2.4: The spectral distribution of BeXRBs in the SMC (dot-dashed) and in the Galaxy (solid). Taken from McBride et al. (2008).

vance throughout this work as it has substantial influence in the evolution of massive stars. The line-driven stellar winds in massive stars are weaker in low metallicity environments (e.g. Kudritzki, Pauldrach & Puls 1987), resulting in lower mass and angular momentum losses from the binary systems in which they reside. This could result in compact object masses different to those seen in the Galaxy and could even affect the evolutionary path of the binary system. The latter may manifest itself as differences in observable parameters of the population, such as spectral distribution, the distribution of orbital sizes and eccentricities or the distribution of mass functions. This is investigated in Chapter 5. McBride et al. (2008) show that, despite the low metallicity in the SMC, the distribution of spectral types of the optical counterparts to Be/X-ray binaries (BeXRB) is consistent with that of Galactic systems (Figure 2.4).

At the time of writing, there are 65 confirmed pulsars in the SMC (see Table 6.1). These are presented in Figure 2.5 as numbers plotted over a radio image of the HI distribution in the SMC, where the numbers represent the spin period of the neutron star. The larger circles represent *RXTE* pointed observations and will be discussed in the following section. The majority of systems lie in the SMC bar whilst only a few occupy the Wing. This is not an observational bias, but evidence that the BeXRBs trace regions of high gas and dust content. Antoniou et al. (2010) investigate this in detail by probing the rate of formation of HMXBs in the SMC in terms of the star formation rate (SFR) in their local environment. Figure 2.6 shows various represen-

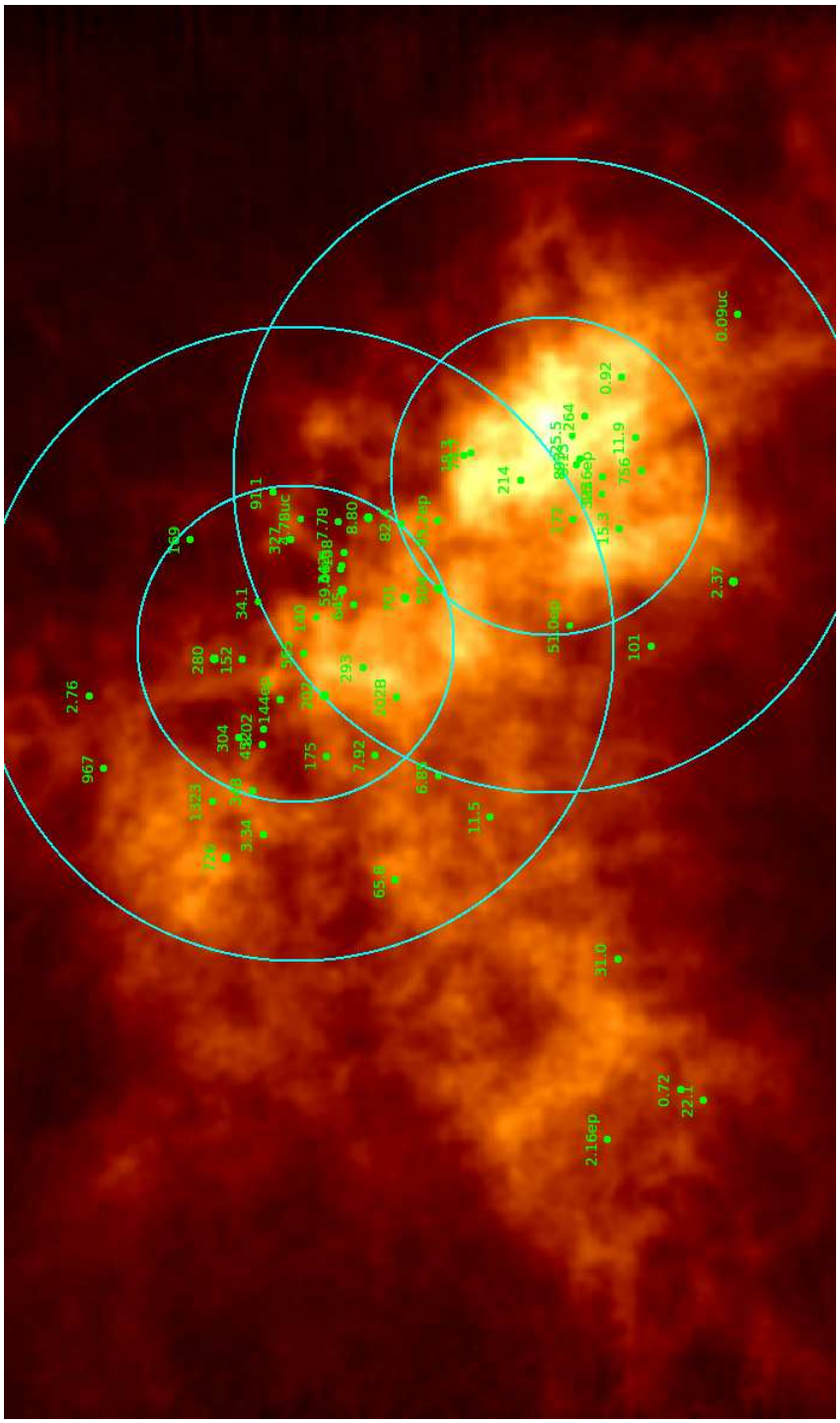

Figure 2.5: HI map of the SMC with the current pulsar population and *RXTE* pointing positions overlaid. The numbers represent the spin period of each system. Pulsars with unknown position have 'ep' following their spin period. The large and small circles denote the 2 degree full field of view and the 1 degree half response field of view of *RXTE* (a circle is an approximation to the actual collimator response which is close to hexagonal).

tations of the star formation history (SFH) of different regions in the SMC. The SFH was derived from the average of the SFHs of individual Magellanic Clouds Photometric Survey (MCPS; Zaritsky, Harris & Thompson 1997) observations that fell within particular regions defined by Antoniou et al. (2010). The individual SFHs were calculated by Harris & Zaritsky (2004) using the MCPS data to map the SFH of the entire SMC at various epochs. Antoniou et al. (2010) used this information to calculate the SFH of regions within various X-ray surveys both with and without a detected XRB to see if local star-formation mapped the current population of HMXBs. The top-left plot in Figure 2.6 is based on the MCPS regions within 5 *Chandra* and 4 *XMM-Newton* observations of the SMC bar described in Antoniou et al. (2010). Two SFHs were calculated: one from the MCPS regions that host one or more BeXRB detected by either X-ray telescope (black squares) and one from those regions with no detected BeXRBs (grey stars). Similar calculations were performed based on whether or not those same MCPS regions hosted *any* known pulsar or not, regardless of detection in their X-ray observations (bottom-left). Both of these plots show a strong SFR at ~ 42 Myr in regions where BeXRBs are known and a minimal SFR at this age for regions without BeXRBs. This demonstrates an obvious difference between the fields with and without BeXRBs and suggests a clear connection between an episode of star-formation and the observed BeXRBs. This age is also consistent with the peak in the age distribution of HMXBs in the SMC bar that occurs ~ 20–50 Myr after a star-formation event (Shtykovskiy & Gilfanov, 2007) and lies at the peak of the age distribution at which Be stars are thought to develop their circumstellar disks (McSwain & Gies, 2005). This all leads to the conclusion that this particularly strong SF episode at ~ 42 Myr formed the population of BeXRBs we see in the SMC today. Antoniou et al. (2010) also note weaker peaks in the SFH at ~ 11 Myr and ~ 422 Myr. The latter cannot have contributed to the HMXB population as all OB stars would have ended theirs lives by this time. The former is too early to produce BeXRB pulsars, but could form a population of black hole binaries due to the faster evolution of a more massive companion. The plot in the top-right of Figure 2.6 shows the same analysis as above, but based on the *Chandra* survey of the SMC Wing (P.I. M.Coe; McGowan et al. 2008b). A peak is seen for regions hosting a BeXRB at ~ 42 Myr, although this is somewhat weaker than in the Bar. There is no peak at this age for regions without a known BeXRB, but these data do show a substantial burst at ~ 11 Myr. These results suggest that the Wing should be deficient in BeXRBs in comparison to the Bar (this is indeed the case) and that SG or black hole systems should dominate the population of massive binaries in the Wing, due to their shorter evolutionary timescale.

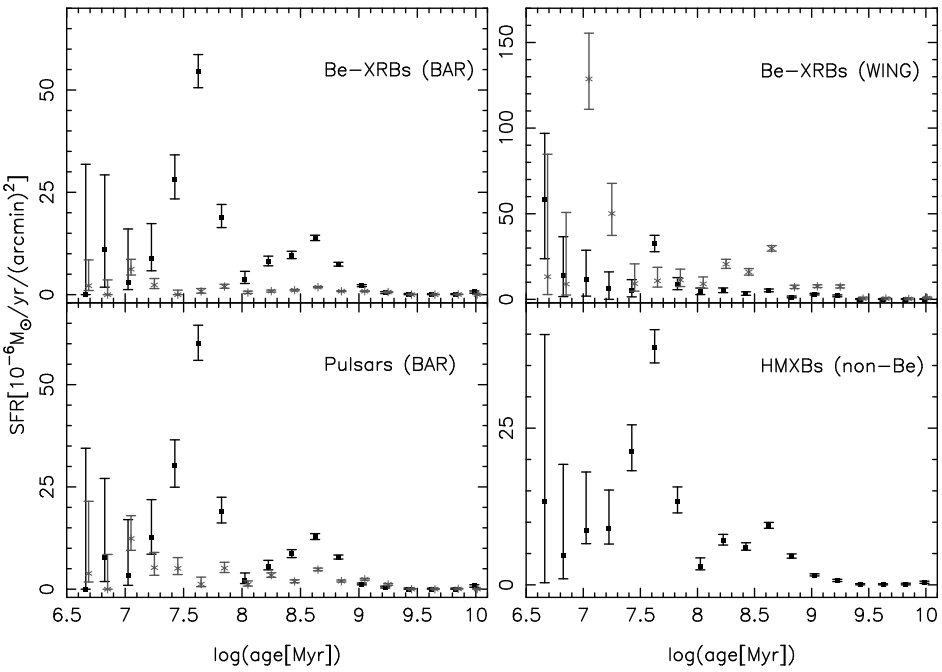

Figure 2.6: *Top-left:* average SFH of the MCPS regions (Zaritsky, Harris & Thompson, 1997) that fall within the *Chandra* or *XMM-Newton* pointing positions of the SMC bar described by Antoniou et al. (2010) that host one or more BeXRB (black) and no BeXRBs (grey) detected in those X-ray observations. *Bottom-left:* SFH of any MCPS region within one of those X-ray pointings in which any known X-ray pulsar resides (black) and does not reside (grey). *Top-right:* SFH of the MCPS regions falling in the pointings of the *Chandra* Wing survey (P.I. M.Coe; McGowan et al. 2008b) in which a BeXRB was (black) and was not (grey) detected in that survey. *Bottom-right:* SFH of MCPS regions that hold one or more candidate (i.e. non-spectroscopically confirmed) BeXRBs from Liu, van Paradijs & van den Heuvel (2005). Taken from Antoniou et al. (2010).

2.2 The SMC monitoring programme with *RXTE*

The *Rossi X-ray Timing Explorer (RXTE)* was launched on December 30, 1995 and is still operational at the time of writing. It is in a low-earth orbit with a period of $\sim$93 minutes. The three science instruments are: The Proportional Counter Array (PCA), the High Energy X-ray Timing Experiment (HEXTE) and the All Sky Monitor (ASM). A schematic of *RXTE* with these instruments labelled is shown in Figure 2.7. The key features of *RXTE* include:

- a broad spectral range of 2–250 keV
- an all-sky monitor
- separate soft and hard X-ray detectors

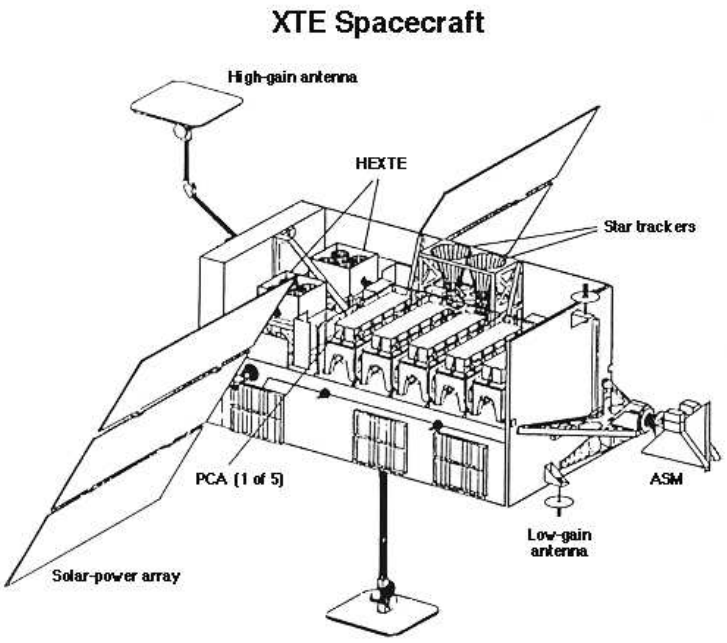

Figure 2.7: Schematic of *RXTE* (credit http://heasarc.nasa.gov/). The PCA, HEXTE and the ASM make up the three science instruments (see text for details).

- very high time resolution of 1 μs at low energies
- very large collecting area on pointed detectors

In the following section, I will give a brief overview of the PCA instrument and discuss the data obtained with this instrument that form the basis of this work. I will not present any data from the HEXTE or ASM detectors so will not discuss them further. For more details on these instruments see Bradt, Rothschild & Swank (1993).

2.2.1 The Proportional Counter Array

The PCA consists of 5 identical proportional counter units (PCUs) placed side by side (see Figure 2.7). For the purposes of this discussion, these will be labelled 0–4. Each PCU has a layer of propane gas on top of xenon/methane detectors acting as a veto for particle background below 2 keV. The xenon/methane detector is further divided into 3 layers, each of which is divided into halves. These 6 xenon compartments provide the means to discriminate between good and bad events. The Event Analysers (EA) on board the spacecraft will record a 'good event' (an X-ray) if only one of the 6 xenon detectors is triggered. The EAs can be told to analyse the incoming events in various different modes. These are chosen by the observer, though 2 EAs are always reserved for the standard modes that are unchanged since

Table 2.2: PCA instrumental properties

Energy range	2–60 keV
Energy resolution	$<18\%$ at 6 keV
Time resolution	1μs
Spatial resolution	collimator with 1° FWHM, 2° FWZI
Detectors	5 proportional counters
Collecting area	6500 cm^2
Sensitivity	0.1 mCrab
Background	2 mCrab

the mission beginning and are made available with the user defined mode data for every observation. The instrumental properties of the PCA are outlined in Table 2.2 and a full description of the instrument can be found in Jahoda et al. (2006).

2.2.2 Data acquisition and analysis

The work presented in the following chapters has made use of the large FOV and high time resolution of the PCA to search for and monitor X-ray binaries in the SMC. The data used come from a key programme in which twice-weekly monitoring observations of the SMC bar region are carried out. Galache et al. (2008) give details of this programme and present light curves of the SMC pulsar population at that time. Here I will summarise the key aspects of the programme, the data analysis methods and changes made to the reduction and analysis pipelines developed by Laycock (2002) and Galache (2006).

Many different positions have been observed during the programme, though in recent years we have settled on two slightly overlapping positions covering most of the Bar. These positions are depicted in Figure 2.5. The large and small circles are the 2° full width zero intensity (FWZI) and 1° FWHM fields of view for the two positions. The observations are made in the GoodXenon event mode which utilises the full timing and energy resolutions of the PCA ($1\,\mu$s and 256 channels). Each photon is tagged with a time, energy and the PCU configuration in this mode. The data are extracted in the 3–10 keV range in order to maximise the signal-to-noise ratio (SNR) for a HMXB. Jahoda et al. (2006) present the quantum efficiency of each of the layers in PCU2. At the energy range of interest, the efficiency of layers 2 and 3 are negligible in comparison to layer 1 and so we only extract data from this top layer. In addition to this, PCUs 0 and 1 unexpectedly vented their propane veto layers on May 12$^{\text{th}}$ 2000 and December 25$^{\text{th}}$ 2006 respectively. Though a new

background model was introduced to account for this in PCU0, it was decided not to use data from this PCU after this date. PCU1 is very rarely used for faint sources, though data are also rejected from this PCU on the rare occasion it is active in our observations.

A reduction pipeline was written in C-shell script to provide a fully automated way of producing a cleaned and barycentre corrected light curve from raw *RXTE* data files. The pipeline uses many of the FTOOLS needed for the standard reduction of *RXTE* data and was originally written by Silas Laycock (Laycock, 2002). Major revisions were made by Jose Galache during his Ph.D to account for changes in the observatory conditions and reduction methods (Galache, 2006). The key points that are important to the discussion in this thesis are described now. After light curves have been extracted from the raw event files they are binned at 0.01s. They are then background subtracted and barycentre corrected before finally having the count rate corrected for the number of active PCUs. The final light curves are passed through a Lomb-Scargle periodogram to search for pulsations. The error associated with any period found is calculated based on the formula for the standard deviation of the frequency given in Horne & Baliunas (1986):

$$\delta\omega = \frac{3\pi\sigma_N}{2N^{1/2}DA} \tag{2.1}$$

where ${\sigma_N}^2$ is the variance of the light curve, N is the number of data points, D is the length of the data and A is the amplitude of the signal given by:

$$A = 2\sqrt{\frac{z_0{\sigma_N}^2}{N}} \tag{2.2}$$

where z_0 is the Lomb-Scargle power. This error analysis is not perfect, but the time and computer power needed to run Monte-Carlo simulations on over 1500 power spectra has meant that a more sophisticated analysis has not yet been implemented. Further minor revisions to the pipeline were made by Matthew Schurch during his Ph.D (Schurch, 2009). Minor revisions made during my Ph.D include:

- addition of new AO information and adaptation of the ObsID recognition section to account for the most recent data sets and newly devised raster observations to try and locate newly discovered pulsars
- changing the ‘epoch selection’ section as an error in the observation dating

within the pipeline meant *all* data were reduced with the energy channels chosen for epoch 5 data. Epochs prior to epoch 5 were meant to be reduced using different gains as the PCUs are constantly changing.[2]

- changing the filtering criteria to remove bad data related to PCU breakdowns. If an observation, or part of an observation occurs less than 150 s before or less than 600 s after a breakdown event (flagged with the TIME_SINCE_BRK keyword) that observation, or part thereof, will be thrown away. The selection expression for PCU2 data, for example, is thus (PCU2_ON == 0 || (PCU2_ON == 1 && (TIME_SINCE_BRK2 <-150 || TIME_SINCE_BRK2 >600))). This expression has been added to the more general selection criteria described in Galache (2006).

Due to the quickly expanding data archive, Galache (2006) developed two further analysis packages designed to automate the period analysis of the light curves. The first program, PUMA (PUlsar Monitoring Algorithm), produces a Lomb-Scargle power spectrum for each light curve and searches it for periodicities from known pulsars. The typical length of an observation is around 10 ks meaning periods of up to $\sim$ 3000s can be searched for. If it finds a known pulsar, it will measure the pulsed amplitude at that frequency. It will also record bright pulsations from previously unknown systems. The second program, ORCA (ORbital Calculation Application), reads in the pulsed amplitude histories of each pulsar as measured by PUMA and makes a long-term light curve for each one. It then searches the light curves for periodic signatures indicative of orbital modulation. Further details on both programs can be found in Galache (2006) or Galache et al. (2008).

2.2.3 Example light curves and programme results

Galache et al. (2008) summarise the results of the *RXTE* monitoring programme between 1999–2008. In total they suggest 14 systems amongst the known population were either newly discovered BeXRB pulsars or were first identified as pulsars by our programme. In addition, they present the long term light curves of every known pulsar at that time which, in many cases, led to a newly determined orbital period from timing analysis of the light curves. In this section, I will briefly summarise the results of the programme between 2008 and the present day and present the light

[2] See http://heasarc.nasa.gov/docs/xte/e-c_table.html for the energy conversion table at different epochs.

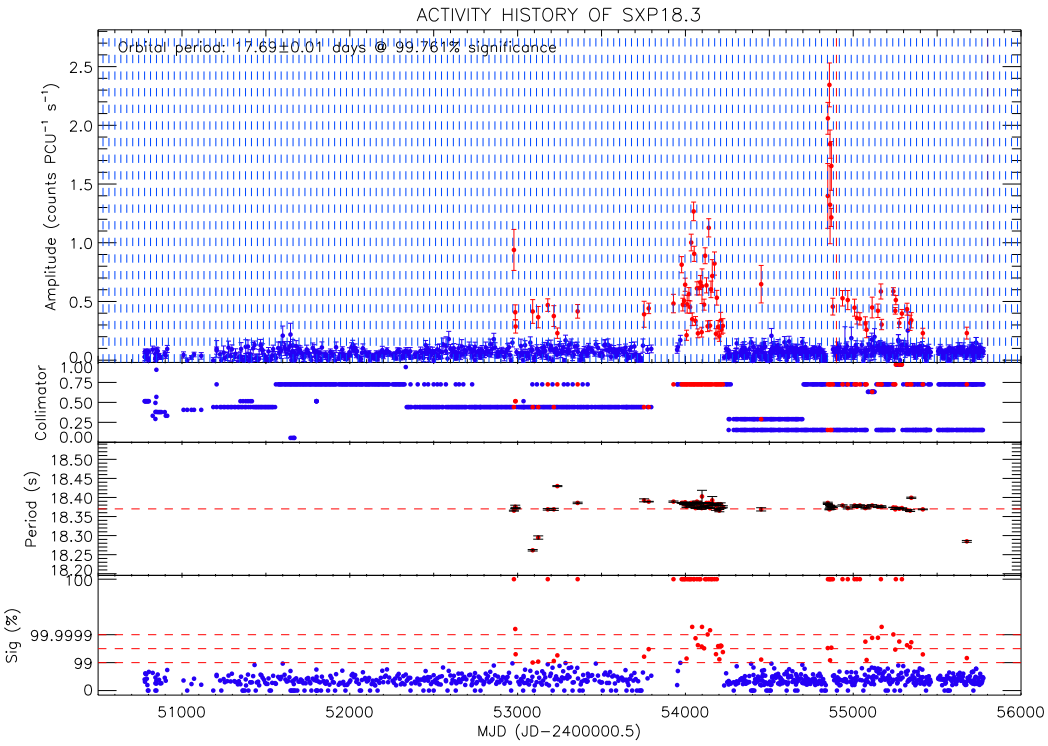

Figure 2.8: Long-term *RXTE*/PCA light curve of SXP18.3 in the 3–10 keV band. The panels are described in the text.

curves of some selected systems that show recent X-ray activity. There are 3 main results coming from the programme in the last 3 years:

- the discovery of 4 new pulsars (SXP7.92, SXP11.5, SXP175 & SXP723) and determination of a small number of binary periods of known pulsars.
- the determination of an accurate spin period of the first known pulsar in the Magellanic Bridge.
- the detection and rapid monitoring of Type II outbursts to track spin period evolution in these outbursts for several systems.

The discovery of new pulsars is an important result for more general studies of the SMC population. When a new pulsation is discovered by *RXTE*, the source needs locating before more detailed studies can be carried out. Chapter 6 discusses what I believe to be the most effective and efficient way of doing this. The latter of these points has proved hugely successful in producing well sampled outbursts to which orbital and spin-up models can be fit. This model fitting to Type II outbursts is the basis on which much of the work presented in this thesis was produced. As I will describe in the following chapters, this adaptation of our traditional observing programme to target large outbursts has for the first time allowed the determination of

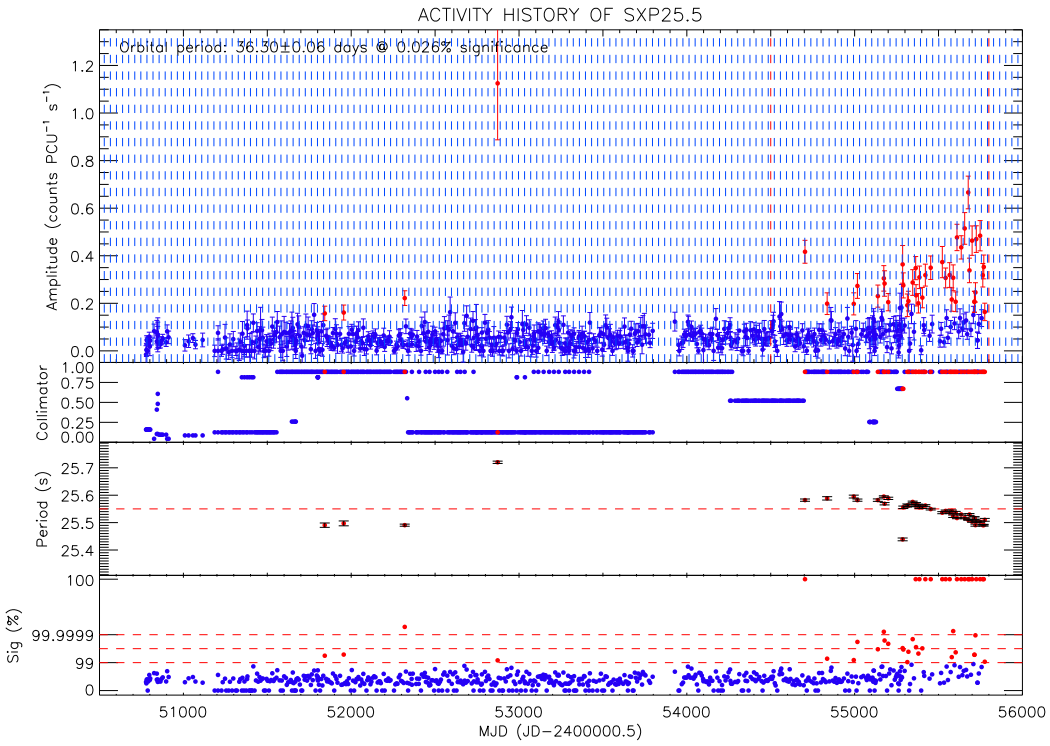

Figure 2.9: Long-term *RXTE*/PCA light curve of SXP25.5 in the 3–10 keV band. The panels are described in the text.

the orbital parameters of several BeXRB systems in another galaxy. Before presenting the results of this analysis, I will introduce examples of the data and highlight some specific systems that are currently very active and discuss this in terms of the outburst types seen in BeXRB. The simplistic view of an outburst either being Type I or II as described in Chapter 1, seems to no longer be satisfactory in categorising outbursts in BeXRBs. The light curves presented in Figures 2.8 – 2.12 are used to emphasise some of the more subtle difference in the outbursts we observe. These differences are seen in Galactic systems, but I believe they can only be characterised by looking at a large population that have the same age, distance and local environment for a long time. Our SMC dataset offers such an opportunity.

The layout of Figures 2.8 – 2.12 is generic and is produced by the ORCA routine. It is described here so as not to be repeated in each figure caption or the following chapters. The top panel shows the amplitude of the pulsed emission in counts/PCU/s, where each point is a single observation. The vertical blue dashed lines show the most likely X-ray ephemeris based on an orbital period search of the light curve. The second panel shows the source position within the *RXTE* FOV. A source at the very centre has a collimator of 1 and a source at the very edge 0. The collimator response is approximately linear with distance from the centre. The

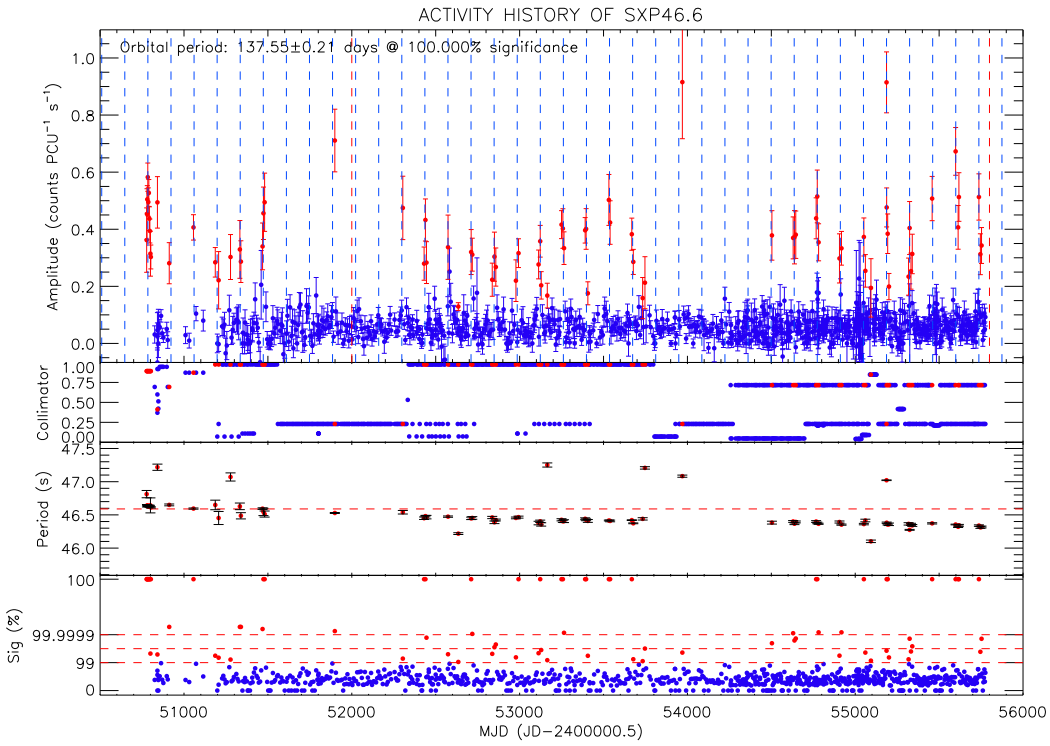

Figure 2.10: Long-term *RXTE*/PCA light curve of SXP46.6 in the 3–10 keV band. The panels are described in the text.

third panel shows the pulse period measurements in seconds. The final panel shows the significance of the detection where the significance, sig, of a given frequency is related to its Lomb-Scargle power, P, by the following formula:

$$\mathrm{sig} = 100 \times \left(1 - e^{-P}\right)^{M} \tag{2.3}$$

where M is the number of independent frequencies and is typically 2×10^5 in our analysis pipeline. As such, a LS power $\gtrsim 17$ is a detection above 99% significance. Only detections above a significance of 99% are plotted in the third panel for clarity reasons. This 99% limit is denoted in the other panels by red points. Blue points are detections below this threshold. The x-axis is in MJD and spans approximately 14 years. Figures 2.8 – 2.10 are the light curves of SXP18.3, SXP25.5 and SXP46.6 respectively. All three pulsars have been extremely active since their light curves were last published by Galache et al. (2008) and they all show different behaviour. SXP18.3 underwent a massive Type II outburst around MJD54000 (see Schurch et al. 2009 for details) and then turned off. It then switched back on around MJD55000 with a much shorter Type II outburst that was over double the luminosity of the first. This Type II did not end abruptly as before, but reduced into a long series of Type I

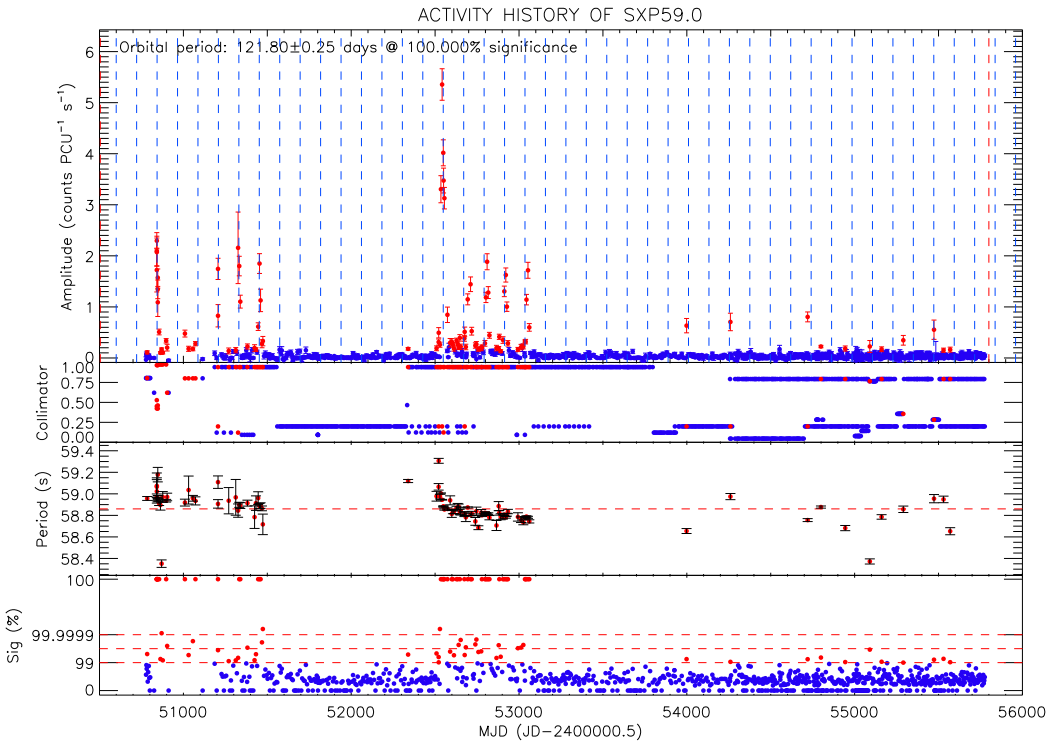

Figure 2.11: Long-term *RXTE*/PCA light curve of SXP59.0 in the 3–10 keV band. The panels are described in the text.

outbursts that peak at around 20% of the Type II luminosity. Timing analysis of this section of the light curve reveals the orbital period of this system at 17.7 d[3]. This light curve alone is evidence that the traditional Type II outbursts show differences in length and intensity and must be caused by differences in the circumstellar disk at the two epochs. SXP25.5 was rarely detected until MJD ∼55000 when it began showing evidence of low luminosity Type I outbursts. These quickly evolved into a more persistent outburst of higher luminosity, though it was still not seen in every observation as a traditional Type II outburst would be. This suggests an intermediate outbursting stage, where a system may be accreting for most of its orbit, but not all of it. This transition also causes the neutron star to strongly spin-up, in contrast to SXP18.3 in which a much more luminous outburst of similar duration has caused almost no spin-up of the neutron star. This implies the torque imparted by the accreted material is different in the two systems. SXP46.6 is the most constant and predictable source in the SMC. Whenever we have had good coverage, we have seen regular Type I outbursts modulated at the binary period. There is a small and constant spin-up and little change in the X-ray luminosity. This is the archetypal Type I outburst as described in the previous chapter.

[3]The orbital period had already been derived from optical light curves (Schurch et al., 2009).

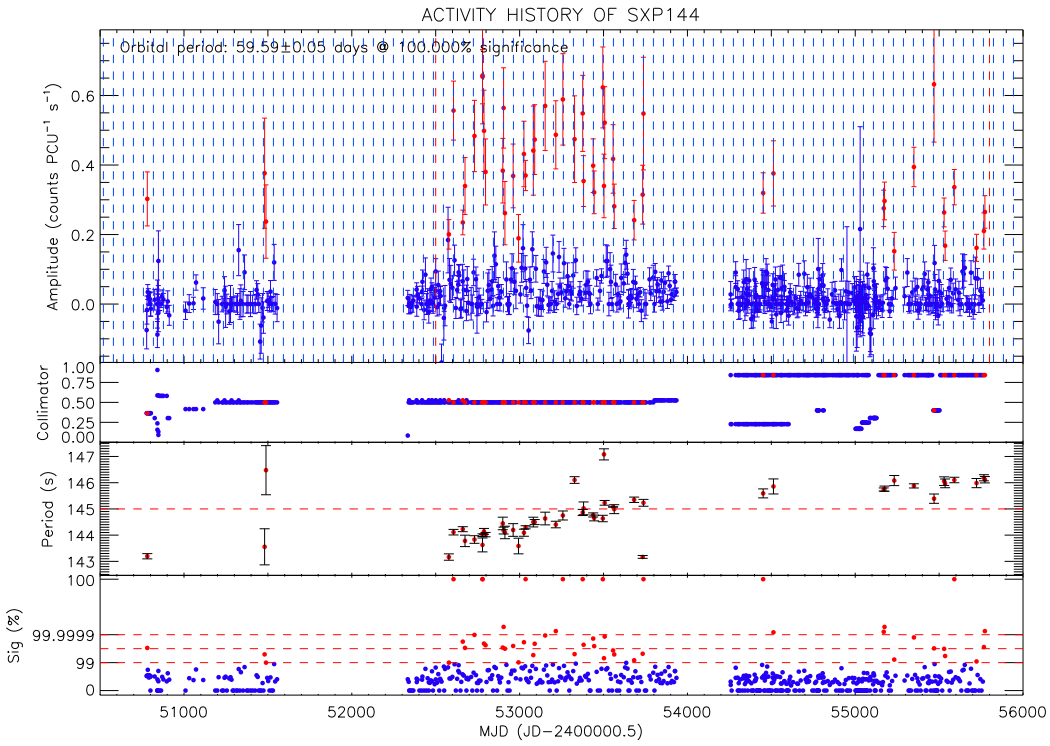

Figure 2.12: Long-term *RXTE*/PCA light curve of SXP144 in the 3–10 keV band. The panels are described in the text.

Figures 2.11 – 2.12 show SXP59.0 and SXP144. These systems have shown little X-ray activity since Galache et al. (2008) presented their light curves, but they show more diversity in the type of outburst in their histories. SXP59.0 has undergone two similar outbursts around MJD51000 and MJD52700. They resemble a persistent (Type II) low luminosity outburst with sharp increases in luminosity at the time of periastron passage (Type I). This shows persistent accretion, but with an increase in accretion rate during periastron. This is very different from SXP18.3 in which the Type II preceded the Type I in a very clear change of state. The spin-up also clearly changes from high to low during the second outburst as the luminosity drops from 5.5 to 2 cts/PCU/s. Finally SXP144 was active for a long time, undergoing regular Type I outbursts, similar to SXP46.6. However, in this case there is very definite spin-*down* of the neutron star whilst accretion is occurring. This is due either to the neutron star spinning in the opposite direction to the accretion flow or the magnetic braking torque of the neutron star is stronger than the torque provided by the accretion flow. Whilst these 5 light curves were chosen as some of the cleanest we have, they demonstrate that care is needed when discussing outburst type. Many factors can affect what type of outburst we see, not least the neutron star spin and its phase in the orbit, the state of the CS disk and the parameters that describe

the binary orbit. Outbursts discussed throughout the rest of this work will often be described in terms of Type I and Type II for ease of understanding, though more specific details will be given when necessary. In the long term however, I believe the nomenclature used in the field should move away from these traditional descriptions. In Chapter 7 I will discuss future plans to try and quantify these differences and produce an more thorough classification regime than currently exists.

2.3 Optical monitoring of SMC BeXRBs

To fully understand the X-ray behaviour we see from BeXRBs, it is vital to have information about the optical counterpart. In Chapter 1 I introduced the OGLE monitoring programme of stars in the Magellanic Clouds. Whilst stellar variability was not a key science goal of the project itself, the data the programme has taken since 1997 has been an invaluable tool in understanding the optical counterparts to the SMC BeXRB population and in many cases the role that the counterparts have in the X-ray activity. The light curve shown in Figure 1.10 was chosen to emphasise the two types of variability seen in the data, though it is representative of all the light curves in the database.

The OGLE project has been steadily monitoring millions of stars in the Magellanic Clouds for the past 12 years (see Udalski, Kubiak & Szymański (1997) and Szymański (2005) for more details on the OGLE instrumentation and catalogue). Photometric images in the I-band are taken almost every night whilst the SMC is visible; these images now make up a decade long database that includes most of the HMXB systems in the SMC. Throughout the following chapters, I will often refer to the OGLE light curves of various BeXRB systems in the context of the optical flux coming from the circumstellar disk or the variability in the system caused by the Be star or the neutron star. The light curves are reduced with the OGLE real time data analysis system (Udalski, 2003), meaning calibrated light curves are provided direct to the user for immediate scientific exploitation.

As a secondary means to optically monitor BeXRBs, my group has been using the 1.4m Infrared Survey Facility (IRSF) telescope at the *South African Astronomical Observatory (SAAO)* for the last 7 years, taking photometry and polarimetry at near-IR wavelengths. This monitoring is not regular, as time on the telescope is awarded via competitive proposals and observations carried out by visitors to the telescope. However, the few observations made of each system over the years have proved a very useful probe of the cooler parts of the circumstellar disks in these sys-

tems, which nicely compliment the OGLE monitoring. The IRSF is a Japanese built telescope designed specifically to take photometric data in the J, H & K_s bands. The SIRIUS (Simultaneous three-colour InfraRed Imager for Unbiased Survey) camera attached consists of three 1024×1024 pixel HAWAII arrays which take simultaneous images in the three bands (Nagashima et al., 1999). The pixel scale of the chip is 0.45 arcsec per pixel, yielding a $7'.7 \times 7'.7$ field of view.

Data reduction was performed using the dedicated SIRIUS pipeline based on the National Optical Astronomy Observatory's (NOAO) IRAF software package. The pipeline was provided by Yasushi Nakajima at Nagoya University, Japan. This performs the necessary dark subtraction, flat fielding, sky subtraction and recombines the dithered images. It has only been during the past couple of years that the IRSF has really been noticed by the astronomical community outside of Japan and South Africa. As such, huge advances have been made improving the pipeline for external use. A moderate amount of time was spent during my Ph.D. setting this pipeline up on the university computer system and testing it for bugs and errors, in conjunction with the Japanese, to produce a pipeline that is suitable and easy to install and run. With the advancement in the understanding of the telescope and the reduction packages, the Japanese astronomers recommended various observing strategies to maximise the data. During my groups early observing runs, a typical setup of 15 dithers of 25s each was generally used for each target. This total exposure time of between 350 and 400s was sufficient to detect sources down to K_s=17 and was used for all but the faintest sources. As my observing experience on the telescope grew, these exposure times were fine-tuned to fit each source and the conditions. I found that shorter exposure times and more dither cycles reduced the background noise significantly (particularly on hot nights) and the total exposure times of bright sources could be reduced slightly. For the readers information throughout the following chapters, systems with a J magnitude of 14-15 were observed with 4 sets of 10 dithers of 10s exposures, totalling 400s. Magnitude 15-16 stars were typically observed for 6 sets of 10×10s exposures, totalling 600. Anything fainter than this needed longer individual exposure times else sources would not be visible above the noise. Typical exposures were 6 sets of 10×15s exposures, totalling 900s.

Photometry on the reduced data was originally done using the NOAO/DAOPHOT package in IRAF to extract the J, H & K_s band magnitudes. The catalogue by Kato et al. (2007) was used to calibrate the data by finding the average magnitude offset of all the stars in my field from those in the same field in the catalogue. This usually incorporated 100s of stars, meaning potential effects of variable stars in the field could be ignored. The error on this fit was added in quadrature to the instrumental

error from the photometry to get the final errors. This method was used until 2010 when a new version of the pipeline included an aperture photometry stage, meaning the whole process could be carried out in one go. As a final test before implementing this new version into my analysis, I reduced a selection of previously analysed images which resulted in the same flux values for the stars of interest via both methods. Thus, the data presented throughout this work are consistent with each other independent of pipeline version or type of photometry performed.

Two things are infinite: the universe and human stupidity;
and I'm not sure about the the universe.

ALBERT EINSTEIN (1879 - 1955)

3

Be/X-ray binary SXP6.85 undergoes large Type II outburst in the Small Magellanic Cloud

The Small Magellanic Cloud Be/X-ray binary pulsar SXP6.85 = XTE J0103-728 underwent a large Type II outburst beginning on 2008 August 10. The source was consistently seen for the following 20 weeks (MJD = 54688–54830). I present X-ray timing and spectroscopic analysis of the source as part of the ongoing *RXTE* monitoring campaign described in Chapter 2 and an *INTEGRAL* key programme monitoring the SMC and 47 Tuc. A comparison with the OGLE III light curve of the Be counterpart shows the X-ray outbursts from this source coincide with times of optical maximum. This is attributed to the circumstellar disk increasing in size, causing mass accretion onto the neutron star. Ground based IR photometry and Hα spectroscopy obtained during the outburst are used as a measure of the size of the circumstellar disk and lend support to this picture. In addition, folded *RXTE* light curves seem to indicate complex changes in the geometry of the accretion regions on the surface of the neutron star, which may be indicative of an inhomogeneous density distribution in the circumstellar material causing a variable accretion rate onto the neutron star. The work presented in this chapter has been published as a

paper, for which Dr. Vanessa McBride performed the *INTEGRAL* data analysis.

3.1 Introduction

The BeXRB that is the subject of this chapter is the SMC pulsar SXP6.85 = XTE J0103-728. It was first detected in 2003 by *RXTE* as a 6.848 second pulsed X-ray source (Corbet et al., 2003). Lomb-Scargle periodograms of the X-ray data reveal a 112.5 day period (Galache et al., 2008), although it is uncertain as to whether this modulation is the orbital period of the system or if it is driven by the interval between X-ray outbursts. The system was later detected in a 2006 *XMM-Newton* observation at the position $01^h02^m53^s.1, -72°44'33''.0$ (J2000.0). This detection led to the identification of a V=14.6 optical counterpart (Haberl & Pietsch, 2008a). Follow-up work by McBride et al. (2008) classified the counterpart as an O9.5V-B0V emission line star.

Previous analysis of MACHO red and blue data by McGowan et al. (2008a) reveals a 620 ± 18 d optical modulation in which the source brightens by ~ 0.5 magni-

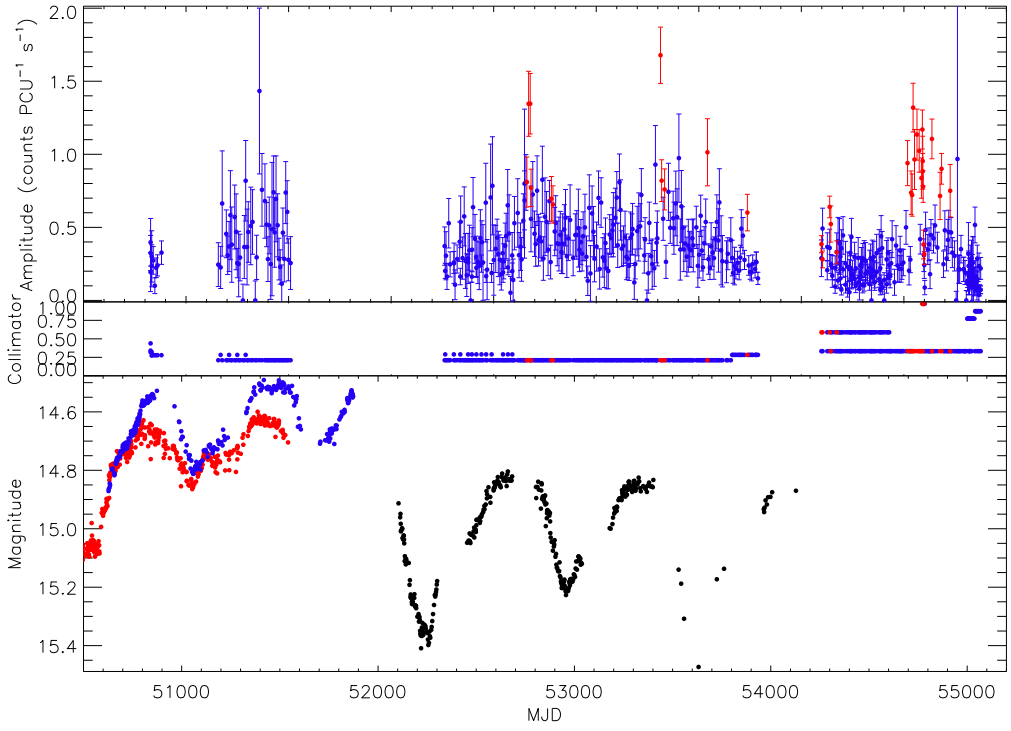

Figure 3.1: SXP6.85 X-ray and optical light curves. The top and middle panels show the pulsed flux and collimator response to SXP6.85 as described in Chapter 2. The final panel shows the combined MACHO (red), OGLE II (blue) and OGLE III (black) light curves in the B (MACHO) and I (OGLE) photometric bands. The MACHO data have been arbitrarily normalised for viewing purposes.

tudes. Those authors also show that the source gets redder as it gets brighter, meaning the plane of the disk is likely at a low inclination to the observer. Schmidtke & Cowley (2007) analysed MACHO and OGLE II data of the source, finding an optical variation of $\sim$658 days. This is similar to the value found by McGowan et al. (2008a), providing evidence for a quasi-periodic growth and decay of a circumstellar disk. Schmidtke & Cowley (2007) also find a possible period of 24.82 days in the OGLE II data. This period is closer to the expected orbital period of the system based on the Corbet diagram (Corbet, 1986) than the X-ray modulation found in Galache et al. (2008). In this chapter I present long X-ray and optical lightcurves of SXP6.85 and analysis of X-ray timing and spectroscopic data taken by *RXTE* and *INTEGRAL*. Near-IR photometric data taken during the most recent outburst are presented and compared to near-IR data taken during quiescence to show the connection between optical and X-ray activity in this system. In Chapter 5 I will return to this source, as a subsequent bright (albeit shorter) outburst allowed a detailed orbital analysis to be performed.

3.2 X-ray Data

Between the start of the *RXTE* monitoring programme of the SMC and the end of 2009 when this work was published, SXP6.85 had been detected above the 99.99% significance level on four separate occasions. The full *RXTE* light curve to this date is shown in Figure 3.1. The PCA collimator response during the most recent outburst was 0.33, except for a period of $\sim$10 days in November 2008 in which an intense set of observations were carried out pointing directly at the source. These observations were in addition to weekly monitoring and were taken due to the unprecedented longevity of the outburst, which lasted for $\sim$20 weeks. The X-ray outbursts are shown in Figure 3.1 between MJD 52700 and MJD 54900, with the detected spin period and detection significance plotted in Figure 3.2. Data reduction was performed using Heasoft v.6.6.2 analysis tools. The four distinct detections of this system previously mentioned refer to the time periods centred at MJDs 52800, 53450, 54300 and 54750. These are believed to be four Type II outbursts that have resulted from an enlarged circumstellar disk, as indicated by the OGLE light curve. The three data points lying furthest away from the horizontal red line in Figure 3.2 are likely unrelated to SXP6.85 and just happen to fall above the significance limit of 99% in the statistics of the power spectra. As these figures are created from an automated pipeline, they often include some ‘significant’ points that are not related

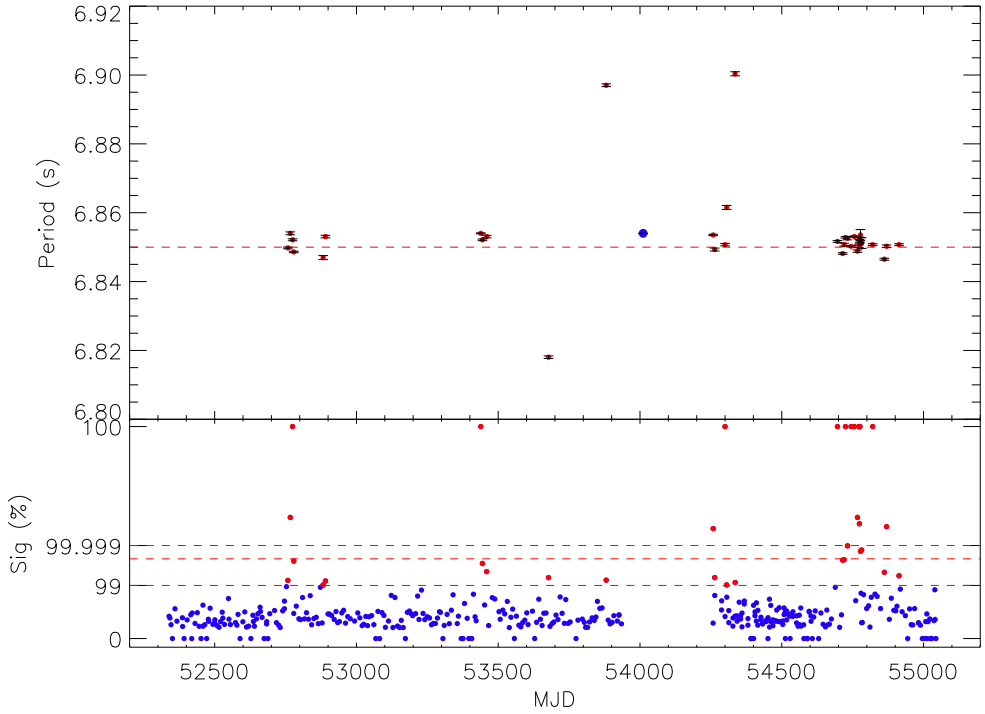

Figure 3.2: X-ray pulse period history of SXP6.85 and the significance of each detection. Only periodicities above the 99% significance level have been plotted (red points in bottom panel). The pulse period detected by *XMM-Newton* in 2006 has been plotted alongside the *RXTE* detections (blue point in upper panel; MJD 54011).

to the pulsar of interest. These are usually noise spikes that fall within the designated frequency search width of any given pulsar. They can usually be identified by eye as points that do not fall at a time of optical maxima, do not follow the general spin-up trends of other outbursts or have a significance only just above the cutoff. At least two, sometimes all three, of these points can be applied to the three points highlighted in the figure.

The timing and spectral analysis presented below is a result of *RXTE* and *INTEGRAL* data taken during the most recent epoch of pulsed X-ray emission. *RXTE* observations were made approximately weekly between 2008 August 10 and 2008 December 30. According to the ephemeris in Galache et al. (2008), the maximum in X-ray luminosity of the system is expected to occur on 2008 November 23 (MJD 54793). Although this date coincides with the detection, it is clear that the length and brightness indicate a Type II outburst that likely spans many neutron star orbits. Figure 3.3 shows *RXTE* pulse profiles in the 3-10 keV energy band for 10 observations throughout the outburst. The light curves were folded at the pulse period and arbitrarily phase shifted to align the point of minimum amplitude. There is clear variability in the accretion mode and pulsed fraction here, which are discussed later

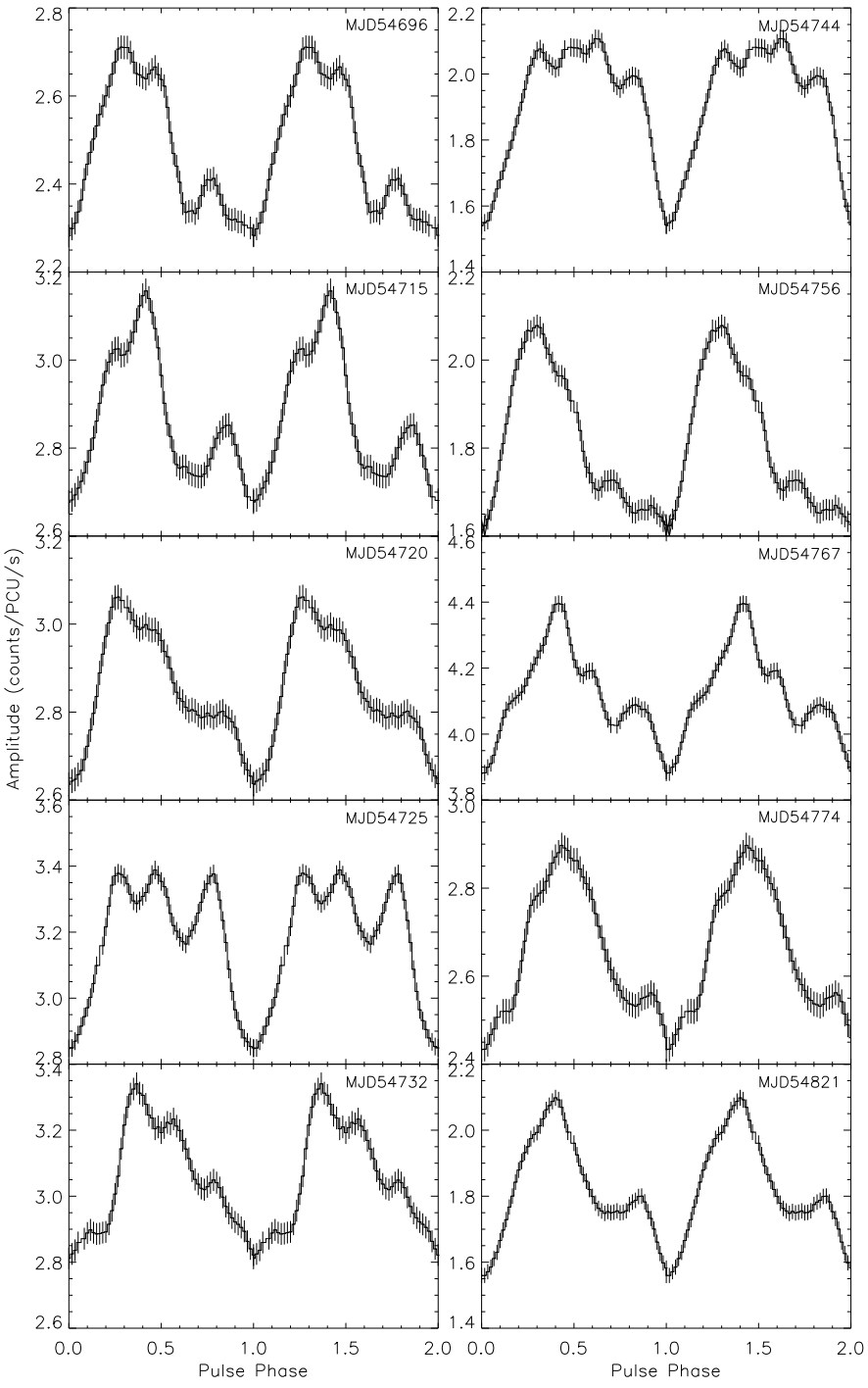

Figure 3.3: Pulse profiles of SXP6.85 during the most recent X-ray outburst (MJD = 54688 - 54830). The profiles are 3-10 keV light curves folded at the pulse period and have been smoothed and arbitrarily shifted in phase to align the minima in amplitude. Thus, they are included as a visual representation of the changes in the X-ray emission regions on the surface of the neutron star and do not contain any absolute information regarding the neutron star phase.

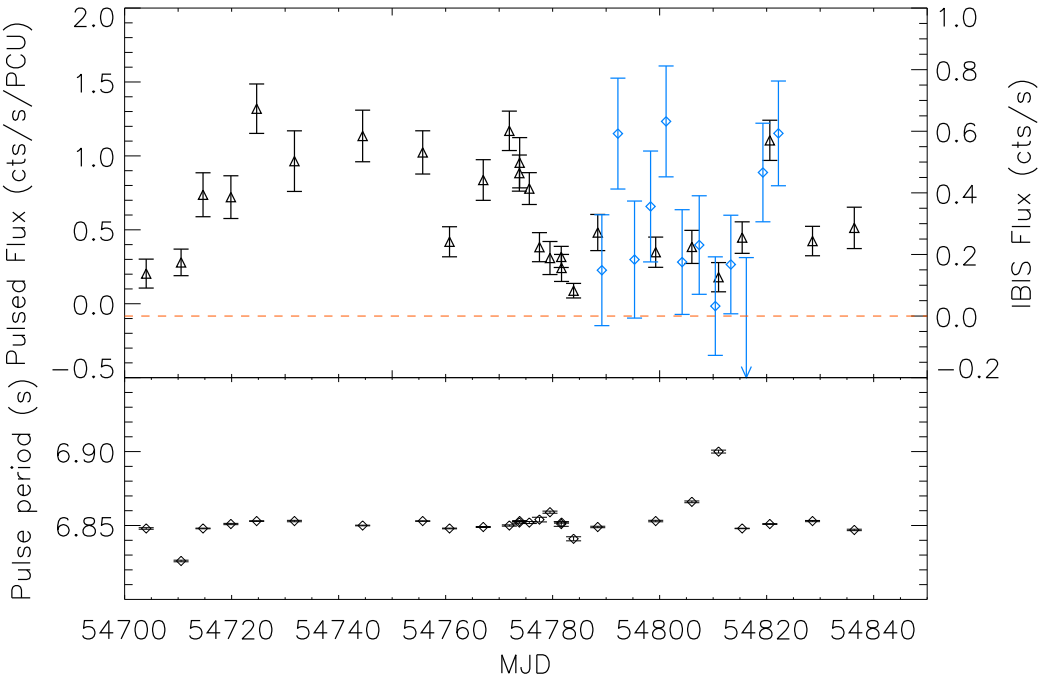

Figure 3.4: Combined *RXTE* and *INTEGRAL* light curve of SXP6.85. The black data points are the 3-10 keV pulsed flux detected with *RXTE*, while the blue data points are the 15-35 keV total flux detected with *INTEGRAL*. The pulse period in the lower panel is from timing analysis of *RXTE* data. The dashed line corresponds to zero flux as detected by IBIS.

in the chapter.

The IBIS telescope aboard *INTEGRAL*, which is optimised for an energy range of 15-200 keV and has a field of view of $30^\circ \times 30^\circ$, is uniquely suited to observing large sky areas for point sources. As part of a key programme monitoring campaign on the SMC and 47 Tuc, *INTEGRAL* observed the SMC and Magellanic Bridge for approximately 80 ks per satellite revolution from 2008 November 11 to 2008 December 21. Individual pointings (science windows) were processed using the *INTEGRAL* Offline Science Analysis v.7.0 (OSA) (Goldwurm et al., 2003) and were mosaiced into revolution sky maps using the weighted mean of the flux in the 15-35 keV energy range. Figure 3.4 shows the IBIS detections of SXP6.85 plotted over a section of the *RXTE* pulsed flux light curve from Figure 3.1. These data represent the hard X-ray flux measured from SXP6.85. The brightest detection at 0.63 cts/s corresponds to a peak luminosity of 1.1×10^{37} ergs s^{-1}. The significance of the detection of the source once all science windows from the 33 d of coverage had been taken into account was 6.4 sigma. We used the four brightest detections to make an X-ray spectrum to compare with the softer *RXTE* spectrum. The *RXTE*

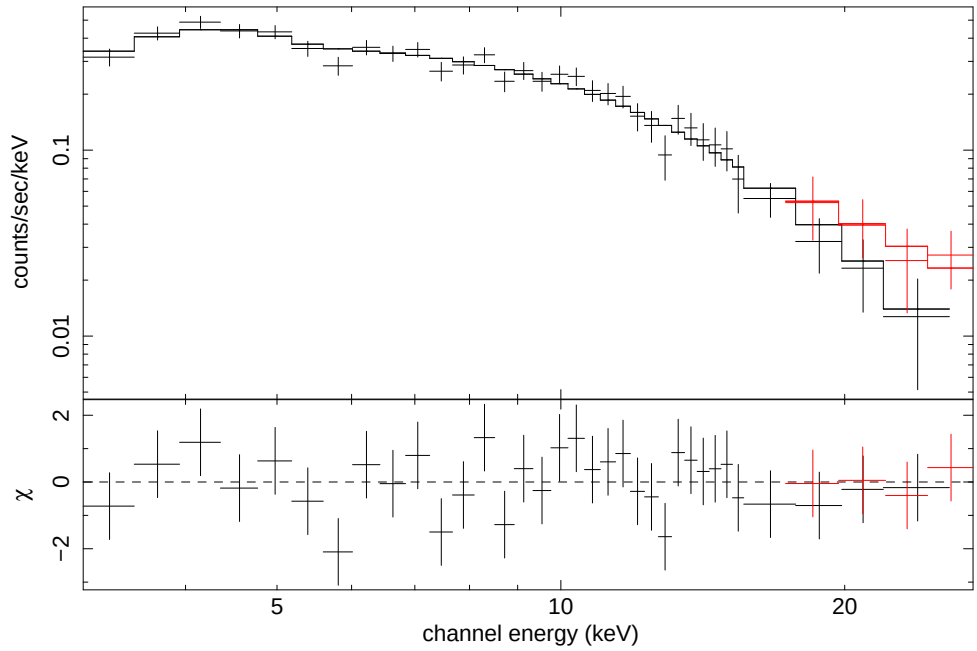

Figure 3.5: Typical X-ray spectrum of SXP6.85 extracted from an observation in which no other pulsating sources were in emission to minimise contamination effects. The harder IBIS spectrum (red) was fit simultaneously with the *RXTE* spectrum (black) with a freely variable offset. The spectrum has been re-binned above 15 keV due to low counts. See text for discussion of model fitted.

spectrum was taken on MJD 54772, approximately 4 weeks before the *INTEGRAL* data. Although this is not ideal for comparison, we are limited to the brightest detections with both satellites and to detections with *RXTE* in which no other source was active.

The *RXTE* and *INTEGRAL* spectra were fitted with an absorbed cutoff powerlaw model using XSPEC version 11.3.2 (Arnaud, 1998). The absorption was frozen at 6×10^{20} cm^{-2} (Dickey & Lockman, 1990). The power law had a photon index of 0.8 ± 0.2 with a cutoff at 14.6 ± 9.6 keV. The two spectra were fit with this model simultaneously with an offset allowed to vary during the fit. A χ^2_ν of 0.75 (33 d.o.f) indicates a good fit to the data (see Figure 3.5). This analysis reveals a peak X-ray luminosity of $\sim 7 \times 10^{36}$ ergs s^{-1} in the 3-10 keV band, assuming a distance to the SMC of 60 kpc. Only *RXTE* spectra in which there was no other detected pulsed X-ray emission were used to calculate L_X. I find that this value varies by a factor of two during the outburst. Analysis of *XMM-Newton* data by Haberl & Pietsch (2008a) show the source at a higher luminosity, $L_X = 2 \times 10^{37}$ ergs s^{-1} in the 0.2-10 keV band, and showing variations of a factor of two in intensity on time scales of ten minutes.

Table 3.1: IR data of the counterpart to SXP6.85.

Catalogue	Date (MJD)	J	H	K_s
2MASS[1]	51034.784	14.83 ± 0.04	14.71 ± 0.05	14.78 ± 0.11
SIRIUS[2]	52894.036	14.82 ± 0.02	14.74 ± 0.02	14.57 ± 0.02
Telescope	Date (MJD)	J	H	K_s
IRSF	54453	14.84 ± 0.02	14.77 ± 0.02	14.67 ± 0.03
	54809	14.53 ± 0.02	14.46 ± 0.02	14.36 ± 0.04

[1]Skrutskie et al. (2006), [2]Kato et al. (2007).

3.3 Optical and IR Data

The bottom panel in Figure 3.1 shows the OGLE II, OGLE III and MACHO *blue* light curves of SXP6.85 (blue, black and red points respectively). The MACHO data have been arbitrarily normalised for viewing purposes. It is clear that the long period oscillations described in McGowan et al. (2008a) are also present in the OGLE data, indicating a quasi-periodic brightening that is intrinsic to the Be star; most likely the growth and decay of the circumstellar disk. Although the OGLE III light curve does not extend up to the most recent *RXTE* detection (this particular source falls on an OGLE chip-gap, thereby needing a different reduction process to the normal pipeline), it is apparent that the most luminous X-ray outbursts seem to coincide with the epochs of maximum optical brightness. This again suggests that the X-ray detections are similar to classical Type II outbursts, being independent of binary phase. The few detections which fall at times of optical minima (Figure 3.1 & 3.2) are likely spurious as the spin periods are significantly different from the other detections and they are of lower significance. It should also be noted that the *XMM-Newton* detection is consistent with an optical maximum.

Table 3.1 shows the J, H & K_s magnitudes of the counterpart to SXP6.85 from both the 2MASS and SIRIUS catalogues (Skrutskie et al., 2006; Kato et al., 2007). The IR position of the source is agreed by both catalogues to be $01^h02^m53^s.3$, $-72^\circ44'35''.1$ (J2000.0). Below the catalogue values are the data from two observing runs at the IRSF observatory during December 2007 and December 2008. Immediately obvious is the increase in near-IR brightness of the source between these two dates, suggesting an increase in the size of the circumstellar disk building up to the most recent X-ray outburst.

In order to more fully understand the circumstellar disk of the system, Hα spectroscopy was obtained simultaneously with the near-IR photometry using the 1.9-m telescope, Sutherland Observatory, South Africa. The spectrograph was used with

Table 3.2: Hα W_{eq} measurements of SXP6.85.

Telescope	Date	Exposure time (s)	Hα W_{eq} (Å)
ESO 3.6-m	2007-09-17	1000	3.53 ± 0.08
SAAO 1.9-m	2008-12-03	1000	5.35 ± 0.76
	2008-12-06	1000	5.31 ± 0.98
	2008-12-07	1000	8.11 ± 2.62
	2008-12-10	1500	4.62 ± 0.43
	2008-12-13	1500	6.21 ± 0.66
	2008-12-14	1500	4.80 ± 0.21
	2008-12-15	1500	5.13 ± 0.27
	2008-12-16	1500	5.96 ± 0.49
	2008-12-16	1500	5.06 ± 0.41

the SITe detector and a 1200 l/mm grating. The dispersion was 1.0Å/pixel and the SNR ~ 10. A total of 9 spectra were taken throughout the two weeks beginning 2008 December 3. This was to check for any short-term variations in the Hα Equivalent Width (W_{eq}) during the ongoing Type II X-ray outburst. Details of the observations made and the measured W_{eq} are shown in Table 3.2. Data reduction was performed using standard IRAF routines. In addition, another Hα spectrum was taken in 2007 September 17 by the European Southern Observatory (ESO) 3.6-m telescope, La Silla, Chile, shortly after the optical counterpart had been verified. The EFOSC2 faint object spectrograph mounted at the Cassegrain focus was used with grism no:18 with lines ruled at 600/mm and which covered the wavelength range 4770-6770 Å. Using a slit width of $1''$ resulted in spectra at a resolution of 5 Å. The data reduction was performed using standard IRAF routines. The 3.6-m spectrum and one of the 1.9-m spectra are shown in the top and bottom panels of Figure 3.6 respectively. All of the spectra described have been smoothed with a boxcar average of either 5 or 7 Å.

It is clear that there is Hα in emission at both epochs, showing the existence of a circumstellar disk. The higher SNR spectrum in the top panel of Figure 3.6 shows a single peaked emission line structure. Using the standard rotation model put forward by Struve (1930), I suggest this system is of low inclination, with the disk near face-on to our line-of-sight. W_{eq} measurements suggest that the Hα line flux has grown in the time since the 2007 observation by over 50 percent. This along with the IR photometry provides strong evidence that the disk has grown. Figure 3.7 shows the 9 W_{eq} measurements from the data taken with the 1.9-m telescope in December 2008. The first three data points have large associated errors due to the shorter exposure times used (1000s as opposed to 1500s for the remaining

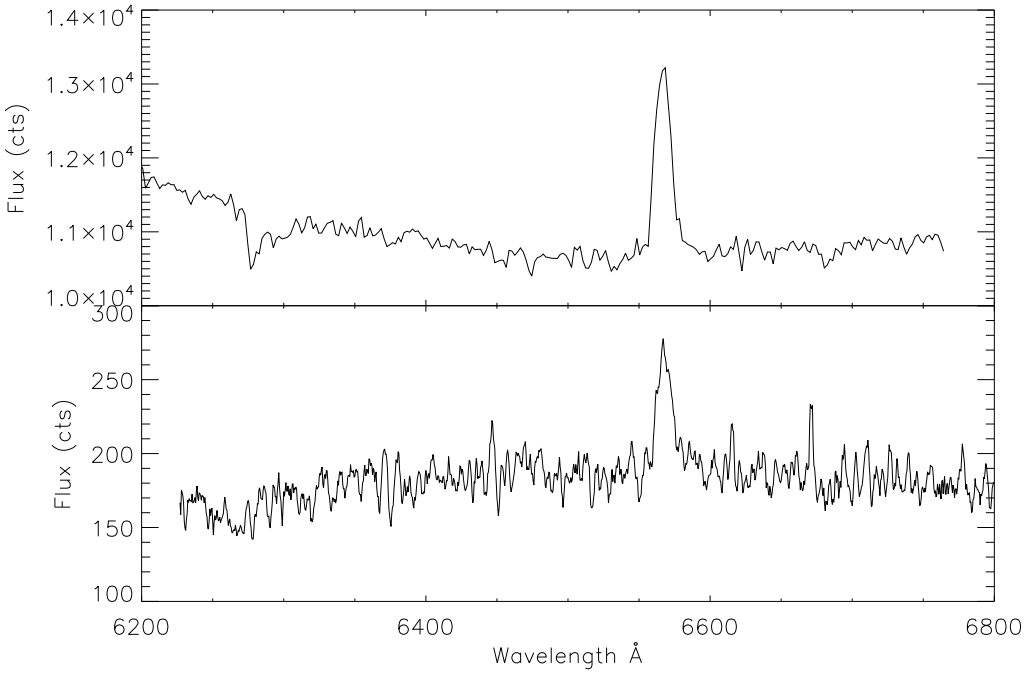

Figure 3.6: Top panel: Hα spectrum of SXP6.85 taken with the ESO 3.6-m telescope on 2007 September 17. Bottom panel: Hα spectrum of SXP6.85 taken with the SAAO 1.9-m telescope on 2008 December 16.

exposures). Even so, it is clear that, within these errors, there is little or no evidence for any variation in Hα emission during the two weeks. If only the 1500s exposures are considered (these having the smallest errors), a limit on the amount of variability can be estimated from the minimum and maximum possible values during this 7 day period. These values are 4.19 and 7.87 Å respectively. Given the errors, I can conclude that the line cannot have changed by more than 3.5 Å during this period and that the actual change, if any, is likely much smaller than this.

3.4 Discussion

The optical light curve of SXP6.85 displays long-term, quasi-periodic variations which are most likely associated with the growth and decay of the Be star's circumstellar disk. Changes in the (B-R) colour support this idea. By comparison with the X-ray light curve I find that at least two of the X-ray outbursts are consistent with optical maximum. This has also been observed in other systems, such as SXP18.3 (see Figure 2 of Schurch et al. 2009).

The X-ray light curve shows no periodic behaviour that can be attributed to a

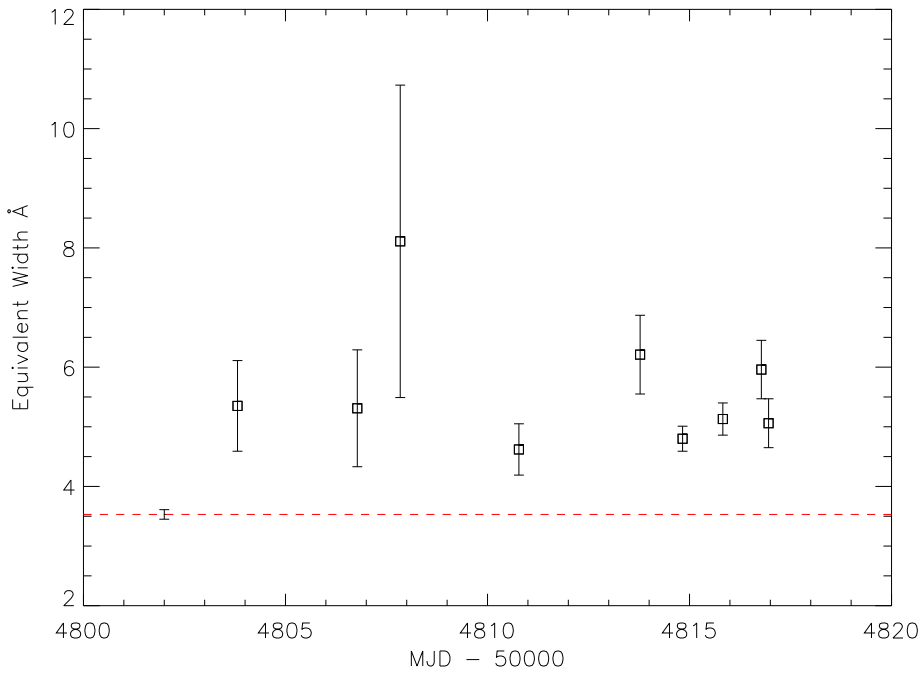

Figure 3.7: Hα W_{eq} measurements of SXP6.85 taken at the SAAO 1.9-m telescope during December 2008. The large error bars associated with the first three values are due to a lower SNR from shorter observations. The horizontal dashed line represents the Hα W_{eq} of the source during the September 2007 observation. The associated error in this case is much lower due to the higher SNR that can be obtained at the ESO 3.6-m telescope.

binary period. All the detected outbursts seem to be driven by the intrinsic behaviour of the Be star. I note that only small fluctuations in the pulse period are observed and that these show no correlation with time. Of greater interest is the pulse period history of the most recent Type II outburst (MJD 54688 - MJD 54830), which shows no general spin-up trend. This is an unusual observation as most HMXB systems show spin up of the neutron star during Type II outbursts due to the high accretion torques present.

The X-ray pulse profiles presented in Figure 3.3 show very complex double and triple peaked structures, that reveal much about the geometry of the system and of the beam emission regions: We see both poles from the pulsar, with the emission from the poles asymmetrical and, except for the profiles corresponding to MJD = 54725 and 54744 in Figure 3.3, always favouring one pole. This implies accretion onto the poles is asymmetric. The variability in the shape and width of the most prominent peak suggests we are seeing both fan and pencil beam emission. However, it has been observed that pulse profiles are very messy at low energies, with the possibility that the absorption is varying with neutron star spin phase, so

it is difficult to confirm that we are indeed seeing both fan and pencil beams in these energy ranges. Basko & Sunyaev (1975) theorise that pencil beams should be dominant under low accretion rates (hence low luminosities) and that fan beams should dominate at high accretion rates, as the radiation is strongly absorbed by the infalling material and can largely only be emitted sideways. However, from the profiles presented here there seems to be no clear dependence of the profile shape on flux.

The pulsed fraction calculated from the folded light curves is shown in Figure 3.8. The formula used in these calculations is given in Equation 3.1. I show that there is considerable variation in the measured pulsed fraction throughout the outburst, with the source appearing to increase and then return to some base level.

$$\text{PulsedFraction} = \frac{(F_{max} - F_{min})}{(F_{max} + F_{min})} \tag{3.1}$$

It is important to note that the pulsed fraction is only correct if SXP6.85 was the only source detected in that observation. If other sources were active, then the base emission includes emission from those objects and as such the pulsed fraction is only the lower limit of the actual value. I find a marginal correlation between source intensity and pulsed fraction, which could be attributed to the fractional change in the ratio of the source flux and the contribution of quiescent sources in the field. Therefore, although I can be sure there was no bright pulsed emission from any source in the field of view, I cannot be certain that there was no continuous emission affecting the pulsed fraction measurements. The values presented in Figure 3.8 are a factor of three lower than the value presented in Haberl & Pietsch (2008a), having taken the method of calculating the pulsed fraction into account. This implies either a significant contribution from background sources to the *RXTE* spectrum or that there has been a dramatic change of pulsed emission between the two observations, which may not be suprising given the observations are separated by more than 2 years. Those authors also find that SXP6.85 has one of the hardest spectra of known HMXB systems with a photon index of ~ 0.4. This also suggests that there is contamination from other sources in the *RXTE* spectrum, softening the powerlaw photon index to the value of 0.8 found in this study. This conclusion is not certain, however, as a slightly different energy range (0.2–10 keV as opposed to 3–10 keV) and spectral model may also be the cause of this difference.

It has been observed in other Be/X-ray binary systems that the (J-K) colour often remains constant for long periods of time despite dramatic changes in near-IR magnitude (e.g. Coe et al. 2006). SXP6.85 also exhibits this behaviour as can be

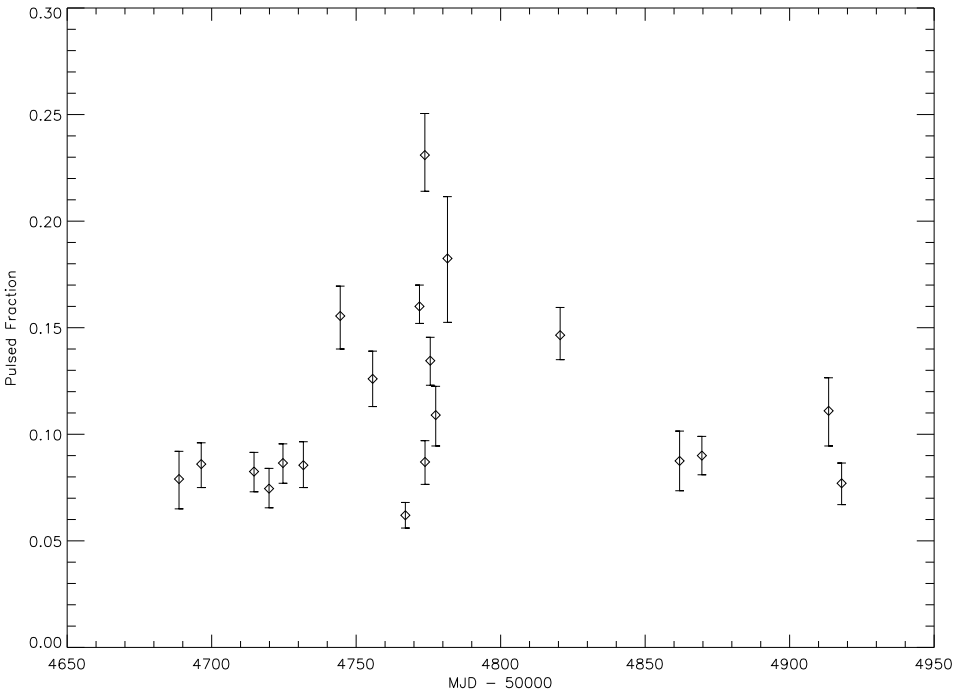

Figure 3.8: Pulsed fraction as a function of time in the 3-10 keV band for the most recent SXP6.85 outburst. The data show variations of a factor of two in pulsed fraction on the timescale of days. The definition of pulsed fraction used in this work is given in Equation 3.1.

seen in Table 3.1. The brightness of the system has increased by almost one third of a magnitude in the year between the two IRSF observations. However, the (J-K) colour has remained unchanged at 0.17. This is indicative of the temperature of the circumstellar disk remaining constant, whilst the increased brightness indicates the surface area of the disk has increased. It is possible to make a rough guess at the size of the circumstellar disk using the Hα W_{eq} measurements and making some assumptions on inclination and optical depth. Using the models of Grundstrom et al. (2007b), I estimate the disk half-width at half-maximum (HWHM) radius to be approximately $3\,R_*$ on 2008 December 16 and approximately $2.7\,R_*$ on 2007 September 17, an increase of over 11 percent in the year leading up to the recent Type II outburst. In this calculation I do not take into account any truncation caused by the neutron star and I make some approximations regarding the binary system: the effective temperature of the star is 30000 K, the inclination is 10°, the optically thin outer boundary of the disk is at $50\,R_*$ and the disk continuum dilution factor is 0.0033 (Dachs et al., 1988). See Grundstrom & Gies (2006) and Grundstrom et al. (2007b) for more details on the model input parameters. The key thing to note is that varying the disk outer boundary by factors of 2-3 changes the calculated

HWHM radius by approximately 10% as the model assumes a small contribution to the Hα flux from the optically thin part of the disk. Thus, the relative growth of the disk is set by the model despite the uncertainty in the actual radius. I also note that the 2008 measurement was made after SXP6.85 had been in outburst for more than 16 weeks, and as such the disk may have been significantly larger at the start of the outburst than the value estimated here. If I consider the IR magnitudes taken in December 2007 and December 2008, this yields a fractional increase in brightness of 1.33; a factor of three higher than the prediction made using the equivalent widths. The OGLE light curve shows variations on the order of 0.7 magnitudes over the entire epoch of coverage, corresponding to a factor of 1.9 in brightness (here I assume that the change in flux is proportional to the change in surface area of the disk, which is reasonable for an optically thick disk). If I assume that the recent X-ray activity occured during an optical maximum and that the disk HWHM at this time was $\sim 3\,R_*$, this implies the minimum, or quiescent, level of the disk is at $\sim 1.5\,R_*$. Clearly these are rough estimates based on some simplistic approximations which would benefit from more detailed modelling, but how do they compare to the theoretical and measured values discussed in this thesis? As mentioned in Chapter 1, Carciofi (2010) present models of isolated Be stars that suggest the Hα flux falls to about half of its maximum value at around $10\,R_*$. Whilst the introduction of a neutron star will reduce this value somewhat, these two estimates are not quite consistent with each other. In Chapter 5 I present data that allow an estimate of the semi-major axis of the orbit of SXP6.85 to be made. The result of this work suggests the optical counterpart sits around $9\,R_*$ from the neutron star at its closest point in the orbit. This implies the disk must be at least this size because of the persistent interaction of the neutron star with the circumstellar material, and is consistent with the predictions of Carciofi (2010). Unfortunately, this too is inconsistent with the size estimates made above using the Hα flux. In Chapter 4 I will repeat this calculation for another SMC pulsar, SXP11.5, for which a semi-major axis is also derived. Should the same result be observed, it would suggest that the models of Grundstrom et al. (2007b) are systematically underestimating the disk size of Be stars, at least in the SMC BeXRB population. The relationship between the orbit and disk sizes in BeXRB systems is important to understand as it can explain why we observe the activity we do and could even be used as a predictive tool for future outbursts. These ideas are discussed further throughout this work.

3.5 Conclusions

The X-ray and optical data presented here are evidence that SXP6.85 is indeed a Be/X-ray binary system. The X-ray light curve shows the transient nature of the source, whilst the optical and near-IR data suggest there are quasi-periodic modulations that are intrinsic to the Be star that are likely to be associated with the extended envelope of matter in the equatorial plane of the companion. Hα flux measurements show that an extended disk is indeed present in this system, with the shape of the emission line suggesting low inclination to the observer. The small variation in the spin period is also evidence of a low inclination system, assuming the circumstellar disk and the neutron star orbit lie in the same plane. W_{eq} measurements of the Hα line reveal a growth in the emission of Hα photons from the system which is most likely a result of an increase in the size of the circumstellar disk; an argument that is supported by the increase in optical luminosity that culminated in the most recent epoch of pulsed X-ray emission from the neutron star. Folded X-ray light curves reveal the geometry of the emission region on the surface of the neutron star and show the highly variable nature of the accretion region. Finally, a simple estimate of the radius of the circumstellar disk was made, quantifying the size of the disk during periods of X-ray activity and during quiescence, though the values obtained seem to be slight underestimates of what other observations and theory suggest.

I much prefer the sharpest criticism of a single intelligent man to the thoughtless approval of the masses.

JOHANNES KEPLER (1571 – 1630)

4

The Orbital Solution and Spectral Classification of the High-Mass X-Ray Binary IGR J01054-7253 in the Small Magellanic Cloud

The system that is the subject of this chapter, IGR J01054-7253, was discovered as a new X-ray source in the direction of the wing of the SMC in June 2009 (Bozzo et al., 2009). It was later confirmed as a BeXRB system through analysis of the optical and X-ray data presented here. I derive the spin and orbital periods of the neutron star and discuss the spectral properties of both the neutron star and optical counterpart. The latter of which resulted in the spectral classification of the star. Dense observations of a moderate Type II outburst with *RXTE* allowed for an orbital solution to be calculated, making it only the second BeXRB outside of the Milky Way to have a well defined orbit. This work has been published as a paper, for which Dr. Adam Hill made significant contributions to the orbital fitting code described here, whilst Dr. Frank Haberl performed the *XMM* data analysis and wrote most of the corresponding text. Students Brian van Soelen and Devanka Pathak obtained

Table 4.1: *INTEGRAL* observations of the SMC and 47 Tuc in which IGR J01054-7253 was detected

Revolution	MJD_{start}	Exposure Time (ks)	Count Rate ($ctss^{-1}$)
812	54989.2	63.3	0.4927
813	54992.2	53.1	1.1790
814	54995.2	60.8	1.1149
815	54998.2	58.8	0.9149
816	55001.2	62.1	0.8718
817	55004.2	63.1	1.31728
818	55007.2	40.2	1.35568

the optical photometry from the SAAO 1.9 m and Faulkes telescopes respectively and reduced the data.

4.1 Introduction

In this chapter, I present X-ray and optical data on the Be/X-ray binary pulsar IGR J01054-7253 = SXP11.5 in the Small Magellanic Cloud (SMC). Section 4.2 gives details of the X-ray observations made and presents X-ray data of the outburst. Section 4.3 describes the orbital model fitting to several weeks of *RXTE* data and presents the orbital solution for the system. Section 4.4 presents optical and IR data of the companion star. In section 4.5 I use Science Verification (SV) data from the new broadband spectrograph X-shooter on the Very Large Telescope (VLT) to spectrally classify the optical counterpart. I review the implications of the accretion properties and orbital solution in a broader context and discuss what might be happening to the circumstellar disk in this system in Section 4.6. I end with conclusions in section 4.7.

4.2 X-Ray Data

As part of a key programme monitoring campaign of the SMC and 47 Tuc, *INTEGRAL* observed the SMC for approximately 90 ks per satellite revolution ($\sim$3 days) between 2008 November 11 and 2009 June 25 (see Coe et al. 2010 for more details). IGR J01054-7253 was detected by an *INTEGRAL/IBIS* observation on MJD 54989 as a new X-ray source (Bozzo et al., 2009). Table 4.1 gives the observation dates and exposures relating to the detection of this object. Unfortunately, these were the

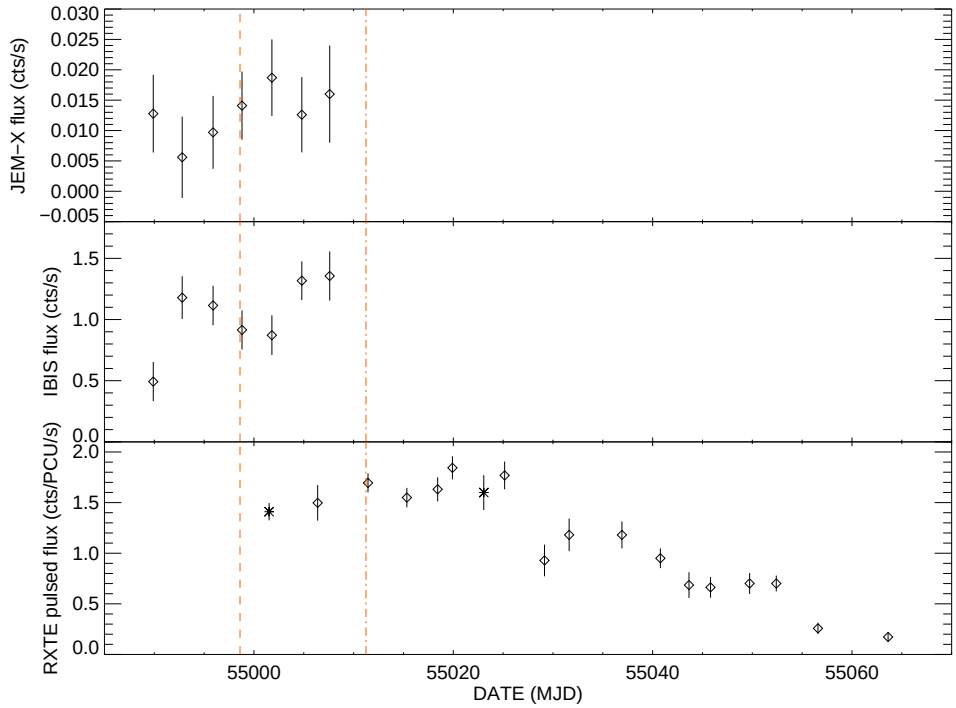

Figure 4.1: Combined *INTEGRAL* and *RXTE* light curve of IGR J01054-7253. The JEM-X flux (top panel) and *RXTE* pulsed flux (bottom panel) are both in the 3–10 keV band, whilst the IBIS flux (middle panel) is in the 15–35 keV band. The two *RXTE* points marked with a cross rather than a diamond are the observations used to extract spectra - see text and Figure 4.6 for details. The vertical dashed and dot-dashed lines represent the time of *Swift* and *XMM-Newton* observations respectively.

last seven observations of the key programme and Rev. 812 was the first observation of the SMC for nearly 45 days. As such I cannot be certain how long the source had been in outburst for before *INTEGRAL* discovered it; it was in the *RXTE* field of view, but only at a collimator response of approximately 0.15, making detection difficult. Likewise, the source was only detected with *INTEGRAL* up to Rev. 818 which, as discussed below, was nearly two months before the source switched off. Data were reduced as described in Chapter 3. Light curves in the 3–10 keV (JEM-X) and 15–35 keV (IBIS) energy bands were generated on science window ($\sim$2000 s) and revolution time-scales. Figure 4.1 shows the JEM-X (top panel) and IBIS (middle panel) revolution light curves of IGR J01054-7253. The JEM-X light curve appears to be mostly constant within errors, whereas some variation in the hard X-ray flux is apparent from the IBIS light curve. By eye it also appears that the hard and soft X-ray flux are anticorrelated with one another. However, plotting the hardness of the outburst in the ratio (15–35)/(3–10) keV against time showed no

real evidence for a change in the hardness of the X-ray emission. Timing analysis on the *INTEGRAL* light curves was not possible due to low count rates.

A *Swift*/XRT follow up observation of the source took place on MJD 54998.6 aimed at refining the *INTEGRAL* position and searching for pulsed X-ray emission. The observation revealed a precise position for this source of RA = 01:04:41.41, Dec = -72:54:04.6 (J2000.0) with a 3.6 arcsec error circle (Coe et al., 2009). This position lies within 3.5 arcsec of the V=14.8 star [M2002] SMC 59977 which is now thought to be the optical counterpart. Further data on the counterpart are presented later in the chapter. Timing analysis performed on the XRT data is reported in Coe et al. (2009). Those authors suggest that the most significant periodicity was 17.49s, although this is now known to be incorrect. The correct 11.48s period was not found in the XRT data until after *RXTE* had found the correct period (Corbet et al. 2009; IGR J01054-7253 will here-on be referred to as SXP11.5). *RXTE* observations began three days after the *Swift* observation, once the source location had been refined, and lasted for just over two months. The PCA made a total of 18 exposures in Good Xenon mode during this time. The average exposure time was $\sim$6ks per observation. These data were then binned at 0.01s before being background subtracted to produce cleaned light curves in the 3–10 keV band. The cleaned light curves were then barycentre corrected and normalised to the number of PCU's on at each time interval during the observation. The *RXTE* pulsed flux detections are presented in the lower panel of Figure 4.1. As can be seen, the pulsed flux peaked at around MJD55020 and steadily declined until dropping below the *RXTE* sensitivity level (about 1×10^{36}ergs s^{-1} at the SMC). The peak detected luminosity of the source was 1×10^{37}ergs s^{-1} in the 3–10 keV band, using the average of several pulsed fraction measurements of 0.16. Although the pulsed fraction was only measured using a simple $\frac{max-min}{max+min}$ method, and as such does not take into account the complex shape of the pulse profile, it is in good agreement with the *XMM-Newton* measurement calculated later in this section and the pulse shape does not change much during the outburst, suggesting that these measurements are quite robust.

More information can be gained about the pulsed component in this system by looking at the power spectra and folded light curves. An example power spectrum that is representative of most of the observations is shown in Figure 4.2. The dominant periodicity detected was the third harmonic, with the fundamental period and the fourth and fifth harmonics detected at lesser powers. This behaviour is also seen in the phase-folded light curves. Figure 4.3 shows two examples of the 3–10 keV light curves folded at the spin period observed by *RXTE*. The profile in the upper panel shows how the third harmonic dominates the emission on MJD 55019

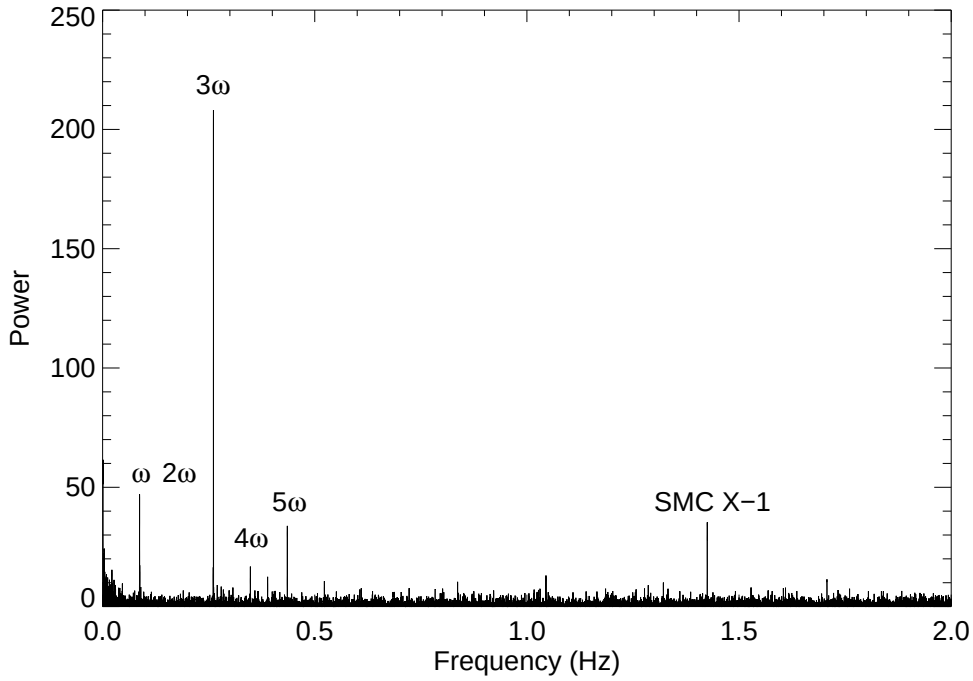

Figure 4.2: Power spectrum of IGR J01054-7253 showing the 11.5s spin period and the third, fourth and fifth harmonics. The second harmonic is not seen. SMC X-1 is also detected at higher frequencies.

with an unusual triple structure; this shape is representative of all of the other profiles until the last few observations of the outburst. The profile in the lower panel shows how the emission geometry had changed into a profile dominated by the fundamental frequency by the end of the outburst, as shown by a much more single peak dominated profile. I also note here that a search over the entire 14 years of monitoring data from *RXTE* reveals no previous detections of this source, although this may be due to a consistently low collimator response of less than 0.2. Another way of exploring the emission on the neutron star surface is to divide an observation up into several energy bands and fold each light curve on the detected period, giving energy dependent phase-folded light curves. Figure 4.4 shows the 3–10 keV (soft) and 10–30 keV (hard) *RXTE* folded light curves from the observation made on MJD 55023. The soft profile is very similar to that shown in the top panel of Figure 4.3, demonstrating that there was little variation in the emission in this energy range. Comparing the soft and hard profiles however, shows evidence for a change in structure; the 3rd peak in the profile changes from being smaller than the other two to a comparable height. This is possible evidence that the emission mechanism is different at different energies. This will be discussed further in section 4.6.

SXP11.5 was serendipitously detected during one observation of the *XMM-Newton*

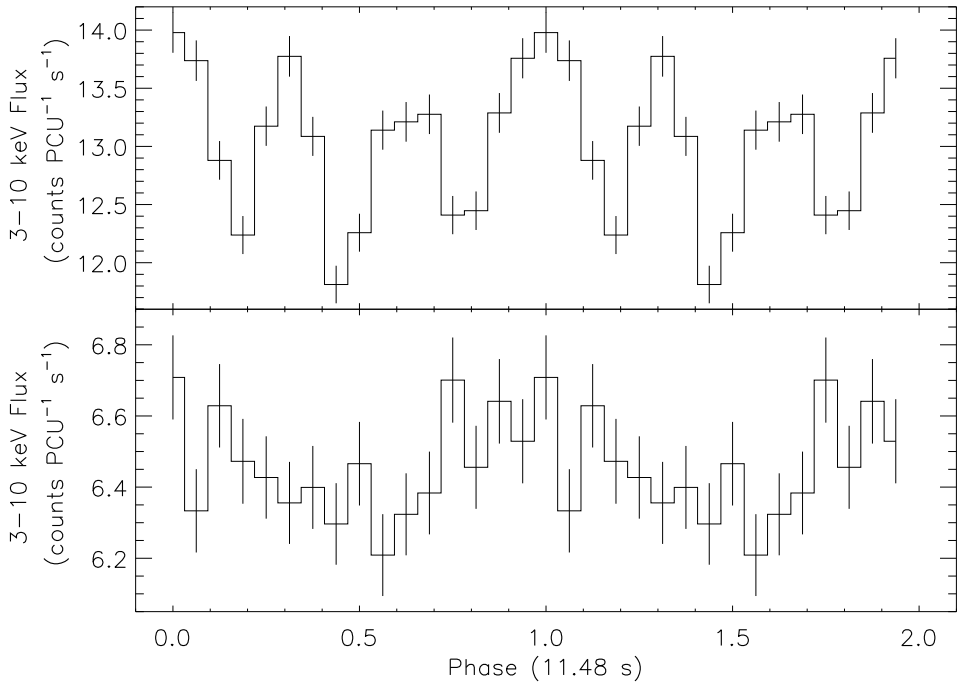

Figure 4.3: *RXTE* 3–10 keV light curves folded at the observed spin period during the peak of the outburst (top panel: MJD 55019) and just before the end of the outburst (bottom panel: MJD55056). The pulse profiles have been smoothed and arbitrarily shifted in phase for viewing purposes.

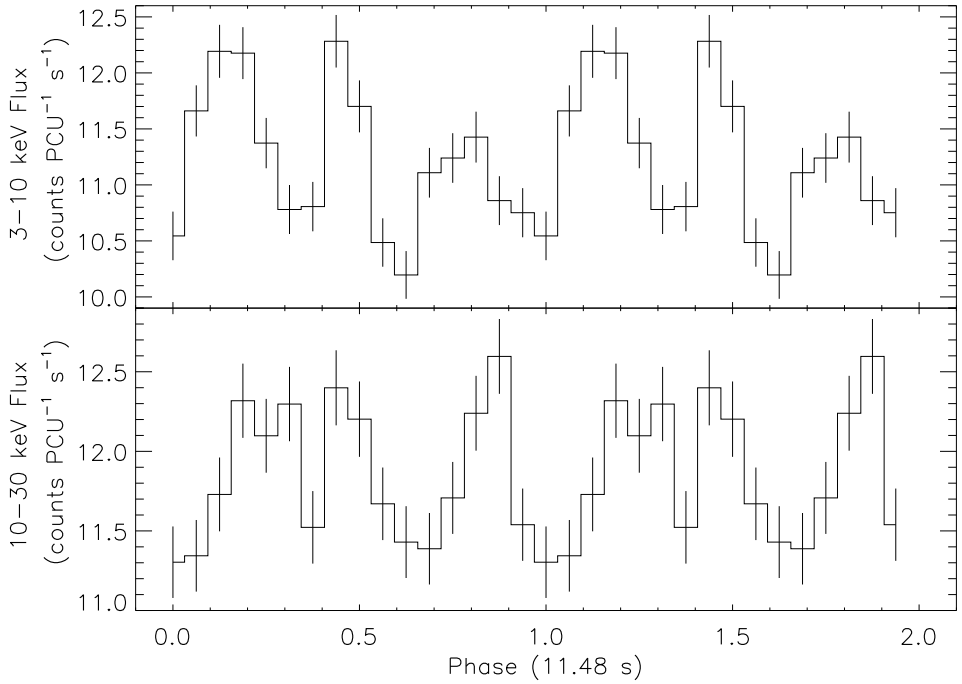

Figure 4.4: *RXTE* pulse profiles in the soft (3–10 keV) and hard (10–30 keV) energy bands from the observation on MJD 55023.

(Jansen et al., 2001) large programme SMC survey (Haberl & Pietsch, 2008b) on MJD 55011.24–55011.59 (ObsID 0601212601). The source was visible only in CCD7 of EPIC-MOS1 (Turner et al., 2001) at the very rim of the detector, where a light path outside the nominal FOV exists due to a gap in the instrument structure (cf. Turner et al. 2001, Figure 11). The calibration for this region might not be as advanced as for the rest of the detector.

XMM-Newton SAS10.0.0[1] was used for data processing. Sources were identified in the FOV for astrometric boresight correction (ΔRA = -3.49", ΔDec = 0.63") and obtained for SXP11.5 a revised *XMM-Newton* position of RA = 01:04:41.60, Dec = -72:54:04.5, which agrees very well with the position determined by *Swift*. A systematic error of ~ 4 arcsec was estimated, since the source lies at a large off-axis angle of ~ 17 arcmin. For data reduction, events were selected with `PATTERN`$\leq$`12` in an elliptical extraction region, placed on the source, and a box, lying on the point source free part of the light-leak region, respectively. Filtering of periods with high background was not necessary, since soft proton flares were at a quiescent level, yielding a net deadtime corrected exposure of 24.3 ks. For spectral analysis, only events with `flag = 0xfffeffff` (similar to `flag=0`, but including events outside the nominal FoV) were used. The spectrum was binned to contain ≥ 20 counts bin^{-1} and response matrices and ancillary files were created using the SAS tasks `rmfgen` and `arfgen`.

The power density spectrum of this observation exhibits a peak at the period found by *RXTE* at 0.087 Hz. Using a Bayesian periodic signal detection method (Gregory & Loredo, 1996) yields a pulse period of (11.483 ± 0.003) s (1σ error). The *XMM-Newton* detection independently confirms both the position of this source and its spin period. The folded pulse profile in different energy bands is plotted in Figure 4.5. The shape of the 0.2–10.0 keV profile is relatively sinusoidal and a calculated pulsed fraction of 0.16 agrees with *RXTE* measurements. Although the third harmonic is not seen in the *XMM-Newton* data, probably because it is close to the detector timing resolution of 2.6s, the profiles show that there is very little variation in the X-ray emission amongst these energy bands.

Figure 4.6 presents the simultaneous fit to the *XMM-Newton* (black) and *RXTE* spectra (red and green taken 10 days before and 12 days after the *XMM-Newton* detection respectively - see Figure 4.1). The two *RXTE* spectra were chosen as they are the ones taken closest in time to the *XMM-Newton* spectrum that contain no other active pulsar in the field of view, based on the *RXTE* power spectrum for that obser-

[1]Science Analysis Software (SAS), http://xmm.esac.esa.int/sas/

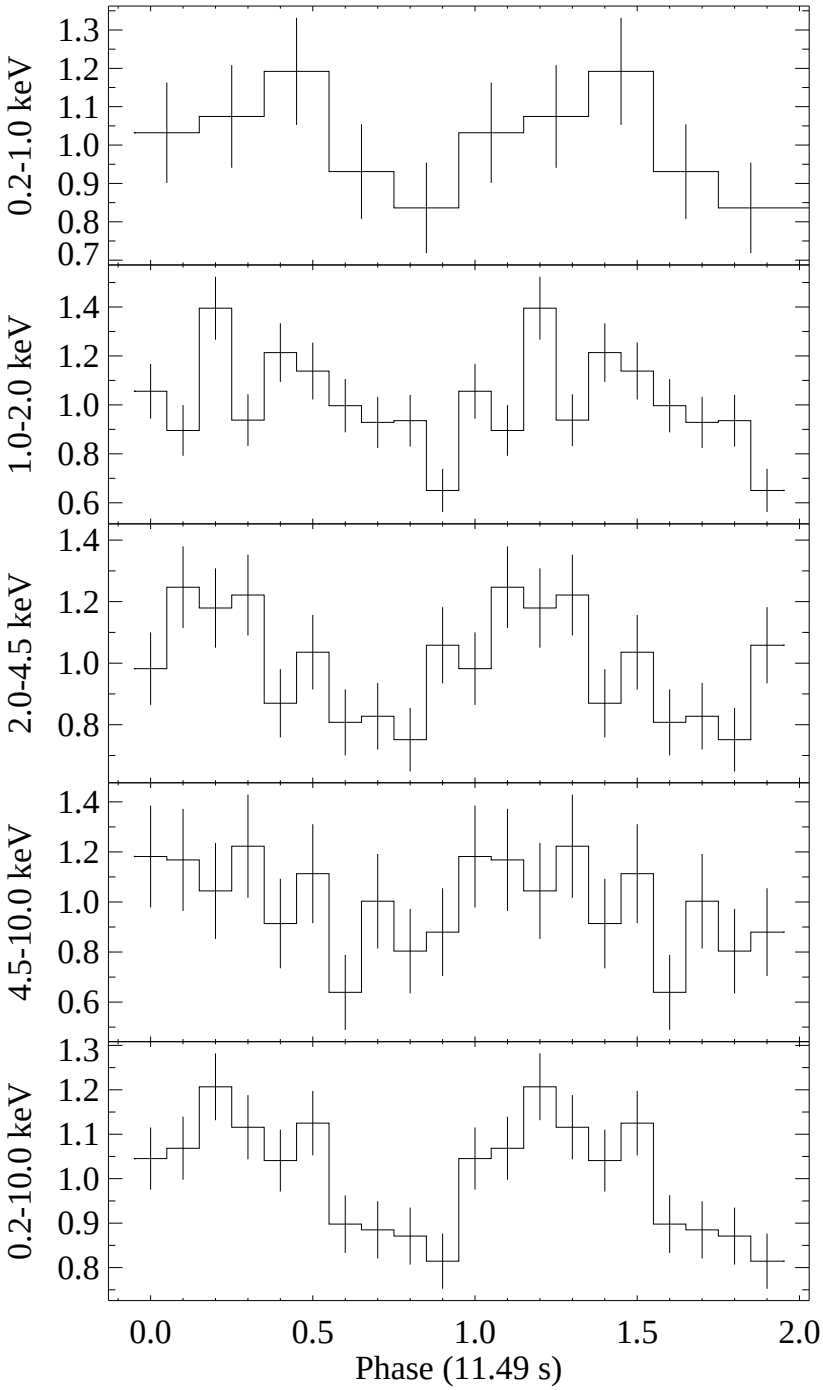

Figure 4.5: *XMM-Newton* pulse profile of SXP11.5 derived from MOS 1 data in different energy bands. The profiles are background subtracted and then plotted as a ratio to the mean count rate. The mean count rates for the energy bands used are (from top to bottom): (1.24, 3.44, 2.88, 1.18 and 8.75) x 10^{-2} cts/s.

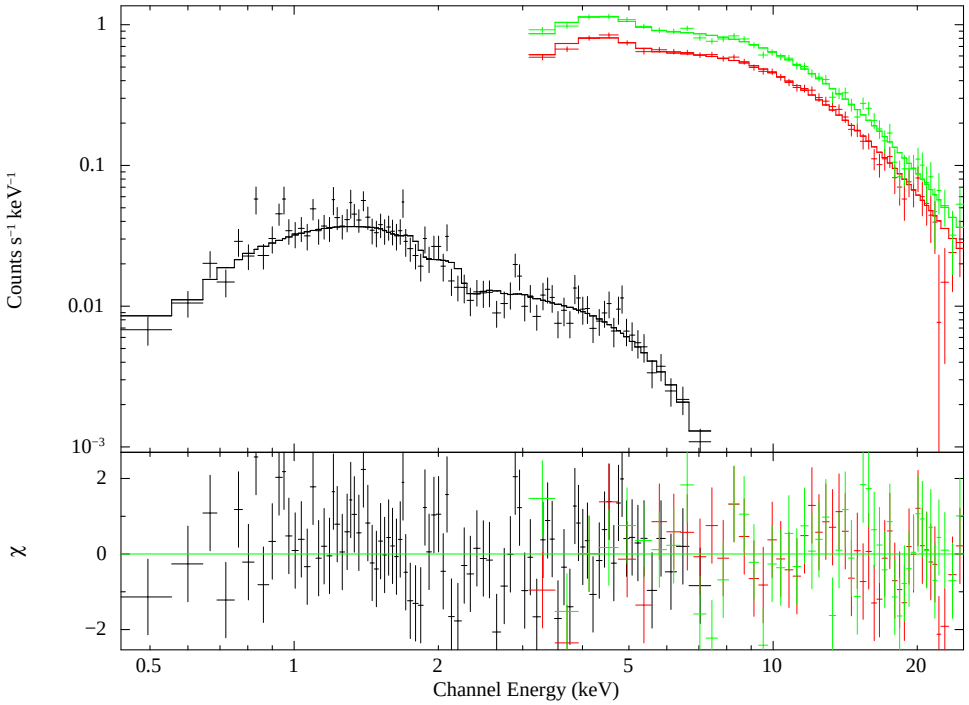

Figure 4.6: *RXTE* & *XMM-Newton* spectra recorded during the outburst. The *XMM-Newton* spectrum was taken on MJD 55011 and is shown in black. The *RXTE* spectra were taken on MJD 55001 & 55023 (red and green respectively). All three spectra were fit simultaneously with an absorbed power-law with high-energy cutoff allowing only a constant normalisation factor between the three spectra under the assumption that the spectral shape does not change. The model fit is presented in the text.

vation. The spectra were modelled with an absorbed power-law with a high-energy cutoff allowing only a constant normalisation factor between the three spectra with the assumption of no change in the spectral shape (only intensity changes). The flux during the *XMM-Newton* observation was apparently significantly lower (although there is some uncertainty due to the far-offaxis source position). The Galactic photoelectric absorption was fixed at $N_H = 6\times10^{20}\mathrm{cm}^{-2}$ (Dickey & Lockman, 1990), whereas the SMC column density with abundances at 0.2 for metals was a free fit parameter. A best-fit was obtained with $\chi^2/\mathrm{dof} = 184/179$ with the best-fit parameters: $N_{H,SMC} = 2.30^{+0.63}_{-0.60}\times10^{21}\mathrm{cm}^{-2}$, $\Gamma = 1.06^{+0.05}_{-0.05}$, cutoff energy = $9.24^{+1.87}_{-0.98}$ keV, folding energy = $22.0^{+4.2}_{-4.2}$ keV and a detected flux of $(7.81\pm0.57)\times10^{-12}$ ergs $\mathrm{cm}^{-2}\mathrm{s}^{-1}$ in the 3–10.0 keV band. Assuming a distance of 60 kpc, this corresponds to an unabsorbed *XMM-Newton* luminosity of $L_{3-10.0} = (3.35\pm0.25)\times10^{36}$ ergs s^{-1}. The luminosity of the two *RXTE* observations found using the normalisation fit are $L_{3-10.0} = (1.79\pm0.07)\times10^{37}$ ergs s^{-1} and $L_{3-10.0} = (2.54\pm0.11)\times10^{37}$ ergs s^{-1} for the red and green spectra respectively. These agree nicely with the value ob-

tained using the pulsed flux light curve and the pulsed fraction. The *XMM-Newton* value is much lower than the values found in the *RXTE* observations. It is unclear how much of this difference is due to source variability and how much is due to the unusually far off-axis position of the source on the MOS detector. For comparison, this model was also fit to the spectrum from the *Swift* observation. The luminosity was found to be $L_{3-10.0} = (9.51 \pm 0.48) \times 10^{36}$ ergs s^{-1}. This value is a factor of 2 smaller than the *RXTE* value measured just 3 days later, but could be explained by variability within the source at the start of the outburst.

SXP11.5 was also in the FOV of a previous *XMM-Newton* observation on MJD 54010.99–54011.26 (ObsID 0402000101), when no significant X-ray emission at this position was detected. Analysis of the EPIC-pn data revealed a 3σ upper limit of 0.002 cts s^{-1} for the 0.2–12.0 keV energy band, which, assuming the same spectrum as above, corresponds to an unabsorbed luminosity limit of $L_{0.2-10.0} \leq 6.4 \times 10^{33}$ ergs s^{-1}.

4.3 Orbital Solution to IGR J01054-7253

It became apparent after the first few *RXTE* observations that there were both spin-up and spin-down trends in the pulse period of SXP11.5, indicative of Doppler shifted X-rays caused by the orbital motion of the neutron star around the companion star. Figure 4.7 shows the detections of the third harmonic of the pulse period during the outburst and the associated errors. Overplotted is the model fit to the data as discussed later. The third harmonic was used to fit the model because it was several times more powerful in the power spectrum than the fundamental frequency (Figure 4.2) and so the associated errors are smaller. The error bars increase in size towards the end of the outburst as the pulsed emission became much weaker as the pulsar switched off. The final two data points are one third of the detected fundamental period as the third harmonic had disappeared by this point (see discussion) and the first data point is the *Swift* detection, which is also one third of the detected period as, like the MOS-1 detector on *XMM-Newton*, it was not possible to detect the third harmonic due to longer binning needed with such a low count rate source. Due to the length of the gaps between observations, it was not possible to match phase between them and do more accurate pulse arrival time analysis.

As mentioned, the oscillatory nature of the spin period is most easily explained by the Doppler shifting of the X-ray light from the neutron star by the binary orbital motion in the system. In the simplest example of the orbital plane being perpen-

dicular to our line-of-sight (inclination, $i = 0$), any change seen in the spin period of the neutron star should be due to torque produced by accretion onto the neutron star surface. The most common result of this is for the spin period to decrease over the length of the outburst. This is known as spin-up. However, in some cases it is seen that the spin period *increases* during phases of accretion. This is known as spin-down. Spin-down also occurs during phases in which there is no accretion due to torques exerted by the magnetic field of the neutron star. In the more generic case of the orbital plane being at some angle to our line-of-sight, we see more complicated spin period variations. Convolved with the standard spin-up of the neutron star, there will be a shifting of the X-ray pulse arrival time caused by the orbital motion of the neutron star around its counterpart. It is because of this that the orbit fitting code simultaneously fits a simple spin-up model and a radial velocity model

$$P_{obs} = \left(1 + \frac{v(t)}{c}\right) P(t) \tag{4.1}$$

where P_{obs} is the detected spin period of the pulsar, c is the speed of light and $v(t)$ is the binary radial velocity. $v(t)$ is calculated using the IDL routine BINRADVEL.PRO from the AITLIB[2] which uses the procedure of Hilditch (2001) and employs the method of Mikkola (1987) to solve Kepler's equation. The spin of the pulsar is given by $P(t)$ which incorporates the spin-up component and is defined below:

$$P(t) = P(t_0) + \dot{P}(t - t_0) - \frac{\ddot{P}(t - t_0)^2}{2} \tag{4.2}$$

where $\dot{P}$ and $\ddot{P}$ are the spin-up and change in spin-up of the neutron star. A least-squares fit is performed on the data which then returns the best fitting parameters. The full spin-up component shown in equation 4.2 was fit to the outburst. Standard values for other HMXB systems were used for initial parameters that were unknown. After first running a simplified version of this model that assumed a circular orbit, it was clear that an acceptable fit could only be achieved by including an eccentricity component and excluding $\ddot{P}$ as the data were not sufficient to fit the second derivative. The final fit gave an orbital period of 36.3 $\pm$ 0.4d and a $\dot{P}$ of (4.7 $\pm$ 0.3) $\times 10^{-10}$ss^{-1} (see also Townsend et al. 2009). The model fit to the data

[2]Developed at the Institut für Astronomie und Astrophysik, Abteilung Astronomie, of the University of Tübingen and at the University of Warwick, UK; see http://astro.uni-tuebingen.de/software/idl/

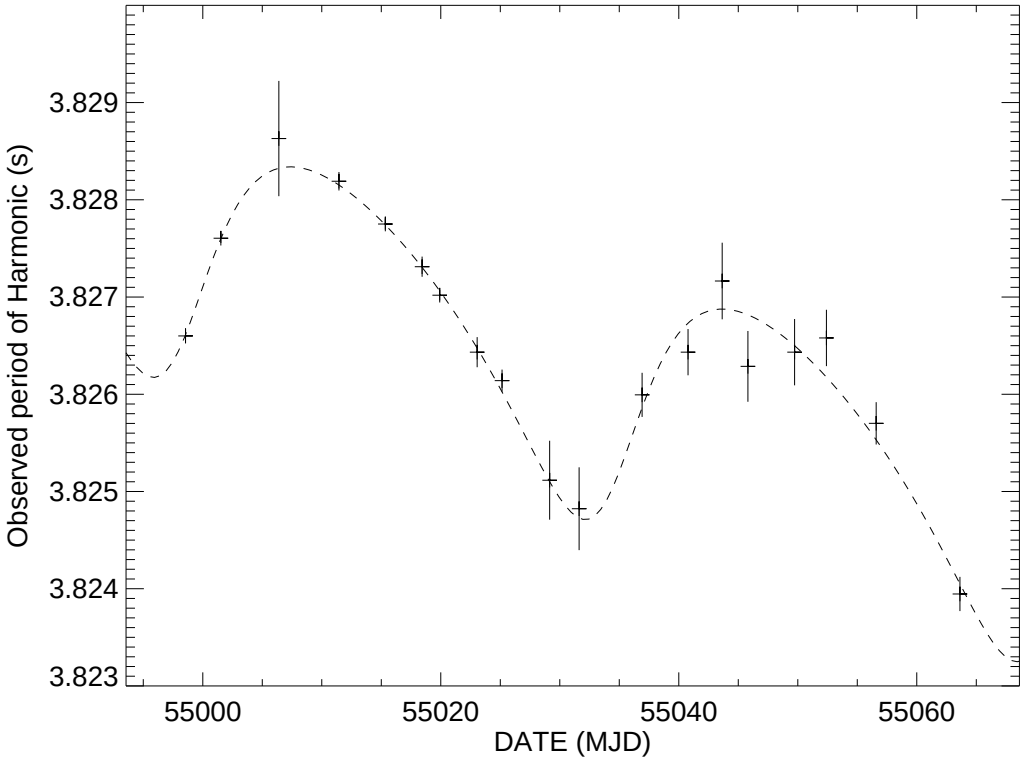

Figure 4.7: Period of the third harmonic of SXP11.5 as detected by *RXTE* during the two months of pointed observations. The final two data points are one third of the detected fundamental period as the third harmonic had disappeared by this point and the first data point is one third of the period detected by *Swift* (see text). Overplotted is the model fit to the data as described in the text.

Table 4.2: The orbital parameters for IGR J01054-7253 from the analysis of 3–10 keV *RXTE*/PCA data.

Parameter		Orbital Solution
Orbital period	$P_{orbital}$ (d)	36.3 ± 0.4
Projected semimajor axis	$a_x \sin i$ (light-s)	167 ± 7
Longitude of periastron	ω (^{o})	224 ± 10
Eccentricity	e	0.28 ± 0.03
Orbital epoch	$\tau_{periastron}$ (MJD)	55034.3 ± 1.0
Spin period	P (s)	11.48143 ± 0.00001
First derivative of P	$\dot{P}$ (10^{-10}ss^{-1})	-4.7 ± 0.3
Goodness of fit	χ^2_ν	0.82

is shown in Figure 4.7 and the various parameter values are displayed in Table 4.2 along with the reduced chi-squared value.

4.4 Optical and IR Data

In this section, I present spectroscopic and photometric data in the optical and NIR wavebands from a variety of ground-based telescopes. The aims of this were to spectrally classify the optical counterpart and to explore the changes in the circumstellar disk leading up to, during and after the X-ray outburst.

4.4.1 Observatories and Instrumentation

- OGLE III & IRSF - see Chapter 2 for details.
- Faulkes Telescope - FT South, located at Siding Spring, Australia is a 2m, fully autonomous, robotic Cassegrain-type reflector which employs a Robotic Control System (RCS) (Tsapras et al., 2009). The telescope was used both in Real Time Interface (RTI) mode and Offline mode for the observations of SXP11.5. All the observations were pipeline-processed which does the flat-fielding and de-biasing of the images.
- 1.9m Radcliffe telescope at the South African Astronomical Observatory (SAAO) - Photometry was done using the SAAO CCD at the Cassegrain focus. The spectra were obtained using the unit spectrograph combined with a 1200 l/mm grating and the SITe detector at the Cassegrain focus. Data reduction was performed using standard IRAF packages.
- X-shooter - The first of the second generation VLT instruments, X-shooter (D'Odorico et al., 2006), is a three arm, single object echelle spectrograph for the Cassegrain focus of one of the VLT UT's. The instrument simultaneously covers the wavelength range 300-2400 nm at resolving powers R = $\frac{\lambda}{\Delta\lambda}$ = 5100, 8800 and 5600 in the UVB ($\Delta\lambda$ = 300-550 nm), VIS ($\Delta\lambda$ = 550-1015 nm), and NIR arms ($\Delta\lambda$ = 1025-2400 nm) respectively. However, the resolution obtained is dependent on the slit width and seeing conditions.

4.4.2 Photometry

Figure 4.8 shows the full 12yr optical light curve of SXP11.5 from OGLE monitoring (open black triangles) and coverage from Faulkes Telescope (FT; closed red

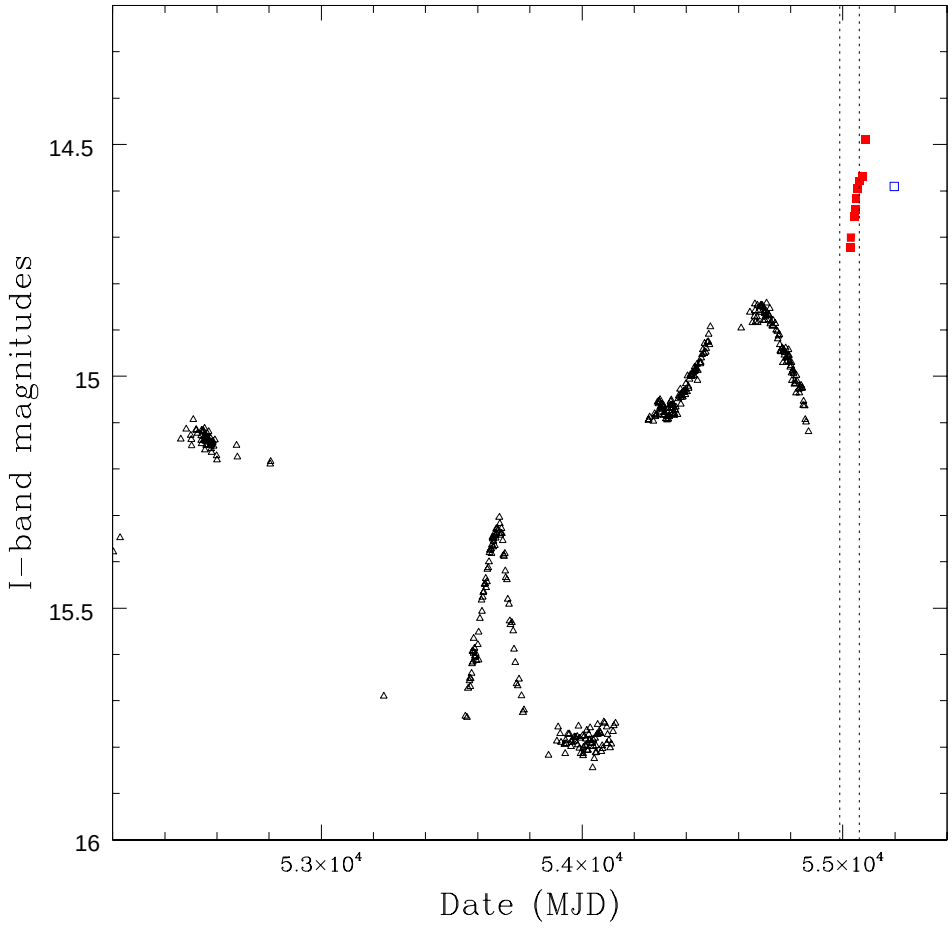

Figure 4.8: Combined OGLE III, Faulkes Telescope (FT) south and SAAO 1.9m I-band light curve of the optical counterpart in SXP11.5 (open black triangles, closed red squares and open blue square respectively). The FT I-band data have been transformed into the OGLE I-band for direct comparison of the magnitude of the star. The vertical dashed lines indicate the start and end of the Type II X-ray outburst as seen by *INTEGRAL* and *RXTE*; this time period spans approximately two orbital cycles, illustrating the scale of the optical variability.

squares) south and the 1.9m, SAAO telescope (open blue square). The FT I-band data were calibrated onto the OGLE I-band using 18 field stars from the OGLE database that show no variability over the set of measurements. The OGLE data are sparse compared to the normal coverage of the SMC because this system occasionally falls onto a gap in the detector chip which is dependent on its orientation angle. Despite this, the data presented were detrended by subtraction of a 50 day moving mean model to remove large amplitude variability, allowing timing analysis to be performed. A Lomb-Scargle periodogram of the detrended light curve shows the presence of a 36.70 $\pm$ 0.03d periodicity above the 99.9% significance

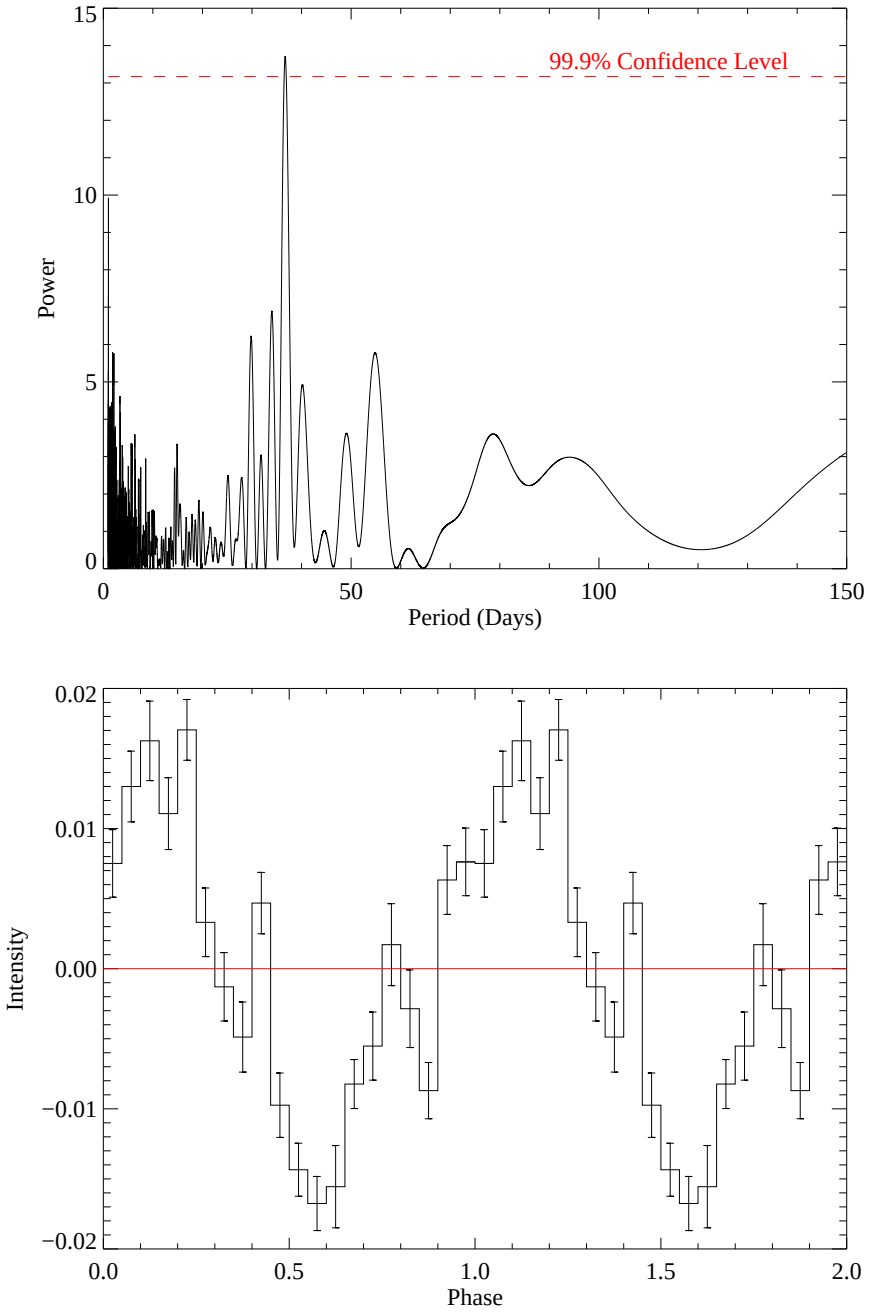

Figure 4.9: Lomb-Scargle periodogram of the detrended section of the OGLE III light curve between MJD 53400 and MJD 54200 (top). A peak at 36.70 $\pm$ 0.03d is seen above the 99.9% significance level, verifying the orbital period predicted by the X-ray data. This period was only detected in this section of the light curve when the disk was seemingly at its lowest flux level. Analysis of other individual sections and the light curve as a whole did not reveal any significant periods. The phase-folded light curve (bottom) is folded such that a phase of 1.0 in the figure corresponds to periastron of the neutron star based on the result of the X-ray fit.

Table 4.3: IR and optical data of the counterpart to SXP11.5.

Catalogue	Date (MJD)	J	H	K_s
2MASS[1]	51035	14.16 ± 0.03	13.70 ± 0.04	13.52 ± 0.04
SIRIUS[2]	52894	14.21 ± 0.08	13.75 ± 0.06	13.74 ± 0.04
Telescope	Date (MJD)	J	H	K_s
IRSF	55196	14.23 ± 0.04	13.75 ± 0.03	13.61 ± 0.04
Telescope	Date (MJD)	B	V	I
1.9m	55200	14.91 ± 0.31	14.91 ± 0.11	14.59 ± 0.10

[1]Skrutskie et al. (2006), [2]Kato et al. (2007).

level, as shown in Figure 4.9. This periodicity was only detected in certain sections of the light curve, but confirms the orbital period predicted from the X-ray data. Figure 4.9 also shows the phase-folded light curve folded at the detected period and phase aligned to the ephemeris given in Table 4.2. The profile seems to be quite sinusoidal, being brightest just after periastron and faintest just after apastron, suggestive of a slight lag between the periodic brightening of the disk with the phase of the neutron star. The narrow peak and trough at phases of approximately 0.4 and 0.9 respectively are somewhat more peculiar; they may suggest something is happening half way between the optical minimum and maximum. However, on folding the light curve at various phases or with different bin sizes these features come and go, suggesting that they may not be a real physical feature of the system. There are no MACHO or OGLE II data of this source. The OGLE, FT and SAAO data were taken before, during and after the X-ray outburst respectively (see discussion section for interpretation). The orbital period found here was also used as a frozen parameter in a second orbital model fit to the X-ray data. This did improve slightly the errors on the parameters presented in Table 4.2 but only on the order of a few percent.

Photometric data taken on the IRSF and the SAAO 1.9m telescope are shown in Table 4.3, along with measurements previously published in catalogues. The IRSF Magellanic Clouds Point Source catalogue by Kato et al. (2007) was used to calibrate the IRSF data. The Magellanic Clouds Photometric Survey (MCPS) catalogue by Zaritsky et al. (2002) was used to calibrate the 1.9m optical data. The optical photometry is not as good as the IR as can be seen from the associated errors. This is due to the poor seeing at optical wavelengths during the observations, and variability in the conditions during the long integration times required because

of a full moon. Also, the smaller field of view of the SAAO CCD compared with the SIRIUS CCD meant there were fewer stars which could be used to perform the calibration. A pipeline provided by SAAO was used to calculate the PSF magnitude of the optical images after performing flat fielding. The error is calculated by taking the average of the square of the magnitude errors from the MCPS catalogue, for the stars used for calibration, and the standard deviation of the stars from the fitted line. The final error is $\sqrt{\sigma^2_{\text{avg,catalogue}} + \sigma^2_{\text{fit}}}$. Data from the IRSF Magellanic Clouds Point Source catalogue and 2MASS catalogue (Skrutskie et al., 2006) are presented as reference to past IR observations of this source. Unfortunately, the IR data are not directly comparable to the I-band data in the OGLE light curve as both measurements fall into gaps in the data and as such I cannot say if the NIR bands follow what is happening in the I-band. However, I can make two cautious observations; firstly, that there is little variation in the J, H & K band values presented in Table 4.3 and, secondly, that at the time of the SIRIUS catalogue measurement the I-band seems to be much fainter than at the time of the IRSF measurement (assuming the I-band at MJD 53000 is around 15.2 magnitudes in comparison to the present value of 14.6). This suggests that there may be a change in the (I-K) colour in this system. This could signify that a change in the size of the circumstellar disk has caused a flux contribution that is dependent on wavelength, contributing more to the I band than the K band. However, the most frequent observation from other BeXRBs is that the flux in all the bands varies by about the same amount, leaving the colour unchanged. This has always been thought to mean that whilst the disk is growing, its surface temperature is approximately constant. Thus, a change in the colour such as what is observed here could be indicative of a temperature change on the surface of the optically thick circumstellar disk.

4.4.3 Spectroscopy

SXP11.5 was observed during the X-shooter Science Verification (SV1) phase in August 2009 (MJD 55055; $\sim$10d before the X-ray outburst ended), with a total integration time of 1200s[3]. The spectra were reduced with a beta version of the ESO X-shooter pipeline (Goldoni et al., 2006), which uses subtraction of the sky lines based on the procedures developed by Kelson (2003). The pipeline reduction used calibration spectra taken during the commissioning run for order location and tracing, flat fielding and wavelength calibration. The final product from the pipeline is an extracted 2D, wavelength calibrated, rectified spectrum with orders combined

[3]Program ID 60.A-9439(A)

using a weighting scheme. For further data processing and analysis I used a combination of IDL programs and standard IRAF tools. The spectra were then smoothed with a boxcar average of 7, normalised to remove the continuum and then shifted by 150 km s^{-1} (Allen, 1973) to account roughly for the recession velocity of the SMC and hence to place spectral features at approximately the correct wavelengths. These spectra are presented in Figs. 4.10 and 4.12. The UVB arm spectrum is used in the next section to spectrally classify SXP11.5, whilst the VIS arm spectrum is used to measure the Hα equivalent width just before the outburst came to an end. This is discussed and compared to a SAAO Hα measurement taken months later in section 4.6.

4.5 Spectral Classification

The classification of SXP11.5 has been made using the X-shooter UVB arm spectrum presented in Figure 4.10. Immediately obvious is the presence of ionised Helium in the spectrum: He II $\lambda\lambda$4686, 4541 are present, meaning the spectral type must be B0 or earlier (Lennon 1997; Evans et al. 2004). He II λ4200 is weak, and much weaker than He I λ4143, meaning it is later in type than O9. There may be evidence of some Si lines in the spectrum which could stretch the classification to B1, although these are very difficult to confirm above the general SNR of the spectrum. Given the presence of He II λ4686 it would seem that, even if the metal lines are suppressed by the low metallicity of the SMC or masked by rotational broadening of the Balmer and helium lines, a spectral type as late as B1 is unlikely. Walborn & Fitzpatrick (1990) also present spectra with apparent Si lines and classify them as B0, indicating that a classification of B0 would be correct in this case if the Si lines are present. Given that the metal lines in the spectrum are not so obvious, I was limited to using the He I λ4121/He I λ4143 ratio to determine the luminosity class (Walborn & Fitzpatrick, 1990). This line ratio strengthens towards more luminous stars, suggesting that this star has a luminosity class of IV-V. I have also performed a check on this luminosity classification by comparing the absolute magnitude of the source in the V-band with a distance modulus for the SMC of 18.9 (Harries, Hilditch & Howarth, 2003), to determine whether the absolute magnitude of the source is consistent with the estimated luminosity class for this spectral type (using absolute magnitudes for OeBe stars from Wegner 2006). A V-band magnitude of 14.9 (Table 6.2) confirms a luminosity class of IV-V for a spectral type of O9.5-B0, as a star of higher luminosity class would need to be of a later spectral type. This

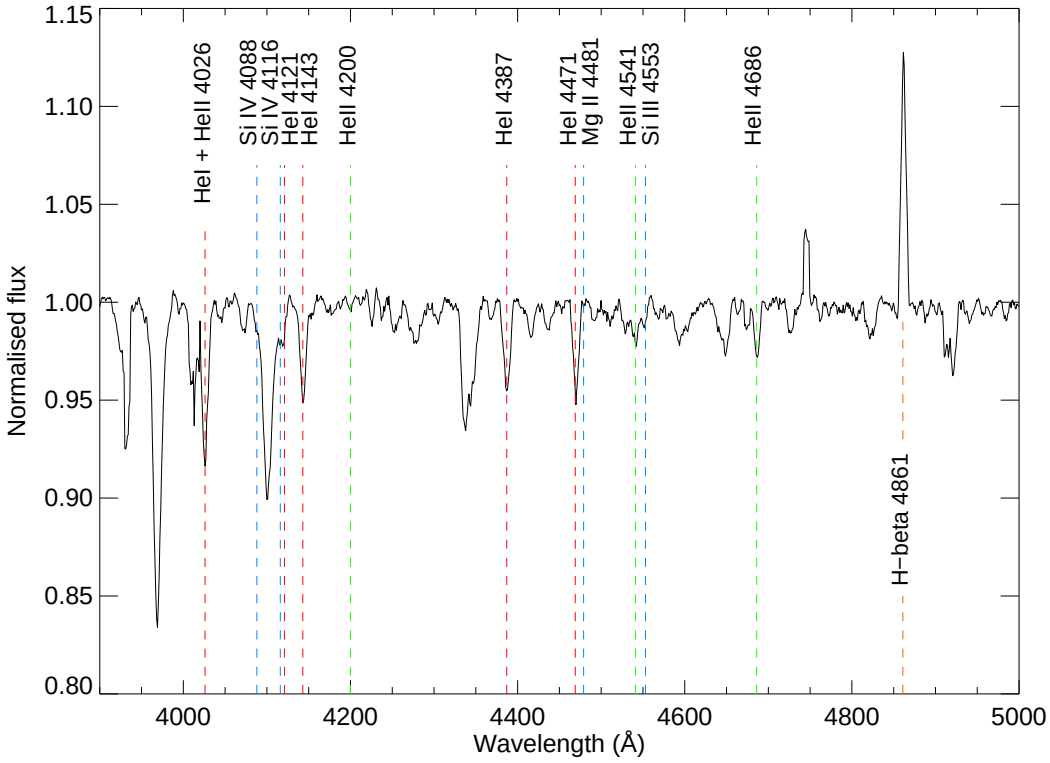

Figure 4.10: Spectrum of SXP11.5 taken with the UVB arm of the X-shooter spectrograph in the wavelength range 300-550nm. The spectrum has been normalised to remove the continuum and the data have been redshift corrected by -150 km s^{-1} to account for the recession of the SMC. Overplotted are various atomic transitions that are significant in the spectral classification of an early type star at their rest wavelengths; He II, He I and metal transitions are in green, red and blue respectively.

spectral classification agrees with recent work done by Masetti et al. (2010) on the SAAO 1.9m telescope, although those authors give a luminosity class of III which may be too early based on the available line ratios in the spectrum.

4.6 Discussion

4.6.1 X-ray behaviour

Strong triple peaked structure is visible in the X-ray pulse profile when the 3rd harmonic was strongest (top panel Figure 4.3). This triple structure remained constant for several observations whilst the outburst was at its most intense. Only once the flux had significantly dropped did the pulse shape begin to evolve into a more familiar single peaked structure (bottom panel Figure 4.3). At this point the 3rd harmonic

fades and the fundamental begins to dominate the pulsed emission. The energy dependent pulse profiles plotted in Figures 4.4 and 4.5 demonstrate a possible change in the X-ray emission at higher energies. The *XMM-Newton* profile seems to show the shape of the folded light curves are very similar within the 0.2–10 keV energy range (although it is noted that some information is being lost here due to the non-detection of the 3rd harmonic). This was also the case for the *RXTE* observations in which the 3–10 keV light curve was split into smaller energy bands (these have not been presented here). However, moving to higher energies in the *RXTE* profiles a change is seen occurring around 10 keV. Below this energy, the pulse profile suggests a combination of a pencil beam from one pole and a fan beam from the other pole, with an orientation that places two sides of the fan beam and the pencil beam approximately one third of a phase apart. The smaller of the three peaks is likely the pencil beam in this picture, being a phase of 0.5 apart from the centre of the fan beam 'double' peak. The hard energy profile shows evidence for a number of possibilities; the pencil beam has increased in strength, becoming comparable to the fan beam. The pencil beam may be narrower, although it remains 0.5 phase away from the centre of the other 2 peaks. The fan beam may have a narrower opening angle at higher energies given the apparent infilling of the gap between the two peaks. At the moment, these are all speculations based on observation and thus more detailed modelling is required to take this discussion further.

The orbital parameters in Table 4.2 are typical of those seen in other BeXRB systems (Okazaki & Negueruela, 2001). Most Be systems have $P_{orb} \sim$ 10-100 d and orbital eccentricities of between 0.3-0.5 (Bildsten et al., 1997). These parameters also place SXP11.5 firmly in the BeXRB regime of the Corbet diagram (Corbet, 1986), lending support to the optical determination that this source is a BeXRB and not a supergiant system.

Ghosh & Lamb (1979) show that there is a relationship for binary pulsars such that $-\dot{P} \propto PL^{\frac{3}{7}}$ for a given neutron star mass and magnetic moment, where $\dot{P}$ is the spin-up in sec/yr, P is the spin period in seconds and L is the X-ray luminosity in units of 10^{37} ergs/s. This relationship has since been verified by Coe, McBride & Corbet (2010) using a much larger database of SMC binary pulsars. The spin period and $\dot{P}$ from the orbital fit above were used along with the highest luminosity recorded by *RXTE* during the outburst to place this new system onto the plot of SMC pulsars presented in Coe, McBride & Corbet (2010). The result is shown in Figure 4.11. The position of this source on the plot seems to follow the general distribution of SMC pulsars and thus agrees with the theoretical laws of binary accretion. Plotted on this figure are some lines showing the expected relationship between the two

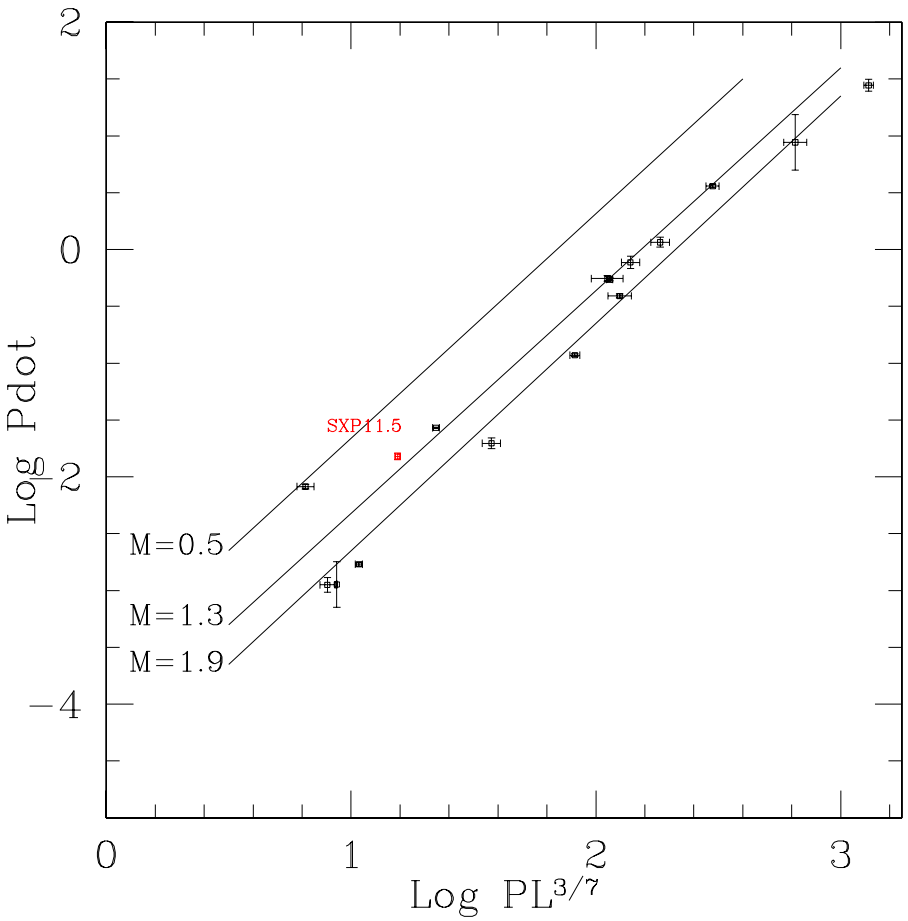

Figure 4.11: The distribution of SMC BeXRB pulsars on the $\dot{P}$ vs $PL^{\frac{3}{7}}$ plane adapted from Coe, McBride & Corbet (2010), where $\dot{P}$ is the spin-up in sec/yr, P is the spin period in seconds and L is the X-ray luminosity in units of 10^{37} ergs/s. SXP11.5 is shown to sit in the low period end of the distribution, confirming that the luminosity, pulse period and spin-up calculated in this analysis agree with the equations originally presented in Ghosh & Lamb (1979) and that this source is, in this sense, normal with respect to the general distribution of SMC pulsars.

parameters for a particular neutron star mass (0.5, 1.3 and 1.9 $M_{\odot}$). The only assumption in producing these relationships is a magnetic moment of 4.8×10^{29} Gauss cm^3 (see Ghosh & Lamb 1979 for further details on the theory behind these relationships). From the position of SXP11.5 on the figure, its mass could be around 1.2 $M_{\odot}$. This value is lower than most other SMC pulsars based on the work of Coe, McBride & Corbet (2010), though not inconsistent with them. In Chapter 5, I consider the orbital solution of SXP11.5 further and what the exact value of the neutron star mass means for the inclination and orbital size of the system.

4.6.2 Optical behaviour

Due to the lower temperatures believed to be present in the circumstellar environment, the photometric I-band data presented in Figure 4.8 are a direct measure of the circumstellar emission. These data show that this system has a highly variable circumstellar disk and that the X-ray outburst was triggered by the disk being in an exceptionally large state, relative to its base level. The vertical dashed lines in Figure 4.8 show the start and end points of the X-ray outburst in relation to the optical activity. A single observation at SAAO in January 2010 (MJD 55200) shows that the disk has started to decrease in size, although the X-ray outburst had finished before the disk had returned to the level at which the X-ray emission began. This could be evidence of a lag between the X-ray and optical emission in this system. Another puzzle that these data introduce is why the orbital modulation in the light curve is only seen at the very lowest flux level. This would suggest that the variability is coming from the stellar atmosphere as the disk would seem to be at a minimum. In contrast Schurch et al. (2011) only detect the orbital modulation from SXP18.3 at the very brightest part of the detrended optical light curve, suggesting that in this system, the variability is coming from the circumstellar disk and not the stellar atmosphere.

It is currently believed that the amount of red and IR emission from the circumstellar disk is directly related to the strength of emission lines in this regime (see Chapter 1). Figure 4.12 shows two spectra of the Hα region taken during and many months after the X-ray outburst. The top panel is a VLT/X-shooter VIS arm spectrum showing clearly Hα being in emission. This corresponds to the peak of the I-band light curve shown in Figure 4.8. Equivalent width measurements of the line profile give a value of -8.0$\pm$0.5Å. The bottom panel is a spectrum taken on the SAAO, 1.9m telescope 4 months after the outburst had ended. This observation was near-simultaneous to the SAAO I-band measurement plotted in Figure 4.8. The poor SNR in this spectrum made it difficult to make a precise equivalent width measurement, the best estimate being -3 $\pm$ 2, so I cannot say by how much the disk has reduced in size. However, I can conclude that both the Hα and I-band measurements suggest the disk is shrinking. Comparison to Hα measurements of other BeXRBs shows that, even during a long Type-II X-ray outburst, the disk in this system was quite small compared to other BeXRBs (see Chapter 1, Figure 1.11). Although SXP11.5 lies below the best fit line of this trend, it is not a complete outlier and may just lie within the distribution. Unfortunately a more quantitative handle on the IR excess seen in the photometry is needed to help verify the true size of the disk

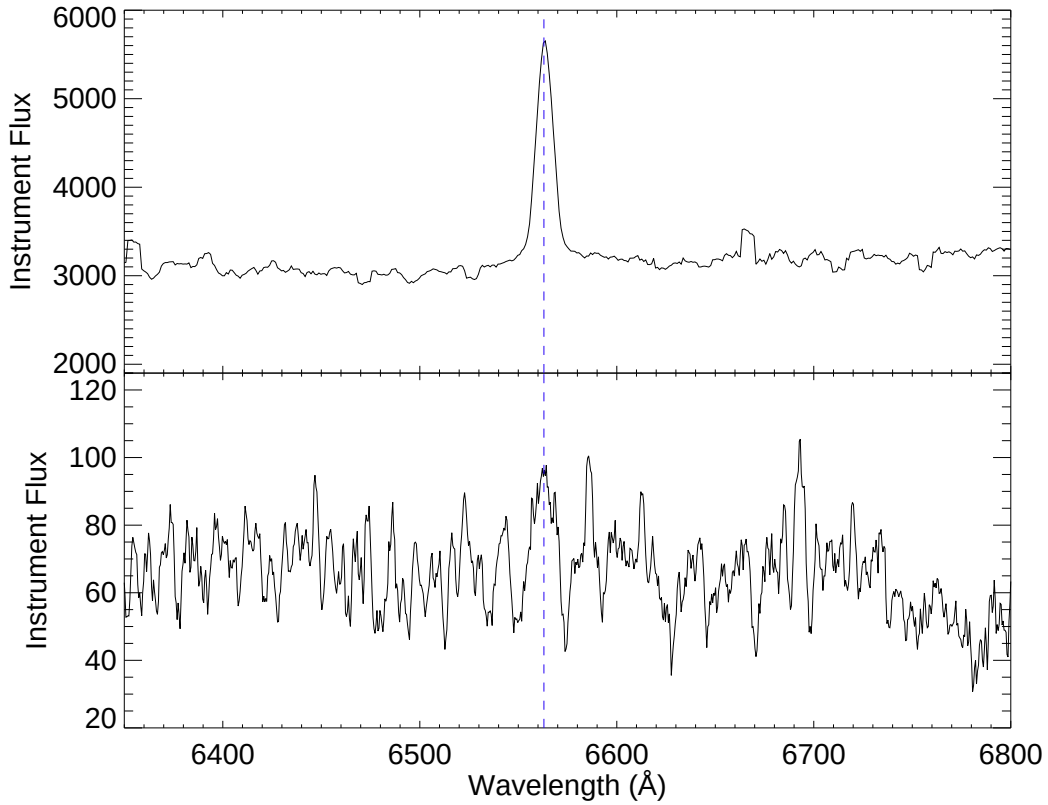

Figure 4.12: Spectra of SXP11.5 taken in the wavelength range of Hα at the VLT (top) and SAAO,1.9m (bottom). The VLT spectrum was taken on 2009-08-12 (MJD 55055), just before SXP11.5 fell below the detection threshold of *RXTE*, therefore showing the disk during an X-ray active phase. The SAAO spectrum was taken on 2009-12-12 (MJD 55177), four months after the X-ray outburst ended.

relative to other systems in the SMC. So given only a small circumstellar disk to accrete from, how does accretion continue for over two months in this system? The most plausible explanation seems to be that an accretion disk has formed around the neutron star, allowing accretion to continue after the neutron star has moved away from the circumstellar disk which may not, in this case, be filling, or be near to filling the orbit of the neutron star. However, it is not easy to detect the presence of an accretion disk in HMXBs and so an unusual orbit or other such geometries cannot be ruled out as an explanation of what is seen, although this seems unlikely based on the fairly standard parameters obtained in the orbital fit of the X-ray data. It is also worth noting that the narrow, single peaked Hα and Hβ emission lines seen in the spectra presented here suggest the disk has a low inclination angle to the observer (Struve, 1930). Comparing this to the value of $a_x \sin i$ presented in Table 4.2 suggests that the semimajor axis of the disk could be over 300 light-s (for $i < 30^\circ$), approximately 18 $R_\star$ assuming a B0 star of radius equal to 7 $R_\odot$.

In order to explore the extent of the emission from the circumstellar disk, the

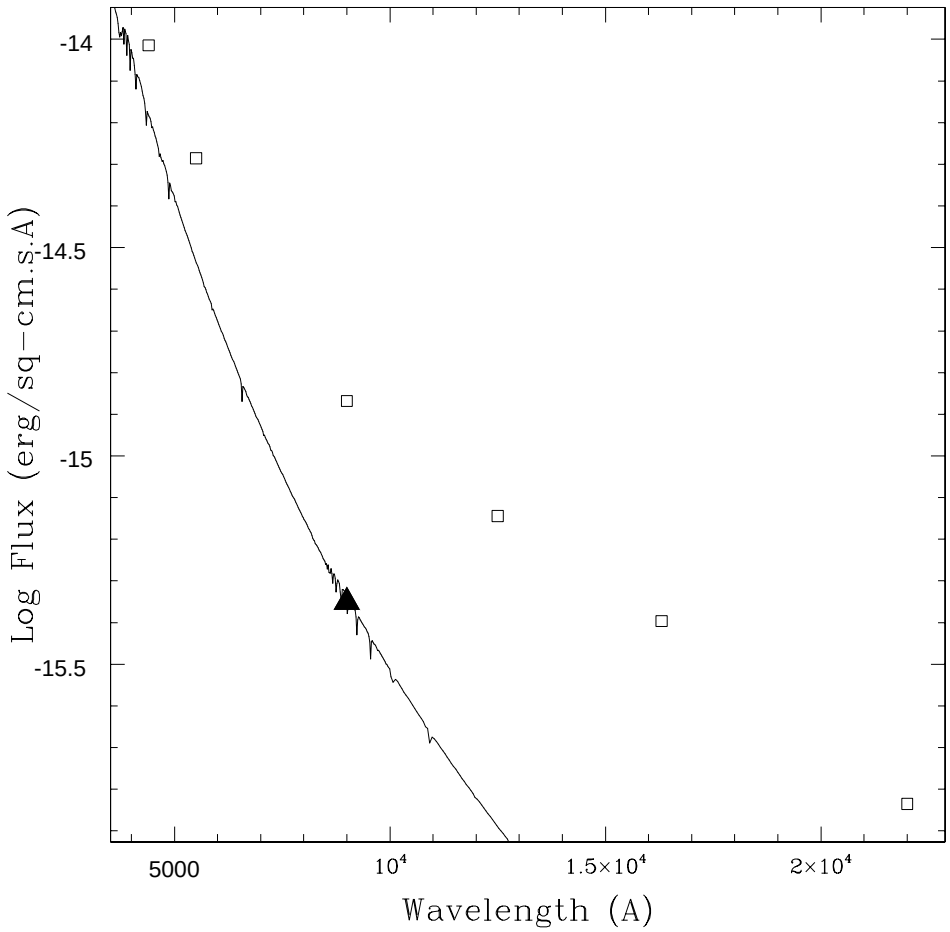

Figure 4.13: The optical & IR photometry (open squares) from MJD 55196-55200 de-reddened and compared to a Kurucz model atmosphere for a B0V star (continuous line). The filled triangle indicates the lowest OGLE III I-band point which has been used to normalise the Kurucz model - see text for details. This demonstrates the extent of the continuum emission from the circumstellar disk in this system.

contemporaneous optical & IR photometric data from MJD 55196-55200 shown in Table 6.2 were used to compare with the predicted stellar emission. The photometric data were first de-reddened by the established value to the SMC of E(B-V)=0.08 (Schwering & Israel, 1991). These were then compared to a Kurucz model atmosphere (Kurucz, 1979) for a B0V star (T_{eff}=30,000K and log g=4.0). To make the comparison, the model atmosphere was normalised to the lowest I-band point in the OGLE III data (taken around MJD 54000) on the assumption that this represents the occasion on which any contribution from the circumstellar disk is at its lowest. The results are shown in Figure 4.13 from which it is immediately apparent that at the time the optical and IR photometry were taken there was a clear disk contribution across the whole of the optical and IR regime. Even the B and V points clearly con-

tain some element of such a component. In trying to quantify this excess, the Kurucz model was normalised to the distance estimate of the SMC (60 kpc) which proved to be very close to the I-band normalised model. Working from this, I converted the I-band flux at this base level into a distance estimate, assuming that all the flux is coming from the star. I find a distance to SXP11.5 of 71$\pm$5 kpc. The error comes from calculating the maximum and minimum distance based on a range of E(B-V) values. Of course, this value is very dependant on obscuration localised to the SMC itself and should be treated with some caution. What this calculation shows is that it is very likely that the I-band measurement used in the normalisation represents very closely the base level of the disk emission in this system. A Hα spectrum is needed to confirm this prediction should the I-band magnitude ever return to this level. Assuming this base flux level contains light only from the star, a simple calculation can be performed to estimate the amount the disk contributes to the flux observed at each wavelength. I estimate that the disk contributes to around 32% of the B-band flux, 43% to the V-band, 67% to the I-band, 83% to the J-band and 90% to the H-band at the time the photometry presented here was taken. This agrees with current ideas that the disk dominates the emission in the near-IR regime. However, it is more interesting to note that the apparent contribution to optical wavebands is rather significant, with around half the red light coming from the disk and around a third of the blue light.

Modelling the disk continuum emission took a significant leap forward with the development of the viscous decretion disk model (see Chapter 1). Whilst I was not able to use this model during this work, the density and size of the disk can be estimated from the disk contributions calculated above and results published in the literature. Touhami, Gies & Schaefer (2011) used such a model to produce tables of flux excess and disk size as functions of disk density and wavelength. The set of parameters that are most similar to those of SXP11.5 published by those authors were used to estimate the disk size and excess. The model parameters are: T_{eff}=30,000K, R_{star}=10 $R_\odot$, M_{star}=15.5 $M_\odot$, inclination=45°, radial density exponent=3, outer disk radius=21.4 $R_\odot$ and disk-to-star temperature ratio of $\frac{2}{3}$. The model does not consider wavelengths shorter than the H-band, so I will consider only this band here. One assumption in their calculations was that there is negligible flux coming from the disk in the V-band. This has been proved a bad assumption here, and indeed those authors also state that the disk can contribute as much as 50% in the largest and densest disks. Thus, it is more precise in this case to use the flux predicted by the normalised stellar atmosphere model than the observed flux. In magnitude space, this excess is of the form

$$E(V-m_\lambda) = 2.5log(1+\frac{F_{disk}}{F_{star}}) \tag{4.3}$$

The result of which is E(V-H)=1.9. Comparing this value with the tables of Touhami, Gies & Schaefer (2011) suggest the disk is very dense, as does the V-band excess, at around $3\times10^{-10}\,\mathrm{g\,cm^{-3}}$. Those authors list a table of Be stars for which they have calculated the IR excesses, most if not all of which have a lower density than SXP11.5. However, the associated disk radius of $\sim 2.6\,R_{star}$ seems quite small and so the estimates made here should be treated as such, until a full calculation can be done based on the exact parameters of SXP11.5. Using the same method for calculating the disk size as in Chapter 3 produces a somewhat larger disk of $\sim 3.5\,R_{star}$ (for an Hα W_{eq} of -8.0$\pm$0.5Å). As was the case for SXP6.85, this is a factor of 3 to 4 smaller than what is suggested by the size of the semi-major axis and the neutron stars persistent interaction with the disk. The ideas raised here and in Chapter 3 will be drawn together in Chapter 7.

4.7 Conclusions

I have presented the complete orbital solution to a newly discovered high-mass binary system in the SMC, making it one of the few well described systems known outside the Galaxy. These parameters are similar to other binary systems in the Galaxy and Magellanic Clouds and place SXP11.5 firmly in the BeXRB region of the Corbet diagram. Under huge accretion torques, it is shown that the neutron star is being spun up and that this satisfies current theoretical predictions of the relationship between spin-up, spin period and luminosity in binary systems. However, it is clear that there is still much to learn about the accretion process itself as shown by the complex triple peaked structure and evolution of the pulse profiles, which are still poorly understood.

Spectral analysis of the companion has allowed a classification of O9.5-B0 IV-V to be made. Timing analysis of the optical light curve confirms the orbital period detected in the X-ray data. Contemporaneous Hα spectra show, along with the optical light curve, that the circumstellar disk is shrinking in the time since the X-ray outburst. Although there is evidence that the disk is unusually small compared to other BeXRBs, making the extended period of accretion seen in this outburst difficult to explain. We show that the lowest flux seen in the optical light curve is likely to be from a period in which the Be star has entirely lost its disk and make estimates of the flux contributions from the disk at each wavelength. This lead to

an estimate of the disk density and size using a viscous decretion disk model with some default parameters. A distance estimate to the source was also made based on the 'diskless' assumption, though Hα spectroscopy is necessary to confirm this prediction should the I-band flux ever return to this level.

SXP11.5 has proved to be a very interesting addition to the SMC binary population; on one hand, it seems to be a very normal system showing orbital parameters and a spectral type that match very well with previously studied systems. However, it also shows peculiarities, such as showing a small Hα equivalent width relative to other systems with similar orbital periods. Should this system go into another X-ray outburst in the future, further simultaneous optical and X-ray measurements are essential to uncovering where this system lies in the overall population of SMC BeXRB systems.

Education is what remains after one has forgotten what one has learned in school.

ALBERT EINSTEIN (1879 - 1955)

5

On the orbital parameters of Be/X-ray binaries in the Small Magellanic Cloud

The orbital motion of a neutron star about its optical companion presents a window through which to study the orbital parameters of that binary system. This has been used extensively in the Milky Way to calculate these parameters for several high-mass X-ray binaries. This chapter describes the use of several years of *RXTE*/PCA data to derive the orbital parameters of four Be/X-ray binary systems in the SMC, increasing the number of systems with orbital solutions by a factor of three. These solutions include one new orbital period, the confirmation of a second and allow for a comparison to the parameters of Galactic systems. Despite the low metallicity in the SMC, these binary systems sit amongst the Galactic distribution of orbital periods and eccentricities, suggesting that metallicity may not play an important role in the evolution of high-mass X-ray binary systems. A plot of orbital period against eccentricity shows that the supergiant, Be and low eccentricity OB transient systems occupy separate regions of the parameter space; akin to the separated regions on the Corbet diagram. Using a Spearman's rank correlation test, a potential correlation between the two parameters is suggested. The mass functions, inclinations and orbital semimajor axes are derived for the SMC systems based on the binary parameters and the spectral classification of the optical counterpart. As a

Table 5.1: Outburst date (T_0), duration and peak X-ray luminosity of the four systems investigated in this study.

Source	T_0 (MJD)	Duration (days)	Peak L_x (10^{37}ergs s^{-1})
SXP2.37	51573	84	21.0
SXP6.85	55435	59	3.3
SXP8.80	55080	39	7.3
SXP74.7	55232	42	3.5

by-product of this work, I present a catalogue of the orbital parameters for every high-mass X-ray binary in the Galaxy and Magellanic Clouds for which they are known. This work has been published as a paper for which Dr. Adam Hill made significant contributions to the orbital fitting code.

5.1 Introduction

The aim of this investigation was to uncover the first sizable sample of orbital parameters of HMXBs in the SMC, using the data taken as part of the *RXTE* monitoring programme described in Chapter 2. This idea was triggered by the orbital fitting of the new pulsar SXP11.5 described in the previous chapter. The *RXTE* data archive was searched for outbursts occurring at any point in the past 14 years that satisfied the following three criteria:

1. The outburst must not be a classical Type I outburst driven by the orbital period of the system (for example, SXP46.6; Chapter 2).

2. The outburst should last for longer than one orbit of the neutron star, where the orbital period is known, or have at least 10 detections during the outburst when the orbital period is not known. This was to ensure enough data was available in the fitting process.

3. Adjacent detections must not have a large gap between them (more than 5 or 6 days) as this would allow for too much ambiguity during the fitting procedure.

This search revealed 12 systems that showed evidence for one or more extended outbursts. Of these, 10 satisfied, or were very close to satisfying, the above criteria. Two of which (SXP11.5 and SXP18.3), had already had their orbits solved. The remaining 8 systems were fit using the method and code introduced in Chapter 4. Half of the systems converged to a satisfactory fit, whilst half did not. It is worth noting here that all 12 systems that could be clearly identified as experiencing an

extended outburst unrelated to the orbital phase of the neutron star have spin periods of less that 100 s. If this can be proven not to be an observational bias, then it may demonstrate a fundamental link between the orbital properties of the binary system and the outbursts seen from them. This idea is discussed further in Chapter 7. Table 5.1 gives a summary of the start time, duration and peak X-ray luminosity in the 3–10 keV band, of the studied outburst for each system that was fitted successfully. The results of the successful fits are presented in the next section. In order to obtain a meaningful fit, the period measurements used in the fitting procedure were restricted to detections greater than a particular significance. This threshold was not kept constant for every source because the luminosity and duration of each outburst was different, meaning fits improved or worsened by including data above different thresholds. As such, a significance threshold was chosen to minimise the (1σ) errors in the binary parameters for each fit. The chosen value is stated in the relevant section. To insure that the errors found on each parameter were not underestimated in the cases of $\chi^2_\nu > 1$, the error bars on each light curve were scaled such that the fit resulted in a χ^2_ν of unity. The result of this is a small increase in the error of each binary parameter. Where this method has been employed, it will be made clear in the relevant table and the original χ^2_ν quoted. In section 5.3 I discuss the orbits derived in the context of the Galactic population and investigate possible relationships between the binary parameters in BeXRBs. The results are summarised in section 5.4.

5.2 Results

5.2.1 SXP6.85 = XTE J0103−728

A detailed history of SXP6.85 is given in Chapter 3 and so will not be repeated here. I mearly remind the reader that, in an analysis of MACHO light curves, McGowan et al. (2008a) find that the source gets redder as it gets brighter, which is suggestive of a low inclination system. Those authors also propose a low eccentricity based on comparison to other systems. There are also four main periodicities associated with the source from the literature: 114.1 ± 0.6 d, 24.8 ± 0.1 d and $\sim$620–660 d from optical analyses and 112 d from X-ray analysis (see Chapter 3). Thus until now, neither the orbital period or eccentricity of this system were known for certain.

To try and resolve this issue, the two longest X-ray outbursts were fit with the orbital model. The outburst occurring around MJD 54800 (this is the main outburst discussed in Chapter 3) turned out to be too sparsely covered, meaning I was unable

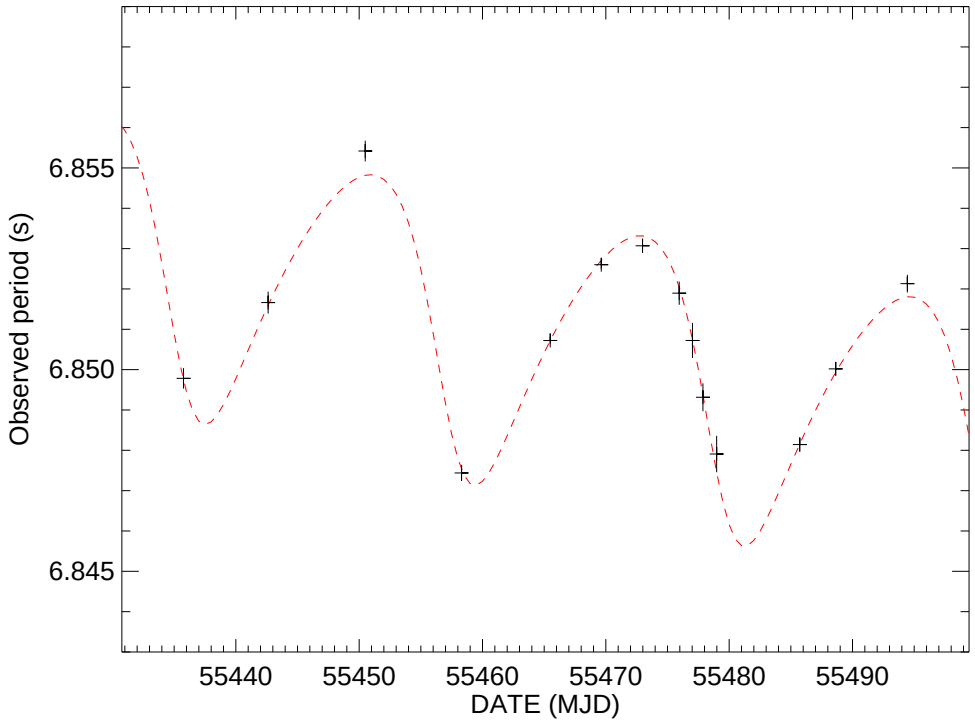

Figure 5.1: The spin period of SXP6.85 as measured by *RXTE* during 2 months of pointed observations. Both the orbital motion of the neutron star and the accretion driven spin-up are visible. Overplotted is the model fit to the data as shown in Table 5.2.

Table 5.2: The orbital parameters for SXP6.85 from the analysis of 3–10 keV *RXTE*/PCA data.

Parameter		Orbital Solution*
Orbital period	$P_{orbital}$ (d)	21.9 ± 0.2
Projected semimajor axis	$a_x \sin i$ (light-s)	151 ± 7
Longitude of periastron	ω (^{o})	125 ± 8
Eccentricity	e	0.26 ± 0.03
Orbital epoch	$\tau_{periastron}$ (MJD)	55479.1 ± 0.5
Spin period	P (s)	6.8508 ± 0.0001
First derivative of P	$\dot{P}$ (10^{-10}ss^{-1})	-8.0 ± 0.6
Goodness of fit	χ^2_ν	1.79*

*This solution is the result of a fit with spin period errors scaled such that $\chi^2_\nu = 1$.

to get an acceptable fit. However, since the work of Chapter 3 (see also Townsend et al. 2010) another luminous, extended outburst occurred, approximately coinciding with the expected time of optical maximum. This outburst, beginning on MJD 55435 (Table 5.1), was sampled very well thanks to dedicated pointings at the position of the source in addition to the regular monitoring. The period evolution is shown in Figure 5.1 with the best model fit overplotted. The data used in the fit were cut at the 99.99 % ($4\,\sigma$) significance level. The very clear changes in the spin period allowed the radial velocity of the neutron star to be found quite simply. Unfortunately, an attempt to fit both outbursts simultaneously was unsuccessful as the amount of spin-down happening between the outbursts is unknown, making the fit hard to constrain. The solution is presented in Table 5.2 and is the best fit to date in the sample of systems presented here. Thus the 21.9 ± 0.1 d period is proposed to be the true orbital period of this system, placing it nicely in the BeXRB region of the Corbet diagram. The other orbital parameters and the nature of the 25 d, 112 d and 114 d periods are discussed in section 5.3.

5.2.2 SXP2.37 = SMC X−2

SXP2.37 was discovered by SAS 3 observations in 1977 (Li, Jernigan & Clark, 1977) as a highly variable X-ray source. Corbet et al. (2001) discovered 2.372 s pulsations from the source during the Type II outburst from January 2000 to May 2000. The proposed optical counterpart to this X-ray source was shown to be a close north-south double (Murdin, Morton & Thomas, 1979). As such, it has been difficult to tell which of the two stars is the true optical counterpart due to large X-ray error circles and the lack of any significant periodicity in OGLE II and the first 5 years of OGLE III data (Schmidtke, Cowley & Udalski, 2006b). It was not until a further 2 years of OGLE III data became available that the correct counterpart revealed itself. Schurch et al. (2011) show there is a clear 18.62 ± 0.02 d periodicity in the final 2 years of the light curve of the northern star, making it very probable that this star is the true counterpart and that the periodicity is the orbital period of the binary system. Schmidtke, Cowley & Udalski (2009) suggest that the 18.6 d period, along with the apparent 9 and 6 d harmonics are caused by 2 nonradial pulsations seen around 0.86 s and 0.9 s. Schurch et al. (2011) argue that because the 18.6 d modulation is visible in the light curve and the folded light curve at this period is typical of other binary systems, the modulation must be orbital in nature. McBride et al. (2008) classify the counterpart as an O9.5 III–V emission line star.

The outburst that led to the discovery of pulsations from SXP2.37 (Corbet et al.,

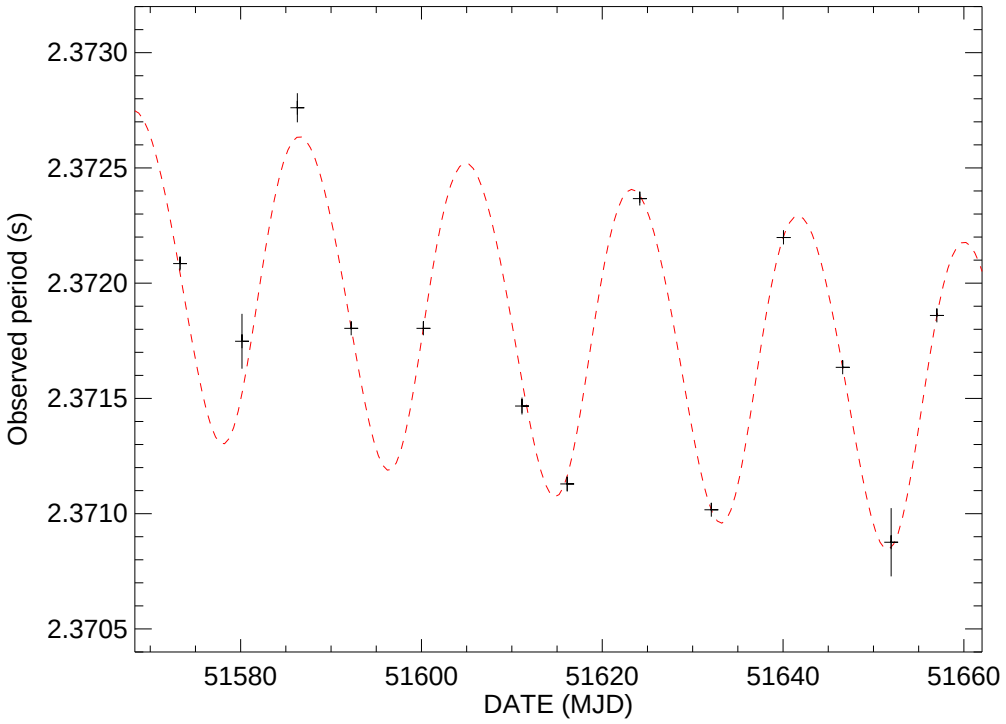

Figure 5.2: The spin period of SXP2.37 as measured by *RXTE*. The orbital modulation is not as obvious as in the case of SXP6.85, but the period deviations around the general spin-up trend suggests we are seeing orbital modulations. Overplotted is the model fit to the data as shown in Table 5.3.

Table 5.3: The orbital parameters for SXP2.37 from the analysis of 3–10 keV *RXTE*/PCA data.

Parameter		Orbital Solution*
Orbital period	$P_{orbital}$ (d)	18.38 ± 0.03
Projected semimajor axis	$a_x \sin i$ (light-s)	73.7 ± 1.7
Longitude of periastron	ω (^{o})	226 ± 16
Eccentricity	e	0.07 ± 0.03
Orbital epoch	$\tau_{periastron}$ (MJD)	51616.8 ± 0.8
Spin period	P (s)	2.37194 ± 0.00001
First derivative of P	$\dot{P}$ (10^{-10}ss^{-1})	-0.720 ± 0.029
Goodness of fit	χ^2_ν	3.58*

*This solution is the result of a fit with spin period errors scaled such that $\chi^2_\nu = 1$.

2001) is the only time *RXTE* has detected the source with any high significance or for any great period of time. Thus, the period measurements from this outburst were fitted with the orbital model. Fits were tried both with the orbital period free to vary and fixed at the value reported in Schurch et al. (2011). Both fits yielded the same parameters to within their errors and very similar goodness of fits, verifying that the 18.6 d periodicity is the orbital period of the system. Figure 5.2 shows the pulse period evolution of the source. The data are cut at the 99.9999% ($5\,\sigma$) significance level. Overplotted is the best model fit to the data in which the orbital period was free to vary. The orbital period measurement is refined to 18.38 ± 0.02 d. I also note here that the fit is more likely providing an upper limit on the eccentricity of 0.1, as a fit with the eccentricity frozen at zero does not result in a statistically worse fit according to an f-test. Thus, I cannot be certain that the eccentricity is non-zero. The other parameters are shown in Table 5.3 and are discussed later.

5.2.3 SXP8.80 = RX J0051.8−7231 = 2E 0050.1−7247

SXP8.80 was discovered by *Einstein* IPC observations in 1980 (Bruhweiler et al., 1987) as a new X-ray source in the SMC wing. The original error circle from these observations led to a tentative association with the optical star AzV 111. Wang & Wu (1992) showed that this source was highly variable, had a moderate X-ray flux and a hard spectrum, suggesting a BeXRB classification. *ROSAT* PSPC observations in May 1993 discovered a periodicity of 8.88163 ± 0.00001 s in the direction of SXP8.80 (Israel et al., 1995). Those authors also showed the transient nature of the source which, along with the spin period, confirmed this as a new BeXRB in the SMC. A refined X-ray position published by Kahabka & Pietsch (1996) cast doubt over the true optical counterpart, with more than one star looking possible. It was not until Haberl & Sasaki (2000) improved the *ROSAT* error circle that the star MA93 506 was identified as the most probable counterpart. The orbital period of SXP8.80 was found to be 28.0 ± 0.3 d (Corbet et al., 2004) during *RXTE* monitoring of the SMC. Subsequent analysis of MACHO and OGLE data of MA93 506 revealed periodicities of 185 d and 33 d respectively (Coe et al. 2005; Schmidtke & Cowley 2006a), casting doubt over the orbital period and the optical counterpart determination. McBride et al. (2008) classify MA93 506 as a O9.5–B0 IV–V emission line star. Only recently has this star been verified as the counterpart with the detection of a 28.51 ± 0.01 d periodicity in the combined OGLE II & III light curve (Rajoelimanana, Charles & Udalski, 2010), in agreement with the X-ray derived period.

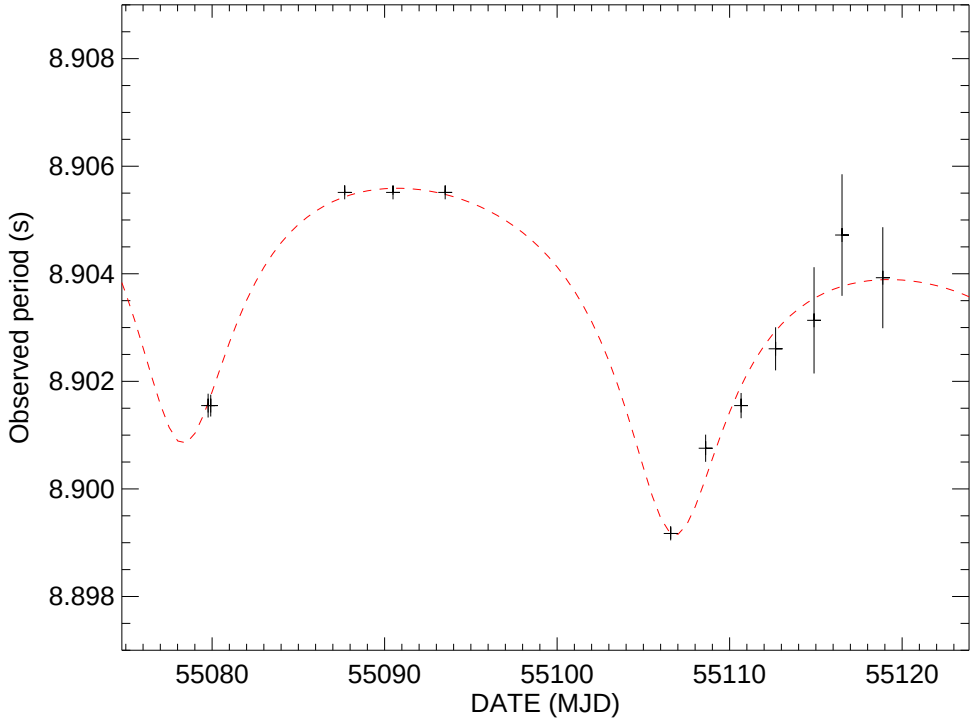

Figure 5.3: The spin period of SXP8.80 as measured by *RXTE*. The orbital modulation is apparent, though the data are sparse over some of the orbit. The orbital period had to be frozen at 28.51 d to produce an acceptable fit. This fit is overplotted and is shown in Table 5.4.

Table 5.4: The orbital parameters for SXP8.80 from the analysis of 3–10 keV *RXTE*/PCA data.

Parameter		Orbital Solution*
Orbital period	$P_{orbital}$ (d)	28.51 *(frozen)*[1]
Projected semimajor axis	$a_x \sin i$ (light-s)	112 ± 6
Longitude of periastron	ω (^{o})	178 ± 6
Eccentricity	e	0.41 ± 0.07
Orbital epoch	$\tau_{periastron}$ (MJD)	55106.7 ± 0.4
Spin period	P (s)	8.9038 ± 0.0002
First derivative of P	$\dot{P}$ (10^{-10}ss^{-1})	-6.9 ± 0.9
Goodness of fit	χ^2_ν	2.60*

*This solution is the result of a fit with spin period errors scaled such that $\chi^2_\nu = 1$.
[1]Orbital period frozen at the period found by Rajoelimanana, Charles & Udalski (2010)

SXP8.80 had been X-ray quiet since a long period of Type I outbursts that began around MJD 52700. The Type II outburst to which I have fit the orbital model began on MJD 55080 and is one of the most luminous outbursts seen in the SMC (see Table 5.1); 6 or more harmonics of the neutron star spin period were often seen in the power spectra. Unfortunately, the coverage during this outburst was sparse and so there are large gaps throughout the outburst. The data are shown in Figure 5.3 and are cut at the 90 % significance level to try and include as much data as possible. This means that some of the data toward the end of the outburst have large associated errors. To aid fitting further, the orbital period was frozen to 28.51 d (Rajoelimanana, Charles & Udalski, 2010). The best fit is plotted over the data in Figure 5.3. The results are given in Table 5.4 and are discussed in section 5.3.

5.2.4 SXP74.7 = RX J0049.1−7250 = AX J0049−729

RX J0049.1−7250 was discovered during a *ROSAT* PSPC observation of the SMC in October 1991 (Kahabka & Pietsch, 1996). It appeared variable by more than a factor of 10 and was highly absorbed. Kahabka & Pietsch (1996) concluded that the source was an XRB on the far side of the SMC, but could not rule out a time variable AGN. A new pulsar was discovered by *RXTE* during pointed observations of SMC X-3, with a periodicity of 74.8 ± 0.4 s (Corbet et al., 1998). This was confirmed by the detection of a 74.675 ± 0.006 s period during an *ASCA* observation on 1997 November 13 (Yokogawa & Koyama, 1998). Kahabka & Pietsch (1998) associated the *ASCA* source with the highly variable *ROSAT* source (Kahabka & Pietsch, 1996) and suggested this as a Be type transient. Optical follow up work by Stevens, Coe & Buckley (1999) deduced one probable and one possible counterpart to the X-ray source (which they refer to as objects 1 & 2). Object 1 has since been confirmed as the correct counterpart from the detection of a 33.4 ± 0.4 d period in the optical light curve (Schmidtke & Cowley, 2005), assumed to be the orbital period of the system. McBride et al. (2008) classify the counterpart as a B3 V emission line star.

There have been sporadic detections of SXP74.7 with *RXTE* since its discovery, although no major outburst was seen until MJD 55232. This Type II outburst was observed regularly by *RXTE*, to try and follow the period evolution. Unfortunately, the outburst lasted for less than one orbit, making fitting difficult. The period history is plotted in Figure 5.4, with the data cut at the 99.9999% ($5\,\sigma$) significance level. Besides a small kink at around MJD 55247, there is very little binary motion visible making fitting more challenging. This could be caused by a low orbital inclination with respect to our line-of-sight or the modulation could be getting swamped by an

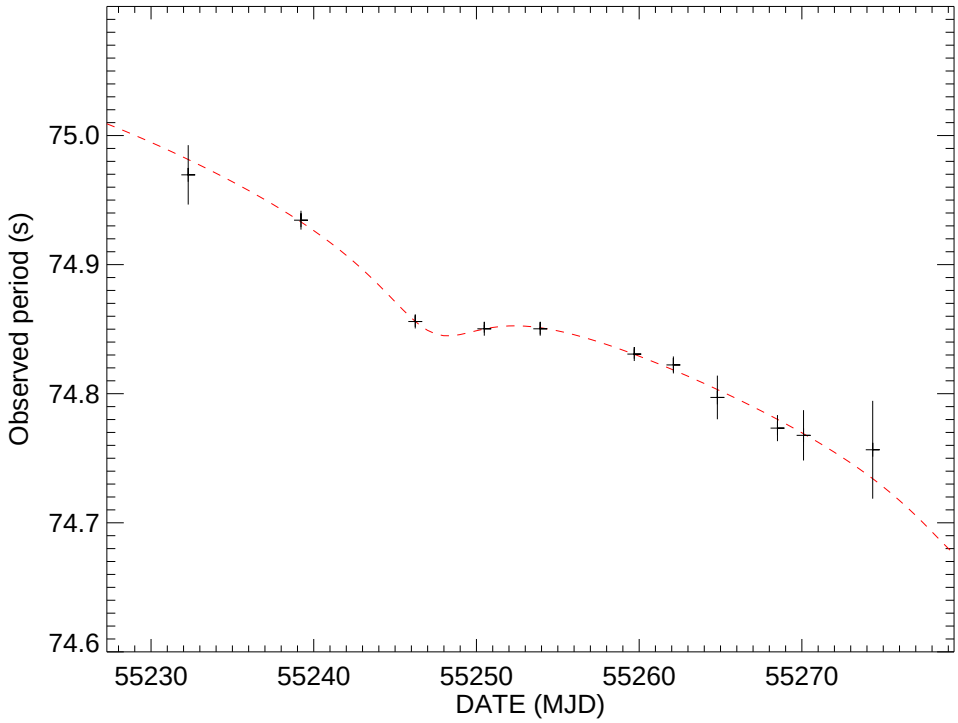

Figure 5.4: The spin period of SXP74.7 as measured by *RXTE*. Very little orbital modulation is apparent, though the outburst is sampled well. To aid fitting, the orbital period was frozen to 33.38 d. The fit is overplotted and is shown in Table 5.5.

Table 5.5: The orbital parameters for SXP74.7 from the analysis of 3–10 keV *RXTE*/PCA data.

Parameter		Orbital Solution
Orbital period	$P_{orbital}$ (d)	33.38 *(frozen)*[1]
Projected semimajor axis	$a_x \sin i$ (light-s)	147 ± 15
Longitude of periastron	ω (^{o})	186 ± 18
Eccentricity	e	0.40 ± 0.23
Orbital epoch	$\tau_{periastron}$ (MJD)	55280.9 ± 1.5
Spin period (MJD 55247.2)	P (s)	74.867 ± 0.002
First derivative of P	$\dot{P}$ (10^{-10}ss^{-1})	-635 ± 37
Goodness of fit	χ^2_ν	0.33

[1] Orbital period frozen at the period found by Rajoelimanana, Charles & Udalski (2010)

exceptionally large spin-up component. The orbital period was frozen to the value found by Rajoelimanana, Charles & Udalski (2010) to help fit the data. The best fit is plotted over the data and the parameters are given in Table 5.5. From the reduced chi-square value it is clear that the model is over-fitting the data. This is reflected in the larger errors on many of the parameters. Again, the results are discussed in the next section.

5.3 Discussion

The 4 systems presented above bring the total number of BeXRBs with reliably measured orbital parameters in the SMC to 6. As such, it is the first time in which there is a large enough sample of SMC systems to compare with the parameters of Galactic HMXBs. In this section I derive mass functions, inclination angles and orbital semimajor axes for the SMC sample and compare them and the other binary parameters to parameters calculated from studying Galactic systems.

5.3.1 The Binary Mass Functions

The masses of the two stars can be described by the X-ray and optical mass functions of the binary system:

$$f_X(M) = \frac{{K_x}^3 P (1-e^2)^{3/2}}{2\pi G} = \frac{M_c \sin^3 i}{(1+q)^2} \tag{5.1}$$

and

$$f_C(M) = \frac{{K_c}^3 P (1-e^2)^{3/2}}{2\pi G} = \frac{M_x \sin^3 i}{(1+1/q)^2} \tag{5.2}$$

respectively. M_x and M_c are the masses of the neutron star and the optical counterpart, i is the inclination of the orbital plane to the line of sight, P is the orbital period, e is the eccentricity and q is the mass ratio (=M_x/M_c). The semiamplitudes of the radial velocity curves are given by

$$K_n = \frac{2\pi a_n \sin i}{P(1-e^2)^{1/2}} \tag{5.3}$$

Table 5.6: The derived X-ray mass function, orbital inclination and semimajor axis for the 4 systems studied in this chapter and the 2 previously studied SMC BeXRBs. M_c is estimated from the spectral classification of the authors referenced here using the table of luminosity and spectral type from de Jager & Nieuwenhuijzen (1987), along with the standard mass-luminosity relationship for main sequence stars ($L \propto M^{3.6}$). $f_X(M)$ is calculated using results from the orbital fits and is shown in solar masses. The inclination and semimajor axis are estimated using equation 5.1, M_c and $M_x = 1.4 M_\odot$.

Source	$(M_c/M_\odot)$	$(f_X(M)/M_\odot)$	$i\ (^\circ)$	$a_x\ (R_\star)$
SXP2.37[1]	18–26	1.27 ± 0.05	$24\ ^{+2}_{-3}$	9
SXP6.85[1]	13–26	7.71 ± 0.92	$50\ ^{+20}_{-9}$	12
SXP8.80[1]	13–23	1.86 ± 0.25	$30\ ^{+6}_{-4}$	13
SXP74.7[1]	6–9	3.06 ± 0.94	$55\ ^{+20}_{-13}$	16
SXP11.5[2]	13–26	3.79 ± 0.48	$37\ ^{+11}_{-6}$	16
SXP18.3[3]	8–13	1.43 ± 0.17	$36\ ^{+5}_{-7}$	10

Note. References for the spectral classification are given: [1]McBride et al. (2008), [2]Chapter 4 of this work and Townsend et al. (2011), [3]Schurch et al. (2009). The spectral type of SXP18.3 in Schurch et al. (2009) is estimated based on optical and NIR photometry as no spectrum allowing for classification is available.

where a_x and a_c are the semimajor axes of the ellipse travelled by the neutron star and the optical counterpart about the centre of mass of the system. Thus, if the radial velocity curves for both stars are known, along with the inclination angle, one can calculate the masses of the two stars to high precision. However, due to the non-eclipsing nature of these SMC binary systems, I am unable to make precise measurements of the neutron star masses as the inclination is not well constrained. Instead, the X-ray mass function for each system can be calculated using their orbital solutions. From this, estimates of the inclination and orbital size ($\simeq a_x$) can be made using masses estimated from the spectral classification of the counterpart and the standard mass of a neutron star of 1.4 $M_\odot$. These results are shown in Table 5.6 for the 6 SMC BeXRBs with orbital solutions. The range in the value of each inclination is based mostly on an uncertainty in the spectral classification of one spectral type either side of the published value. The uncertainty in the mass function also contributes to the range in inclination, albeit less significantly. The semimajor axes are estimated based on the most probable mass and radius of the primary star.

The orbital inclinations seen in this sample are as expected given the method of detection. Very low inclinations would mean the delays in pulse arrival times would

not be detected, whilst very high inclinations would mean the X-ray source gets eclipsed by the primary star. More specifically, one can compare the inclinations to Hα profiles of the Be star to investigate the (mis-)alignment of the orbital plane and the circumstellar disk. I find that SXP6.85 and SXP74.7 have quite narrow, single peaked Hα emission (see Chapter 3), despite having the highest estimated inclinations. Conversely, SXP18.3 has a lower inclination but shows prominent double peaked Hα emission in its optical spectrum. However, I note that the mass of SXP18.3 has been estimated photometrically, not spectroscopically. Although this may provide some qualitative evidence of orbit-disk misalignment in these systems, more quantitative evidence may only be obtained from detailed polarimetric studies of the disk itself.

The estimated semimajor axes in Table 5.6 are quite similar and range from 9 to 16 stellar radii, but are these values what one might expect? The use of complex models that describe the dynamics and thermal structure of the circumstellar disk around the primary star helps explain what is observed here. Okazaki (2007) shows that the density of the disk is several orders of magnitude lower beyond 10 $R_\star$ than it is closer to the star, whilst Carciofi (2010) shows most of the optical and NIR flux and polarisation is emitted from within 10 $R_\star$ and nearly all FIR and Hα flux is produced inside 20 $R_\star$ (see Chapter 1). Thus, these models are predicting that a very large fraction of the matter in the disk is within approximately 10 $R_\star$. This prediction goes some way to explaining the nature of the X-ray outbursts that are seen in the SMC binary systems. SXP74.7 and SXP11.5 have the largest predicted orbital size (relative to the radius of the counterpart) and are observationally the least active of the sample, rarely undergoing a Type I outburst and only once being seen in a Type II outburst. SXP6.85, SXP8.80 and SXP18.3 have smaller predicted orbital sizes and are much more active, often being detected in Type I or Type II outbursts, or outbursts in-between these classical types as discussed in Chapter 2. This is likely due to the neutron star passing closer to, or further into, the circumstellar material than those in larger orbits. The exception to this seems to be SXP2.37 which has the smallest predicted orbital size, but is very rarely detected in X-ray outburst. This can be explained when considering the low eccentricity of the orbit. Okazaki & Negueruela (2001) predict that for low eccentricity HMXBs, the circumstellar disk will get truncated at the 3:1 resonance radius, in contrast to intermediate and high eccentricity systems in which truncation is much less efficient and occurs at larger distances near the Roche lobe radius of the star. Thus, the disk in SXP2.37 could be truncated at a much smaller radius than those of the other systems in the sample, explaining the small number of X-ray outbursts seen.

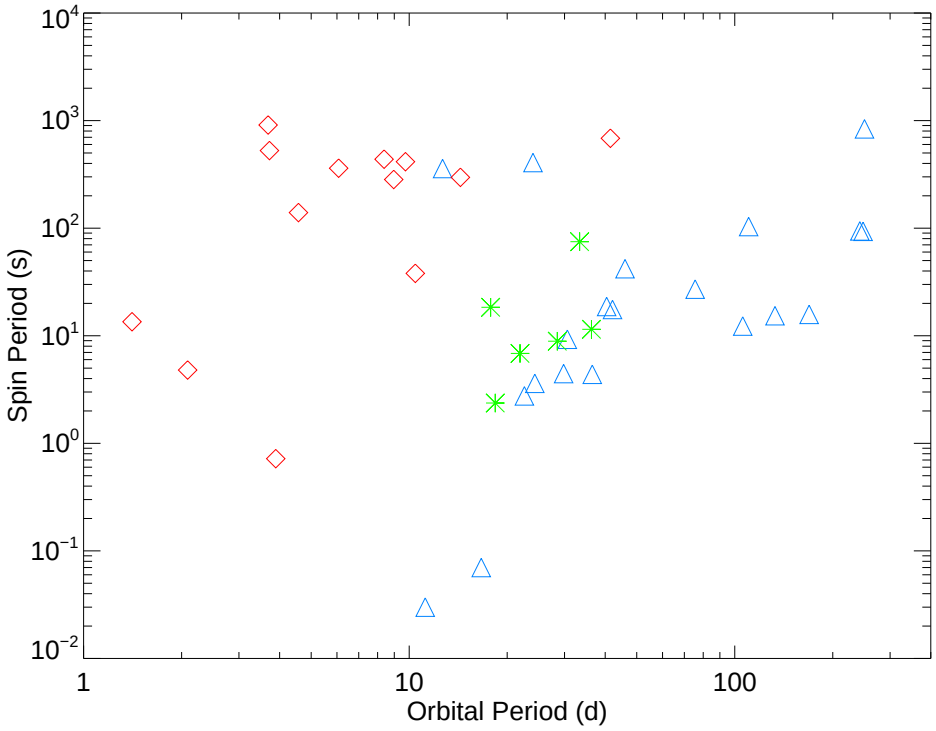

Figure 5.5: Corbet Diagram for all the HMXBs in Table 5.7 that have a known spin period (excluding the PSR systems). The red diamonds represent the SG systems, the blue triangles are the Galactic BeXRBs and the green stars are the SMC BeXRBs.

5.3.2 Comparison with the Galactic population

In order to properly compare this new sample to those found in the Galaxy, a thorough review of the literature was made and a database compiled of all known HMXB systems for which the orbital period and the eccentricity are known. This list is intended to be exhaustive, although this cannot be guaranteed. In total I find 24 HMXB systems with a Be companion and 17 with a giant or supergiant companion in addition to the 6 systems discussed so far in this chapter. Tables 5.7 & 5.8 present the orbital parameters of all 47 HMXBs. Table 5.7 shows the orbital periods and eccentricities, as well as spin periods and longitudes of periastron where known. Table 5.8 shows the spectral types, mass functions and projected semimajor axes where known. This source list is based mostly, but not solely, on tables presented in Bildsten et al. (1997), Pfahl et al. (2002) and Martin, Tout & Pringle (2009). I also used the updated database of BeXRBs of Raguzova & Popov (2005) and the online database of *INTEGRAL* sources maintained by Jerome Rodriguez and Arash Bodaghee[1]. Figure 5.5 shows the orbital and spin periods of these HMXBs (less 8

[1]http://irfu.cea.fr/Sap/IGR-Sources/

Table 5.7: Spin period, orbital period, eccentricity and longitude of periastron for all high-mass X-ray binaries with a reliable eccentricity measurement.

Source name	P_{spin} (s)	$P_{orbital}$ (d)	e	ω (^{o})
Be/X-ray binaries				
PSR J0045−7319[1]	0.93	51.169	0.808	115.236 ± 0.002
RX J0049.1−7250 (SXP74.7)	74.9	33.38 ± 0.01	0.40 ± 0.23	186 ± 18
2E 0050.1−7247 (SXP8.80)	8.89	28.51 ± 0.01	0.41 ± 0.04	178 ± 4
MX 0053+604 (γ Cas)[2]		203.59 ± 0.29	0.260 ± 0.035	47.9 ± 8.0
XTE J0055−727 (SXP18.3)[3]	18.4	17.79 ± 0.01	0.43 ± 0.03	15 ± 6
SMC X−2 (SXP2.37)	2.37	18.38 ± 0.02	0.07 ± 0.02	226 ± 8
XTE J0103−728 (SXP6.85)	6.85	21.9 ± 0.1	0.26 ± 0.03	125 ± 6
IGR J01054−7253 (SXP11.5)[4]	11.5	36.3 ± 0.4	0.28 ± 0.03	224 ± 10
4U 0115+63[5]	3.61	24.317	0.342 ± 0.004	48.5 ± 0.9
LS I +61 303[6]		26.496 ± 0.003	0.537 ± 0.034	40.5 ± 5.7
V0332+53 (BQ Cam)[7]	4.38	36.50 ± 0.29	0.417 ± 0.007	283.49 ± 0.91
4U 0352+32 (X Per)[8]	837.7	250.3 ± 0.6	0.111 ± 0.018	288 ± 9
A 0535+26[9]	103.5	110.3 ± 0.3	0.47 ± 0.02	130 ± 5
A 0538−66[10]	0.07	16.646	0.82 ± 0.04	222 ± 21
SAX J0635.2+0533[11]	0.03	11.2 ± 0.5	0.29 ± 0.09	356 ± 24
GS 0834−430[12]	12.3	105.8 ± 0.4	0.14 ± 0.04	140 ± 44
PSR 1259−63[13]	0.05	1236.724	0.87	138.665

Table 5.7: (continued)

Source name	P_{spin} (s)	$P_{orbital}$ (d)	e	ω (^{o})
GRO J1008−57[14]	93.5	247.8 ± 0.4	0.68 ± 0.02	
1A 1118−616[15]	407.7	24.0 ± 0.4	< 0.16	310 ± 30
2S 1417−624[16]	17.5	42.12 ± 0.03	0.417 ± 0.003	298.85 ± 0.68
XTE J1543−568[17]	27.1	75.56 ± 0.25	< 0.03	
2S 1553−542[18]	9.27	30.6 ± 2.2	< 0.09	
SWIFT J1626.6−5156[19]	15.4	132.89 ± 0.03	0.08 ± 0.01	340 ± 9
GRO J1750−27[20]	4.45	29.806 ± 0.001	0.360 ± 0.002	206.3 ± 0.3
2S 1845−024[21]	94.3	242.18 ± 0.01	0.879 ± 0.005	252.2 ± 9.4
4U 1901+03[22]	2.76	22.583	0.036	268.812 ± 0.003
GRO J1944+26[23]	15.8	169.2 ± 0.9	0.33 ± 0.05	269 ± 23
GRO J1948+32[24]	18.7	40.415 ± 0.010	0.033 ± 0.013	33 ± 3
EXO 2030+375[25]	42	46.021	0.412 ± 0.001	211.3 ± 0.3
SAX J2103.5+4545[26]	358.6	12.665	0.406 ± 0.004	244.3 ± 6.0
Giant & Supergiant X-ray binaries				
SMC X−1[27]	0.72	3.892	0.0002	317 ± 9
2S 0114+650[28]		11.598	0.18 ± 0.05	51 ± 17
LMC X−4[29]	13.5	1.408	0.006 ± 0.002	
Vela X−1[30]	283.5	8.964	0.090 ± 0.001	152.59 ± 0.92
Cen X−3[31]	4.8	2.087	< 0.0001	

Table 5.7: (continued)

Source name	P_{spin} (s)	$P_{orbital}$ (d)	e	ω (^{o})
1E 1145.1−6141[32]	297	14.365 ± 0.002	0.20 ± 0.03	308 ± 8
GX 301−2[33]	685	41.498 ± 0.002	0.462 ± 0.014	310.4 ± 1.4
4U 1538−52[34]	526.8	3.723	0.174 ± 0.015	64 ± 9
IGR J16393−4643[35]	910.4	3.688	0.15 ± 0.05	
IGR J16493−4348[36]		6.782 ± 0.002	< 0.15	
OAO 1657−415[37]	38.2	10.444 ± 0.004	0.104 ± 0.005	93 ± 5
EXO 1722−363[38]	414.8	9.740	< 0.19	
PSR J1740−3052[39]	0.57	231.030	0.579	178.646
IGR J18027−2016[40]	139.6	4.570	< 0.2	
LS 5039[41]		3.906	0.337 ± 0.036	236.0 ± 5.8
XTE J1855−026[42]	361.0	6.072	0.04 ± 0.02	226 ± 15
4U 1907+09[43]	437.5	8.375	0.28 ± 0.04	330 ± 7

Note. Included are all HMXBs in the Galaxy and Magellanic Clouds that I have been able to find reference to in the literature for which the orbital period and eccentricity are reliably known. If the parameter is known to better than 3 decimal places, it is truncated and the error is smaller than 0.001. References for quantities presented in the table are given here for each individual system: [1]Kaspi et al. (1994); [2]Harmanec et al. (2000); [3]Schurch et al. (2009); [4]Chapter 4 of this work and Townsend et al. (2011); [5]Raichur & Paul (2010b); [6]Aragona et al. (2009); [7]Raichur & Paul (2010b); [8]Delgado-Martí et al. (2001); [9]Finger, Wilson & Hagedon (1994); [10]Hutchings et al. (1985); [11]Kaaret, Cusumano & Sacco (2000); [12]Wilson et al. (1997); [13]Wang, Johnston & Manchester (2004); [14]Coe et al. (2007);

[15]Staubert et al. (2011); [16]Raichur & Paul (2010b); [17]in't Zand, Corbet & Marshall (2001); [18]Kelley, Rappaport & Ayasli (1983); [19]Baykal et al. (2010); [20]Scott et al. (1997), Shaw et al. (2009); [21]Finger et al. (1999); [22]Galloway, Wang & Morgan (2005); [23]Wilson et al. (2003); [24]Galloway, Morgan & Levine (2004); [25]Wilson, Finger & Camero-Arranz (2008); [26]Baykal et al. (2007); [27]Raichur & Paul (2010a); [28]Grundstrom et al. (2007a); [29]Levine (1991), van der Meer et al. (2007); [30]Kreykenbohm et al. (2008); [31]Raichur & Paul (2010a); [32]Ray & Chakrabarty (2002); [33]Koh et al. (1997); [34]Clark (2000); [35]Thompson et al. (2006); [36]Cusumano et al. (2010); [37]Chakrabarty (1993); [38]Thompson et al. (2007); [39]Stairs et al. (2001); [40]Hill et al. (2005); [41]Aragona et al. (2009); [42]Corbet & Mukai (2002); [43]Baykal et al. (2006).

Table 5.8: Spectral type, projected semi-major axis and mass function for all high-mass X-ray binaries with a reliable eccentricity measurement. See Table 5.7 for references.

Source name	Spectral type	$a_x \sin i$ (light-s)	$f_X(M)$ ($M_\odot$)
Be/X-ray binaries			
PSR J0045−7319[1]	B1 V	174.235 ± 0.002	2.169
RX J0049.1−7250 (SXP74.7)	B3 V	147 ± 15	3.06 ± 0.94
2E 0050.1−7247 (SXP8.80)	O9.5-B0 IV-V	112 ± 5	1.86 ± 0.25
MX 0053+604 (γ Cas)[2]	B0.5 IV		
XTE J0055−727 (SXP18.3)[3]	B1-B3 V	75 ± 3	1.43 ± 0.17
SMC X−2 (SXP2.37)	O9.5 III-V	73.7 ± 0.9	1.27 ± 0.05
XTE J0103−728 (SXP6.85)	O9.5-B0 IV-V	151 ± 6	7.71 ± 0.92
IGR J01054−7253 (SXP11.5)[4]	O9.5-B0 IV-V	167 ± 7	3.79 ± 0.48
4U 0115+63[5]	B0.2 V	140.69 ± 0.72	5.06 ± 0.08
LS I +61 303[6]	B0 V		
V0332+53 (BQ Cam)[7]	O8.5 V	82.49 ± 0.94	0.45 ± 0.02
4U 0352+32 (X Per)[8]	O9.5 III-B0 V	454 ± 4	1.60 ± 0.04
A 0535+26[9]	B0 III-V	267 ± 13	1.68 ± 0.25
A 0538−66[10]	B2 III		
SAX J0635.2+0533[11]	B1 III-B2 V	83 ± 11	4.9 ± 2.0
GS 0834−430[12]	B0-2 III-V	128 ± 43	0.2 ± 0.2
PSR 1259−63[13]	B2		

Table 5.8: (continued)

Source name	Spectral type	$a_x \sin i$ (light-s)	$f_X(M)$ ($M_\odot$)
GRO J1008−57[14]	B1-B2 V	530 ± 60	2.6 ± 0.9
1A 1118−616[15]	O9.5 IV-V	54.9 ± 1.4	0.31 ± 0.03
2S 1417−624[16]	B1 V	207.1 ± 1.0	5.37 ± 0.08
XTE J1543−568[17]	Be	353 ± 8	8.27 ± 0.56
2S 1553−542[18]	Be	164 ± 22	5.1 ± 2.2
SWIFT J1626.6−5156[19]	Be	401 ± 5	3.92 ± 0.15
GRO J1750−27[20]		101.8 ± 0.5	1.27 ± 0.02
2S 1845−024[21]	Be	689 ± 38	6.0 ± 1.0
4U 1901+03[22]	OB	106.989 ± 0.015	2.578 ± 0.001
GRO J1944+26[23]	B0-1 IV-V	640 ± 120	9.8 ± 5.5
GRO J1948+32[24]	B0 V	137 ± 3	1.69 ± 0.11
EXO 2030+375[25]	B0 V	244 ± 2	7.36 ± 0.18
SAX J2103.5+4545[26]	B0 V	74.07 ± 0.86	2.72 ± 0.09
Giant & Supergiant X-ray binaries			
SMC X−1[27]	B0 Ib	53.577	10.897
2S 0114+650[28]	B1 Ia		
LMC X−4[29]	O8 III	26.343 ± 0.002	9.893 ± 0.002
Vela X−1[30]	B0.5 Ia	113.89 ± 0.13	19.73 ± 0.07
Cen X−3[31]	O6-8 III	39.661	15.373 ± 0.001

Table 5.8: (continued)

Source name	Spectral type	$a_x \sin i$ (light-s)	$f_X(M)$ ($M_\odot$)
1E 1145.1−6141[32]	B2 Ia	99.4 ± 1.8	5.11 ± 0.28
GX 301−2[33]	B1 Ia^+	368.3 ± 3.7	31.14 ± 0.94
4U 1538−52[34]	B0 Iab	56.6 ± 0.7	14.04 ± 0.52
IGR J16393−4643[35]		55 ± 2	13.1 ± 1.5
IGR J16493−4348[36]	B0.5 Ib	< 128	< 49
OAO 1657−415[37]	Ofpe/WN9h	106.0 ± 0.5	11.72 ± 0.17
EXO 1722−363[38]	B0-1 Ia	101 ± 3	11.7 ± 1.0
PSR J1740−3052[39]	B	756.909	8.721
IGR J18027−2016[40]	B1 Ib	68 ± 1	16.16 ± 0.71
LS 5039[41]	ON6.5 V(f)		
XTE J1855−026[42]	B0 Iaep	80.5 ± 1.4	15.19 ± 0.79
4U 1907+09[43]	O8.5 Iab	83 ± 2	8.75 ± 0.63

systems with unknown spin periods or PSR designations). The red diamonds represent the supergiant (SG) systems, the blue triangles are the Galactic BeXRBs and the green stars are the SMC BeXRBs. As expected, the SG and Be systems occupy separate parts of the plot (Corbet, 1986) and the SMC BeXRBs sit amongst the Galactic Be systems. This sample will be used to compare with the results from my analysis throughout this discussion.

An observation that emerges from this work, is that there are often many different periodicities found in the optical and X-ray light curves of individual sources and that these periods do not always agree. As such, great care must be taken when deciding which periodicity is the orbital period and which can be attributed to stellar pulsations, disk oscillations, superorbital periods or even aliasing between different periodicities. Figure 5.5 supports my interpretation of the 21.9 d orbital period in SXP6.85 as a longer 114 d period would see it sit towards the edge of the BeXRB region. The 112 d period reported by Galache et al. (2008) came from timing analysis of the long term *RXTE* light curve. A periodogram of the updated light curve (including over 4 years of new data) refines this period to 117 ± 1 d. The X-ray period seems to be driven by the time between outbursts, although considered with the 114 d optically derived period and the ~ 620 d disk relaxation timescale (McGowan et al., 2008a), a superorbital period cannot be ruled out. An additional argument for the 21.9 d period being orbital in nature is the relationship between the orbital and superorbital periods found by Rajoelimanana, Charles & Udalski (2010) (see Figure 1.10, Chapter 1). The strong correlation between these parameters, if physical, suggests that for a superorbital period of ~ 620 d, the expected orbital period is around 15–20 d. SXP8.80 also shows evidence for many different periodicities in its optical and X-ray light curves. The possible period of 185 d reported in Coe et al. (2005) was only found in the MACHO red data. Those authors comment that they could not find the same period in the early OGLE data implying that the result should be taken with some caution. It is also very close to half a year – a period that always needs to be treated with care in such data sets. The period of 33 d reported by Schmidtke & Cowley (2006a) is described as 'weak' by those authors and possibly only seen in some early OGLE data. They accept that this could actually be the same as the 28 d reported by Corbet et al. (2004). Although these periodicities could be real, possibly a signature of stellar pulsations in the Be star, it is likely that they are non-orbital in nature. Indeed, as the optical data sets have grown in size over the years, so has the confidence in what is found. Hence, the optical period of 28 d found by Rajoelimanana, Charles & Udalski (2010) is much more likely to be real as it was found in a much longer data set. In this case, it is very likely to be the

orbital period of SXP8.80 as it also agrees with the X-ray derived period of Corbet et al. (2004).

As mentioned previously, the low metallicity environment in the SMC may have a significant impact on the evolution of HMXBs which may manifest itself as observable differences in the population from that of the Milky Way. Figure 5.5 suggests that there is little difference in the relationship between spin and orbital periods of SMC and Galactic systems. McBride et al. (2008) also show there to be no difference in the distribution of spectral types. In the following section I investigate if there is evidence of such a difference in the distribution of eccentricities and, by inference, supernova kick during the formation of the neutron star.

5.3.3 The relationship between orbital period and eccentricity

The orbital solutions presented here mean that, for the first time, one can investigate the relationship between the orbital period and eccentricity for a sample of SMC BeXRBs and compare this to what is seen in the Galaxy. In Figure 5.6 I plot these two parameters for the 6 SMC sources and the Galactic sample. For clarity I have removed the PSR designated systems from the comparison as these are almost certainly not 'normal' HMXBs. I have also excluded the millisecond binary pulsars A0538–66 and SAX J0635.2+0533 from the comparison as their spin periods suggest that they have not evolved through the same pathway as most HMXBs that result in quasi-equilibrium spin periods between 1–1000 s as discussed in Chapter 1. A0538–66 has also been seen at extremely high (super-Eddington) luminosities, which is highly unusual for 'normal' HMXBs. There are several things of note here. Firstly, there seems to be little difference between the parameter space occupied by SMC and Galactic systems. This may suggest that the metallicity difference between the galaxies is not a large factor in binary evolution, although many more orbits of SMC systems need to be solved before a firm conclusion can be drawn. Secondly, the Be and SG systems occupy separate regions of the plot much like on the Corbet diagram. This is what might be expected considering the tight, circular orbits in SG systems and the wide, eccentric orbits in Be systems. The upper-right most red diamond (GX 301-2) has shown evidence of behaving like a Be system despite its B1 Ia^{+} classification (Koh et al., 1997), and so may be an exception to this relationship. Thirdly, there is a possible correlation between the two parameters, particularly when the small class of low eccentricity, long orbit OB transients

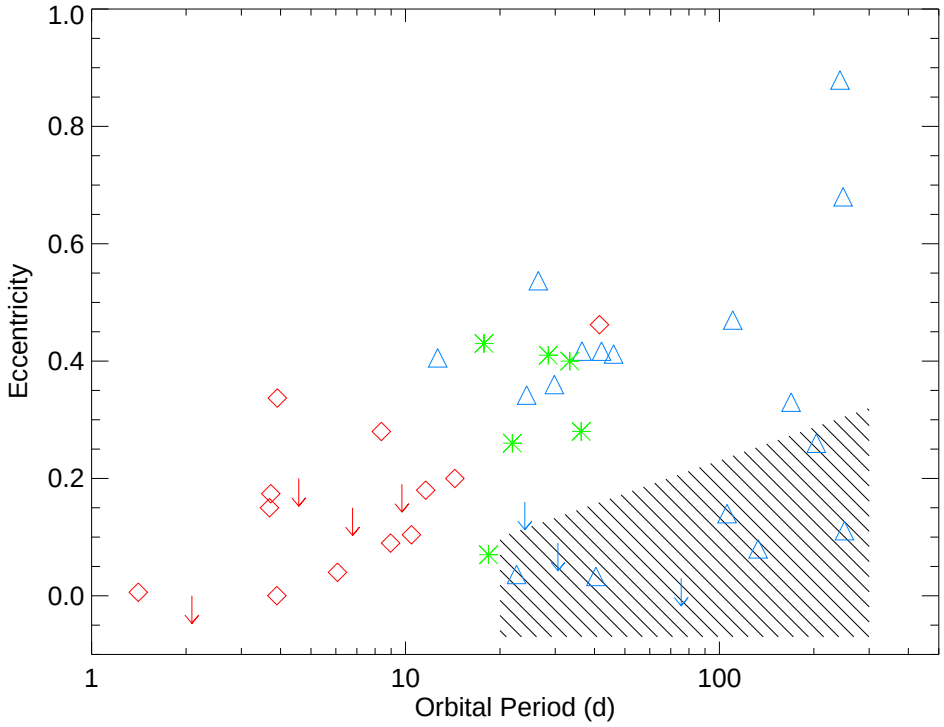

Figure 5.6: Orbital period against eccentricity for all the systems presented in Table 5.7, excluding the millisecond pulsars. The red diamond, blue triangle and green star symbols represent SG, Galactic Be and SMC Be systems respectively, as in Figure 5.5. The red and blue arrows are upper limits for the eccentricity of SG and Galactic Be systems respectively. The 1 σ errors are not plotted here for clarity, but are approximately the size of the data point or smaller. The 8 systems within the shaded region belong to the new class of low eccentricity, long orbit HMXB (Pfahl et al., 2002).

(Pfahl et al., 2002) in the shaded region are excluded[2]. The size and shape of this region was chosen purely to included only the systems documented in the literature with this low eccentricity, long orbital period nature and was not chosen in a subjective way or to lead the eye of the reader.

To try and quantify any possible relationship between the two parameters, a Spearman rank correlation coefficient was derived. This was preferred over a linear Pearson correlation as the relationship seems to be linear-log as opposed to simply linear. The rank correlation coefficient for the whole dataset was computed to be 0.412 with a p-value of 0.007 (significant at the 3 σ level). A second correlation test was performed excluding the 8 sources proposed to belong to the low eccentricity

[2]Pfahl et al. (2002) argue that these objects make up a new group of HMXB that received a much smaller kick from the supernova explosion that created the X-ray binary. This work was originally based on 6 systems, though now there are currently 8 members of this group. See Galloway, Wang & Morgan (2005) and Baykal et al. (2010) for details on the other two systems.

group of OB transients, resulting in a coefficient of 0.79 and p-value of 2.6×10^{-8} (significant at the $6\,\sigma$ level). The more significant correlation resulting from the removal of this small group of systems may reinforce the idea put forward by Pfahl et al. (2002) that these are a separate population of Be systems that receive a smaller supernova kick compared to 'classical' Be systems. It may also suggest that orbital period and eccentricity in HMXBs are somehow intrinsically related. However, fitting any function to the current data is difficult given the spread of values and the unknown contribution to the trend from factors such as mass, orbital size and tidal circularisation timescales. Whilst the correlation seems significant, there is an obvious alternative to this scenario. Separate correlation tests on the SG systems and Be systems yield lower correlation coefficients of 0.54 (p-value of 0.03) and 0.49 (p-value of 0.04) respectively. This means much of the overall correlation could be a result of the two groups occupying different parameter space. With the low eccentricity transients included in the Be group, this correlation coefficient drops to 0.08 (p-value 0.69). Again this favours the interpretation that we are seeing 3 different populations with different evolutionary histories, rather than one continuous population.

Conversely, we can think of the weak correlations shown in both groups as evidence for a relationship between the parameters, which is only enhanced when the two groups are combined. This could be telling us something significant about the pre-supernova phase of the binary evolutionary path. Delgado-Martí et al. (2001) simulate binary periods and eccentricities resulting from SN kicks imparted onto the neutron star with varying initial orbital separations. Somewhat intuitively, the results show that as the initial separation is increased, a higher fraction of systems are found to have larger orbital periods and larger eccentricities. If we consider each binary system to have the same evolutionary path, the correlation in Figure 5.6 may be telling us that SG systems generally have tighter pre-supernova orbits than Be systems. As for the question of whether there is a difference between SMC and galactic systems in this parameter space, any potential correlation in these data can only be confirmed by including more binary systems in the comparison, particularly more long orbital period Galactic systems and both long and short orbital period SMC systems. However, this will be difficult given the nature of the analysis method. Finally, I note the location of SXP2.37, immediately left of the shaded region in Figure 5.6. I postulate that this source is the latest member of this growing class of low eccentricity OB transient HMXB and the first member from outside the Galaxy.

5.4 Conclusions

The orbital parameters of four BeXRB systems in the SMC have been derived, taking the total number of extra-Galactic BeXRBs with orbital solutions to six. I find one new orbital period and confirm a second. Two further fits were made possible by freezing the orbital period parameter to known values from analysis of optical light curves. I find that one system (SXP2.37 = SMC X-2) is consistent with being part of the small class of HMXBs with low eccentricities and long orbital periods proposed by Pfahl et al. (2002), or at least lies between this class and the 'normal' population. On comparing the SMC sample to Galactic systems I find there to be little difference in their binary parameters, suggesting that the low metallicity environment in the SMC does not contribute strongly to the evolution of the binary. The different types of HMXB are found to occupy different regions on a plot of orbital period and eccentricity, similar to what is seen in the Corbet diagram. A possible correlation between the two parameters is noted, although it is unclear whether this is an effect of the position of the groups on the plot or if it demonstrates a physical connection between the parameters in HMXB systems. The data clearly suffer from selection effects, in particular the lack of many long orbital period systems that will ultimately determine the answers to the questions posed here. As a by-product of this work, I present a catalogue of the orbital parameters for every HMXB in the Galaxy and Magellanic Clouds for which they are known.

Sorry Meg. Daddy loves ya, but Daddy also loves Star Trek,
and in all fairness, Star Trek was here first.

PETER GRIFFIN, FAMILY GUY

6

Using *XMM-Newton* and *INTEGRAL* to locate new pulsars found by *RXTE*

In this chapter, I present two newly detected pulsations coming from the direction of the SMC. On detection with *RXTE*, both pulsations were considered to originate from new BeXRB pulsars with unknown locations. Using follow-up *INTEGRAL* and *XMM-Newton* observations, I show the first pulsar to be coincident with a candidate HMXB in the northern bar region of the SMC. The second pulsar is shown not to be a new pulsar at all, but is consistent with being the first ever pulsar detected by the *RXTE* monitoring programme. This source shows large spin-up of the neutron star during apparent phases of quiescence that is hard to quantify. This work is currently unpublished. A PhD student at Southampton, Sebastian Drave, performed all of the *INTEGRAL* analysis presented here.

6.1 Introduction

The major drawback of the SMC monitoring programme with *RXTE* is that newly discovered pulsars are positionally very poorly constrained. In the past my colleagues and I have tried various raster monitoring observations with *RXTE* to try

and locate a pulsar, failing on almost all occasions. A much more successful route is to apply for observing time on imaging X-ray instruments. For two new pulsations detected in the last 18 months, this is the route I was able to take. When these periodicities were confirmed by a second successive *RXTE* detection, *INTEGRAL* Target of Opportunity (ToO) observations were triggered to observe the entire SMC and locate the source of the X-ray emission. When a position was found with *INTEGRAL*, an *XMM-Newton* ToO was triggered to improve on the position allowing for optical identification of the counterpart. Two unidentified pulsations detected in August 2010 and March 2011 have allowed this tactic to be employed. The X-ray and subsequent optical observations made are presented in sections 6.2 and 6.3 respectively. The results are discussed in section 6.4 and brief conclusions given in section 6.5.

6.2 X-ray observations

6.2.1 SXP175 = RX J0101.8–7223

The *RXTE*/PCA detected 175.4 ± 0.1 s pulsations coming from the direction of the SMC on 2011 March 19 (MJD 55639). This period was confirmed by a second detection at 175.1 ± 0.1 s on 2011 March 26 (MJD 55646). It does not coincide with the spin period of any known pulsar in the *RXTE* field of view, and so was concluded to be a new HMXB pulsar in the SMC. The entire *RXTE* data archive was subsequently searched in order to build up an activity history of the pulsar (herein SXP175 under the naming convention of Coe et al. 2005). Unfortunately, this source has shown very little X-ray activity despite good coverage with the PCA over approximately 9 of the last 13 years. Only a handful of low significance detections are seen in the long-term light curve. These detections are sporadic and no orbital information could be drawn from the data.

An *INTEGRAL* (Winkler, 2003) ToO follow up observation was performed on 2011 April 2 (MJD 55653) to localise any X-ray sources within the *RXTE* field of view. The observation consisted of 50 individual Science Windows (ScW) summing to a total good time exposure of $\sim$89.5 ks, nominally a ScW represents an $\sim$2000 s exposure. Both the hard IBIS/ISGRI (Ubertini et al. 2003; Lebrun et al. 2003) and soft JEM-X (Lund et al., 2003) X-ray data were analysed using the *INTEGRAL* Offline Science Analysis software (OSA v9.0, Goldwrum et al 2001). Images were generated at ScW level in the $3-10$ keV and 15-60 keV energy bands for JEM-X and IBIS respectively and combined into mosaics of the total observation. These

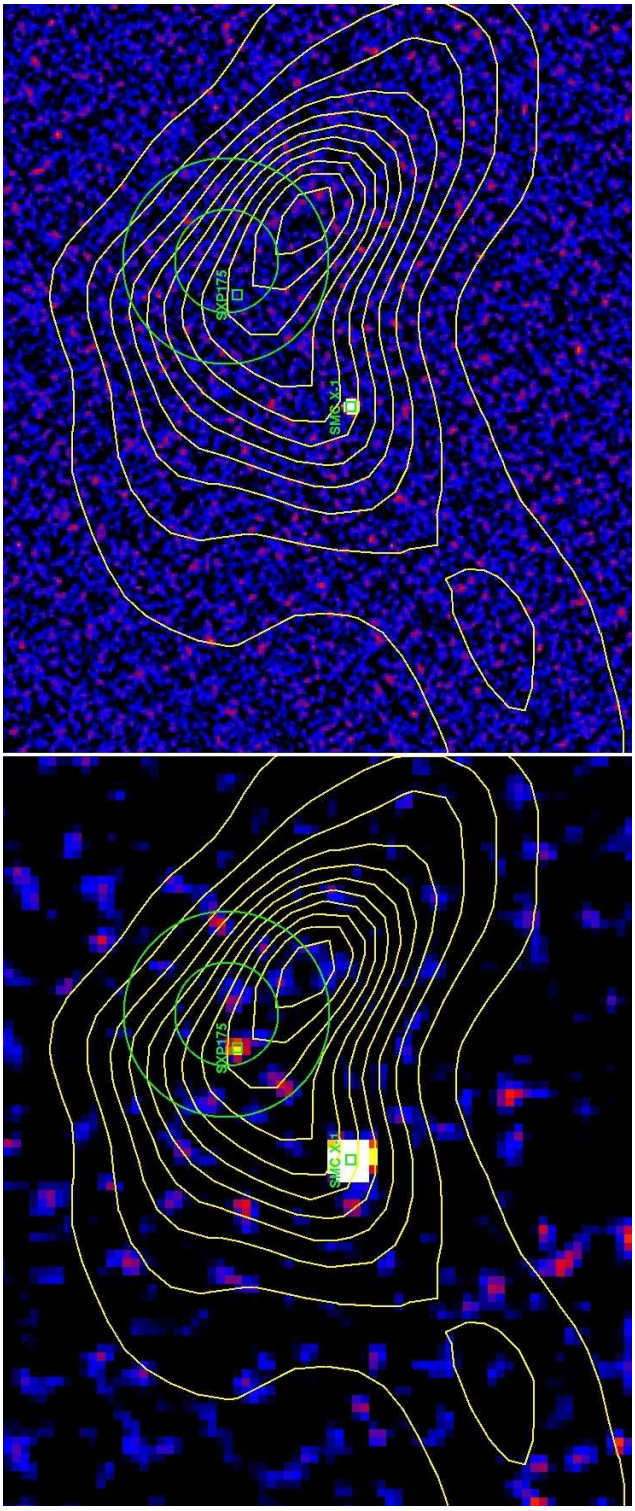

Figure 6.1: Top: JEM-X 3−10 keV significance map showing a non-detection at the location of the IBIS source. Bottom: IBIS/ISGRI 15−60 keV significance map. A single source is detected within the PCA FOV at a significance of 6.2σ. The circles indicate the *RXTE*/PCA half and zero response of the pointing used whilst the contours are those of the HI column density of Putman et al. 2003.

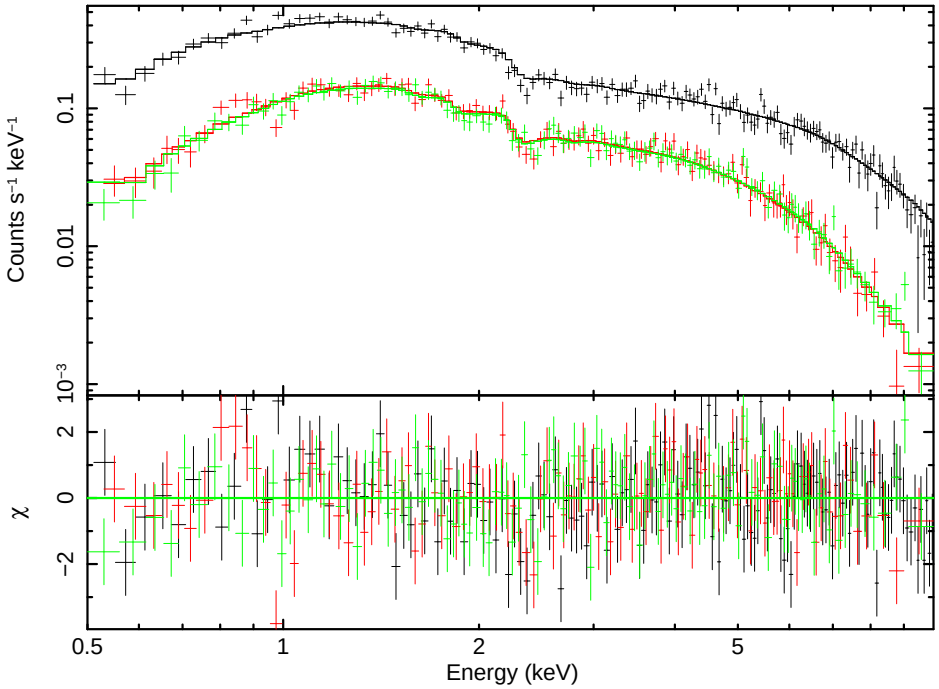

Figure 6.2: *XMM-Newton* EPIC spectra of SXP175. EPIC-PN is shown in black and EPIC-MOS in red (MOS1) and green (MOS2). The three spectra were fitted simultaneously with an absorbed power law allowing only a constant normalisation factor between the three spectra under the assumption that the spectral shape does not change. The model fit is presented in Table 6.1.

mosaics are shown in Figure 6.1 with the *RXTE*/PCA pulsation detection pointing overlaid. A single source is detected within the PCA field of view with a significance of 6.2σ in the IBIS revolution map, with a 90% error circle on its position of radius 3.9 arcmin (Scaringi et al., 2010). The other fluctuations visible in the significance maps were not identified as real sources by the OSA source detection algorithms either because they are beneath the new source detection limit or their PSF is inconsistent with the known IBIS PSF which is well characterised at all positions within the FOV of the instrument. The detection limit is set at 4σ for a source at a position coincident with a known X-ray source and 6σ for a potential new source that is not coincident with a known X-ray source. These values are higher than those of a normal focusing X-ray telescope as the coded mask design used by *INTEGRAL* creates random fluctuations and artefacts within single images to occur at higher significance levels than normal, especially at the extremes of the FOV. Combining single images into a mosaic acts to average out these artefacts, however within a single revolution there is insufficient exposure to remove them completely, hence more conservative detection limits are required to prevent false source identification. The reader should also note that the figures are plotted in log-

Table 6.1: Results of absorbed power-law fits to EPIC spectra of SXP175 and SXP91.1.

Spectral Parameter	SXP175	SXP91.1
Date	2011/04/08	2009/09/27
SMC $N_{\rm H}$ (10^{22} cm^{-2})	0.47 ± 0.03	6.55 ± 0.44
Photon index	0.96 ± 0.02	0.95 ± 0.06
χ^2_ν/degrees of freedom	1.08/391	1.13/158
Model flux (10^{-12} erg cm^{-2} s^{-1})$^{(a)}$	8.50 (M2)	1.92 (M2)
Luminosity (10^{36} erg s^{-1})$^{(b)}$	3.65	0.82

$^{(a)}$ The median 0.2–10 keV flux from the three detectors is presented, with the detector indicated in brackets. M2=MOS2. $^{(b)}$ The 0.2–10 keV luminosity at a distance to the SMC of 60 kpc (Hilditch, Howarth & Harries, 2005). Errors signify the 90% confidence level.

arithmic space. As such, fluctuations that appear by eye to be of similar magnitude may be quite different. The source was not detected in the $3-10$ keV energy band in the corresponding JEM-X map. The detection permitted an *XMM-Newton* ToO observation to identify the nature of the source.

An *XMM-Newton* observation was carried out on 2011 April 8 (MJD 55659) with the EPIC cameras in full frame, imaging mode. For data reduction I selected events with `PATTERN`$\leq$`12` in a circular extraction region, placed on the source. Filtering of periods with high background was not necessary, since soft proton flares were at a quiescent level, yielding a net exposure time of 18.5 ks. A background region was chosen from a source free region of the chip in which the source was seen, such that the RAWY positions were the same to minimise the background variation across each chip. Source detection and light curve extraction were carried out using standard SAS[1] tools. A single bright X-ray source was found within the IBIS error circle at the position RA = 01:01:52.53, dec = -72:23:34.98 (J2000.0) with a 1-sigma error circle of radius 1.1 arcsec. A Lomb-Scargle periodogram of the 0.2–10 keV light curve revealed a period of 175.1 ± 0.1s, confirming the *RXTE*, *INTEGRAL* and *XMM-Newton* detections are of the same source.

For spectral analysis I used only events with `PATTERN`$\leq$`4`. The response matrices and ancillary files were created using the SAS tasks `rmfgen` and `arfgen`. The X-ray spectrum was fit with an absorbed power law with Galactic photoelectric absorption, $N_{\rm H}$, fixed at 6×10^{20} cm^{-2} (Dickey & Lockman, 1990) and the SMC

[1]Science Analysis Software (SAS), http://xmm.esac.esa.int/sas/

column density with abundances at 0.2 for metals a free fit parameter (Figure 6.2). This resulted in a photon index of 0.96 ± 0.02 and intrinsic SMC absorption of $(4.7 \pm 0.3) \times 10^{21}$ cm^{-2}. The full list of model parameters are presented in Table 6.1. The 0.2–10 keV flux from the fit is 8.5×10^{-12} ergs cm^{-2} s^{-1}, corresponding to 3.7×10^{36} ergs s^{-1} at the distance of the SMC (60 kpc; Hilditch, Howarth & Harries 2005). These spectral parameters are fairly standard for a BeXRB and suggest that the non-detection with JEM-X is more likely due to a low SNR in the less sensitive of the two *INTEGRAL* instruments, rather than the hardness of the emission. The pulsar is coincident with the HMXB candidate RX J0101.8-7223 (Haberl & Sasaki 2000, Yokogawa et al. 2003) and is believed to be the same object. The counterpart is likely the emission line star [MA93] 1288. Optical and IR data of this star are explored in the next section.

6.2.2 SXP91.1 = AX J0051–722 = RX J0051.3–7216

SXP91.1 was the first pulsar to be discovered in the *RXTE* monitoring programme at a period of 92 ± 1.5 s (Marshall et al. 1997, Galache et al. 2008). The source was regularly seen during the first 2 years of the programme and again briefly during the fifth year of the programme. It was not detected again with any certainty for several years.

RXTE observations made on 2010 August 16 and 2010 August 21 showed the presence of pulsations with a period of 85.4 ± 0.1 s in their power spectra (Corbet et al., 2010). On seeing this pulsation, it was believed not to be consistent with any known pulsar in the SMC. The period is close to the second harmonic of the known pulsars SXP169 and SXP172, but neither appeared likely to be the source of the 85.4 s pulsations. Recent measurements of SXP169 have shown a spin-up trend that has produced a period significantly different from twice 85.4 s (e.g. Galache et al. 2008) and the detection times are not consistent with the known orbital period or ephemeris of SXP169. The collimator response to SXP172 in the pointed observation is only about 5%, making this source unlikely to be the origin of the pulsations unless it was accreting close to the Eddington limit for a 1.4 $M_\odot$ neutron star. In addition, we see no evidence for modulation near twice 85.4 s in the power spectra of the light curves, but the second harmonic of this period is present at 42.7 s. This pulsation was thus concluded to be from a new HMXB which was designated SXP85.4.

Subsequent observations of the field showed the pulsar was undergoing several small outbursts at regular intervals. From the peak of maximum flux, a rough or-

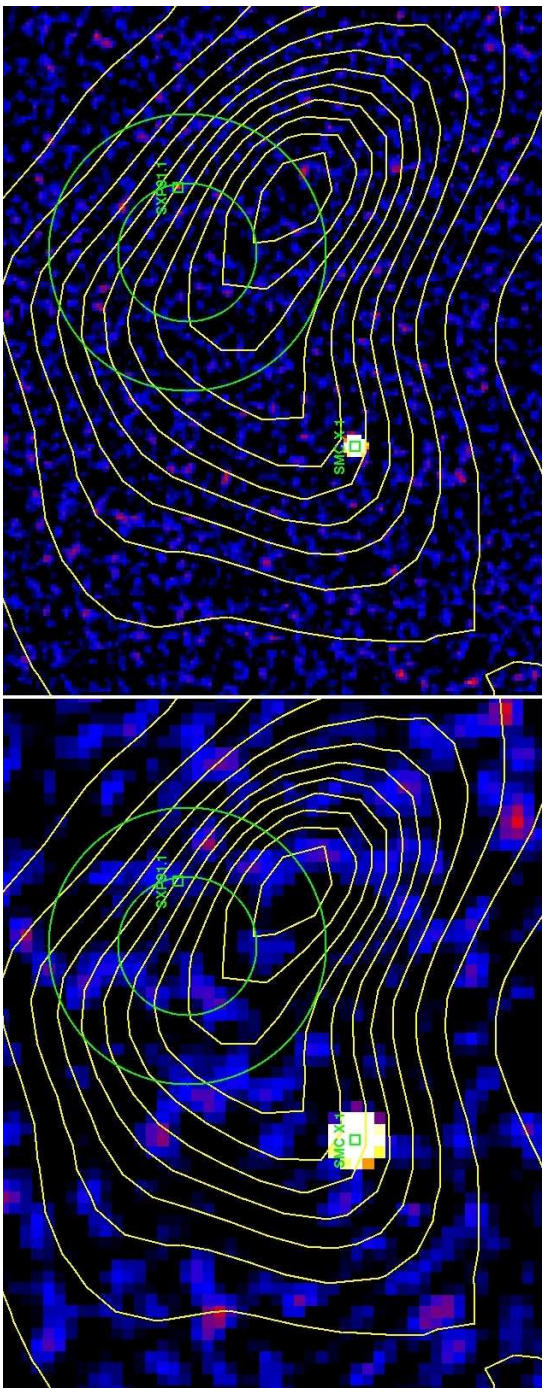

Figure 6.3: Top: JEM-X 3−10 keV significance map. The JEM-X source locator tool (j_ima_src_locator) identified a single source within the *RXTE*/PCA FOV detected at a significance of 5.6σ. Bottom: IBIS/ISGRI 15−60 keV significance map. No significant sources are detected within the *RXTE*/PCA FOV. Again, the circles indicate the *RXTE*/PCA half and zero response of the pointing used whilst the contours are those of the HI column density of Putman et al. 2003.

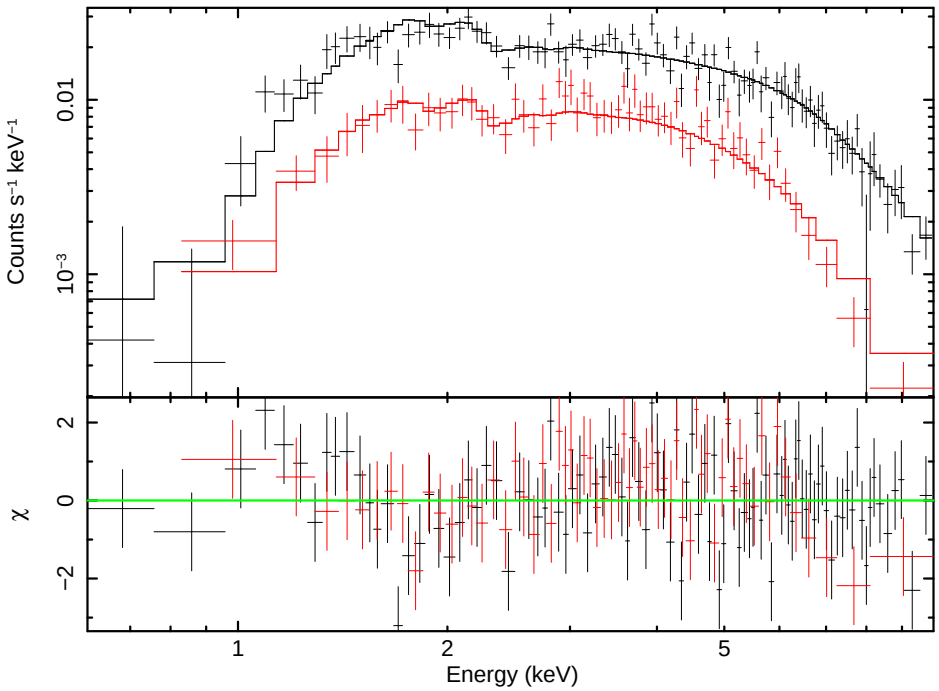

Figure 6.4: *XMM-Newton* EPIC spectra of SXP91.1. EPIC-PN is shown in black and EPIC-MOS2. The two spectra were fitted simultaneously with an absorbed power law allowing only a constant normalisation factor between the three spectra under the assumption that the spectral shape does not change. The model fit is presented in Table 6.1.

bital period was seen at around 88 days. After several orbits, a Lomb-Scargle periodogram of the light curve allowed an ephemeris of maximum amplitude to be calculated. An orbital period of 88.42 ± 0.14 d is the best estimate derived from the X-ray data. From this ephemeris, the time of the next outburst was predicted to allow scheduling of an *INTEGRAL* follow-up observation. An *INTEGRAL* ToO observation was carried out on 2011 May 20. The data were processed using the same methods and energy bands as the SXP175 observations. No sources were detected within the *RXTE*/PCA FOV by IBIS (Figure 6.3, bottom). However the JEM-X source locator tool (j_ima_src_locator) identified a clear source in the JEM-X combined mosaic at RA,Dec (2000)=(12.753,-72.239) with a significance of 5.6σ and an uncertainty of 3 arcminutes (Figure 6.3, top). This position turned out to be consistent with that of SXP91.1. Along with SMC X−1, SXP91.1 was the only source identified by the source locator tool within the image. Comparison of the pulse period history of the two sources confirmed that they were the same source, assuming a constant spin-up over the 13 year *RXTE* monitoring campaign. This result is discussed in detail later in the chapter.

Since the *INTEGRAL* position and spin period history show conclusively that

SXP85.4 is in fact SXP91.1, an *XMM-Newton* follow-up observation was not needed. A search through the *XMM-Newton* archive showed two observations were previously made containing the position of SXP91.1 (observations 0301170201 and 0601210701), taken on MJD 53817.3 and 55101.7 respectively. A similar search of the *Chandra*, *ROSAT* and *Swift* archives did not return any useful observations. The latter of the two *XMM-Newton* observations was taken just before *RXTE* detected the 85.4 s pulsations, though no periodicities were found in the data. A spectrum was extracted for the PN and MOS2 detectors as described for SXP175 (the source was not inside the MOS1 detector FoV). These spectra were fit simultaneously with parameters fixed as described earlier. This resulted in a photon index of 0.95 ± 0.06 and intrinsic SMC absorption of $(6.55 \pm 0.44) \times 10^{22}\,\mathrm{cm}^{-2}$. The full list of model parameters are presented in Table 6.1. The 0.2–10 keV flux from the fit is $1.9 \times 10^{-12}\,\mathrm{ergs\,cm^{-2}\,s^{-1}}$, corresponding to $8.2 \times 10^{35}\,\mathrm{ergs\,s^{-1}}$ at the distance of the SMC. The source was not observed to be active in the other *XMM-Newton* observation. An upper limit for the flux was derived, corresponding to a limiting luminosity of $\sim 4 \times 10^{33}\,\mathrm{ergs\,s^{-1}}$ (Haberl 2011, priv. comm.).

6.3 Optical observations

In this section I present an optical light curve, near-IR fluxes and optical spectra of SXP175 with the aim of understanding more fully the circumstellar disk and its role in the X-ray outburst. I spectrally classify the optical counterpart from the absorptions lines in its spectrum. I also present an optical light curve and spectra of SXP91.1 to try and understand the large variations in X-ray flux seen during the last 14 years.

6.3.1 SXP175

Figure 6.5 shows the OGLE III light curve of SXP175[2]. It shows very little periodic or long-term variability, besides a small increase in brightness just before the end of the light curve by ~ 0.05 magnitudes. At this time, there was good coverage of the source position with *RXTE*, though no X-ray activity was seen. This suggests the circumstellar disk must have grown in the time between the end of the OGLE III light curve and the X-ray outburst. On three occasions IR data of the counterpart

[2]Light curves of objects associated with variable X-ray sources can be found in the OGLE real time monitoring of X-ray variables (XROM) programme. See http://ogle.astrouw.edu.pl/ogle3/xrom/xrom.html and Udalski (2008) for details.

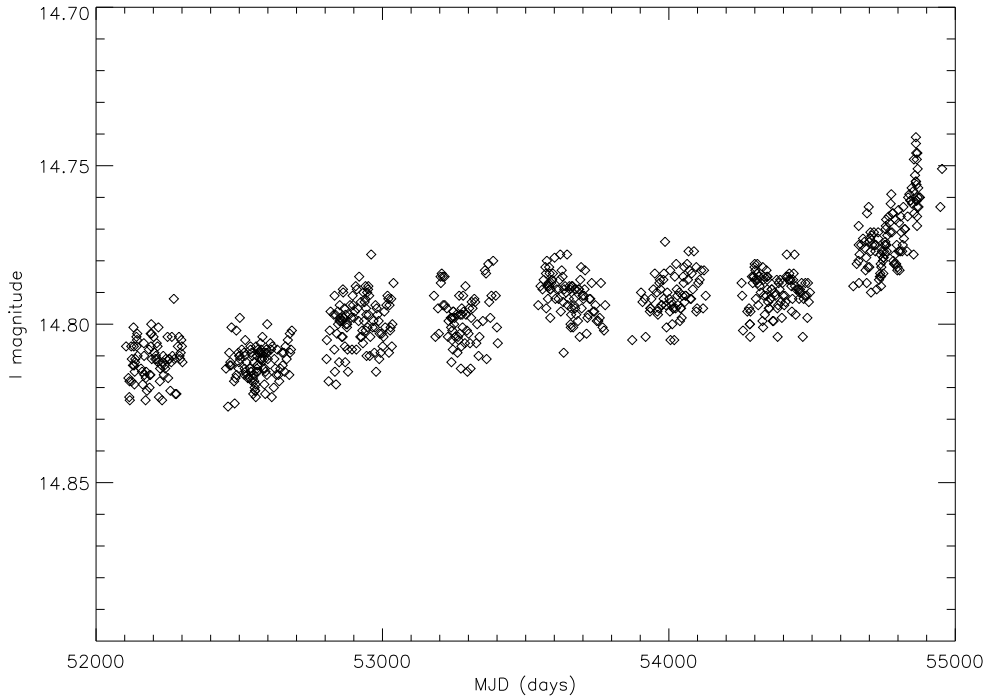

Figure 6.5: OGLE III light curve of SXP175.

Table 6.2: IRSF IR photometry of the counterpart to SXP175.

Date (MJD)	J	H	K_s
18-12-2007 (54452)	14.83 ± 0.01	14.67 ± 0.02	14.50 ± 0.03
08-12-2008 (54808)	14.82 ± 0.01	14.65 ± 0.01	14.47 ± 0.02
14-12-2009 (55179)	14.83 ± 0.02	14.65 ± 0.02	14.45 ± 0.05

were obtained to get a better idea of the disk activity. These data are presented in Table 6.2 and confirm the very stable nature of the disk over a long period of time. Unfortunately, no data for this source are available closer to the X-ray outburst to confirm or not whether the disk has grown.

A red and blue spectrum of this source were taken from the ESO 3.6 m telescope at La Silla, Chile on 2007 September 18 and 2007 September 19. In the following section I will used the blue spectrum to classify the star based in its absorption lines and their ratios. The red end spectrum is presented in Figure 6.6, from which some important information can be gained. Firstly, the presence of Hα and Hβ lines in emission confirm the identification of this system as a BeXRB. The shape of both lines is very narrow and single peaked, suggesting the disk has a low inclination to our line-of-sight. Secondly, the equivalent widths of the lines can be measured.

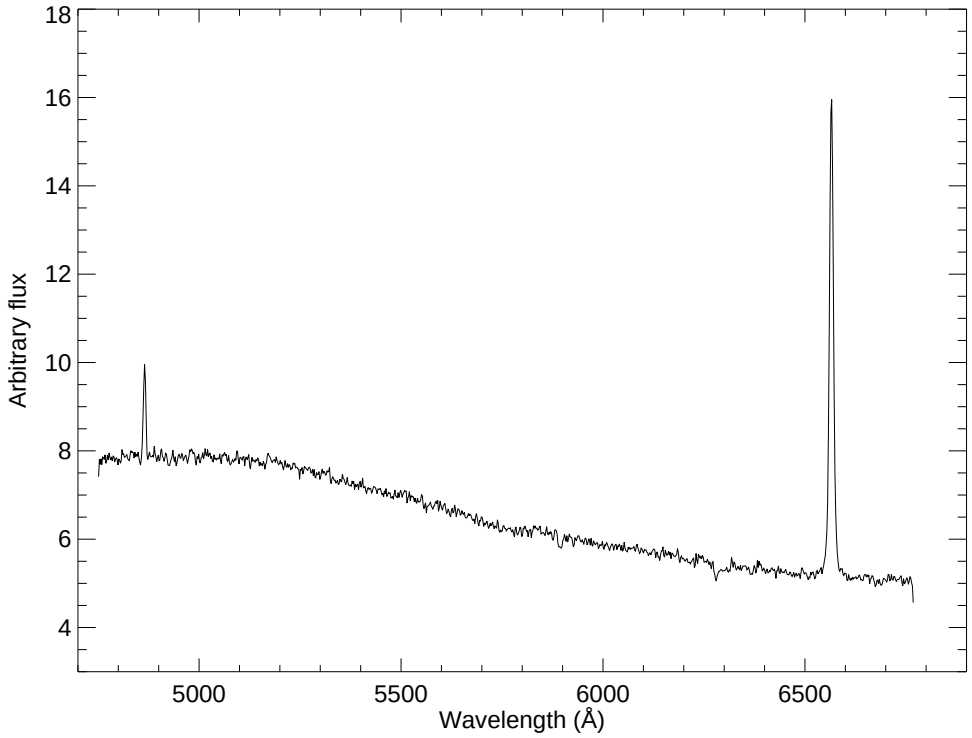

Figure 6.6: Optical spectrum of SXP175 taken with the ESO Faint Object Spectrograph and Camera (EFOSC) on the 3.6 m telescope at La Silla, Chile. Hα and Hβ are observed to be in emission.

I estimate the equivalent width of the Hα and Hβ lines to be -25.7Å and -1.9Å respectively. This value places the system nicely amongst the BeXRB region in Figure 1.13 and suggests the system should have an orbital period of approximately 90–100 d (see Figure 1.12). This number is also implied from the Corbet diagram. To this end, the light curve in Figure 6.5 was detrended and searched for periodicities. The power spectrum is shown in Figure 6.7. A peak at 87.2 ± 0.2 d is found at greater than the 99.9999% confidence level. This seems likely to be the orbital period of the system though, as I have already discussed, great care must be taken with optically derived periods. Until there is evidence of this period in the X-ray light curve, it cannot be certain that it is orbital in nature. The secondary peak at 91.3 d is probably due to beating of the actual period with the gap between observations or the annual sampling, or created in the detrending process. Detrending was done with a simple third order polynomial, though a more precise way to do this would be with a rolling mean or boxcar average. The main peak may move around slightly with a different detrending method, though it is safe to conclude the presence of a significant peak in the power spectrum at ~ 90 d that is likely the orbital period of the binary.

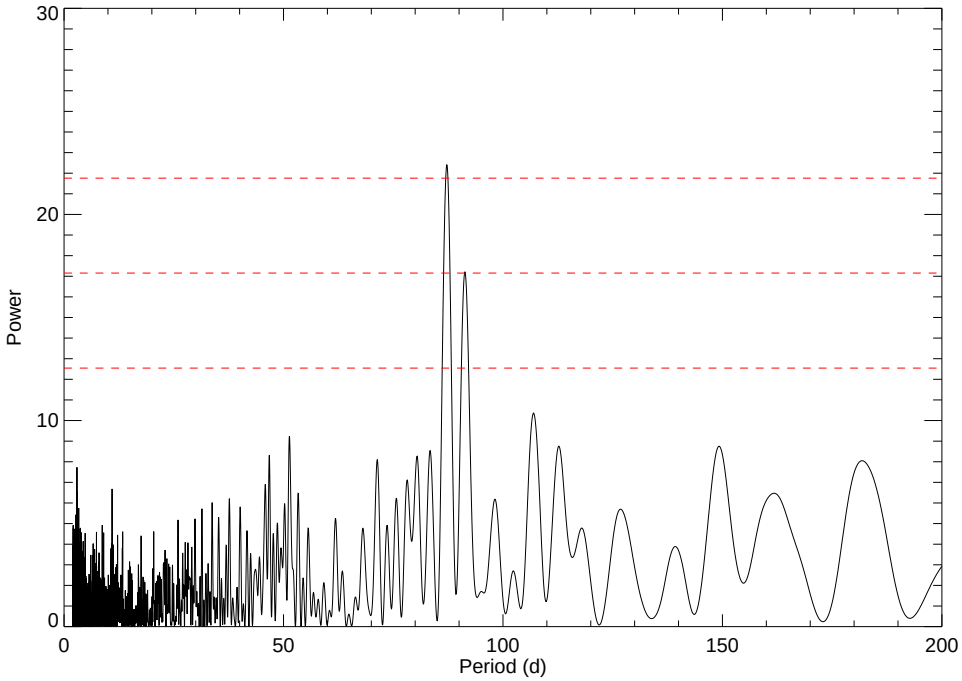

Figure 6.7: Power spectrum of the optical light curve of SXP175. Horizontal lines are 99%, 99.99% and 99.9999% confidence levels. The peak period is 87.2 ± 0.2 d. A secondary peak is visible at 91.3 d. This is most likely due to beating of the actual period with the gap between observations or the annual sampling, or created from the simplistic detrending method used.

6.3.1.1 Spectral classification

The normalised and redshift corrected spectrum used to spectrally classify SXP175 is presented in Figure 6.8. The classification method and references are the same as described in Chapters 1 and 4. The spectrum shows evidence of He II λ4686 absorption, albeit fairly weak, meaning the star must be of type earlier the B 1 (Lennon 1997; Evans et al. 2004). Other ionised helium lines (He II $\lambda\lambda$4200, 4541) may be present, but at a very weak level. This rules out a spectral type earlier than O 9.5. Given all of the He II lines are weak, I would suggest a B 0.5 class. However, if He II $\lambda\lambda$4200, 4541 are present, the spectral type is more likely B 0. As it is difficult to confirm this above the noise in the continuum, I suggest a B 0–B 0.5 classification. As stated in Chapter 4, the lack of strong metal lines makes the luminosity classification difficult. The He I λ4121/He I λ4143 ratio strengthens towards more luminous stars and is the only ratio that can be used here. The ratio in this spectrum is reasonably high, suggesting the luminosity class may be closer to III than V. A V-band magnitude of 14.6 (Haberl, Eger & Pietsch, 2008) allows a check of this classification by comparing the absolute magnitude of the source with a distance

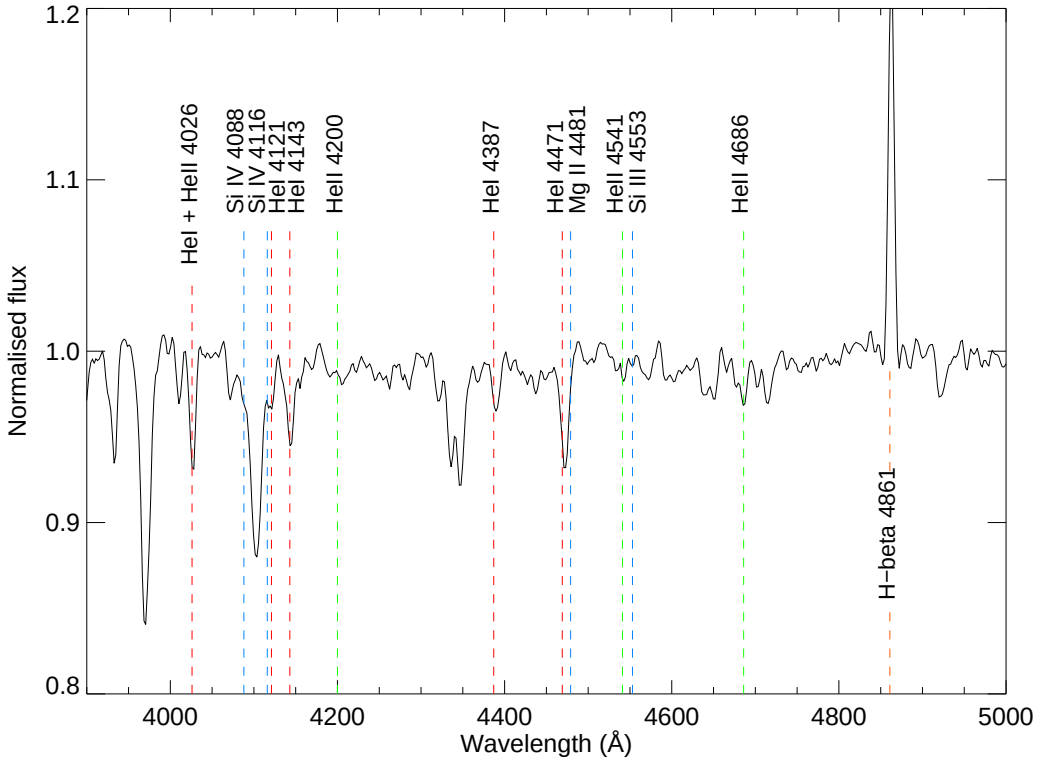

Figure 6.8: Spectrum of SXP175 taken with the EFOSC spectrograph on the 3.6 m telescope at La Silla, Chile. The spectrum has been normalised to remove the continuum and the data have been redshift corrected by -150 km s^{-1} to account for the recession of the SMC. Overplotted are various atomic transitions that are significant in the spectral classification of an early type star at their rest wavelengths; He II, He I and metal transitions are in green, red and blue respectively.

modulus for the SMC of 18.9 (Harries, Hilditch & Howarth, 2003). Thus, an absolute magnitude of -4.3 suggests (using absolute magnitudes for OeBe stars from Wegner 2006) a luminosity class of III, as a V–IV classification would suggest a spectral type as early as O 9. The reader can see from the discussion that a certain amount of personal interpretation is required in estimating spectral types of stars from spectral lines, but I suggest a classification of B 0–B 0.5 IIIe is the most likely for this system given the information available. This is consistent with that of other BeXRBs in the SMC and in the Galaxy (for example McBride et al. 2008; Antoniou et al. 2009).

6.3.2 SXP91.1

Figure 6.9 shows the OGLE III light curve of SXP91.1. It shows clear periodic variability, brightening by $\sim$0.06 magnitudes every 90 days, which is undoubtedly due

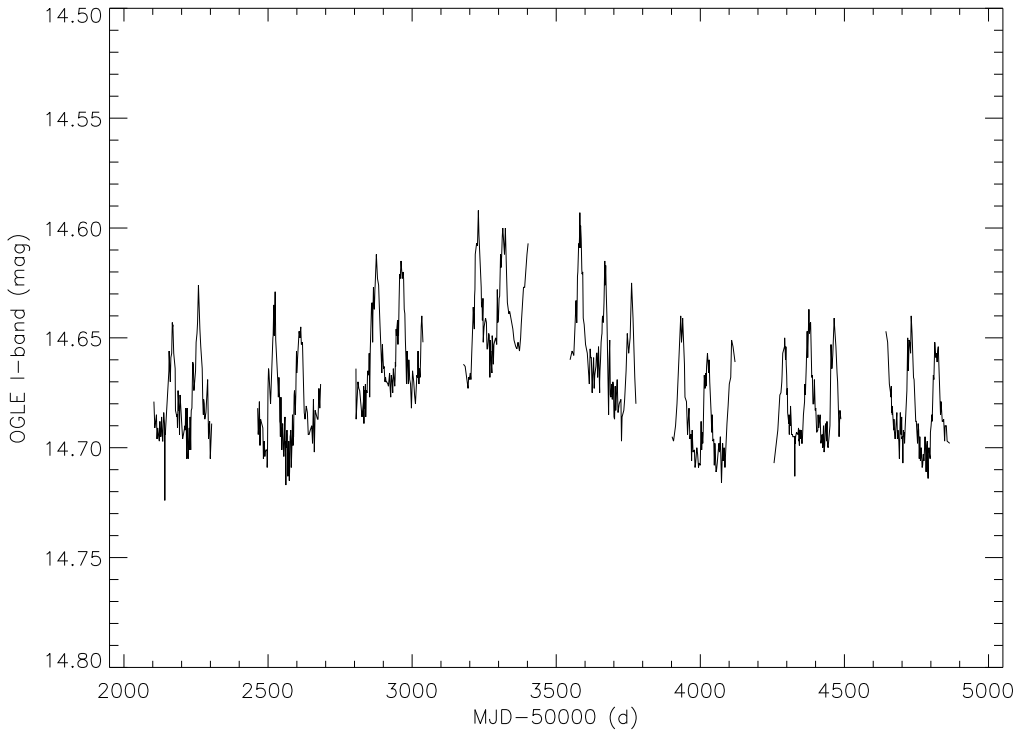

Figure 6.9: OGLE III light curve of SXP91.1.

to the orbital motion of the neutron star. A Lomb-Scargle analysis of the light curve reveals an extremely significant periodicity at 88.37 ± 0.03 d. The power spectrum is shown in Figure 6.10. This period is consistent with that found from analysis of the X-ray light curve and the period originally reported in Schmidtke et al. (2004) and is thus confirmed as the orbital period. There is very little long-term variability, besides a small increase in brightness between MJD 52800 and 53800 by ~ 0.05 magnitudes. Unfortunately, the light curve finishes just before the current series of Type I X-ray outbursts began, so it is impossible to conclude the state of the disk during this phase of X-ray activity. What is very interesting to note here, however, is that at the time of maximum optical flux in the light curve (MJD 53000–53500) there is no X-ray emission detected from this source. However, in the years preceding this small increase in optical flux, when the system appears to be in a constant low state, there were three consecutive Type I X-ray outbursts recorded in the *RXTE* monitoring data (MJD 52300–52600). This suggests X-ray emission only occurs, or at least only reaches the observer, at times of optical minima. Even in the low state, X-ray emission is not always seen as is evident from the lack of X-ray activity between MJD 54000–55000. NIR photometry taken around MJD 55200 suggest the disk is in a similar state to the last 3 years of the OGLE III light curve, which implies

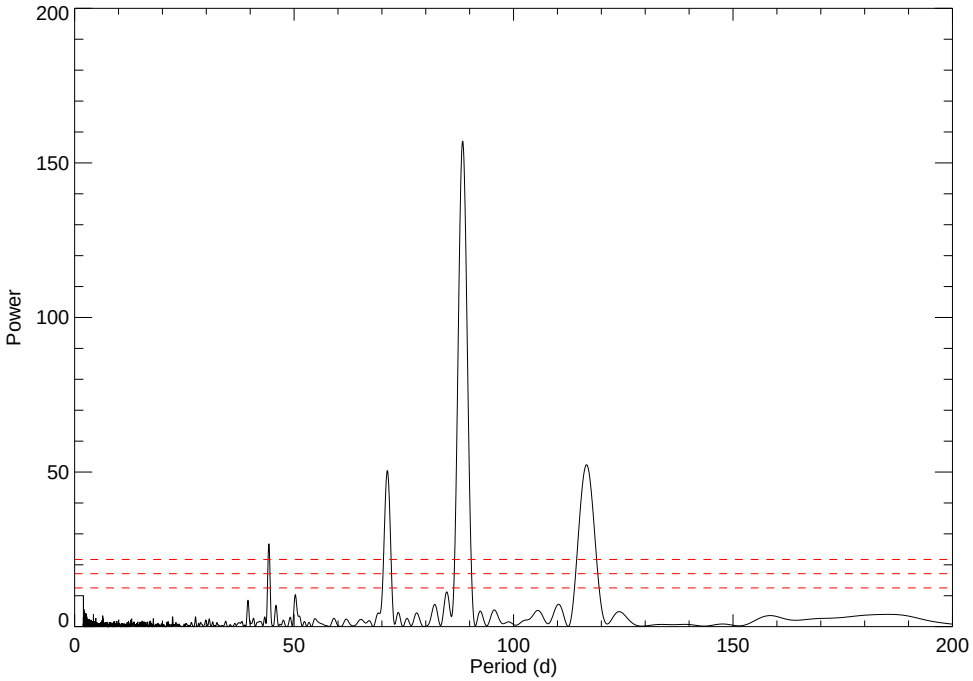

Figure 6.10: Power spectrum of the optical light curve of SXP91.1. Horizontal lines are 99%, 99.99% and 99.9999% confidence levels. The peak period is 88.37 ± 0.03 d. The second harmonic is visible at 44.2 d.

that no dramatic change in the circumstellar environment induced the current long series of X-ray outbursts. Several Hα spectra were also taken during this time period and are shown in Figure 6.11. Five of the seven spectra available show almost constant equivalent widths (W_{eq}) of the Hα line, with an average of -21.0 Å and range between -20.2 and -21.4 Å. Errors on these measurements are between 0.7 and 1.1 Å. These spectra cover the time period of the OGLE light curve, reinforcing the idea of a very stable disk. The sixth and seventh spectrum, however, show equivalent widths of -17.2$\pm$1.6 and -27.3$\pm$1.2 Å respectively. Both were taken after the end of the OGLE light curve, suggesting there may have been some variability in the disk emission after this time. The full *RXTE* light curve for this source is presented in the next section where the discussion of these observations is continued.

6.4 Discussion

The utilisation of *INTEGRAL* and *XMM-Newton* to follow up on unidentified *RXTE* pulsars has proven to be very successful. In this chapter I have discussed the discovery and localisation of a new SMC pulsar to the HMXB candidate RX J0101.8–7223 and the association of a suspected new pulsar with an already known one, that may

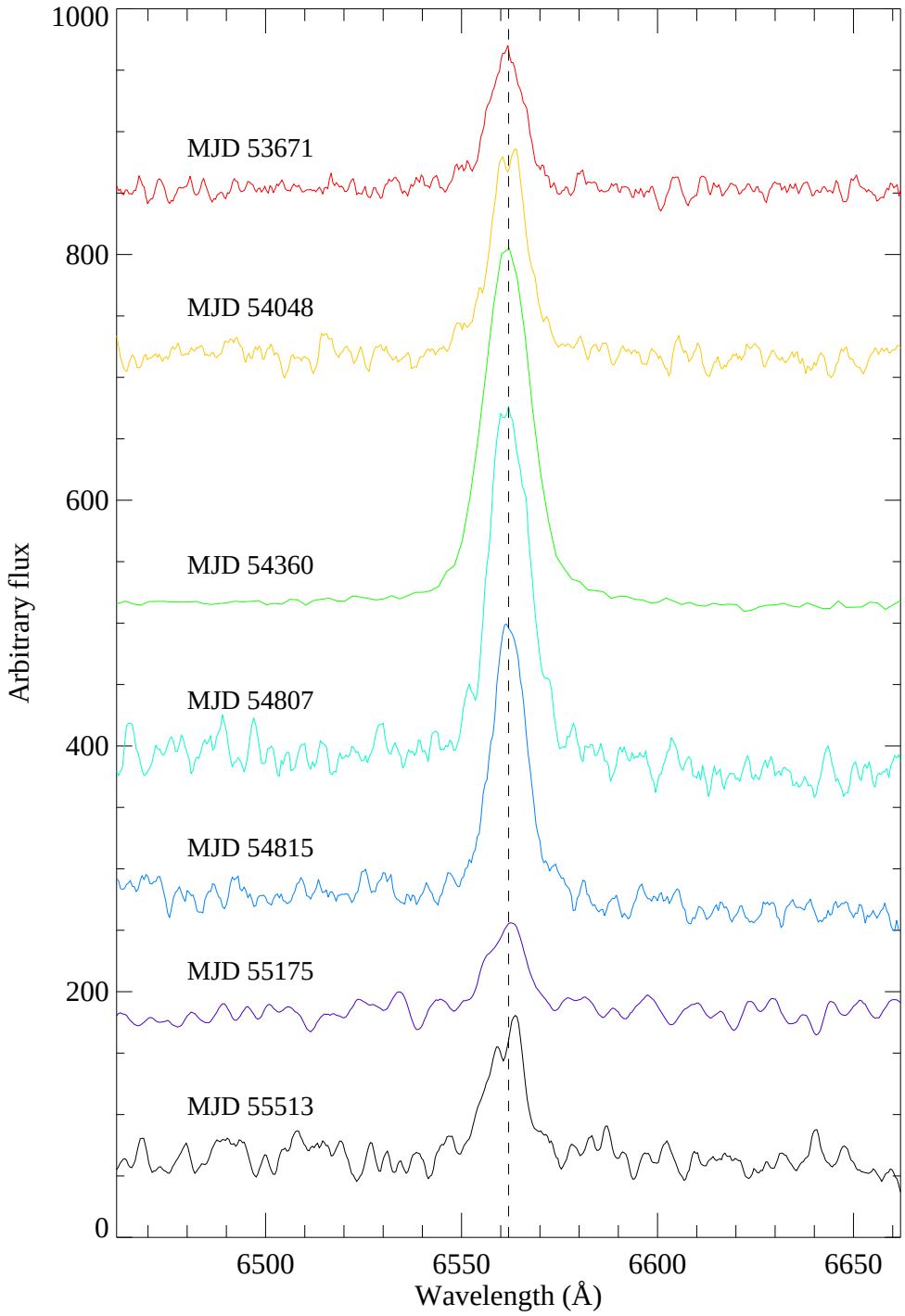

Figure 6.11: Optical spectra of SXP91.1 taken on the 1.9 m telescope at SAAO. The spectrum dated MJD 54360 was taken on the 3.6 m telescope at La Silla. The vertical line denotes the rest wavelength of Hα. All spectra have been arbitrarily shifted in flux and smoothed with a boxcar average of 5 Å for viewing purposes.

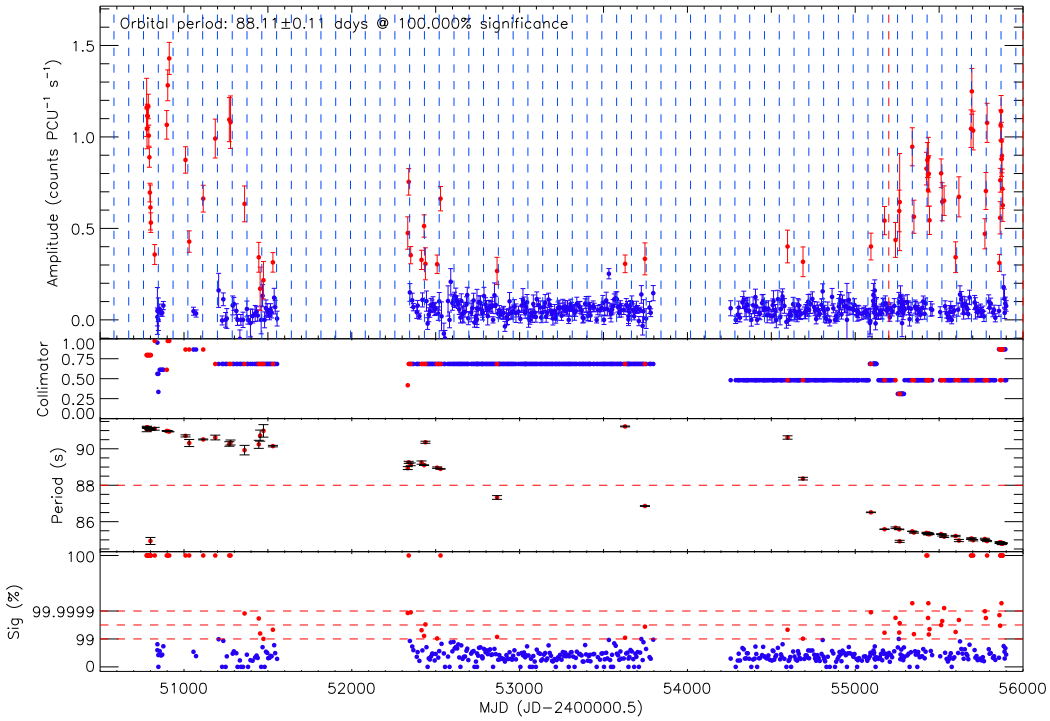

Figure 6.12: Long-term *RXTE*/PCA light curve of SXP91.1 in the 3–10 keV band. The vertical blue lines denote the orbital ephemeris which was calculated from data taken after MJD 55000, as indicated by the vertical red lines. The source had good coverage with *RXTE* between MJD 52300–55000, though very few X-ray outbursts were detected. A constant spin-up can be fit to the entire spin period history, despite this apparent lack of accretion. This is discussed in greater detail in the text.

otherwise not have been so easy. The cause of the X-ray outburst from SXP175, which is the largest known from this HMXB, is not clear as the state of the disk at the time of the outburst is not known. It is likely that the disk increased in size, causing a small outburst. Previous observations of the region by *XMM-Newton* resulted in a positive detection of the source on 5 occasions, each time being at a flux level approximately 10% of that detected in the ToO observation presented here (Haberl, 2011, private communication). This not only explains why it has never been seen with *RXTE* at a significant level before, but reinforces the idea that the disk may have grown and induced an outburst. The most recent of the aforementioned *XMM-Newton* detections was analysed by Haberl, Eger & Pietsch (2008). They present a power law fit to the spectrum that yields a photon index and intrinsic SMC absorption that are almost identical to those values presented here, despite the flux being $< 11\%$ of the flux measured in outburst. This shows that there was no change in the accretion column or surrounding material during the transition into outburst.

The analysis of data on SXP91.1 has shown that this particular BeXRB is quite

abnormal from the rest of the population. Figure 6.12 shows the full spin period history of SXP91.1 along with the pulsed amplitude detections in the same format as was used in previous chapters. The following accounts a short summary of the key observations made before potential explanations are given for the peculiar behaviour of the pulsar:

- it has a high intrinsic absorption column of $(6.55 \pm 0.44) \times 10^{22}\,\mathrm{cm}^{-2}$
- it was shown to be emitting unpulsed X-ray emission at a luminosity comparable to a Type I outburst ($8.2 \times 10^{35}\,\mathrm{ergs\,s}^{-1}$) only one or two orbits before the first detection of pulsations with *RXTE*.
- it must have become much softer between the *XMM-Newton* detection and the *INTEGRAL* detection to be seen in JEM-X and not IBIS. This could mean it is softer in outburst (pulsed emission) but harder just before an outburst or at a slightly lower flux level (unpulsed emission)
- the long-term light curve suggests a constant spin-up under phases of outburst and quiescence. Real quiescence is verified by the *XMM-Newton* non-detection with limiting luminosity of $\sim 4 \times 10^{33}\,\mathrm{ergs\,s}^{-1}$
- its outbursting state seems not to be dependent on a change in the circumstellar disk. X-ray emission is detected, and not, when the disk is unchanged. If anything, the X-ray outbursts are seen at the lowest optical flux level. If the state of the disk does not change and the orbital parameters do not change, then there is nothing to cause accretion to start or stop. This may mean there is always X-ray emission but, for some reason, this does not always reach the observer.

The first point on the spin period plot after MJD 55000 is not real as a huge outburst from another pulsar caused multiple spurious peaks in this observations power spectrum. The second point around MJD 55175 is a very weak detection and, if real, is likely to have underestimated error bars meaning the set of outbursts here probably did not start with a small spin-down before the more obvious spin-up. The detection is probably real, however, as it falls very close to periastron. The *XMM-Newton* observation on MJD 55101 falls 0.2 of an orbital phase after periastron. Comparing this to the *RXTE* folded light curve suggests this lies very close to the point at which pulsed emission ceases to be detected by *RXTE*. This limit is known to be around $10^{36}\,\mathrm{ergs\,s}^{-1}$ in the SMC, which makes sense when the *XMM-Newton* derived luminosity is considered. The *RXTE* observation near MJD 55240

is the first confirmed detection of the source at a luminosity of 6×10^{36} ergs s^{-1}. Thus it seems that pulsed X-ray emission in this pulsar may only begin between luminosities of (0.8–6) $\times 10^{36}$ ergs s^{-1}. From the theory of magnetospheric accretion (e.g. Corbet 1996), it is highly unlikely that this lack of pulsations at such a high luminosity is due to material not making its way to the neutron star surface. More likely, it is due to changes in the absorbing material around the system or changes in the hardness of the X-ray emission. Spectral fits to the few *RXTE* observations in which no other pulsar was active seem to suggest a softer power law than the *XMM-Newton* observation[3]. This makes the later *INTEGRAL* detection with JEM-X more understandable as the source may have softened beyond what is detectable with IBIS, but it still does not explain why *XMM-Newton* did not see pulsations with sufficient counts and a normal value for the photon index. Another explanation is an energy dependence of the pulsed profile. Since the *RXTE* and *XMM-Newton* light curves were extracted in almost the same energy ranges, the pulsed fraction must have increased at softer energies between the *XMM-Newton* and *RXTE* detections. However, since energies much above 10 keV cannot be probed with XMM, this possibility is not testable. There was marginal evidence for variability in the HI column density between the *XMM-Newton* and *RXTE* observations, though this parameter was much less well constrained in the fits than the photon index and so drawing conclusions from this is not desirable.

The *RXTE* pulsed profiles were studied to investigate variability in the pulsed fraction and shape throughout the series of outbursts. The profile shown in Figure 6.13 is representative of most of the profiles available. The pulsed shape is always double or triple peaked due to the presence of multiple harmonics in the power spectrum, with lots of variability in the relative strengths of the peaks. The pulsed emission seems to occur over almost all phases of the neutron stars spin, with the folded light curve looking more like an eclipse than profiles from other pulsars. The pulsed fraction is approximately constant between outbursts, between 0.1–0.2, but shows a strong correlation with pulsed flux (and hence time) during individual outbursts. This may suggest an almost constant unpulsed component and that the pulsed component is much more variable under changing accretion rates. Again, it is hard to quantify the level of background emission in *RXTE* data, so these pulsed fractions are lower limits. As well as showing broad pulsed profiles, SXP91.1 has a broad orbital profile not in keeping with the fast-rise, exponential decay shape that is usually present in eccentric accreting binaries. Figures 6.14 & 6.15 show

[3]These spectral fits are never fully believable as it is impossible to quantify the background contribution from unpulsed point source emission when observing with *RXTE*.

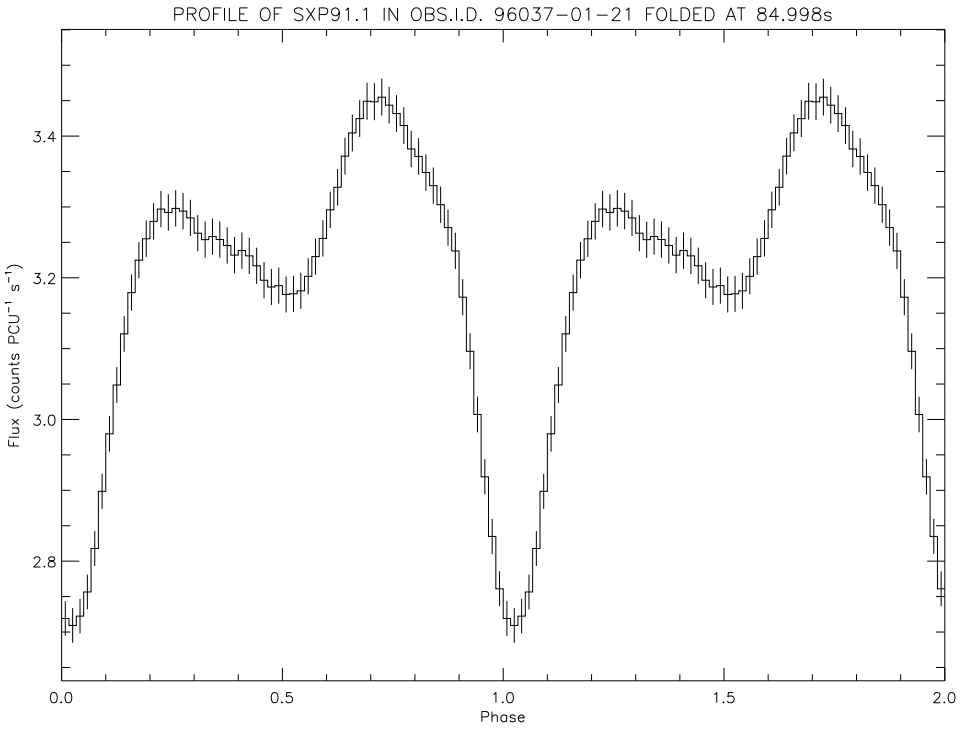

Figure 6.13: Example pulsed profile of SXP91.1 in the 3–10 keV band, folded at the detected spin period. The profile has been arbitrarily shifted in phase for viewing purposes.

the folded orbital X-ray and optical light curves respectively. Both show a broad emission region spanning around half an orbital period. This is indirect evidence of a low eccentricity in this system as the neutron star is accreting well beyond periastron, putting it into a minority group amongst BeXRB pulsars. This may help to explain the unusual spin-up that is observed through phases of quiescence in this system. If the orbit is near-circular, it could be accreting at a very low level all the time, spinning the neutron star up, whilst only becoming an X-ray pulsar when the accretion rate increases. However, as mentioned earlier, the cause of such an increase is hard to understand given the stability of the circumstellar disk. The optically and X-ray derived ephemerides agree well, with a suggestion that the peak in optical flux may lag the X-ray peak by no more than 6 days. The errors are large, however, so this value could be much less. Should the lag be real (5–10% of an orbital period), it reinforces what is currently thought to occur during periastron passage; that the disk only begins to be disturbed after the neutron star passes periastron.

The constant state of the circumstellar disk is unusual during such a dramatic change in X-ray activity. NIR fluxes suggest that the constant nature of the disk seen in the OGLE light curve has continued well into the current X-ray active phase

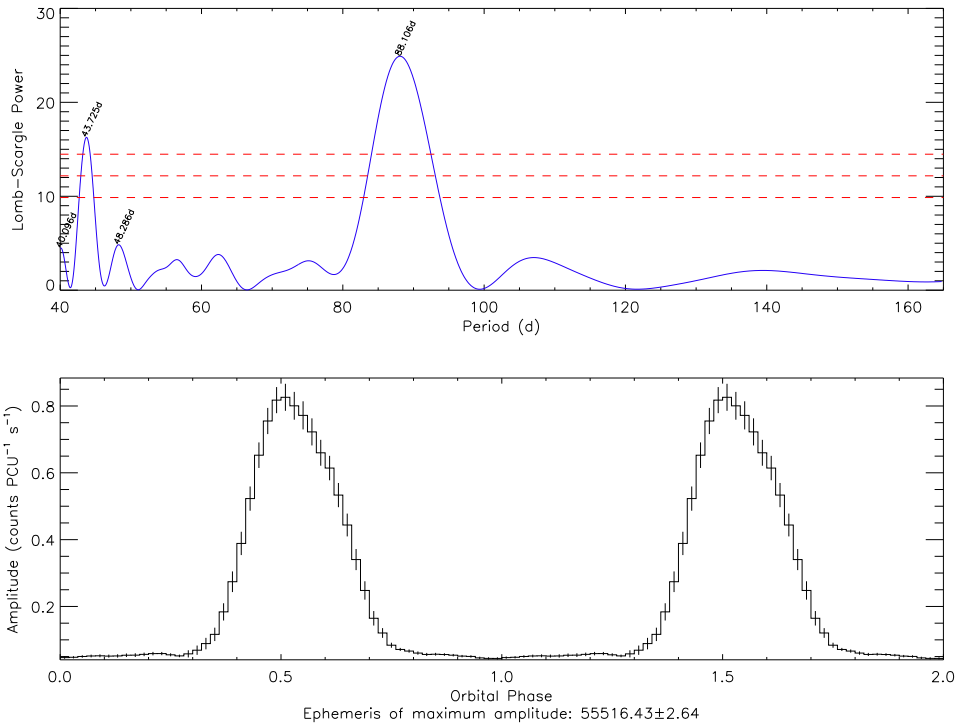

Figure 6.14: Top: orbital power spectrum of the long-term X-ray light curve of SXP91.1. The peak at 88.1 d signifies the orbital period of the system and agrees well with the optically derived period. The horizontal lines are 99%, 99.99% and 99.9999% significances. Bottom: the X-ray light curve folded on the orbital period. Increased flux is apparent over a phase space of 0.4, higher than most other BeXRBs.

as discussed above. Hα spectra taken before and during the X-ray active phase (see Figure 6.11) shed some light on the problem, but also raise some further issues. The Hα equivalent width measurement on MJD 55175 suggests a small decrease in the disk emission at the onset of the X-ray outburst, whilst the following measurement is evidence of a significant increase in the disk emission. At first, this may appear as evidence for the growth of the disk many hundreds of days into the series of X-ray outbursts. However, on closer inspection this observation falls nearly 2 weeks before periastron and so could just have been induced by the interacting neutron star rather than being an intrinsic change in the disk. A counter argument to this though, is that four of the other spectra were taken as close or closer to periastron than this one and show no sign of an increase in flux. If the flux increase is intrinsic to the disk, it could indicate a significant lag between the start of the X-ray outburst and increased optical activity. Beyond this variability, these Hα spectra show some far more intriguing features. Firstly, they show evidence of both single peaked and double peaked profiles that may correlate with flux. The two observations with the

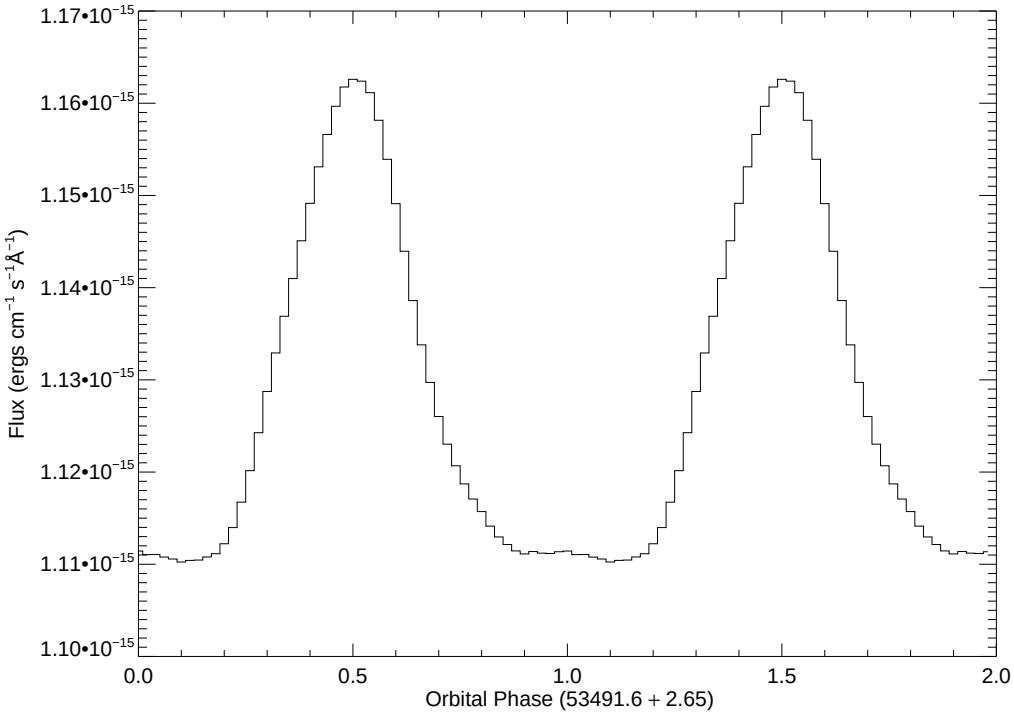

Figure 6.15: Folded optical light curve of SXP91.1. As with the X-ray light curve, a broad peak is observed suggesting the disturbance in the disk lasts for almost half an orbit.

largest measured W_{eq} show evidence of a double peaked line profile, whilst the 5 smallest W_{eq} are all single peaked. Secondly, the flux and shape of the profiles may correlate with orbital phase. The 3 profiles with the smallest W_{eq} (all single peaked) were taken within a few days of periastron, whilst the 3 with the largest W_{eq} (2 of which are double peaked) were taken at least 2 weeks before or after periastron. This could be evidence of the neutron star truncating the disk slightly (see the discussion on disk modelling in Chapter 1), though the reason for the changing profile shapes and their orbital phase distribution is very hard to understand with the data available.

6.5 Conclusions

This chapter has presented the discovery of a new 175 s pulsar in the SMC and its association with the HMXB candidate RX J0101.8–7223. This system seems to be a very standard BeXRB system that has shown low levels of X-ray activity fairly regularly and a rare larger outburst that allowed the pulse period to be found. The large outburst is likely caused by an increase in the size of the circumstellar disk

around the counterpart that, until now, has been very stable. Analysis of the optical light curve allowed an estimate of the orbital period of the system of 87.2 ± 0.2 d. An archival spectrum has allowed the counterpart to be classified as a B 0–B 0.5 IIIe star, similar to most other known BeXRBs.

SXP91.1 has proven to be very different to SXP175, with its very regular outbursts, large modulation in its optical light curve and peculiar spin-up and X-ray emission characteristics. I have endeavoured to explain these aspects by combining all available X-ray, optical and IR data. It seems clear that the neutron star has always, and is continuing to, interact with the circumstellar disk at every periastron passage from the periodic variations in the OGLE light curve, though this interaction does not always lead to X-ray emission, pulsed or otherwise, reaching the observer. The idea of constant accretion in this system, despite the lack of X-ray emission is backed up by the relatively constant spin-up of the neutron star throughout the entire *RXTE* monitoring campaign. Since the lack of pulsations at such a high flux is improbable for this spin period, the most likely explanation from the data presented here is that either a nearby absorbing material sometimes acts to prevent the X-ray emission reaching the observer, or a change in the geometry of the emission column or magnetic field of the neutron star directs the emission away from us at certain times. The other possible scenario is that a near-circular orbit brings the neutron star into contact with the disk, causing a weak interaction every periastron passage. This could spin the neutron star up and cause a spike in the optical light curve without resulting in an X-ray outburst. At the times when an outburst is seen, the accretion rate is likely to have increased, though with a very stable disk it is unclear what could cause the system to outburst. Solving the orbit of this system would provide a huge step to understanding its strange behaviour, though this would have to be done through optical radial velocity work, as the X-ray outbursts are not suitable for such an analysis.

We are all in the gutter, but some of us are looking at the stars.

OSCAR WILDE (1854 – 1900)

7

Conclusions & Future work

In this chapter, I give a brief overview of the main results of this thesis and discuss the implications in a broader context. This is closely linked to work I hope to continue with and embark upon in the near future.

7.1 Impact of this work

Throughout this work I have tried to emphasise the importance of a multi-wavelength approach to understanding high-mass X-ray binaries, as the plethora of different X-ray outbursts seen can only be understood by considering the behaviour of the optical counterpart in the system. This approach can also prove fruitful in reverse, as the HMXB family are ideal to study the effects a compact object has on main sequence and supergiant stars. The second main concept that has been addressed in this work is the importance of the SMC population of HMXBs. These systems are the most homogeneous group known and offer our best opportunity to study the statistical properties of X-ray binary systems. The third and final idea put forward is the opportunities the SMC population provides for studying the affects the local environment has on the formation, evolution and activity of these systems by comparison to the Galactic population. Though not as homogeneous as the SMC

population, largely due to uncertainties in distance and absorption to many systems, the Galactic population is of similar size and has already allowed similarities and differences to be discovered through statistical analyses of the populations. Many of these have been discussed throughout the preceding chapters and will be summarised in this section, along with the general conclusions that can be drawn from this work. The reader is also referred to the more detailed conclusion sections at the end of each chapter for more information.

The main aims of this thesis were to further our understanding of the outburst properties and orbital dynamics of BeXRBs in the SMC and to improve the statistical properties of the SMC population by finding and following up new systems. The calculation of the orbital parameters of some of the systems in the SMC forms probably the most significant result in this work and is discussed later.

It will forever be important to find and understand new BeXRB systems as some of the most fundamental knowledge of these systems comes from their global properties. The more properties that are known, the better the statistical analysis will be. In Chapter 2 I touch on the new systems found during the RXTE monitoring programme and describe the two most recent attempts to localise and follow-up new systems in detail in Chapter 6. The details presented in these two chapters signify a significant increase in the number of spin periods, orbital periods, spectral types, emission line strengths, positions, spectral hardnesses, local absorptions and outbursts known in the SMC thanks to this monitoring programme and the follow-up of many optical and X-ray telescopes. In total, RXTE has identified 18 new pulsars in the SMC and 1 in the Magellanic Bridge as part of this programme. When added to the other known systems in the SMC, the population is of a good size to investigate their global properties. The spectral classifications have been used by McBride et al. (2008) and subsequently by Antoniou et al. (2009) to show that the low metallicity in the SMC does not result in a different distribution to that of Galactic counterparts (see Chapter 1). The positions have been used by Antoniou et al. (2010) to show that regions of higher SFR in the SMC coincide with regions containing HMXBs (see Chapter 2). The ever-increasing number of spin and orbital periods known have been used to make a more complete Corbet diagram, though this extra information has started to blur the distinction between Be systems and supergiant systems, rather than result in an empirical relationship between the two parameters. These two parameters have also very recently shown evidence for a bimodal distribution, which may be evidence for two distinct formation channels in BeXRBs (Knigge, Coe & Podsiadlowski, 2011). This is discussed further in the next section. It is clear that new systems presented in earlier chapters, and those

presented in Galache et al. (2008), are small but important stepping stones in understanding BeXRBs as an entire population and have already helped find similarities between the SMC and Galactic populations and shed light on the fundamental formation processes.

Chapters 2, 3 & 4 present many of the different types of X-ray outburst observed in BeXRBs and try to emphasise that these are closely linked to the activity of the optical counterpart and to the orbital motion of the neutron star. As such, I suggest that each outburst needs to be described differently and not cast into groups of simply Type I or Type II. The 5 light curves in Chapter 2 really demonstrate the range of outbursts possible: Long, bright outbursts can be followed by fainter, orbitally induced outbursts; systems can be active over many years; they can have a brief, bright outburst and then switch off again; or they can be inactive for many years then in outburst for many years; periastron outbursts can be seen superimposed over continual non-orbital outbursts; neutron stars can spin up, down or stay almost constant during outburst, or shift sharply from one state to another. Future plans to provide a more quantitative view of these ideas is something that is discussed in the next section. In Chapter 3 it is shown that the X-ray outbursts in SXP6.85 are related to the disk-loss timescale of the counterpart and not the orbital period. Optical and IR light curves and emission line strengths are used to show the disk increases in size before every X-ray outburst and an estimate is made of the disk size at the time of outburst. However, this value may be underestimated by a factor of ~ 3 when the calculations made in Chapter 5 regarding the size of the orbital semi-major axis of the system are considered. The result is very similar for SXP11.5, with the size predicted from the emission line profiles and from a viscous disk model a factor 3–4 smaller than that estimated from the size of the semi-major axis. The radius calculated in the former is considered to be approximately the boundary radius of the disk, after which it becomes optically thin and so contributes negligibly to the line flux. If this value really represents the size of the disk, it is hard to understand how the extended X-ray outbursts occur when the closest approach of the neutron star is 3 or 4 times further away. On the other hand, these values do agree with recent interferometric measurements of the disk sizes of many Be stars, as stated in Grundstrom & Gies (2006), so it may be that the neutron only interacts with the optically thin part of the disk out at many stellar radii. Of course, the calculation of the semi-major axes in Chapter 5 relies heavily on assumed stellar masses and radii and so it is entirely possible that the inconsistency in these two measurements arises from uncertainties in the stellar parameters. Uncertainties may also exist in the input parameters to the models of Grundstrom et al. (2007a), in particular the

effective temperature of the star and the disk continuum correction factor. Grundstrom & Gies (2006) correct all their radius estimates by a certain factor to account for the continuum contribution of the disk in the V-band. They use an average value found by Dachs et al. (1988) as they lacked knowledge of the value for individual systems. However for SXP11.5, this information is available, as the correction factor to the W_{eq} is just $(1+\frac{F_{disk}}{F_{star}})$. From the values found in Chapter 4, this is ~ 1.75, which corresponds to an increase of $\sim 10\%$ in the disk radius from that found using the value in Dachs et al. (1988). Similar increases of $\sim 10\%$ are apparent when changing the inclination and effective temperature slightly. For a B0 V star, the effective temperature should not be lower than 25000 K and the inclination should be less than $\sim 30^{\circ}$ for SXP11.5 given the shape of its line profiles. Using these limits, I estimate a disk size ~ 2 times smaller than the radius of the semi-major axis. This is an improvement on the factor of 3–4 from earlier calculations, but it certainly seems to suggest that the neutron star is not within the densist parts of the disk, even at periastron. The question remains whether or not this is the case for all BeXRB systems, if indeed it is the correct interpretation of the data in this system.

Whilst one can observe the various properties of the X-ray emission in these systems and put forward explanations based on the activity of the counterpart or on the orbital path, very little is still understood about the physics of the emission regions very close to the neutron star surface. In particular, very little is understood about the X-ray pulsed profiles. In Chapters 3 & 4 I present some profiles of outbursts of SXP6.85 and SXP11.5, but venture very little in the way of a quantitative explanation. This is because detailed modelling or a systematic approach to explain what is observed has as yet not been undertaken by the community. The basic concept of a fan or pencil beam is the only way to explain what is observed at this time. The profiles of SXP11.5 show very strong triple peaked profiles that fade into a single peak as the luminosity drops. More regularly, a double peaked profile can be explained by both poles being visible to the observer. A third peak is much harder to quantify. In this case, a combination of a pencil beam from one pole and a fan beam from the other pole was suggested as the dip between the two closest peaks is half of an orbit away from the third peak. Thus, it could be that we observe both poles and both edges of a fan beam as the neutron star spins. This idea could also explain some of the (albeit less apparent) triple peaked structure in the profiles of SXP6.85. However, the rapid changes observed in these profiles on timescales of days is much harder to understand and demonstrates the variability that is occurring around the accretion columns in some systems that cannot be explained at this time. Discussion of the pulsed component in these systems, its shape, strength

and variability, also highlights the peculiar nature of SXP91.1 found in the previous chapter. As discussed, the amount of material available to be accreted in this system seems unchanged, even though the X-ray flux detected changes by at least 4 orders of magnitude. Whilst this could be explained by a variable absorber around the system, it could also be caused by a change in the accretion or emission regions around the magnetic poles of the neutron star. With the available data it is very hard to say what the actual cause of this is, but SXP91.1 undoubtedly offers itself as a very intriguing candidate for future multi-wavelength campaigns.

The orbital analysis presented in part in Chapter 4 and more fully in Chapter 5 is perhaps the most significant result of this thesis. The 5 orbital solutions found in these chapters mark a significant increase in the number known outside of the Milky Way. Prior to this work there were only 3 BeXRBs with orbital solutions outside of the Galaxy (SXP18.3, PSR J0045–7319 & A 0538–66, only the first of which is considered a 'normal' BeXRB), compared to the 23 known in the Galaxy. Whilst the knowledge of the Galactic systems has produced some very exciting science, this is now the first time the orbital parameters of another group of systems can be compared to them. In general, the parameters of the SMC systems seem to be similar to the Galactic parameters, suggesting the effect a low metallicity environment has on massive stars is not so important in the formation or evolution of the massive binaries. The position of one of the SMC systems in the orbital period against eccentricity parameter space highlights yet a other similarity these systems have with their Galactic cousins. SXP2.37 lies very near the much discussed low eccentricity BeXRBs that are theorised to have received a smaller kick from the natal supernova (Pfahl et al., 2002). The existence of this group implies a fundamentally different formation channel, the details of which are more closely linked to my future work and so is discussed in the next section. The important point here is that, along with spectral type, spin period, orbital period and Hα W_{eq}, the eccentricity distribution seems to be consistent with the Galactic distribution and shows evidence of the same low and high eccentricity sub-groups. The other potentially important result of this work is the apparent relationship between eccentricity and orbital period amongst the entire HMXB population. As discussed in Chapter 5, this may just be due to Be systems being at a different evolutionary stage than the supergiant systems, rather than there being a fundamental link between the two parameters. Indeed, if this were the case, the relationship should hold for just the Be systems which, at the moment, the data are not sufficient to prove. Improving the available data to try and solve this puzzle is, again, something that is discussed in the next section.

7.2 Future work

Previous discussion of the binary parameters of HMXBs has highlighted the orbital period and eccentricity as the most important, as they give an insight into the birth of the X-ray binary from the natal supernova explosion and also the pre-supernova phase of the binary. Unfortunately, the smallness of the SMC population and some more general observational biases affecting the entire HMXB population mean that the conclusions drawn are currently not certain. In order to overcome this problem and be able to say something statistically significant about the formation of these systems in other galaxies, many more orbits need to be modelled and the biases resolved. This is an area of investigation that I would like to continue with in the future, through the following avenues:

1. Improved analysis of *RXTE* SMC monitoring data, either by improving the orbital fitting code described in Chapter 4 or by using an alternative method, such as pulse arrival time analysis. There are outbursts from 4 systems in these data that are long enough and well sampled enough to extract the orbital information from, which would be a good starting place for this work.

2. Optical radial velocity work with 8m class telescopes such as SALT, GTC or the VLT. Solving the orbits of binary systems from X-ray data requires a large outburst of significant duration. These are quite rare in many systems and tend to be less numerous in longer orbital period systems. This is a major bias in the data set, which may only be resolved by optical analysis.

The necessity to understand these ideas and to find as many orbital solutions as possible has never been more apparent, since the publication of a recent paper in Nature announcing the discovery of a bi-modal population of BeXRBs (Knigge, Coe & Podsiadlowski, 2011). The data leading to the discovery are shown in Figure 7.1. The authors conclude that the group of pulsars with a low neutron star spin period are likely to have formed through electron-capture supernovae (ECS; less massive core) and those with high spin period through core-collapse supernovae (CCS; more massive core). This could be analogous to the BeXRBs inside and outside of the shaded region in Figure 5.6 as an ECS is thought to impart a smaller kick to the neutron star than the CCS, resulting in a lower eccentricity. However, the authors also state that the bi-modal distribution is most significant in the spin period and that they could find no statistically significant relationship between the orbital period and eccentricity. Thus, it is vital that as many of these systems have

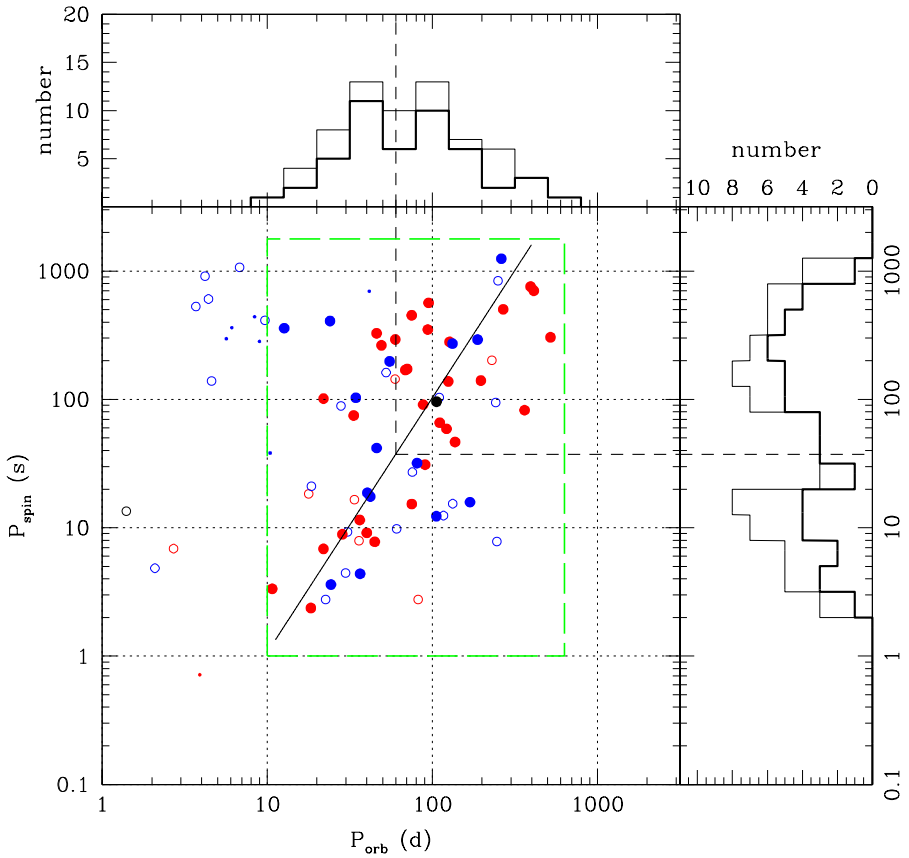

Figure 7.1: Orbital period against spin period for all the HMXBs for which these two parameters are known. Filled circles correspond to spectroscopically confirmed BeXRBs, small dots to confirmed supergiant X-ray binary systems and open circles to candidate BeXRBs. Blue corresponds to Milky Way systems, red to SMC and black to LMC. The dashed green lines mark a selection box that conservatively includes all confirmed BeXRBs for which orbital and spin periods have been measured. The values within this box have been projected onto the plot at the top and right of the main plot respectively. Taken from Knigge, Coe & Podsiadlowski, (2011).

their orbits calculated as possible to test this theory of bi-modality, investigating whether it extends to the orbital period against eccentricity distribution and to explore whether different extra-Galactic environments have an effect on these results. Not only would these results help understand the formation mechanisms of one of the largest class of X-ray binary, but they will also help place limits on the neutron star mass. The neutron star mass can only be determined precisely for eclipsing systems as it is important to know the orbital inclination. However, knowing the orbital dynamics, mass function and spectral type of the optical companion can lead to a somewhat more constrained neutron star mass. It is possible that even limits such as

these would be important in areas such as understanding the neutron star equation of state or whether neutron stars formed in other galaxies or via a particular supernova channel have statistically different masses. The former would help understand how matter behaves in hyper-dense environments whilst the latter two points have been predicted by star formation theory and so this avenue of study would provide a means of testing this theory.

Throughout this work I have spoken about the need for a better characterisation of the outbursts seen in BeXRBs and that this should be linked to the orbital parameters of the system and the activity of the optical counterpart. This need became apparent during discussion sessions at a recent conference on BeXRBs, where I learnt that many systems show behaviour that is intermediate to the classical Type I and II outbursts and cannot easily be placed into one of these two groups. It could be that the exact nature of each outburst is different in subtle ways and that these differences are intrinsically related to the orbital period and eccentricity of the system as well as the variability produced by the optical counterpart. The large database of *RXTE* SMC observations is an obvious starting point for such a study, with the *RXTE*/ASM monitoring of Galactic systems a natural extension to include many Galactic systems in the analysis. I would also like to perform an archival search of *XMM*, *INTEGRAL*, *Swift* and *Chandra* observations of known BeXRBs to enhance the data set. Such a categorisation would involve examining the outburst intensity, duration, phase, spectral features, and the strength, shape and variability of the pulsed component. My initial aim would be to devise a basis by which this information can be used to categorise each outburst more thoroughly than is possible at this time. Once a categorisation scheme has been set out, my secondary aim is to link the observed types of outburst with the orbital and spin periods and eccentricities (where known) of each system. If this is achieved, it may be possible to use as a predictive tool for when an outburst may occur and how large it will be, though the aperiodic variability of the Be star counterpart will likely make some outbursts impossible to predict. Conversely, it may allow better informed estimates of the orbital parameters of a system based on the characteristics of its outbursts. This project could be concluded by searching the fundamental parameters (orbital period, eccentricity, semi-major axis, disk size etc) for correlations, like that done in Chapter 5, to investigate links that may provide information about the formation or activity in these systems. One such correlation that may already exist in the data is the much higher frequency with which short spin period systems seem to show extended outbursts over long spin period systems. This was first suggested in Chapter 5, but the RXTE dataset shows that all of the 12 systems in the SMC showing

huge, extended outbursts in the past 14 years have a spin period under 100 s, even though the number of systems with spin period above and below 100 s is almost split evenly. Though not all the orbital periods are known in this sample, it should map directly to onto orbital period space using the Corbet diagram. If correct, this may be analogous to the findings of Okazaki & Negueruela (2001) in which higher eccentricity systems tend to only show smaller, periastron outbursts, whereas low eccentricity systems show more luminous, extended outbursts. Though Knigge, Coe & Podsiadlowski (2011) found no statistical correlation between orbital period and eccentricity, the outburst behaviour of the BeXRBs seem to suggest there may be a qualitative relationship between the parameters which should be looked into further.

A third project that I will work on in the near future is a population study of the Magellanic Bridge. As touched on earlier, work done by McBride et al. (2010) has started to uncover a new HMXB population in the Bridge that likely formed separately from the SMC and LMC populations. Knowledge of this emerging population is important for our understanding of how the environment (e.g. local metallicity, gas content) affects star formation and evolution in turbulent intergalactic environments. However, to date there have only been shallow observations of the region with RXTE and INTEGRAL, probing only the outbursting systems. As such, my colleagues and I have proposed the first deep survey of its Western-most region with XMM. Two 35 ks observations were carried out at the start of January 2012, that are deep enough to probe the quiescent population of X-ray binaries. These observations are important as they have the potential to form a population of systems different from that of the Milky Way and SMC, which may be the first step in expanding the extra-Galactic comparisons outlined throughout this thesis for yet another population of XRBs. The two regions observed have been well studied optically, which will allow rapid characterisation of sources detected and make further optical follow-up easier. The proposal has also been resubmitted for the upcoming XMM observing round and has been given priority C time. If carried out, a variability study would be possible, further helping in the source characterisation.

Finally, I have several active and future projects in mind studying the optical counterparts of the SMC systems, that have not yet been discussed in this work. My collaborators and I are working on the analysis of near-IR spectra of 12 sources, with the aim of better understanding the structure of the disks beyond the Hα region. These are the first such observations made in the SMC. The data have been reduced, but have not yet been properly calibrated to allow satisfactory analysis of the Brγ line or any other lines that may be present. There also exists simultaneous

Hα spectra of these sources to allow the prominent optical and near-IR emission lines to be compared. On top of this, I wish to more fully exploit the wealth of data my group and I have obtained from the IRSF telescope at SAAO. Whilst these data have been useful in conjuncture with the OGLE light curves in understanding certain systems, the amount of data accrued warrents a full statistical study of the flux and colour changes in around 50 systems over the past 6 years. This has been done for some systems in the past, but never with this much data or this number of systems. I would also like to continue trying to understand the flux contribution of the disk across the optical and IR regime as was tried for SXP11.5 in Chapter 4. Although this relies on there being some near-simultaneous optical photometry, the disk in several systems should be able to be probed in this way. A final project that I think would be very interesting is a disk polarisation study. Using the IRSF in polarimetry mode, I have data that will allow the Stokes parameters to be calculated for several systems in the SMC. Whilst these data have yet to be exploited, it could potentially give an idea of the disk size and orientation to the observer, as the amount of polarised flux that is observed likely depends most heavily on these two parameters. Many of the results from such studies of the counterpart are likely to link in with work done and work that will be done in the X-ray regime, allowing a more complete understanding of the BeXRB population.

BIBLIOGRAPHY

Allen C.W., 1973, Astrophysical Quantities, 3rd edn. Athlone Press, London

Antoniou V., Hatzidimitriou D., Zezas A., Reig P., 2009, ApJ, 707, 1080

Antoniou V., Zezas A., Hatzidimitriou D., Kalogera V., 2010, ApJ, 716L, 140

Aragona C., McSwain M.V., Grundstrom E.D., Marsh A.N., Roettenbacher R.M., Hessler K.M., Boyajian T.S., Ray P.S., 2009, ApJ, 698, 514

Arnaud, K.A., 1996, ASPC, 101, 17

Barsukova E.A., Borisov N.V., Burenkov A.N., Klochkova V.G., Goranskij V.P., Metlova N.V., 2005, Atel, 416

Basko, M.M., Sunyaev, R.A., 1975, A&A, 42, 311

Baykal A., Inam S.C., Beklen E., 2006, MNRAS, 369, 1760

Baykal A., Inam S.C., Stark M.J., Heffner C.M., Erkoca A.E., Swank J.H., 2007, MNRAS, 374, 1108

Baykal A., Gögüş E., Inam S.C., Belloni T., 2010, ApJ, 711, 1306

Belczynski K., Ziolkowski J., 2009, ApJ, 707, 870

Besla G., Kallivayalil N., Hernquist L., Robertson B., Cox T.J., van der Marel R.P., Alcock C., 2007, ApJ, 668, 949

Bildsten L., et al., 1997, ApJS, 113, 367

Bird A.J., et al. 2007, ApJS, 170, 175

Bird A.J., et al. 2011, Priv. Comm.

Blum S., Kraus U., 2000, ApJ, 529, 968

Bodaghee A., Courvoisier T.J.L., Rodriguez J., et al., 2007, A&A, 467, 585

Bozzo E. et al. 2009, ATel, 2079

Bradt H.V., Rothschild R.E., Swank J.H., 1993, A&AS, 97, 355

Bruhweiler F.C., Klinglesmith D.A. III, Gull T.R., Sofia S., 1987, ApJ, 317, 152

Campana S., Stella L., Mereghetti S., Colpi M., 1995, A&A, 297, 385

Campana S., Stella L., Israel G.L., Moretti A., Parmar A.N., Orlandini M., 2002, ApJ, 580, 389

Carciofi A.C., Bjorkman J.E., 2006, ApJ, 639, 1081

Carciofi A.C., 2010, arXiv:1009.3969

Chakrabarty D., et al., 1993, ApJ, 403, L33

Chaty S., Rahoui F., Foellmi C., Tomsick J.A., Rodriguez J., Walter R., 2008, A&A, 484, 783

Clark G.W., 2000, ApJ, 542, L131

Coe M.J., Edge W.R.T., Galache J.L., McBride V.A., 2005, MNRAS, 356, 502

Coe M.J., Reig P., McBride V.A., Galache J.L., Fabregat J., 2006, MNRAS, 368, 447

Coe M.J., et al., 2007, MNRAS, 378, 1427

Coe M.J. et al. 2008, The Magellanic System: Stars, Gas, and Galaxies, Proceedings of the International Astronomical Union, IAU Symposium, Volume 256, p. 367-372.

Coe M.J., Bird A.J., McBride V.A., Townsend L.J., Corbet R.H.D., Udalski A., 2009, ATel, 2088

Coe M.J., McBride V.A., Corbet R.H.D., 2010, MNRAS, 401, 252

Coe M.J. et al. 2010, MNRAS, 406, 2533

Corbet R.H.D., 1986, MNRAS, 220, 1047

Corbet R.H.D., 1996, ApJ, 457, L31

Corbet R.H.D., Charles P.A., Southwell K.A., Smale A.P., 1997, ApJ, 476, 833

Corbet R.H.D., Marshall F.E., Lochner J.C., Ozaki M., Ueda Y., 1998, IAU Circ. 6803

Corbet R.H.D., Marshall F.E., Coe M.J., Laycock S., Handler G., 2001, ApJ, 548, L41

Corbet R.H.D., Mukai K., 2002, ApJ, 577, 923

Corbet R.H.D., Markwardt C.B., Marshall F.E., Coe M.J., Edge W.R.T., Laycock S., 2003, ATel, 163, 1

Corbet R.H.D., Coe M.J., Edge W.R.T., Laycock S., Markwardt C.B., Marshall F.E., 2004, ATel, 277, 1

Corbet, R. H. D., Coe, M. J., McGowan, K. E., Schurch, M. P. E., Townsend, L. J., Galache, J. L., Marshall, F. E., 2008, The Magellanic System: Stars, Gas, and Galaxies, Proceedings of the International Astronomical Union, IAU Symposium, Volume 256, p. 361-366.

Corbet R.H.D., Bird A.J., Coe M.J., McBride V.A., Townsend L.J., Marshall F.E., 2009, ATel, 2092

Corbet R.H.D., Bartlett E.S., Coe M.J., McBride V.A., Townsend L.J., Schurch M.P.E., Marshall F.E., 2010, Astron. Telegram, 2813

Cusumano G., La Parola V., Romano P., Segreto A., Vercellone S., Chincarini G., 2010, MNRAS, 406, L16

Dachs, J., Kiehling, R., & Engels, D., 1988, A&A, 194, 167

de Jager C., Nieuwenhuijzen H., 1987, A&A, 177, 217

Delgado-Martí H., Levine A.M., Pfahl E., Rappaport S.A., 2001, ApJ, 546, 455

de Wit W.J., Lamers H.J.G.L.M., Marquette J.B., Beaulieu J.P., 2006, A&A, 456, 1027

Diaz J., Bekki K., 2011, MNRAS, 413, 2015

Dickey J. M. & Lockman F. J., 1990, ARA&A, 28, 215

D'Odorico S. et al. 2006, SPIE, 6269, 626933

Doroshenko V., Santangelo A., Suleimanov V., 2011, A&A, 529, 52

Dray L.M., 2006, MNRAS, 370, 2079

Ekström S., Meynet G., Maeder A., Barblan, F., 2008, A&A, 478, 467

Emilio M., et al., 2010, A&A, 522, 43

Evans C.J., Howarth I.D., Irwin M.J., Burnley A.W., Harries T.J., 2004, MNRAS, 353, 601

Fender R.P., Belloni T.M., Gallo E., 2004, MNRAS, 355, 1105

Finger M.H., Wilson R.B., Hagedon K.S., 1994, IAUC, 5931, 1

Finger M.H., Bildsten L., Chakrabarty D., Prince T.A., Scott D.M., Wilson C.A., Wilson R.B., Zhang, S.N., 1999, ApJ, 517, 449

Frank J., King A.R., Raine D.J., 2002, Accretion Power in Astrophysics, Cambridge University Press, 3rd Edition

Galache J.L., 2006, Ph.D Thesis, University of Southampton

Galache J.L., Corbet R.H.D., Coe M.J., Laycock, S., Schurch M.P.E., Markwardt C., Marshall F.E., Lochner, J., 2008, ApJS, 177, 189

Galloway D.K., Morgan E.H., Levine A.M., 2004, ApJ, 613, 1164

Galloway D.K., Wang Z., Morgan E.H., 2005, ApJ, 635, 1217

Gardiner L.T., Noguchi M., 1996, MNRAS, 278, 191

Ghosh P. & Lamb F.K., 1979, ApJ, 234, 296

Goldoni, P., Royer, F., Franois, P., Horrobin, M., Blanc, G., Vernet, J., Modigliani, A., Larsen, J., 2006, SPIE, 6269E, 80

Goldwurm, A., David, P., Foschini, L., Gros, A., Laurent, P., Sauvageon, A., Bird, A. J., Lerusse, L., Produit, N., 2003, A&A, 411, L223

Gregory, P.C., Loredo, T.J., 1996, ApJ, 473, 1059

Grundstrom, E.D. & Gies, D.R., 2006, ApJ, 651, L53

Grundstrom E.D., et al., 2007, ApJ, 656, 431

Grundstrom, E.D., et al., 2007, ApJ, 660, 1398

Haberl F., Sasaki M., 2000, A&A, 359, 573

Haberl F., Pietsch W., 2008, A&A, 484, 451

Haberl F., Pietsch W., 2008, xng, conf, 32, X-ray source populations in the Magelanic Clouds

Haberl F., Eger P., Pietsch W., 2008, A&A, 489, 327

Harmanec P., et al., 2000, A&A, 364, L85

Harris J., Zaritsky D., 2004, AJ, 127, 1531

Harries T.J., Hilditch R.W., Howarth I.D., 2003, MNRAS, 339, 157

Heindl W.A. Rothschild R.E., Coburn W., Staubert R., Wilms J., Kreykenbohm I., Kretschmar P., 2004, X-RAY TIMING 2003: Rossie and Beyond. AIP Conference Proceedings, Volume 714, pp. 323-330

Hilditch R. W., 2001, An Introduction to Close Binary Stars, Cambridge Univ. Press, Chapter 3

Hilditch R.W., Howarth I.D., Harries T.J., 2005, MNRAS, 357, 304

Hill A.B., et al., 2005, A&A, 439, 255

Hill A.B., Dubois R., Torres D.F., on behalf of the Fermi-LAT collaboration, 2010, To be published in the book of proceedings of the 1st Sant Cugat Forum on Astrophysics, ”ICREA Workshop on the high-energy emission from pulsars and their systems”, held in April, 2010, arXiv:1008.4762

Horne J.H., Baliunas S.L., 1986, ApJ, 302, 757

Hutchings J.B., Crampton D., Cowley A.P., Olszewski E., Thompson I.B., Suntzeff N., 1985, PASP, 97, 418

in't Zand J.J.M., Corbet R.H.D., Marshall F.E., 2001, ApJ, 533, L165

Israel G.L., Stella L., Angelini L., White N.E., Giommi P., 1995, IAUC, 6277, 1

Jahoda K., Markwardt C. B., Radeva Y., Rots A. H., Stark M. J., Swank J. H., Strohmayer T. E., Zhang W., 2006, ApJS, 163, 401

Jansen, F. et al., 2001, A&A, 365L, 1

Kaaret P., Cusumaon G., Sacco B., 2000, ApJ, 542, L41

Kahabka P., Pietsch W., 1996, A&A, 312, 919

Kahabka P., Pietsch W., 1998, IAU Circ. 6840

Kallivayalil N., van der Marel R.P., Alcock C., Axelrod T., Cook K.H., Drake A.J., Geha M., 2006, ApJ, 638, 772

Kallivayalil N., van der Marel R.P., Alcock C., 2006, ApJ, 652, 1213

Kaspi V.M., Johnston S., Bell J.F., Manchester R.N., Bailes M., Bessell M., Lyne A.G., D'Amico N., 1994, ApJ, 423, L43

Kato S., 1983, PASJ, 35, 249

Kato D., Nagashima C., Nagayama T., Kurita M., et al., 2007, PASJ, 59, 615-647

Kelley R.L., Rappaport S., Ayasli S., 1983, ApJ, 274, 765

Kelson, D.D., 2003, PASP, 115, 688

King A., Cominsky L., 1994, ApJ, 435, 411

Knigge C., Coe M.J., Podsiadlowski P., 2011, accepted for publication in Nature (arXiv 1111.2051)

Koh D.T., et al., 1997, ApJ, 479, 933

Kreykenbohm I., et al., 2008, A&A, 492, 511

Kudritzki R.P., Pauldrach A., Puls J., 1987, A&A, 173, 293

Kurucz, R.L., 1979, ApJS, 40, 1

Lamb F.K., Pethick C.J., Pines D., 1973, ApJ, 184, 271

Laycock S.G.T., 2002, Ph.D Thesis, University of Southampton

Laycock S., Corbet R.H.D., Coe M.J., Marshall F.E., Markwardt C., Lochner J., 2005 ApJS, 161, 96

Laycock S., Zezas A., Hong J., Drake J.J., Antoniou V., 2010, ApJ, 716, 1217

Lebrun F., et al., 2003, A&A, 411, 141

Lee U., Saio H., Osaki Y., 1991, MNRAS, 250, 432

Lennon D.J., 1997, A&A, 317, 871

Levine A., Rappaport S., Putney A., Corbet R., Nagase F., 1991, ApJ, 381, 101

Lewin W.H.G., van der Klis M., 2006, *Compact stellar X-ray sources*, Compact stellar X-ray sources, Cambridge, UK: Cambridge University Press, 2006, Cambridge Astrophysics Series, No. 39. Edited by Walter Lewin & Michiel van der Klis. ISBN 978-0-521-82659-4

Li F., Jernigan G., Clark G., 1977, IAU Circ., 3125, 1

Linden T., Sepinsky J.F., Kalogera V., Belczynski K., 2009, ApJ, 699, 1573

Liu Q.Z., van Paradijs J., van den Heuvel E.P.J., 2005, A&A, 442, 1135

Liu Q.Z., van Paradijs J., van den Heuvel E.P.J., 2006, A&A, 455, 1165

Lund N., et al., 2003, A&A, 411, 231

Maccarone T.J., Gallo E., Fender R.P., 2003, MNRAS, 345, 19

Marshall F.E., Lochner J.C., Takeshima T., 1997, IAU Circ., 6777, 2

Martin R.G., Tout C.A., Pringle J.E., 2009, MNRAS, 397, 1563

Masetti N. et al., 2010, arXiv, 1006, 4513

McBride V.A., Coe M.J., Negueruela I., Schurch M.P.E., McGowan K.E., 2008, MNRAS, 388, 1198

McBride V.A., Bird A.J., Coe M.J., Townsend L.J., Corbet R.H.D., Haberl F., 2010, MNRAS, 403, 709

McCray R.A., Shull J.M., Boynton P.E., Deeter J.E., Holt S.S., White N.E., 1982, ApJ, 262, 301

McGowan K.E., Coe M.J., Schurch M.P.E., Corbet R.H.D., Galache J.l., Udalski A., 2008, MNRAS, 384, 821

McGowan K.E., Coe M.J., Schurch M.P.E., McBride V.A., Galache J.L., Edge W.R.T., Corbet R.H.D., Laycock S., Buckley D.A.H., 2008, 383, 330

McHardy I.M., Papadakis I.E., Uttley P., Page M.J., Mason K.O., 2004, MNRAS, 348, 783

McSwain M.V., Gies D.R., 2005, ApJS, 161, 118

Mennickent R.E., Vogt N., 1991, A&A, 241, 159

Mennickent R.E., Sterken C., Vogt N., 1997, A&A, 326, 1167

Mikkola S., 1987, CeMec, 40, 329

Morgan W.W., Keenan P.C., Kellman E., 1943, An Atlas of Stellar Spectra, with an Outline of Spectral classification. Univ. Chicago Press, Chicago

Murdin P., Morton D.C., Thomas R.M., 1979, MNRAS, 186, 43P

Nagashima C., et al. 1999, in Star formation 1999, ed. T. Nakamoto, (Nobeyama Radio Observatory), 397

Negueruela I., 1998, A&A, 338, 505

Negueruela I., Okazaki A.T., 2000, ASPC, 214, 713

Negueruela I., Okazaki A.T., 2001, A&A, 369, 108

Nidever D.L., Majewski S.R., Butler B.W., Nigra L., 2010, ApJ, 723, 1618

North P., Gauderon R., Barblan F., Royer F., 2010, A&A, 520A, 74

Okazaki A.T., 1991, PASJ, 43, 75

Okazaki, A. T. 2001, PASJ, 53, 119

Okazaki A.T., Negueruela I., 2001, A&A, 377, 161

Okazaki A.T., 2007, ASPC, 361, 230

Percy J.R., Bakos A.G., 2001, PASP, 113, 748

Pfahl E., Rappaport S., Podsiadlowski P., Spruit H., 2002, ApJ, 574, 364

Pollock, A.M.T., 1987, ApJ, 320, 283

Porter J.M., Rivinius T., Publ. Astron. Soc. Pac. 115, 1153

Putman M.E., Staveley-Smith L., Freeman K.C., Gibson B.K., Barnes D.G., 2003, ApJ, 586, 170

Raguzova N.V., Popov S.B., 2005, A&AT, 24, 151

Raicher H., Paul B., 2010, MNRAS, 401, 1532

Raichur H., Paul B., 2010, MNRAS, 406, 2663

Rajoelimanana A.F., Charles P.A., Udalski A., 2010, arXiv, 1012, 4610

Ray P.S., Chakrabarty D., 2002, ApJ, 581, 1293

Reig P., Fabregat J., Coe M.J., 1997, A&A, 322, 193

Russell S.C., Dopita M.A., 1992, ApJ, 384, 508

Scaringi S., et al., 2010, A&A, 516, 75

Schmidtke P.C., Cowley A.P., Levenson L., Sweet K., 2004, AJ, 127, 3388

Schmidtke P.C., Cowley A.P., 2005, AJ, 130, 2220

Schmidtke P.C., Cowley A.P., 2006, AJ, 132, 919

Schmidtke P.C., Cowley A.P., Udalski A., 2006, AJ, 132, 971

Schmidtke P.C., Cowley A.P., 2007, Astron. Telegram, 1181

Schmidtke P.C., Cowley A.P., Udalski A., 2009, Astron. Telegram, 1992

Schönherr G., Wilms J., Kretschmar P., Kreykenbohm I., Santangelo A., Rothschild R.E., Coburn W., Staubert R., 2007, A&A, **472**, 353

Schurch M.P.E., 2009, Ph.D Thesis, University of Southampton

Schurch, M.P.E. et al. 2009, MNRAS, 392, 361

Schurch M.P.E., Coe M.J., McBride V.A., Townsend L.J., Udalski A., Haberl F., Corbet R.H.D., 2011, MNRAS, 412, 391

Schwering, P.B.W. & Israel, F.P., 1991, A&A, 246, 231

Scott D.M., Finger M.H., Wilson R.B., Koh D.T., Prince T.A., Vaughan, B.A., Chakrabarty D., 1997, ApJ, 488, 831

Sguera V., et al., 2005, A&A, 444, 221

Shaw S.E., Hill A.B., Kuulkers E., Brandt S., Chenevez J., Kretschmar P., 2009, MNRAS, 393, 419

Shtykovskiy P., Gilfanov M., 2005, MNRAS, 362, 879

Shtykovskiy P., Gilfanov M., 2005, A&A, 431, 597

Shtykovskiy P.E., Gilfanov M.R., 2007, Astron. Lett., 33, 437

Sidoli L., 2011, Invited talk at the 25th Texas Symposium on Relativistic Astrophysics, held in Heidelberg, Germany, on December 6-10, 2010, arXiv1103.6174

Skrutskie M.F., Cutri R.M., Stiening R., Weinberg M.D., et al., 2006, AJ, 131, 1163

Stairs I.H., et al., 2001, MNRAS, 325, 979

Staubert R., Pottschmidt K., Doroshenko V., Wilms J., Suchy S., Rothschild R., Santangelo A., 2011, A&A, 527, 7

Stella L., White N.E., Rosner R., 1986, ApJ, 308, 669

Stevens J.B., Coe M.J., Buckley D.A.H., 1999, MNRAS, 309, 421

Struve, O., 1930, ApJ, 72, 1S

Szymański M., 2005, Acta Astron., 55, 43

Tauris T.M., van den Heuvel E.P.J., 2006, In: *Compact stellar X-ray sources*, Compact stellar X-ray sources, Cambridge, UK: Cambridge University Press, 2006, Cambridge Astrophysics Series, No. 39. Edited by Walter Lewin & Michiel van der Klis. ISBN 978-0-521-82659-4, arXiv:0303.456

Thompson T.W.J., Tomsick J.A., Rothschild R.E., in 't Zand J.J.M., Walter R., 2006, ApJ, 649, 373

Thompson T.W.J., Tomsick J.A., in 't Zand J.J.M., Rothschild R.E., Walter R., 2007, ApJ, 661, 447

Touhami Y., Gies D.R., Schaefer G.H., 2011, ApJ, 729, 17

Townsend L.J., Corbet R.H.D., Coe M.J., McBride V.A., Hill A.B., Bird A.J., 2009, Astron. Telegram, 2202

Townsend L.J., et al, 2010, MNRAS, 403, 1239

Townsend L.J., et al, 2011, MNRAS, 410, 1813

Townsend L.J., Drave S.P., Corbet R.H.D., Coe M.J., Bird A.J., 2011, Astron. Telegram, 3311

Townsend L.J., Coe M.J., Corbet R.H.D., Hill A.B., 2011, MNRAS, 416, 1556

Tsapras Y. et al., 2009, RoboNet-II: Follow-up observations of microlensing events with a robotic network of telescopes, Astronomische Nachrichten, 330, 1, pp 4-11

Turner, M.J.L., 2001, A&A, 365L, 27

Ubertini P., et al., 2003, A&A, 411, 131

Udalski A., Kubiak M., Szymański M., 1997, Acta Astron., 47, 319

Udalski A., 2003, Acta Astron., 53, 291

Udalski A., 2008, Acta Astron., 58, 187

Uttley P., McHardy I.M., Papadakis I.E., 2002, MNRAS, 332, 231

van den Heuvel E.P.J., 1975, ApJ, 198, L109

van der Meer A., Kaper L., van Kerkwijk M.H., Heemskerk M.H.M., van den Heuvel E.P.J., 2007, A&A, 473, 523

Walborn N.R., Fitzpatrick E.L., 1990, PASP, 102, 379

Wang Q., Wu X., 1992, ApJS, 78, 391

Wang N., Johnston S., Manchester R.N., 2004, MNRAS, 351, 599

Wegner W., 2006, MNRAS, 371, 185

White N.E., Swank J.H., Holt S.S., 1983, ApJ, 270, 711

Wilson C.A., Finger M.H., Harmon B.A., Scott D.M., Wilson R.B., Bildsten L., Chakrabarty D., Prince T.A., 1997, ApJ, 479, 388

Wilson C.A., Finger M.H., Coe M.J., Negueruela I., 2003, ApJ, 584, 996

Wilson C.A., Finger M.H., Camero-Arranz A., 2008, ApJ, 678, 1263

Winkler C., et al., 2003, A&A, 411, 1

Wisniewski J.P., Draper Z.H., Bjorkman K.S., Meade M.R., Bjorkman J.E., Kowalski A.F., 2010, ApJ, 709, 1306

Yokogawa J., Koyama K., 1998, IAU Circ. 6835

Yokogawa J., Imanishi K., Tsujimoto M., Koyama K., Nishiuchi M., 2003, PASJ, 55, 161

Zaritsky D., Harris J., Thompson I., 1997, AJ, 114, 1002

Zaritsky D., Harris J., Thompson I.B., Grebel E.K., Massey P., 2002, AJ, 123, 855

Zorec J., Briot D., 1997, A&A, 318, 443